Helena Isabel Nogueira Ramos Rocha

Seeking for new p53-activating agents: effective therapies for colorectal cancer

Tese de Candidatura ao grau de Doutor em Biotecnologia Molecular e Celular Aplicada às Ciências da Saúde

Programa Doutoral do Instituto de Ciências Biomédicas de Abel Salazar e da Faculdade de Farmácia, Universidade do Porto

Orientador
Lucília Helena Ataíde Saraiva
Professora Auxiliar
LAQV/REQUIMTE; Faculdade de Farmácia, Universidade do Porto

Co-orientadores
Pedro Lopes Granja
Professor Afiliado
Instituto de Ciências Biomédicas de Abel Salazar, Universidade do Porto; i3S – Instituto de Investigação e Inovação em Saúde, Universidade do Porto; INEB - Instituto de Engenharia Biomédica

Joana Gama Soares
LAQV/REQUIMTE; Faculdade de Farmácia, Universidade do Porto

The work presented in this thesis was developed at:

Host institution

LAQV/REQUIMTE, Laboratório de Microbiologia, Departamento de Ciências Biológicas, Faculdade de Farmácia, Universidade do Porto, Porto, Portugal

Collaborating institutions

Department of Chemistry, University of Coimbra, Coimbra, Portugal

CEB, Centre of Biological Engineering, University of Minho, Campus Gualtar, Braga, Portugal

UCIBIO/REQUIMTE, Departamento de Química, Faculdade de Ciências e Tecnologia, Universidade Nova de Lisboa, Caparica, Portugal

Departamento de Biomedicina, Unidade de Biologia Experimental, Faculdade de Medicina da Universidade do Porto, Porto, Portugal

Laboratory of Pharmacology and Experimental Therapeutics, Institute for Biomedical Imaging and Life Sciences (IBILI), Faculty of Medicine, & CNC.IBILI Research

Laboratory of Tumor Biology, Department of Experimental Biology, Faculty of Science, Masaryk University, Brno, Czech Republic

CIBIO, Centre for Integrative Biology, Laboratory of Transcriptional Networks, University of Trento, Trento, Italy

FUNDING

This work received financial support from PT national funds (FCT/MCTES, Fundação para a Ciência e Tecnologia and Ministério da Ciência, Tecnologia e Ensino Superior) through project (3599-PPCDT) PTDC/DTP-FTO/1981/2014—POCI-01-0145-FEDER-016581 and grant UIDB/50006/2020. We also thank FCT for the financial support through fellowships SFRH/BD/119144/2016 (H. Ramos), and the Programa Operacional Potencial Humano (POCH), specifically the BiotechHealth Programme (Doctoral Programme on Cellular and Molecular Biotechnology Applied to Health Sciences; PD/00016/2012).

Acknowledgements

First and foremost, I would like to express my deep gratitude to Professor Lucília Saraiva, my supervisor, who firmly believed in my potential and aptitudes to step forward in my research career. Professor Lucília always valued me and my work, and pushed me to improve continually. I need to thank her all the personal and professional valuable advices and lessons. I learned so much with her. Mostly, I thank her for “giving” me MANIO, for which we work so hard, believed so much, and that took us so far.

I would like to thank Professor Pedro Granja, my co-supervisor. He was one of the best professors I ever had, having inspired me with his amazing lectures, his great scientific knowledge and creativity.

To Joana Soares, my co-supervisor, also my profound gratefulness. I learned so many things with her. I want to acknowledge her careful supervision and all the scientific sharing. Joana definitely pushed me to think more critically and to progress my scientific capabilities. Thank you for that. It was a real pleasure to work alongside with the exceptional researcher that she is.

I am thankful to my lab colleagues Joana Loureiro, Ana Sara Gomes, Cláudia Bessa, Sara Gomes, Liliana Raimundo, Nair Nazareth, Juliana Calheiros, and Joana Almeida. It’s been a long journey, but definitely easier because of their companionship. Most of all, I am proud of us being so united, even in the differences and conflicts. Thank you for all the scientific and personal sharing. I learned so much with each one of these girls. Especially, to Joana Loureiro, who, besides being a great work colleague and companion, also became a dear and close friend. I cannot forget to thank Cristina Pinto da Costa, our lab technician, for all the attention, kindness and readiness, every single day.

I also want to thank Professor Alberto Inga for welcoming me so well in his research group, in Trento, Italy. I really appreciated the efforts and the valuable contribution to progress further with MANIO studies.

Also, I would like to thank Dr. Célia Gomes and Dr. Flávio Reis for the assistance and training in the *in vivo* experiments, Dr. Filipe Monteiro for the support with chromatin immunoprecipitation assays, Professor Renata Veselska and Dr. Peter Chlapek for making it possible to test MANIO in patient-derived primary colorectal cells, and also Professor Salette Reis and Dr. Cláudia Nunes for the support with the fluorescence quenching assays. Also, my sincere appreciation to Professor Lucília Domingues and MSc Joana Silva for the invaluable collaboration in the production of recombinant protein and for their perseverance, even when the preliminary results were discouraging.

To my dearest friends Bartolomeo Bosco, Giulia Montuori, and Kalina Badowska for making me feel like home in the period abroad in Italy. Only people with such great and generous hearts would receive me that way. Although missing home, my family and friends, I never felt alone because of them. Thank you very much.

Não poderia deixar de agradecer à Catarina, Diana, Filipe e Sarah. O melhor que a Bioengenharia me trouxe. Quanto mais conheço pessoas, mais os adoro. Mais, nutro por eles dos sentimentos de amizade mais puros que alguma vez senti. Agradeço profundamente por me terem acolhido no seu núcleo já tão coeso e por tão sincera e genuinamente festejarem as minhas vitórias e alegrias. Acompanharam de perto estes últimos anos e sei que estão verdadeiramente felizes por mim.

À Ju, à Carlinha e à Pi, as minhas amigas do coração e de tantos anos. Agradeço-lhes por me conhecerem tão bem, por me entenderem tão bem, por desconstruírem tantas vezes os meus problemas. Por não me julgarem e me valorizarem sempre. Foram pilares nesta longa e inquietante fase, proporcionando-me muitas vezes o equilíbrio que precisava, com simples conversas ou abraços. Obrigada por tudo. Obrigada por serem família.

À Soninha e ao Nelson, pelo maior presente que alguma vez tive, a minha afilhada Mimi, a personificação da doçura, que me alegra e motiva diariamente. São incontáveis os dias em que vejo os seus vídeos de tão ternurentos momentos a palrar ou a cantarolar, só para recuperar o fôlego e simplesmente continuar. Com o seu nascimento, senti que deveria ser mais um entre os seus (já muitos) exemplos de força, empenho e garra. Gostaria que um dia, mais crescida, sinta orgulho destas conquistas da madrinha.

À D. Sãozinha e Sr. Miguel, pelas constantes palavras de motivação e encorajamento, pelo reforço positivo e por me fazerem sentir sempre capaz de tudo. Sinto-os como minha família há já muitos anos e agradeço-lhes profundamente todo o carinho, conforto e amor que me sempre proporcionaram. Sei que estão genuinamente orgulhosos e felizes por mim.

Aos meus pais e aos meus irmãos, que são o meu núcleo. São-me tudo. Devo-lhes tudo. A minha maior recompensa é saber que se orgulham de mim. Um obrigado especial à minha irmã Vera, pelo bom exemplo que sempre foi para mim e pelos sobrinhos maravilhosos que me deu, Duarte e Dinis, que amo como se fossem meus filhos, e que enchem os meus dias de alegria. Foi muitas vezes nas brincadeiras ou passeios com o Dinis que encontrei paz, que relativizei tantos maus resultados, e encontrei alguma força e motivação.

Em último lugar, o meu maior e mais sentido agradecimento ao companheiro da minha vida toda, a pessoa que viveu as minhas batalhas, as minhas dúvidas, bons e maus resultados, a minha ânsia e ansiedade, como se fossem as suas próprias batalhas, as suas dúvidas, os seus bons e maus resultados, as suas ânsias e ansiedades. Estou-lhe tão grata por incansavelmente cuidar de mim todos os dias destes últimos 4 anos, por estar sempre atento a todas as minhas necessidades, mesmo quando me esquecia de mim própria. Agradeço a força e os longos e apertados abraços. Por nunca me largar a mão. Agradeço-lhe profundamente toda a compreensão, carinho e amor, sobretudo quando o meu foco era tudo, exceto ele. Foi tudo e todos, todos os dias, sempre, e este doutoramento é também dele! Obrigada Nunes, do fundo do meu coração.

ABSTRACT

Despite the continuous investment in research and care, the increasing cancer incidence and mortality remains a matter of great concern. Although the high rate of metastasis and patient relapse, traditional anticancer strategies, including surgery, radiation, and/or conventional chemotherapy, still constitute the cornerstone of cancer therapy. In particular, the success of conventional therapy remains overshadowed by the recurrent resistance of malignant cells and severe side effects, given its low selectivity to cancer cells. In this context, the targeted therapy has arisen as an encouraging opportunity in precision medicine, representing a new hope in the therapy of cancer patients. Indeed, these therapies specifically act on well-defined targets or pathways altered in tumor cells, aiming to improve the efficacy of the antitumor therapeutic response, while minimizing adverse effects on normal tissues. The tumor suppressor protein p53, often referred as the "guardian of the genome", is among the most privileged targets in precision cancer therapy due to its key role in virtually all cancer hallmarks. In fact, p53 is found impaired in the majority of human cancers, either by mutation or inhibition by negative regulators, being the pharmacological restoration of p53 activity a highly challenging anticancer strategy.

Based on this premise, the present doctoral thesis was mainly focused on the discovery and development of new p53-targeted anticancer drug candidates. In Chapter 2, it was aimed an in-depth elucidation of the molecular mechanism of (*S*)-tryptophanol-derived oxazoloisoindolinone (SLMP53-1), which was previously reported by our group as a new (re)activator of p53, wild-type (wt) and mutant (mut) R280K. Its promising *in vitro* and *in vivo* p53-dependent antitumor activity led us to further investigate the mechanism underlying the p53 activation, as well as its potential to reactivate other mutp53 forms. The results obtained demonstrated that SLMP53-1 induced wt and mutp53 R280K thermal stabilization, strongly evidencing the occurrence of intermolecular interactions between the compound and p53 DNA-binding domain (DBD). Accordingly, *in silico* studies on protein-ligand interactions unveiled that SLMP53-1 binds at the interface of the p53 DBD homodimer with the DNA minor groove, disclosing a novel mode of p53 reactivation, distinct from those reported so far. Moreover, using yeast and p53-null tumor cells ectopically expressing distinct hotspot mutp53, the ability of SLMP53-1 to reactivate different mutp53 forms, namely R175H, G245D, R248Q/W, R273H, and R282W, was also evidenced. In fact, this work further reinforces the reliability of the yeast model to search for new small molecule reactivators of distinct mutp53 forms.

In Chapter 3, the ability of SLMP53-1 to induce a non-canonical p53 antitumor response, through modulation of glucose metabolism of cancer cells, was also investigated.

Different *in vitro* and *in vivo* evidences are provided showing the ability of SLMP53-1 to counteract the Warburg effect, with a direct inhibition of migration and angiogenesis of colorectal cancer (CRC) cells. Moreover, synergistic effects between SLMP53-1 and dichloroacetic acid (DCA) metabolic modulator were observed.

In Chapter 4, the (3*S*)-6,7-bis(hydroxymethyl)-5-methyl-3-phenyl-1*H*,3*H*-pyrrolo[1,2-c]thiazole (MANIO) was identified as a new p53-targeting anticancer drug. MANIO exhibited a remarkable selectivity to the p53-pathway, activating both wt- and multiple hotspot mutp53 forms. Moreover, the successful production and purification of recombinant DBD of wt and mutp53 R248W, allowed to confirm the direct interaction of MANIO with these proteins. *In vitro* and *in vivo* data, obtained from immortalized and patient-derived cancer cells, as well as xenograft mouse models, strongly supported its great efficacy as anticancer agent against cancers harboring wt- or mutp53, particularly CRC, without apparent undesirable toxic side effects. Further, MANIO displayed promising synergistic effects with different chemotherapeutic drugs commonly used in CRC therapeutic regimens. Importantly, *in vitro* and *in vivo* pharmacokinetic studies have predicted adequate drug-like properties of MANIO.

As a whole, the work developed in this doctoral thesis represents a valuable contribution to the advance of p53 pharmacology. Most importantly, promising clinical candidates, with great potential to integrate the panel of precision cancer therapy, are disclosed. Particularly, the enormous benefits that MANIO may bring to cancer therapy, especially of CRC, either as single agent or in combination therapy, make it worthy of future investments to boost its clinical translation.

Keywords: Anticancer targeted therapy; Cancer; p53; Small molecules

RESUMO

Apesar do contínuo investimento na investigação e cuidados de saúde, o aumento da incidência e mortalidade do cancro continua a ser motivo de grande preocupação. Mesmo com uma elevada ocorrência de metástases e recidivas dos pacientes, as terapias anticancerígenas convencionais, incluindo a cirurgia, radioterapia e/ou quimioterapia, continuam a representar as principais opções de tratamento no combate ao cancro. Em particular, o sucesso da terapia convencional continua a ser limitado pelo desenvolvimento frequente de resistências e efeitos secundários severos, devido à sua reduzida seletividade para as células cancerígenas. Neste contexto, as terapias direcionadas têm surgido como oportunidades promissoras para a medicina de precisão, constituindo uma nova esperança para a terapia dos doentes oncológicos. De facto, estas terapias atuam especificamente em alvos ou vias moleculares que se encontram alterados nas células tumorais, permitindo uma resposta terapêutica antitumoral mais eficaz e com menos efeitos adversos nos tecidos normais. A proteína supressora tumoral p53, genericamente referida como a "guardiã do genoma", constitui um dos principais alvos da terapia personalizada anticancerígena devido ao seu papel-chave em praticamente todos os *hallmarks* do cancro. De facto, a função da p53 encontra-se comprometida na maioria dos cancros humanos, por mutação ou inibição pelos seus moduladores negativos, constituindo o seu restabelecimento farmacológico uma estratégia anticancerígena muito desafiante.

Neste âmbito, a presente tese de doutoramento focou-se essencialmente na descoberta e desenvolvimento de novos candidatos a fármacos anticancerígenos reguladores da p53. No Capítulo 2, pretendeu-se elucidar o mecanismo molecular da oxazoloisoindolinona derivada do triptofanol (SLMP53-1), descrita em trabalhos anteriores do nosso grupo como um novo (re)ativador da p53 nativa e mutante (mut) R280K. A sua promissora atividade antitumoral dependente da p53, *in vitro* e *in vivo*, conduziu-nos à investigação do mecanismo subjacente à ativação da p53, assim como do seu potencial para reativar outras formas mutadas da p53. Os resultados obtidos demonstraram que o composto SLMP53-1 induziu a estabilização térmica da p53 nativa e mutp53 R280K, evidenciando a ocorrência de ligações intermoleculares entre o composto e o domínio de ligação ao DNA (DBD) da p53. Da mesma forma, estudos *in silico* das interações proteína-ligando demonstraram que o SLMP53-1 foi capaz de se ligar na interface formada entre homodímero de DBD da p53 e a região *minor groove* do DNA, revelando um novo modo de reativação da p53, distinto dos atualmente reportados. Além disso, usando células de levedura e células tumorais humanas sem p53, a expressar ectopicamente mutp53 de elevada relevância clínica, demonstrou-se a capacidade do SLMP53-1 de reativar outras mutp53, nomeadamente R175H, G245D, R248Q/W, R273H e R282W. Este estudo reforça também a fiabilidade da levedura como modelo de pesquisa de novas moléculas reativadoras de diferentes formas mutadas da p53.

No Capítulo 3, investigou-se a capacidade do SLMP53-1 de induzir uma resposta antitumoral não canónica da p53, através da modulação do metabolismo da glucose das células cancerígenas. Diferentes evidências, *in vitro* e *in viv*o, demonstraram a capacidade do SLMP53-1 antagonizar o efeito de Warburg, inibindo diretamente a migração e a angiogénese, em células do cancro colo-rectal (CCR). Além disso, foram também observados efeitos sinérgicos entre o SLMP53-1 e o modulador do metabolismo, o ácido dicloroacético (DCA).

No Capítulo 4, a pequena molécula (3*S*)-6,7-bis(hidroximetil)-5-metil-3-fenil-1*H*,3*H*-pirrolo[1,2-c]tiazole (MANIO) foi identificada como um novo agente anticancerígeno ativador da p53. O composto MANIO demonstrou uma marcada seletividade para a via da p53, ativando tanto a p53 nativa como diferente formas mutadas da p53 de elevada prevalência. Adicionalmente, a produção e purificação dos DBD da p53 nativa e mutp53 R248W permitiu confirmar a interação direta entre o MANIO e estas proteínas. Resultados obtidos *in vivo* e *in vitro,* utilizando células tumorais imortalizadas e derivadas de pacientes oncológicos e xenografos de tumores humanos em ratinhos, corroboraram a eficácia do MANIO como agente anticancerígeno em cancros que expressam as formas nativa e mutada da p53, particularmente o CCR, sem aparentes efeitos secundários indesejados. O MANIO também apresentou efeitos sinérgicos com diferentes quimioterápicos usualmente utilizados nos regimes terapêuticos do CCR. Por último, os estudos de farmacocinética, *in vitro* e *in vivo*, permitiram a previsão de propriedades *drug-like* adequadas do MANIO.

Em conclusão, os estudos desenvolvidos no âmbito da presente tese de doutoramento constituem uma contribuição relevante no avanço da farmacologia da p53. Fundamentalmente, são revelados promissores candidatos clínicos, os quais poderão representar novas opções na terapia personalizada do cancro. Em particular, os enormes benefícios que o MANIO poderá proporcionar à terapia anticancerígena, especialmente do CCR (quer isolado ou em combinação), justificam futuros investimentos nesta molécula potenciadores da sua translação clínica.

Palavras-chave: Cancro; p53; Pequenas moléculas; Terapia anticancerígena direcionada

ABBREVIATIONS

5-FU – 5-Fluorouracil
CETSA – Cellular Thermal Shift Assay
CFU – Colony forming unit
CHIP – Carboxy terminus of HSP70-interacting protein
ChIP – Chromatin immunoprecipitation
CHK – Checkpoint kinase
CHX – Cycloheximide
CI – Combination index
CIN – Chromosomal instability
CMS – Consensus molecular subtype
COX4 – Cytochrome *c* oxidase subunit 4
CRC – Colorectal cancer
CRD – C-terminal regulatory domain
Cyt *c* – Cytochrome *c*
DBD – DNA-binding domain
DCA – Dichloroacetic acid
DMSO – Dimethyl sulfoxide
DNE – Dominant negative effect
DOXO – Doxorubicin
DRI – Dose reduction index
DSB – DNA double-strand breaks
E-CAD – E-cadherin
ECM – Extracellular matrix
EGFR – Epidermal growth factor
EMT – Epithelial-mesenchymal transition
ETOP – Etoposide
GLUT – Glucose transporter
GOF – Gain-of-function
HIF – Hypoxia-inducible factor
HK2 – Hexokinase 2
HSP – Heat shock protein
IC_{50} – Half maximal inhibitory concentration
IHC – Immunohistochemistry
Kd – Dissociation constant
LFS – Li-Fraumeni syndrome
LOH – Loss of heterozygosity
MD – Molecular dynamics
MCT – Monocarboxylate transporter
MDM – Murine Double Minute
MMP – Matrix metalloproteases
MOMP – Mitochondrial outer membrane permeabilization
MSI – Microsatellite instability
Mut – Mutant
N-CAD – N-cadherin

OD – Oligomerization domain
OXPHOS – Oxidative phosphorylation
PARP – Poly(ADP ribose) polymerase
PDK – Pyruvate dehydrogenase kinase
PFKFB3 – Phosphofructokinase-2 isoform 6-phosphofructo-2-kinase/fructose-2,6-biphosphatase 3
PI – Propidium iodide
PK - Pharmacokinetic
PRD – Proline-rich domain
PTM – Post-translational modifications
RE – Response elements
RNA-seq – RNA sequencing
ROS – Reactive oxygen species
SCO2 – Synthesis of cytochrome *c* oxidase 2
siRNA – Small interfering RNA
SRB – Sulforhodamine B
TAD – Transactivation domain
TCA – Tricarboxylic acid
TGF-β —Transforming growth factor activation β
VEGF – Vascular endothelial growth factor
Wt – Wild-type

TABLE OF CONTENTS

ACKNOWLEDGEMENTS **VII**

ABSTRACT **XI**

RESUMO **XIII**

ABBREVIATIONS **XV**

CHAPTER 1 LITERATURE OVERVIEW **25**

- **1.1. Cancer epidemiology and biology** **27**
  - 1.1.1. Colorectal cancer pathogenesis and therapy 29
- **1.2. The p53 tumor suppressor** **33**
  - 1.2.1. p53 structure and DNA binding 34
  - 1.2.2. p53 regulation and biological functions 36
    - 1.2.2.1. Classical p53 functions 39
    - 1.2.2.2. Emerging p53 functions 41
- **1.3. Inactivation of p53 in human cancers** **44**
  - 1.3.1. Impaired wtp53 pathway 46
  - 1.3.2. *TP53* mutations 46
- **1.4. Anticancer therapeutic approaches targeting p53** **51**
  - 1.4.1. Targeting wtp53-expressing tumors 53
  - 1.4.2. Targeting mutp53-expressing tumors 55
    - *1.4.2.1.* Restoration of wt-like function to mutp53 60
    - *1.4.2.2.* Depletion of mutp53 64
    - *1.4.2.3*. Disruption of protein-protein interactions 64
    - *1.4.2.4*. Inhibitors of mutp53 aggregation 65
- **1.5. Targeting p53 in cancer chemoprevention** **65**
- **1.6. Aims** **68**

CHAPTER 2 SLMP53-1 INTERACTS WITH WILD-TYPE AND MUTANT P53 DNA-BINDING DOMAIN AND REACTIVATES MULTIPLE HOTSPOT MUTATIONS **69**

- **2.1. Background** **71**
- **2.2. Materials and methods** **71**
  - 2.2.1. Compounds 71
  - 2.2.2. Construction of yeast and mammalian expression vectors 71
    - 2.2.2.1. Yeast expression vectors 71
    - 2.2.2.2. Mammalian expression vectors 72
  - 2.2.3. Modeling 72
    - 2.2.3.1. Molecular docking 72
    - 2.2.3.2. Molecular dynamics (MD) simulations 73
  - 2.2.4. Yeast assay 73

2.2.5. Human tumor cell lines and growth conditions 73
2.2.6. Cellular thermal shift assay (CETSA) 74
2.2.7. Transient transfection assay of mutp53 in human H1299 tumor cells 74
2.2.8. Sulforhodamine B (SRB) assay 74
2.2.9. Western blot analysis 74
2.2.10. Statistical analysis 75
2.3. Results 75
2.3.1. SLMP53-1 binds to wt and mutp53 R280K 75
2.3.2. SLMP53-1 potentially binds to a hydrophobic pocket formed at the interface of the p53 homodimer with the DNA minor groove 76
2.3.3. SLMP53-1 reactivates distinct hotspot mutp53 78
2.4. Discussion 80
CHAPTER 3 SLMP53-1 INHIBITS TUMOR CELL GROWTH THROUGH REGULATION OF GLUCOSE METABOLISM AND ANGIOGENESIS IN A P53-DEPENDENT MANNER 83
3.1. Background 85
3.2. Materials and Methods 85
3.2.1. Compounds and reagents 85
3.2.2. Human cell lines and growth conditions 85
3.2.3. Immunohistochemistry (IHC) 85
3.2.4. Western Blot 86
3.2.5. Measurement of extracellular lactate 86
3.2.6. Angiogenesis assay 86
3.2.7. Generation of colon cancer spheroids 87
3.2.9. Cell cycle analysis 87
3.2.10. Statistics 88
3.3. Results 88
3.3.1. SLMP53-1 regulates the Warburg effect and angiogenesis in cancer cells, with interference in ECM remodeling and EMT events 88
3.3.2. SLMP53-1 regulates the Warburg effect and angiogenesis, interfering with ECM remodeling and EMT events in a p53-dependent manner, in tumor tissues of xenograft mouse models 90
3.3.3. SLMP53-1 synergizes with dichloroacetic acid (DCA), enhancing its antitumor efficacy in cancer cells 92
3.4. Discussion 93
CHAPTER 4 MANIO: MECHANISM OF WILD-TYPE AND MUTANT P53 ACTIVATION AND THERAPEUTIC POTENTIAL IN COLORECTAL CANCER 97
4.1. Background 99
4.2. Materials and Methods 99
4.2.1. Compounds and reagents 99

4.2.2. Human cell lines and culture conditions 99
4.2.3. Patient-derived CRC cells 100
4.2.4. Cell viability and proliferation assays 100
4.2.5. Transient transfection assay of mutp53 in human H1299 tumor cells 101
4.2.6. Cell cycle and apoptosis analysis 101
4.2.7. Western blot analysis 101
4.2.8. Cycloheximide (CHX) assay 101
4.2.9. RNA extraction and RT-qPCR 102
4.2.10. Chromatin immunoprecipitation (ChIP) assay 102
4.2.11. RNA sequencing (RNA-seq) 103
4.2.12. p53 small interfering RNA (siRNA) 103
4.2.13. CETSA 104
4.2.14. Comet assay 104
4.2.15. Micronucleus test 104
4.2.16. Recombinant human wt- and mutp53 R248W protein DBD production 105
4.2.17. Protein-ligand interaction by fluorescence quenching 105
4.2.18. *In vivo* antitumor and toxicity assays 106
4.2.19. IHC 106
4.2.20. Combination therapy assays 106
4.2.21. Statistical analysis 107

4.3. Results 107

4.3.1. MANIO displays p53-dependent growth inhibitory effect in human cancer cells, inducing cell cycle arrest and apoptosis, but not genotoxicity 107
4.3.2. Activation of the p53 response pathway by MANIO in HCT116 cells is associated with p53 stabilization, and enhancement of p53 DNA-binding and transcriptional activity 109
4.3.3. MANIO reactivates distinct contact and structural mutp53, restoring wt-like properties to mutp53 R248W in CRC cells 114
4.3.4. MANIO leads to wt and mutp53 R248W thermal stabilization through direct binding to protein DBD 116
4.3.5. MANIO has *in vivo* p53-dependent antitumor activity in CRC xenograft mouse models, with no apparent toxic side effects 118
4.3.6. MANIO inhibits the growth of patient-derived CRC cells through regulation of p53 transcriptional targets 121
4.3.7. MANIO has synergistic effects with conventional chemotherapeutics, in immortalized and patient-derived CRC cells 122

4.4. Discussion 124

CHAPTER 5 GENERAL DISCUSSION 129

CHAPTER 6 REFERENCES 139

ANNEX I HUMAN CELL LINES, ANTIBODIES AND PRIMERS 159

ANNEX II SUPPORTING INFORMATION OF CHAPTER 2 165

ANNEX Ⅲ SUPPORTING INFORMATION OF CHAPTER 3 **171**

ANNEX Ⅳ SUPPORTING INFORMATION OF CHAPTER 4 **177**

ANNEX Ⅴ PHARMACOKINETIC STUDIES OF MANIO **183**

LIST OF FIGURES

Figure 1. Hallmarks of cancer. 28

Figure 2. Classical pathway of CRC carcinogenesis and transcriptomic subtypes. 30

Figure 3. p53 structure and DNA binding. 34

Figure 4. p53 signaling pathway. 37

Figure 5. The role of p53 in glucose metabolism. 44

Figure 6. Modes of p53 inactivation in human cancers. 45

Figure 7. Mutp53 GOF activities impact multiple hallmarks of cancer cell biology, affecting the chromatin structure, transcriptional regulation, and microRNA biogenesis, shaping the proteome, and rewiring tumor cell metabolic pathways. 49

Figure 8. Yeast-based assay for the screening of p53-targeting p53 agents. 53

Figure 9. SLMP53-1 thermally stabilizes wt and mutp53 R280K. 76

Figure 10. SLMP53-1 potentially binds at the interface of the p53 homodimer with the DNA minor groove. 77

Figure 11. SLMP53-1 reactivates distinct hotspot mutp53. 79

Figure 12. SLMP53-1 modulates the Warburg effect and angiogenesis in cancer cells, with impact on endothelial cell tube formation, ECM remodeling and EMT events *in vitro*. 89

Figure 13. SLMP53-1 modulates the Warburg effect and angiogenesis, interfering with ECM remodeling and EMT events, through a p53-dependent manner, in tumor tissues of xenograft mouse models. 91

Figure 14. SLMP53-1 sensitizes cancer cells to DCA. 92

Figure 15. Growth inhibitory effect of MANIO in human cancer cells is dependent on p53 and is associated with induction of cell cycle arrest and apoptosis, but not genotoxicity. 108

Figure 16. Gene expression profile changes in human cancer cells by MANIO reveal a p53-activating signature. 111

Figure 17. MANIO enhances p53 stabilization and transcriptional activity, regulating the expression of several p53 target genes by increasing its DNA-binding ability, in HCT116 p53$^{+/+}$ cells. 113

Figure 18. MANIO reactivates distinct contact and structural mutp53, inhibiting the growth of mutp53 R248W-expressing SW837 cells through restoration of wt-like p53 transcriptional activity and DNA-binding ability. 115

Figure 19. MANIO binds directly to the DBD of wt and mutp53 R248W, leading to their thermal stabilization. 117

Figure 20. MANIO has *in vivo* p53-dependent antitumor activity by inhibiting proliferation and enhancing apoptotic cell death. 120

Figure 21. MANIO inhibits the growth of patient-derived CRC cells through regulation of p53 transcriptional targets. 122

Figure 22. Schematic representation of the major outcomes achieved in this doctoral thesis. 137

Figure S1. Effect of wtp53 and mutp53 expression on yeast growth. 167

Figure S2. SLMP53-1 does not interfere with wtp53 and mutp53 half-life. 167
Figure S3. SLMP53-1 binds to human recombinant mutp53 R280K DBD. 168
Figure S4. Structural mutp53 R282W DBD exhibits the same conformational structure as wtp53, with exception for L1 region. 169
Figure S5. Anti-angiogenic effect of SLMP53-1, in HMVEC-D cells, after 12 h treatment, using the endothelial tube formation assay. 173
Figure S6. Expression levels of HK2 and GLUT1, after 24 h treatment with SLMP53-1, in HCT116 p53$^{-/-}$ cancer cells. 175
Figure S7. Representative images of the colony forming assays in HCT116 (p53$^{+/+}$ and p53$^{-/-}$) and SW837, after 14 or 11 days of MANIO treatment, respectively. 179
Figure S8. MANIO is non-genotoxic in tumor cells. 179
Figure S9. Pathway analysis and features of the repressed gene signature elicited by MANIO treatment in HCT116 cells. 180
Figure S10. Western blot analysis of mutp53 protein levels in SW837 cells transfected with sip53 or CTRL. 181
Figure S11. MANIO sensitizes SW837 and patient-derived primary CRC cells to conventional chemotherapeutic agents. 181
Figure S12. MANIO does not inhibit the p53–MDM2 interaction in HCT116 p53$^{+/+}$ cells. 182
Figure S13. The mean exposure levels of MANIO in plasma samples versus time (semi-log plot). 190

List of tables

Table 1. Mutp53-targeting agents. Compounds are organized according to their mechanism of mutp53 targeting. 56
Table 2. Toxicological studies of MANIO in Swiss nude mice. 120
Table 3. Characterization of patient-derived CRC cells and growth inhibitory effect of MANIO. 121
Table 4. Effect of MANIO in combination with conventional chemotherapeutic agents, in SW837 and patient-derived CCZ3 cells. 123

Table S1. Human cell lines description. 161
Table S2. List of antibodies used in immunohistochemistry (IHC) or western blot (WB) experiments. 161
Table S3. List of primers used in RT-qPCR experiments. 163
Table S4. List of primers used in ChIP experiments. 164
Table S5. Distances of SLMP53-1 and its enantiomer to wtp53 and mutp53 R280K with DNA models by MD simulations. 167
Table S6. SLMP53-1 physicochemical properties. 174

Table S7. SwissADME shows that SLMP53-1 do not violate any of the drug-likeness criteria. 174
Table S8. Medicinal chemistry evaluation of SLMP53-1. 174
Table S9. Pharmacokinetic evaluation of the SLMP53-1. 174
Table S10. Water solubility evaluation of SLMP53-1 (ESOL and Ali *et al*. models). 174
Table S11. Water solubility evaluation of SLMP53-1 (SILICOS-IT model). 175
Table S12. Lipophilicity evaluation of SLMP53-1. 175
Table S13. Growth inhibitory effect of MANIO and PRIMA-1^{MET} in human tumor cell lines. 182
Table S14. Description of *in vitro* PK assays. 185
Table S15. Animal Dosing Design - *In vivo* PK, non-fasted animals. 188
Table S16. Solubility of MANIO in different aqueous samples. 189
Table S17. Human intestinal permeability of MANIO, evaluated in Caco-2 cell monolayer. 189
Table S18. *In vitro* hepatic metabolism of MANIO. 189
Table S19. Protein binding ability of MANIO. 190
Table S20. The PK parameters of MANIO in mouse plasma samples. 190

CHAPTER 1

LITERATURE OVERVIEW

The Literature Overview contains parts of the following publications:

Liliana Raimundo[#], **Helena Ramos[#]**, Joana B. Loureiro, Juliana Calheiros, Lucília Saraiva, 2020. *BRCA1/p53: two strengths in cancer chemoprevention*. Biochimica Biophysica Acta Reviews on Cancer 1873 (1), 188339. DOI: 10.1016/j.bbcan.2020.188339.

Ana Sara Gomes, **Helena Ramos**, Joana Soares, Lucília Saraiva, 2018. *p53 and glucose metabolism: an orchestra to be directed in cancer therapy*. Pharmacological Research, 131:75-86. DOI: 10.1016/j.phrs.2018.03.015.

Sara Gomes, Mariana Leão, Liliana Raimundo, **Helena Ramos**, Joana Soares, and Lucília Saraiva, 2016. *p53 family interactions and yeast: together in anticancer therapy*. Drug Discovery Today 21(4): 616-624. DOI: 10.1016/j.drudis.2016.02.007.

[#]Authors equally contributed to this work

1.1. Cancer epidemiology and biology

Cancer is nowadays the second leading cause of death worldwide, accounting for an incidence of 18.1 million new cases and 9.6 million deaths, in 2018 [1, 2]. Epidemiological evidences suggest that incidence and mortality are increasing and, in the incoming years, it is predicted that cancer will rank as the leading cause of death in several countries, surpassing mortality rates of coronary heart disease and stroke [1]. The causes for this trend are complex, but mostly reflect the rapid growth and aging of the population [3]. In general population, lung cancer has the highest incidence rate (11.6% of the total cases) and constitutes the leading cause of cancer death (18.4% of the total cancer deaths). It is followed by female breast (11.6%), colorectal (10.2%), and prostate (7.1%) cancers for incidence, and by colorectal (9.2%), stomach (8.2%), and liver (8.2%) cancers for mortality [1]. In Portugal, cancer accounts for 25% of the overall total mortality, and around 58,000 new cancer cases were diagnosed in 2018. The most frequent types of cancers follow the worldwide trends, including colorectal, female breast, prostate, and lung [2]. As in other countries, cancer also places a significant burden to the Portuguese national health care and the communities they assist. Despite the advances and investments on cancer prevention, diagnosis and treatment, the negative impact on productivity and suffering by cancer patients, and the rising costs of treatment make cancer a priority at the socio-economic level [4].

Cancer, malignant tumors or neoplasms are different generic terms to designate a large group of diseases. In fact, tumor development relays on the continuous and unregulated proliferation of cells of any part of the organisms, giving rise to more than a hundred distinct types of cancer, which can vary considerably in their behavior and therapeutic outcomes. Malignant tumors differ from benign ones in having the ability to invade surrounding normal tissues and to spread throughout the body via the circulatory or lymphatic systems, a process called metastization [5].

In 2001, Hanahan and Weinberg discussed for the first time the major events that govern the transformation of normal human cells into malignant cancers [6]. The authors referred that the acquired capabilities are transversal to most cancer types, as they share similar molecular, biochemical, and cellular traits [5]. As such, they attempted to organize the dense complexity of cancer biology into major alterations in the cell physiology, called hallmarks, that collectively dictate the malignant growth, namely self-sufficiency in growth signals, limitless replicative potential, insensitivity to growth inhibitory signals, evasion of apoptosis, sustained angiogenesis, and tissue invasion and metastasis [6] (Figure 1). One decade later, these authors proposed two additional attributes of cancer cells that are functionally important for the development of cancer. The first one refers to the reprogramming of energy metabolism of cancer cells, in order to fuel continuous cell growth and proliferation. The second involves the active evasion by cancer cells from the immune response [7] (Figure 1).

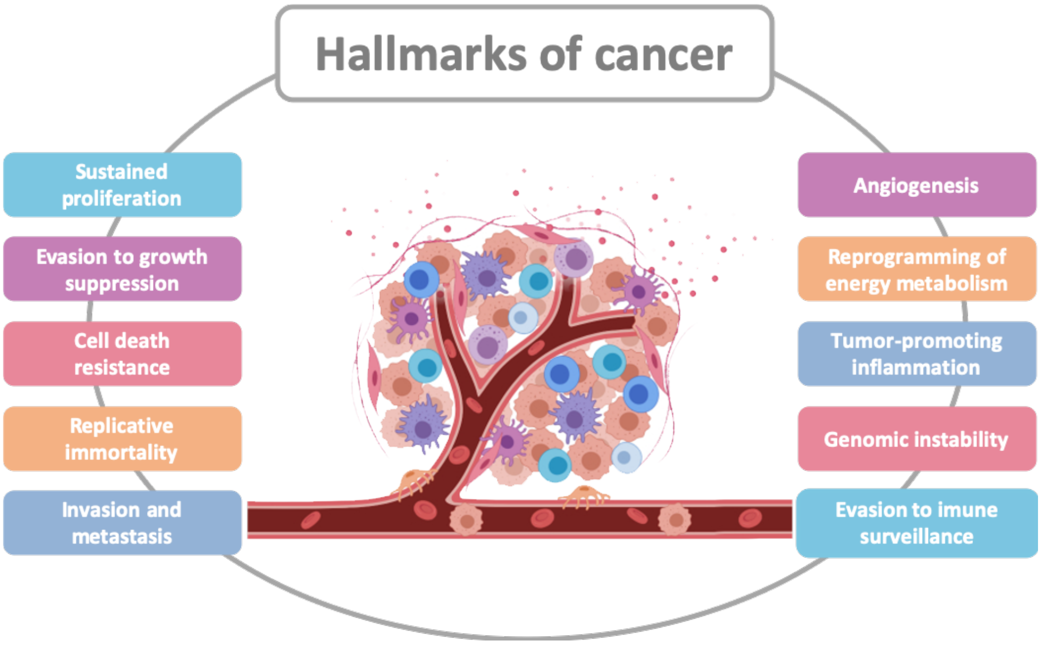
Hallmarks of cancer
Sustained proliferation
Evasion to growth suppression
Cell death resistance
Replicative immortality
Invasion and metastasis
Angiogenesis
Reprogramming of energy metabolism
Tumor-promoting inflammation
Genomic instability
Evasion to imune surveillance

Figure 1. Hallmarks of cancer. Illustration encompassing the ten acquired traits of tumor cells to proliferate, survive, and disseminate.

The same authors also unveiled that the acquired ability of cancer cells to survive, proliferate, and disseminate is mainly possible due to two enabling characteristics: tumor-promoting inflammation and genomic instability [7]. In fact, inflammation can contribute to the acquisition of core hallmark features by providing the tumor microenvironment with growth and survival factors (that sustain proliferation and viability), pro-angiogenic factors, and enzymes that modify the extracellular matrix (ECM), facilitating angiogenesis, invasion, and metastasis [7]. On the other hand, typical genomic instability of cancer cells is achieved by increased sensitivity to mutagenic agents and, consequently, increased mutability. In addition, the accumulation of mutations is enhanced by compromised genomic integrity surveillance and maintenance mechanisms [7]. In fact, different genes controlling the DNA-maintenance machinery were found to be defective in distinct cancers, including tumor suppressor genes. They are involved not only in DNA damage sensing and repair, but also in the induction of apoptosis, inhibition of cell cycle progression, and suppression of metastasis [8]. Among them, the p53 protein has a central role, being frequently called as the “guardian of the genome”.

1.1.1. Colorectal cancer pathogenesis and therapy

Colorectal cancer (CRC) accounts for approximately 10% of all annually diagnosed cancers, representing nowadays one of the deadliest cancer worldwide [1]. Predictions point toward an increase of 60% of the CRC global burden, with an estimated incidence of more than 2.2 million new cases and 1.1 million deaths by 2030 [9]. The distribution of CRC burden differs globally, with the highest rates of mortality and incidence observed in the most developed countries. Also, a rapid increase in these rates has been observed in the developing countries, particularly in Eastern Europe, Asia and South America [9, 10]. Nevertheless, stabilizing and declining tendencies begin to be observed in highly developed countries such as USA, Australia, New Zealand and some Western European countries [9, 10]. This can be partially attributed to the implementation of efficient prevention programs, in particular the detection by colonoscopy of polyps and primary adenomas before their development into CRC [11]. In fact, CRC has a long latency period, allowing enough time for preventive procedures. Changes in factors like diet, tobacco consumption, gastrointestinal microbiome, use of antibiotics, nonsteroidal anti-inflammatory drugs and statins, hormone-replacement therapy have also shown a positive impact in CRC epidemiology [12]. Moreover, the availability of more efficient therapies for early and advanced disease stages has successfully improved the overall survival and disease-free survival of CRC patients [12].

The CRC carcinogenesis is a multi-step and slow process. It involves histological alterations and the accumulation of several genetic and epigenetic events that inactivate tumor suppressor genes and activate oncogenes [13]. The molecular characterization of CRC is already well-established, with the identification of different genes and pathways implicated in tumor initiation and development [13, 14]. In common solid tumors, as those originated in colon and rectum, an average of 66 genes present subtle somatic mutations [15]. However, key "driver" alterations were described to be required for the development and malignant progression of CRC, namely mutations in the tumor suppressor genes adenomatous polyposis coli (*APC*), *TP53* and SMAD family member 4 (*SMAD4*), and in the oncogenes *KRAS* and PI3K catalytic subunit-α (*PIK3CA*) [13-15]. In fact, in human normal intestinal organoids, the simultaneous introduction of mutations in these major driver genes for CRC induced epithelial cell transformation and the development of tumors with invasive features after implantation in mice [16, 17]. There are two major distinct precursor lesion pathways. The serrated neoplasia pathway represents 10-20% of CRC [10]. It is associated with *RAS* and *RAF* mutations and epigenetic instability, with frequent hypermethylation of different gene promoter regions in sessile serrated adenoma, which promotes dysplasia, and ultimately leading to carcinoma development [11]. In 70-90% of cases, referring to the classical model of CRC carcinogenesis (Figure 2), CRC arises from adenomatous polyps, which progresses to advanced adenoma with high-grade dysplasia, invasive adenocarcinoma, and metastasis to distant organs [13].

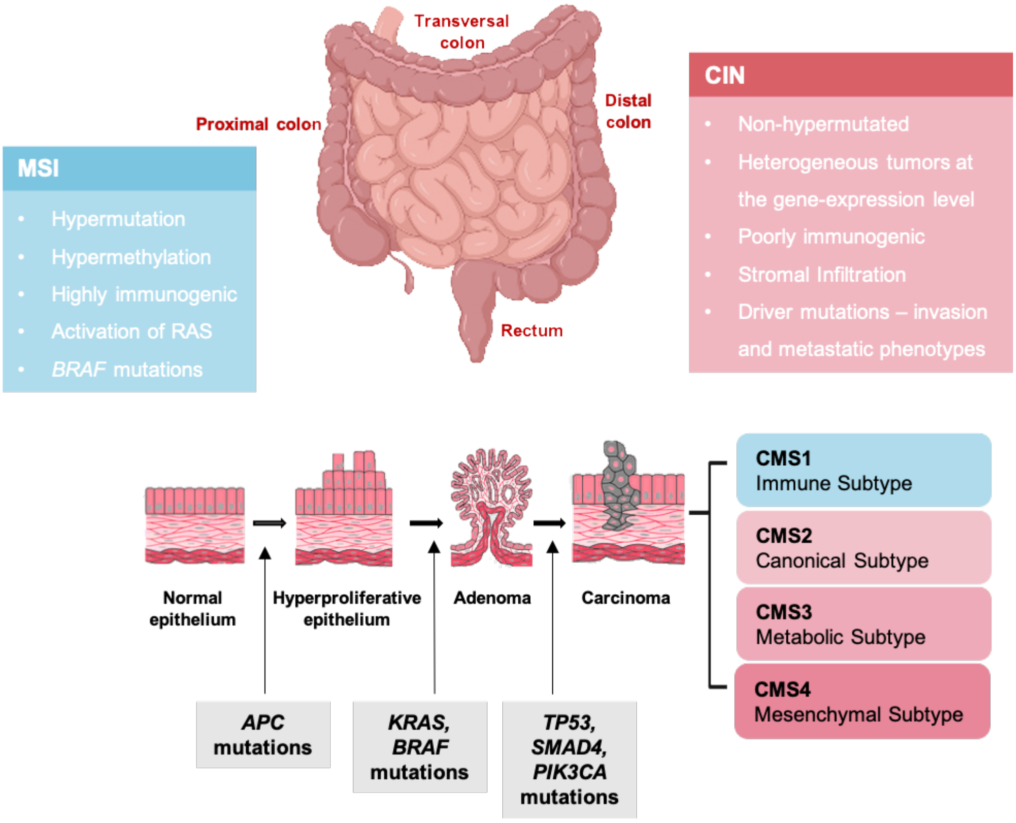
Transversal colon
Proximal colon
Distal colon
Rectum
MSI
Hypermutation
Hypermethylation
Highly immunogenic
Activation of RAS
BRAF mutations
CIN
Non-hypermutated
Heterogeneous tumors at the gene-expression level
Poorly immunogenic
Stromal Infiltration
Driver mutations – invasion and metastatic phenotypes
Normal epithelium
Hyperproliferative epithelium
Adenoma
Carcinoma
APC mutations
KRAS, BRAF mutations
TP53, SMAD4, PIK3CA mutations
CMS1 Immune Subtype
CMS2 Canonical Subtype
CMS3 Metabolic Subtype
CMS4 Mesenchymal Subtype

Figure 2. Classical pathway of CRC carcinogenesis and transcriptomic subtypes. The stepwise genetic and pathologic alterations that transform normal colonic epithelium into invasive carcinoma are represented. Tumors with microsatellite instability (MSI) are generally diagnosed in the proximal colon and are mostly consensus molecular subtype (CMS)1, exhibiting patterns associated with hypermutation, hypermethylation, activation of *RAS*, *BRAF*^{V600F} mutations, and prominent immune infiltration of the tumor microenvironment. Tumors with chromosomal instability (CIN) are mostly CMS2-4 and are commonly diagnosed in the distal colon and rectum, being poorly immunogenic, with marked stromal infiltration.

CRC has pronounced tumor heterogeneity, since almost all of the tumors arise from genomic instability in the form of either chromosomal (CIN) or microsatellite (MSI) instability [18, 19]. Indeed, the concomitant occurrence of CIN and driver mutations was shown to be required for tumors invasion and metastasis [16]. Accordingly, 85% of invasive CRC are characterized by aneuploidy and loss of heterozygosity. CIN results from defects in chromosomal segregation, telomere instability, and abrogated DNA damage responses [20]. On the other hand, 15% of early-stage CRC present defective DNA mismatch repair systems as the main genomic feature, leading to hypermethylation of key genes implicated in tumor development and MSI [19]. Tumors with CIN or MSI differ in the sequence and pattern of total genetic and epigenetic load, as MSI tumors are generally prone to high mutation rates (hypermutated), and CIN tumors are non-hypermutated [21]. In the case of tumors with MSI, the hypermutation feature is expected to increase the probability not only of cancer-promoting mutations, but also of mutations that limit cell viability. As such, robust MSI might limit tumor progression, leading to a more favorable prognosis than that observed for tumors with CIN [11]. The most frequent mutation observed in non-hypermutated CRC is in *APC* gene (>80%), followed by mutations in *TP53* (55–60%) [22]. *KRAS* mutations are found across the different disease subsets, and *BRAF*^{V600F} mutations are mostly found in hypermutated MSI tumors [21].

CRC has recently been categorized into four consensus molecular subtypes (CMS), with distinctive features related with gene expression pattern, cellular phenotype, and tumor behavior: microsatellite instability immune (CMS1), canonical (CMS2), metabolic (CMS3), and mesenchymal (CMS4) [23] (Figure 2). The CMS1 encompasses the majority of MSI CRC (14% or early-stage tumors) and is linked to tumors of the proximal colon. It is characterized by hypermutation, hypermethylation, activation of *RAS* and *BRAF*^{V600F} mutations, and prominent immune infiltration of the tumor microenvironment (Figure 2). CMS1 tumors are associated with the serrated pathway model of the colorectal carcinogenesis [11].

On the other hand, CIN tumors, mostly CMS2-4, are more heterogeneous at the gene-expression level, and develop through the classical model [6] (Figure 2). CMS2 (37% of early-stage tumors) and CMS4 (13% of early-stage tumors) are mainly diagnosed in the distal colon and rectum, and are poorly immunogenic, with marked stromal infiltration. CMS2 and CMS4 present the same somatic copy number alteration patterns and mutation spectrum [21]. However, CMS2 tumors exhibit upregulation of WNT and MYC downstream targets and higher expression of several oncogenes, namely *EGFR*, *ERB2, IGF2, IRS2,* and *HNF4A* [23]. Conversely, CMS4 tumors are characterized by activation of pathways related to epithelial-mesenchymal transition (EMT) (promoted by transforming growth factor activation β (TGF-β) activation), stemness, ECM remodeling, and angiogenesis. As such, higher risk of metastasis and poor prognosis are observed for patients diagnosed with CMS4 CRC [23]. CMS3 encompasses a subset of colorectal tumors enriched for *RAS* mutations, with a strong metabolic adaptation and intermediate levels of mutation, methylation and copy number variations [23].

In a histopathological context, adenocarcinomas of each CMS display distinct characteristics, including solid and/or trabecular or mucinous features in CMS1, complex tubular structure in CMS2, papillary morphology in CMS3, and desmoplastic reaction (growth of dense fibrous connective tissue around the tumor) with high stroma in CMS4 [21].

CRC treatments comprise surgery, downstaging preoperative radiotherapy and systemic therapy, local ablative therapies for metastases, palliative chemotherapy, targeted therapy, and immunotherapy [10]. Regarding chemotherapy, as in other cancer types, CRC treatments encompass the use of conventional chemotherapeutic cytotoxic drugs, which target rapidly proliferating cells, enhancing its sensitivity to DNA damage and triggering cell death. First-line regimens for CRC and metastatic CRC treatment comprise the use of 5-fluorouracil (5-FU; an antimetabolite that blocks the pyrimidine thymidine synthesis required for DNA replication), capecitabine (prodrug converted to 5-FU in the tumor), oxaliplatin (a platinum-based alkylating agent), and irinotecan (a topoisomerase 1 inhibitor, with inhibition of DNA repair and replication) [24]. More recently, a new cytotoxic drug, Lonsurf, was approved by the Food and Drug Administration (FDA) and the European Medicines Agency (EMA) for the treatment of refractory metastatic CRC patients. Lonsurf combines the trifluridine (thymidine-based nucleoside analogue) with the tipiracil (a potent inhibitor of thymidine phosphorylase), interfering with DNA synthesis and inhibiting cancer cell growth [25]. A phase III randomized clinical trial showed that Lonsurf treatment resulted in a 1.8-month improvement in median overall survival in patients with refractory metastatic CRC, when compared to the placebo group [26]. Also, the humanized antibody pembrolizumab, targeting programmed cell death 1 (PD-1) receptor of lymphocytes, was recently approved for advanced CRC with mismatch repair deficiency or MSI [27].

Nevertheless, a significant proportion of CRC patients does not respond to those regimens, with variable levels of chemoresistance, and/or experiencing numerous severe side effects [28]. As such, the inclusion of targeted agents in the therapeutic regimens, in combination with conventional drugs, greatly improved the median overall survival and reduced undesirable side effects [29]. Targeted agents (monoclonal antibodies and small molecules) are cornerstones of modern precision (or personalized) medicine, which takes into account the individual genetics and disease history, before a treatment plan is established [28]. Hence, targeted therapies specifically act on altered genes or proteins, that contribute to cancer development, while limiting the damage in healthy cells. In the case of CRC, targeted therapies comprise epidermal growth factor (EGFR) inhibitors and anti-angiogenesis therapy [24]. Overexpression of EGFR is a common event in various cancer types, including CRC [30]. Studies showed that the inhibition of EGFR by monoclonal antibodies cetuximab or panitumumab, combined with 5-FU, leucovorin plus oxaliplatin (FOLFOX) or with 5-FU, leucovorin plus irinotecan (FOLFIRI), resulted in improved outcomes in metastatic CRC patients [31, 32]. On the other hand, the overexpression of vascular endothelial growth factor (VEGF; an important signaling protein involved in vasculogenesis and angiogenesis) is related with tumor progression and dissemination, as well as with lower survival rates [33, 34]. Currently, three different drugs targeting VEGF were approved for CRC patients, namely ramucirumab (prevents VEGFR-2-dependent signaling), ziv-aflibercept (binds and inhibits placental growth factor (PIGF), VEGF-A, and VEGF-B) and bevacizumab (blocks VEGF-A by causing ligand sequestering) [35]. The combination of FOLFIRI with ziv-aflibercept [36], bevacizumab [37], or ramucirumab [38] treatments showed to improve to median overall survival, when compared to FOLFIRI combined with placebo, in patients with metastatic CRC. However, similar adverse side effects were observed.

Currently, several clinical trials testing new targeted therapies for CRC patients are underway, which explore specific CRC biomarkers, namely *BRAF*, *KRAS*, *NRAS*, *PIK3CA*, and MSI tumor status [24]. The focus of these current studies is therefore the development of more adjusted treatments for each CRC patient, based on the use of specific CRC biomarkers. The major goal is to maximize the therapeutic outcomes and the quality of life of CRC patients.

1.2. The p53 tumor suppressor

The discovery of p53, a ~53 kDa protein, dates back 1979 [39]. The gene encoding p53 (*TP53;* located on chromosome 17p13.1) was initially believed to be an oncogene, but ten years later it was correctly characterized as a tumor suppressor [40]. Since its discovery, p53 has been intensively investigated, including fundamental aspects of its structure, molecular biology, and pharmacology [41]. The p53 protein is a transcription factor activated in response to oncogenic or other cellular stresses, with the modulation of several cellular processes related to basically all cancer hallmarks [42]. In fact, genome-wide data analysis has identified from hundred up to thousands of potential target genes to which p53 can directly bind [43]. The transcriptional activity of p53 is a reflection of its structure [44], being tightly controlled by a complex feedback-regulated network involving major endogenous negative regulators, by different post-translational modifications (PTM), and by interactions with a variety of signaling proteins [44-46].

1.2.1. p53 structure and DNA binding

Active p53 is a homotetramer of four identical chains of 393 amino acid residues. Each monomer presents a modular structure divided into different domains: an acidic *N*-terminal region, comprising the transactivation domain (TAD; residues 1-61) and the proline-rich domain (PRD; residues 64-92); a central core sequence-specific DNA-binding domain (DBD; residues 93-292); a *C*-terminal region, encompassing an oligomerization domain (OD; residues 324-355) and a *C*-terminal regulatory domain (CRD; residues 356-393) [44] (Figure 3A).

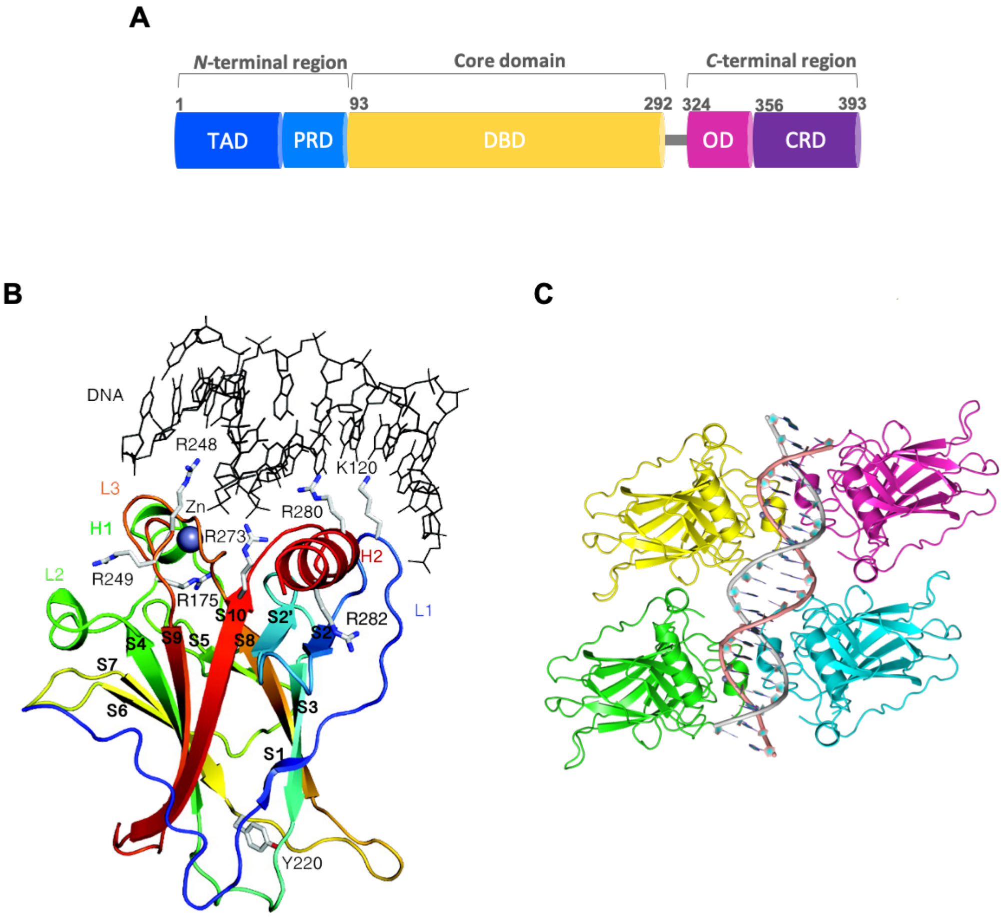
A
N-terminal region
Core domain
C-terminal region
1
93
292
324
356
393
TAD
PRD
DBD
OD
CRD
B
DNA
R248
K120
L3
Zn
R280
H1
R273
H2
L2
R249
R175
S10
S2'
R282
L1
S4
S9
S5
S8
S2
S7
S6
S3
S1
Y220
C

Figure 3. p53 structure and DNA binding. (A) Modular structure of p53 protein, comprising TAD (transactivation domain), PRD (proline-rich domain), DBD (DNA-binding domain), OD (oligomerization domain), and CRD (*C*-terminal regulatory domain). **(B)** 3D immunoglobulin-like β-sandwich structure of p53 DBD bound to DNA, with the representation of its organization in helixes (H1 and H2), loops (L1, L2, and L3), and sheets (S1-10). The zinc ion is colored purple. Important amino acidic residues involved in DNA recognition and residues needed for the correct binding positioning or structural stability are also depicted. **(C)** Four p53 DBD bind cooperatively with DNA response elements (RE), in a dimer-of-dimers topology (PDB ID 4HJE; [47]). Adapted from [48, 49].

The modular structure of p53 encompasses large regions of intrinsic disorder, which is typical of signaling proteins, providing conformational adaptability to p53 and facilitating its interaction with different binding partners [50]. In fact, the intrinsically disordered *N*-terminal TAD is the binding site for a variety of p53-interacting proteins, namely components of the transcription machinery, the transcriptional coactivators p300/CBP (CREB-binding protein), and the negative modulators Murine Double Minute (MDM)2 and MDMX [44, 51]. Simultaneous mutations of key hydrophobic residues in the TAD (L22Q/W23S and W53Q/F54S) result in transactivation-deficient phenotypes [52]. The PRD links the TAD to DBD and mediate several protein-protein interactions, namely proteins containing Src homology 3 domains [44].

The *C*-terminal region of p53 governs its structure and function. CRD is involved in p53 activation, degradation, cellular localization, and scanning along DNA for p53-binding sites [50]. It is subjected to extensive PTM, interacting with a set of regulatory proteins, regulating p53 activity [51]. The OD mediates the oligomerization of p53 in its tetrameric active conformation, being essential for the stability of the DBD in its binding to DNA [44].

As a transcription factor, p53 recognizes and binds to specific double-stranded DNA target sequences, termed p53-response elements (p53REs), through its DBD, eliciting its transcriptional activity. The p53 target RE binding sites consist in two decameric half-site motifs with the general consensus sequence RRRCWWGYYY (R = A, G; W = A, T; Y = C, T), located near the promoters of the p53 target genes [50]. The DBD adopts an immunoglobulin-like β-sandwich structure, with a DNA-binding surface comprising a loop (L)-sheet (S)-helix (H) motif and two loops stabilized by zinc coordination, which bind to DNA major- and minor grooves of target DNA, respectively [24] (Figure 3B). Particularly, residues involved in DNA recognition are K120 (L1), S241 (L3), R248 (L3), R273 (S10), A276 (H2), C277 (H2), and R280 (H2). On the other hand, residues implicated in the correct binding arrangement and structural stability of p53 include R175 (L2), Y220 (S7-S8), G245 (L3), and R282 (H2) [49] (Figure 3B).

The p53 tetramers have a dimer-of-dimers topology [53] (Figure 3C). Initially, two DBD are associated and stabilized within a half-site DNA motif, forming a symmetrical dimer. Two dimers then assemble to form tetramers via protein-protein and base-stacking interactions [53]. Four DBD bind cooperatively to DNA, both within and between half-sites [54, 55] (Figure 3C). This process of formation of dimers followed by the tetramer configuration is favored in the presence of DNA, where either protein-protein and protein-DNA interactions contribute to the complex stability [55]. In homeostatic states, with low p53 levels, all the three p53 oligomeric states (monomeric, dimeric, and tetrameric) are present in varying ratios. However, DNA damage triggers rapid tetramer assembly, even before the increase of p53 protein levels [50].

1.2.2. p53 regulation and biological functions

The crucial role of p53 as tumor suppressor was unequivocally confirmed by the observation of a complete penetrant cancer phenotype in p53-null mice [56]. In fact, p53 is the central hub of a complex and intricated network, regulating major signaling and cell fate decision pathways, in order to prevent tumor development. p53 acts by sensing different cellular stress stimuli, such as DNA damage, diverse physical or chemical distress, hypoxia, and nutrient deprivation, that eventually lead to its activation, stabilization, and accumulation in the cell [57] (Figure 4). Once active, p53 transcriptionally regulates several genes involved in major cellular processes, namely cell cycle arrest, cellular senescence, DNA damage repair, metabolic adaptation, and apoptosis [41] (Figure 4).

The cell fate specified by p53 activation is context- and tissue-dependent, being mainly related with the nature of cellular stress [58]. In case of mild DNA damage, p53 drives cell cycle arrest for DNA repair, while in case of severe and irreparable DNA damage, p53 stimulates apoptotic or senescence programs. Furthermore, other crucial factors, including the expression levels and PTM status of p53, cellular location, co-factor enrollment, and the architecture of the promoters of target genes, also dictate the type of p53-activated cellular responses. As such, p53 levels and PTM are changed to adapt to the context, and different subsets of p53 effectors are transcribed to yield the appropriate responses [58, 59].

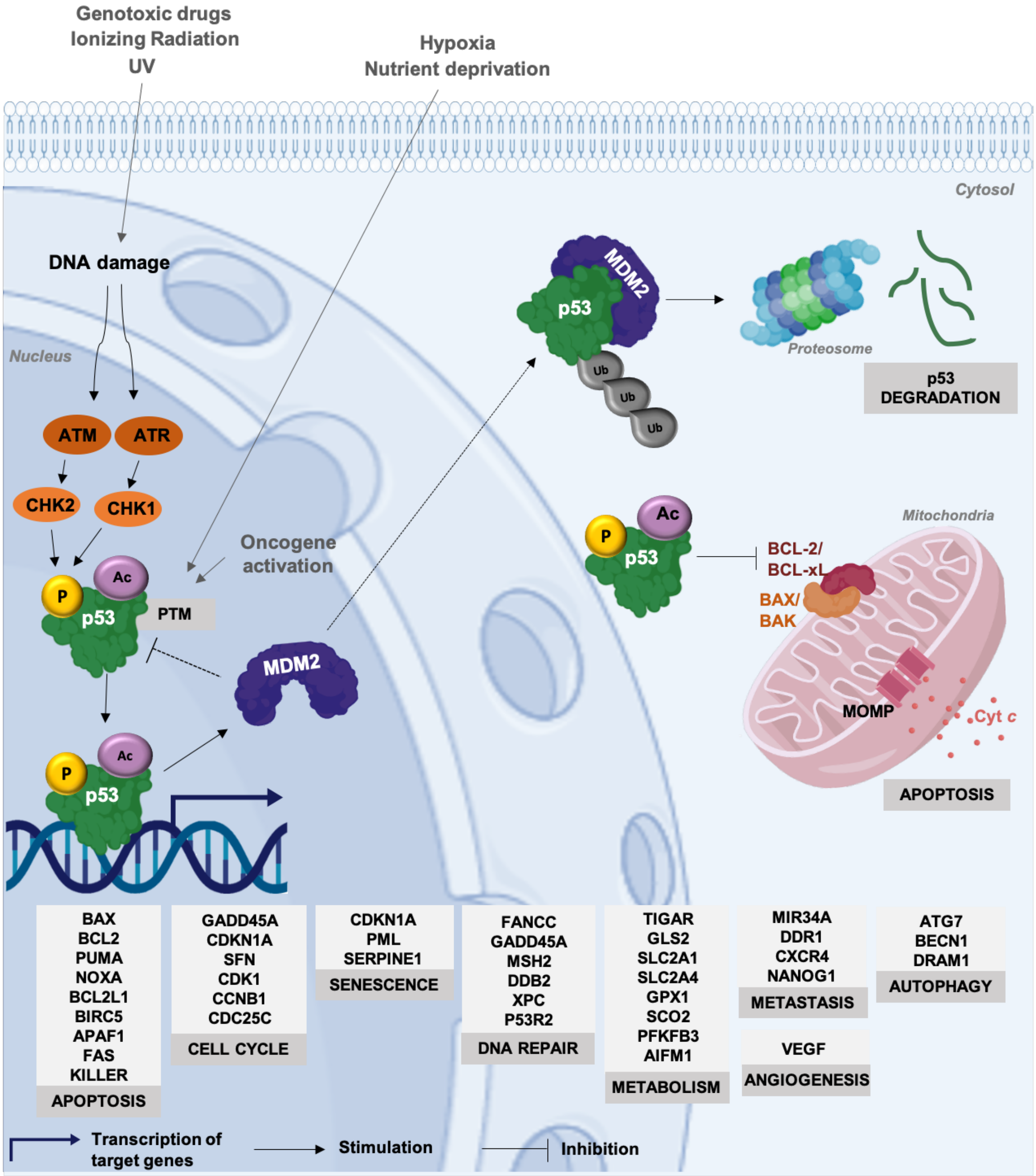
Genotoxic drugs
Ionizing Radiation
UV
Hypoxia
Nutrient deprivation
Cytosol
DNA damage
Nucleus
ATM
ATR
CHK2
CHK1
Oncogene activation
P
Ac
p53
PTM
MDM2
MDM2
p53
Ub
Ub
Ub
Proteosome
p53 DEGRADATION
Mitochondria
BCL-2/ BCL-xL
BAX/ BAK
MOMP
Cyt c
APOPTOSIS
BAX BCL2 PUMA NOXA BCL2L1 BIRC5 APAF1 FAS KILLER
APOPTOSIS
GADD45A CDKN1A SFN CDK1 CCNB1 CDC25C
CELL CYCLE
CDKN1A PML SERPINE1
SENESCENCE
FANCC GADD45A MSH2 DDB2 XPC P53R2
DNA REPAIR
TIGAR GLS2 SLC2A1 SLC2A4 GPX1 SCO2 PFKFB3 AIFM1
METABOLISM
MIR34A DDR1 CXCR4 NANOG1
METASTASIS
VEGF
ANGIOGENESIS
ATG7 BECN1 DRAM1
AUTOPHAGY
Transcription of target genes
Stimulation
Inhibition

Figure 4. p53 signaling pathway. In unstressed conditions, p53 has a short half-life, being normally kept at low levels by MDM2, an E3 ubiquitin ligase that inhibits p53 transcriptional activity and targets it for proteasomal degradation via polyubiquitination. p53 protein is activated by stress stimuli, such as DNA damage, which activates the upstream kinases ataxia telangiectasia mutated (ATM) and ataxia telangiectasia and Rad3-related protein (ATR), leading to p53 phosphorylation by checkpoint kinase (CHK)1 and CHK2. Other cellular stresses include hypoxia, nutrient deprivation, or oncogene activation, which dislocate p53 from the regulation of inhibitors (MDM2) through post-translational modifications (PTM), like phosphorylation (P) and acetylation (Ac), inducing stabilization, rapid accumulation and activation of p53. Depending on the stimulus, cell context or PTM pattern, active p53 transcriptionally regulates the expression of several target genes involved in major cellular processes, including cell cycle arrest, apoptosis, DNA repair, autophagy, senescence, metabolism, metastasis, and angiogenesis. p53 also plays transcription-independent roles, as it can bind to BCL-2 or BCL-xL at the mitochondria, inhibiting their anti-apoptotic functions, through the disruption of inhibitory complexes between BCL-xL or BCL-2 with BAK and BAX, with mitochondrial outer membrane permeabilization (MOMP), cytochrome c (cyt *c*) release, and subsequent apoptosis.

Although p53 has essential cellular functions, its unintentional activation will culminate in deleterious effects on normal and developing tissues. Therefore, under physiologic conditions, p53 has a short half-life, being normally kept at low levels by different negative regulators, such as MDM2, MDMX, COP1, ARF-BP1, and PIRH2 [60]. Particularly, MDM2 and MDMX are recognized as the main endogenous negative modulators of p53, sharing significant structural and functional similarity [61]. The mechanisms by which MDM2 and MDMX interact with and inhibit p53 are well characterized. Both MDMs bind to p53 TAD, and these interactions are mediated by three essential p53 amino acid residues (*Phe19*, *Trp23*, *Leu26*) and the hydrophobic pockets at the *N*-terminal of MDMs [62]. As such, since transcriptional co-activator p300 and MDMs compete for the same p53 TAD binding site, the binding of MDMs hinders the p53 access to the transcriptional machinery [44, 62, 63]. MDM2 also presents an acidic domain that binds the p53 DBD, blocking its interaction with DNA, which efficiently prevents p53 transcriptional activity [64]. Moreover, MDM2 homo-oligomers have an E3 ubiquitin ligase activity [65, 66], targeting p53 for proteasomal degradation via polyubiquitination or nuclear export via monoubiquitination [66]. Under stress conditions, the p53-MDM2 interaction is impaired, with subsequent stabilization and activation of p53 transcriptional functions. Conversely, MDMX does not form homo-oligomers and, consequently, has no ubiquitin ligase function. Despite this, it can regulate MDM2 ubiquitin ligase activity, through formation of MDM2/MDMX heterodimers [61]. In fact, hetero-oligomerization of MDM2 and MDMX creates a more effective p53 E3 ubiquitin ligase complex and leads to a more efficient inhibition of p53 transactivation [67]. The non-overlapping roles of MDM2 and MDMX have been corroborated by the observation that either *MDM2*$^{-/-}$- or *MDMX*$^{-/-}$-mice are not viable due to a p53-dependent embryonic lethality. Nonetheless, with a p53-null background, deletion of *MDM2* or *MDMX* does not affect mice viability, confirming that neither protein can compensate for one another to inhibit p53 and that both proteins are critical regulators of p53-induced growth suppression [68]. Importantly, *in vivo* and *in vitro* experiments showed that MDM2 is transcriptionally regulated by p53, thereby generating a tight autoregulatory feedback loop, important for p53 turnover [58]. Conversely, *MDMX* is not a p53 transcriptional target [69].

The p53 function and modulation is also a consequence of diverse PTM. Over 60 residues of p53 can be post-translationally modified, mostly occurring in p53 TAD and CRD, and markedly influencing the expression of p53 target genes [70]. The most commonly reported PTM of p53 include phosphorylation of serine (S) and/or threonine (T) residues, and acetylation, ubiquitylation and sumoylation of lysine (K) residues [70, 71]. Phosphorylation was the first p53 PTM to be described as functionally relevant. p53 phosphorylation pattern shows a significant redundancy, as a single site can be phosphorylated by multiple kinases and a single kinase can phosphorylate multiple sites [72]. The protein kinases ataxia telangiectasia mutated (ATM) and ataxia telangiectasia and Rad3-related protein (ATR), and their downstream checkpoint kinase (CHK)1 and CHK2, play a central role in genome surveillance, phosphorylating p53 at S9, S15, S20, and S46 residues [73]. The most extensively studied *N*-terminal p53 phosphorylation sites are S15, T18, and S20, which were shown to have determinant roles in p53 sequence-specific DNA binding, by reducing p53 affinity for MDM2 [74-76]. Upon DNA damage, phosphorylation at S46 was shown to be critical for p53-mediated induction of pro-apoptotic genes, namely apoptosis-inducing protein 1 (p53AIP1) [77], NOXA and PUMA [78, 79]. On the other hand, acetylation of p53, at key lysine residues of DBD and CRD, was shown to be a crucial event for the regulation of p53 DNA-binding affinity and transcriptional activity, determining the cellular outcome upon genomic stress. In general, acetylation is mainly mediated by p300/CBP/PCAF or Tip60/MOF/MOZ [80].

1.2.2.1. Classical p53 functions

Apoptosis, cell cycle arrest and senescence represent the most evident outcomes of p53 tumor suppressive functions, being therefore considered as the classical or canonical p53 responses. p53-mediated growth arrest is crucial for cell cycle checkpoint and maintenance of chromosomal integrity, after DNA double-strand breaks (DSB) by ionizing radiation. The cell injury activates ATM, inhibits MDM2, with rapid accumulation of p53 and induction of its target genes [81] (Figure 4). p53 was first described to halt cell proliferation by inducing a transient G1-phase cell cycle arrest in response to DNA damage. This gives the cells time to repair the potentially lethal damage that could initiate tumor development [82, 83]. The p53-induced cell cycle arrest is mainly mediated by the transcription of *CDKN1A*, encoding the cyclin-dependent kinase (Cdk) inhibitor p21 [83, 84]. Increased p21 binds and inactivates cyclin E/Cdk2 or cyclin D/Cdk4 complexes, resulting in the hypophosphorylation of retinoblastoma protein (pRB) and cell cycle arrest [81, 84]. pRB is a negative regulator of the transcription factor E2F, which is required for the expression of S-phase-associated genes [81]. Some studies involving p21-null mouse embryonic fibroblasts (MEFs) showed that these cells presented a substantial deficiency in their ability to arrest cell cycle after induced DNA damage [85]. However, other features of p53 function, namely the induction of thymocyte apoptosis and the normal mitotic spindle checkpoint, were verified, suggesting that other p53 targets, such as *GADD45A*, also contribute to p53-

mediated cell cycle arrest [85-88]. In fact, p53 was also shown to arrest G2/M-phase cell cycle arrest, mainly involving the prevention of cyclin B1/Cdk1 complex formation by the p53 transcriptional targets GADD45, p21, and 14-3-3σ [89-91]. Besides that, p53 was also reported to downregulate Cdk1, cyclinB1 and Cdc25c, contributing to block the entry of cells into mitosis phase [92-94] (Figure 4). In addition to provide a cell cycle checkpoint, p53 also modulates a set of genes associated with DNA recombination and repair mechanisms. In fact, p53 was shown to induce the expression of two components of nucleotide excision repair mechanism, DDB2 and XPC [95], and to regulate the transcription of *OGG1* [96] and *MUTYH* [97] genes involved in base excision repair mechanism. Some studies also showed that p53 synergized with the c-jun transcription factor to regulate the transcription of *MSH2,* which encodes a constituent of the DNA mismatch repair system [98]. Also, p53 presents a direct role in the fidelity control of homologous recombination and non-homologous end-joining, ensuring error-free DSB repair [99].

The cell proliferation arrest after DNA damage is a reversible process, as soon as DNA is repaired and p53 is downregulated. However, cells can enter into a p53-triggered replicative senescence state, an irreversible cell cycle arrest occurring in response to stress signals like telomere dysfunction, oncogene activation, and DNA damage [100]. Therefore, several studies have already linked cellular senescence with p53-mediated tumor suppression in specific contexts [101-103]. In addition, the molecular markers p21, PML, PAI-1, and DEC1 were shown to be sufficient to mediate senescence downstream of p53 activation [104]. Nevertheless, the cell fate decision between the reversible cell cycle arrest and senescence is complex, being mainly affected by cellular context, and by the functional status of different pathways (namely pRb, factor nuclear kappa B (NF-kB), and mammalian target of rapamycin (mTOR) activities) and their crosstalk with p53 [81].

One of the most extensively studied p53 tumor suppressive function relates to its ability to induce apoptotic cell death. Different studies demonstrated that the pro-apoptotic activity of p53 is mainly linked to its transactivation capabilities [105-109]. Different studies have indicated that p53 mediates apoptosis through both extrinsic (or death receptor) and intrinsic (or mitochondrial) apoptotic programs. The extrinsic pathway leads to the activation of a caspase cascade, whereas the intrinsic pathway coordinates the balance in the BCL-2 family towards the pro-apoptotic members, triggering the formation of the apoptosome, and consequently caspase-mediated apoptosis [57]. p53 is capable of triggering an extrinsic apoptotic pathway through the transactivation of *KILLER/DR5* [110], *Fas/CD95* [111] death receptors, and Fas ligand *TNFSF6* [112]. Also, p53 transactivates the BCL-2 family member BID, facilitating the crosstalk between the extrinsic and intrinsic pathways [113]. In fact, death receptors can activate the intrinsic apoptotic pathway through caspase-8-mediated cleavage of BID. In turn, active BID interacts with the pro-apoptotic BCL-2 family members, causing the release of cytochrome *c* (cyt *c*) and Smac/DIABLO, with activation of caspase-9 and -3 [114]. Interestingly, p53 is also able to transactivate caspase-8 [115].

The initiation of the intrinsic pathway is made by the release of BAX, through inhibition of anti-apoptotic proteins BCL-2/BCL-xL by NOXA or PUMA activation, or through direct activation of BAX/BAK, leading to mitochondrial outer membrane permeabilization (MOMP) and cyt *c* release (Figure 4). In turn, cyt *c* binds APAF-1, promoting the formation of the apoptosome complex, which ultimately leads to the recruitment of executioner caspases to induce cell death [116]. p53 was shown to control the transcription of pro-apoptotic members of the BCL-2 family, including BAX [117], PUMA [118], and NOXA [77]. p53 also transactivates APAF-1, which binds to cyt *c*, forming the apoptosome, with caspase-9 cleavage [119]. Furthermore, p53 transactivates executioner caspases-6 and -10, which are important downstream effectors of mitochondrial apoptotic program [120, 121]. Besides that, p53 showed transrepression capabilities that may also contribute to apoptosis, namely the downregulation of BCL-2 [117] and survivin [122] anti-apoptotic proteins. Importantly, several evidences have suggested that p53 has a transcription-independent apoptotic activity, by acting directly on the mitochondria. Different apoptotic signals prompt cytoplasmic p53 to interact with mitochondrial BCL-2 and BCL-xL, leading to the disruption of inhibitory complexes between BCL-xL or BCL-2 with inducers of the MOMP, BAK and BAX [123] (Figure 4). Some authors have also demonstrated that p53 interacts with the pro-apoptotic mitochondrial protein BAK, causing its oligomerization and the release of cyt *c*. They also showed that the formation of the p53-BAK complex coincides with loss of the interaction between BAK and the anti-apoptotic BCL2 family member MCL1 [124]. Interestingly, p53 mitochondria-mediated apoptosis was shown to be a faster response than the apoptosis triggered by p53 transactivation activity, suggesting that these two mechanisms are coordinated to decide cell fate accordingly with the stress signal [125].

1.2.2.2. Emerging p53 functions

The tumor suppressive activity of p53 go far beyond its roles in mediating cell cycle arrest, apoptosis, and senescence. It is already well-stablished that p53 is also critically involved in various non-canonical pathways, including autophagy, energetic metabolism, invasion and metastasis, and angiogenesis [126] (Figure 4).

p53 represents one of the key regulators of metastasis, direct or indirectly controlling the expression of genes involved in major metastatic pathways, namely cell adhesion, ECM remodeling, cell motility and invasion, EMT, stemness, and anoikis [104, 127]. Different studies implicated p53 in the regulation of stem cell function and differentiation [128-131]. Particularly, p53 was shown to promote differentiation after DNA damage by directly suppressing the expression of the pluripotency gene *NANOG* [130], and also to regulate stemness by transcriptionally inhibiting the expression of the key stem cell marker CD44 [132]. Additionally, p53 induces the transcription of miR-34a, indirectly inhibiting different pluripotency genes, in order to restrain somatic cell reprogramming [133]. p53-mediated transcription of miR-34a also negatively regulates factors implicated in EMT programs, namely Snail, Slug, Twist, and Zeb1 [127, 134]. On the other hand, the induction of MDM2 by p53 leads to Slug degradation, enhancing E-cadherin (E-CAD) expression and opposing EMT [135]. The proteolytic enzymes matrix metalloproteases (MMP), MMP-1 and -9, involved in the ECM disruption, were shown to be downregulated by p53 [136], as well as fibronectin that is involved in cell growth, differentiation, and migration [137]. Moreover, p53 negatively regulates angiogenesis by both inhibiting the expression of proangiogenic factors as VEGF and by increasing the production of antiangiogenic ones as thrombospondin [138].

Particular attention has been given to the involvement of p53 in metabolic reprogramming, mainly focusing on glucose metabolism as the major source of cell energy. Metabolic reprogramming constitutes a hallmark of cancer with a crucial impact on tumor cell growth and survival, dissemination, and therapeutic resistance [7]. Otto Warburg was the first to describe the differences in cellular metabolism between normal and cancer cells. While the production of ATP in normal cells occurs preferentially by oxidative phosphorylation (OXPHOS) in mitochondria, tumor cells frequently increase glycolysis to produce lactate and ATP, even in the presence of oxygen, a process known as the "Warburg effect" [139, 140]. Glycolysis is a faster but less efficient process than OXPHOS in ATP production. However, this inefficiency can be compensated by increasing glucose uptake through upregulation of transmembrane glucose transporters (GLUT) [141]. Thus, the Warburg effect confers several advantages to cancer cells, particularly by providing intermediates for different biosynthetic pathways required for unrestrained proliferation, and an adaptation to hypoxic conditions often observed in solid tumors [142]. Increased glycolysis benefits not only the tumor growth, but also its dissemination. The spreading of cancer cells in a multicellular environment is a direct consequence of the elevated glucose consumption and subsequent lactate secretion, which decreases the pH of the microenvironment. An acidic environment leads to the death of surrounding normal cells and ECM remodeling by proteolytic enzymes, including MMPs [142, 143], and depletion of cell-cell adhesion proteins, such as E-CAD [144]. This promotes EMT [145, 146], which enables cancer cells to migrate and invade. Low pH also promotes angiogenesis through the enhanced expression of VEGF by cancer [147] and endothelial [148] cells. Additionally, lactate activates the transcriptional hypoxia-inducible factor (HIF), which was shown to regulate a myriad of genes involved in angiogenesis [149] and metastasis [150] processes. Another consequence of the Warburg effect is the decreased usage of the mitochondrial respiratory chain, due to reduced OXPHOS and oxygen consumption. Accordingly, less reactive oxygen species (ROS) are produced, which promotes cancer cell proliferation and apoptosis evasion [151]. For these reasons, the control of aberrant cellular metabolism can prevent or delay tumorigenesis.

Metabolic reprogramming in cancer cells is driven by activation of oncogenes (*e.g.*, c-Myc and HIF) and/or inactivation of tumor suppressors, including p53 [152, 153]. Particularly, p53 has shown to counteract the Warburg effect, reducing the glycolytic flux and favoring OXPHOS (Figure 5). Primarily, p53 halts the sustained tumor growth by promoting the diversion of metabolic intermediates from biosynthetic pathways to the tricarboxylic acid (TCA) cycle, enhancing OXPHOS and ROS production. This ultimately promotes an imbalance in the redox cell state that contributes to cell death [154]. This emphasizes the importance of mitochondrial maintenance and biogenesis, also promoted by functional p53 through induction of ribonucleoside-diphosphate reductase subunit M2B (p53R2) and mitochondria-eating protein (Mieap) [155, 156]. On the other hand, p53 was shown to regulate several intermediates of the glycolytic pathway. Namely, p53 downregulates directly GLUT1 and GLUT4 [157], and indirectly GLUT3 (through inhibition of NF-κB), limiting glucose uptake by tumor cells [158]. Also, p53 transcriptionally downregulates hexokinase 2 (HK2) [159], and phosphofructokinase-2 isoform 6-phosphofructo-2-kinase/fructose-2,6-biphosphatase 3 (PFKFB3) [160], and participates in phosphoglycerate mutase (PGM) degradation routes [161], compromising glycolysis flux. p53 transcriptionally induces the expression of TP53-induced glycolysis and apoptosis regulator (TIGAR) that decreases the levels of fructose-2,6-bisphosphate (F-2,6-P). Once F-2,6-P is the most potent activator of phosphofructoskinase-1 (PFK-1; catalyzes the conversion of F-6-P to F-1,6-P), a TIGAR-dependent reduction in F-2,6-P levels promoted by p53 results in glycolysis inhibition [162]. p53 also downregulates the monocarboxylate transporter (MCT) 1, suppressing lactate secretion, which also stimulates the shift to OXPHOS, as a consequence of the accumulation of pyruvate that cannot be converted to lactate [163]. In order to promote OXPHOS, p53 was also shown to induce the expression of synthesis of cytochrome *c* oxidase 2 (SCO2), which assists in the assembly of mitochondrial complex IV of the mitochondrial electron transport chain [164], as well as of apoptosis-inducing factor (AIF), which ensures the proper assembly and function of mitochondrial respiratory complex I [165] (Figure 5).

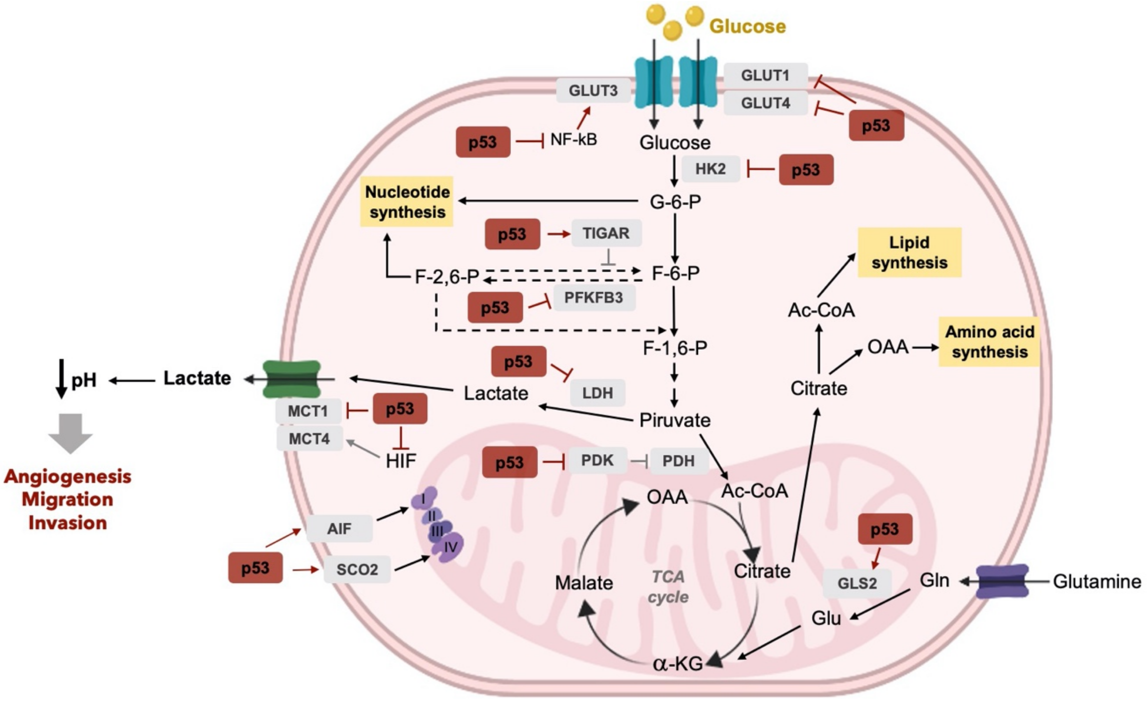
Glucose
GLUT3
GLUT1
GLUT4
p53
NF-kB
Glucose
HK2
G-6-P
Nucleotide synthesis
TIGAR
F-2,6-P
F-6-P
PFKFB3
F-1,6-P
Lipid synthesis
Ac-CoA
OAA
Amino acid synthesis
Citrate
pH
Lactate
LDH
Piruvate
MCT1
MCT4
HIF
Angiogenesis
Migration
Invasion
PDK
PDH
OAA
Ac-CoA
AIF
I
II
III
IV
SCO2
TCA cycle
Malate
Citrate
GLS2
Gln
Glutamine
Glu
α-KG

Figure 5. The role of p53 in glucose metabolism. p53 counteracts the Warburg effect often observed in cancer cells, reducing the glycolytic flux and favoring OXPHOS. p53 can also promote the pentose phosphate pathway to generate NADPH and ribose 5 phosphate (essential precursor of nucleotides). Activated p53 enhances the mitochondrial tricarboxylic acid cycle rate, through transactivation of glutaminase 2. The decrease of the microenvironment pH as a consequence of elevated lactate secretion prompts events related to cancer cells dissemination, namely angiogenesis, migration and invasion. α-KG, α-Ketoglutaric acid; Ac-CoA, Acyl-Coenzyme A; AIF, apoptosis-inducing factor; F-6-P, frutose-6-phosphate; F-1,6-P, frutose-1,6-phosphate; G-6-P, Glucose-6-phosphate; Gln, glutamine; Glu, glutamate; GLUT, glucose transporter; GLS2, glutaminase 2; HIF, hypoxia inducible factor; HK, hexokinase; LDH, lactate dehydrogenase; MCT, monocarboxylate transporter; NF-kB, nuclear factor kappa B; OOA, oxaloacetate; PDH, pyruvate dehydrogenase; PDK, pyruvate dehydrogenase kinase; PFKFB3, 6-phosphofructo-2-kinase/fructose-2,6-biphosphatase 3; PGM, phosphoglycerate mutase; TCA, tricarboxylic acid; SCO2, synthesis of cytochrome *c* oxidase 2.

1.3. Inactivation of p53 in human cancers

The tumor suppressor p53 is mutated in nearly 50% of all human cancers, and in many of the remaining cases, which express wild-type (wt) p53, the p53 pathway is found abrogated [166] (Figure 6). As such, loss of p53 function is clearly a pre-requisite for tumor growth. The understanding of the mechanisms underlying p53 inactivation in human cancers is of great relevance for its therapeutic targeting.

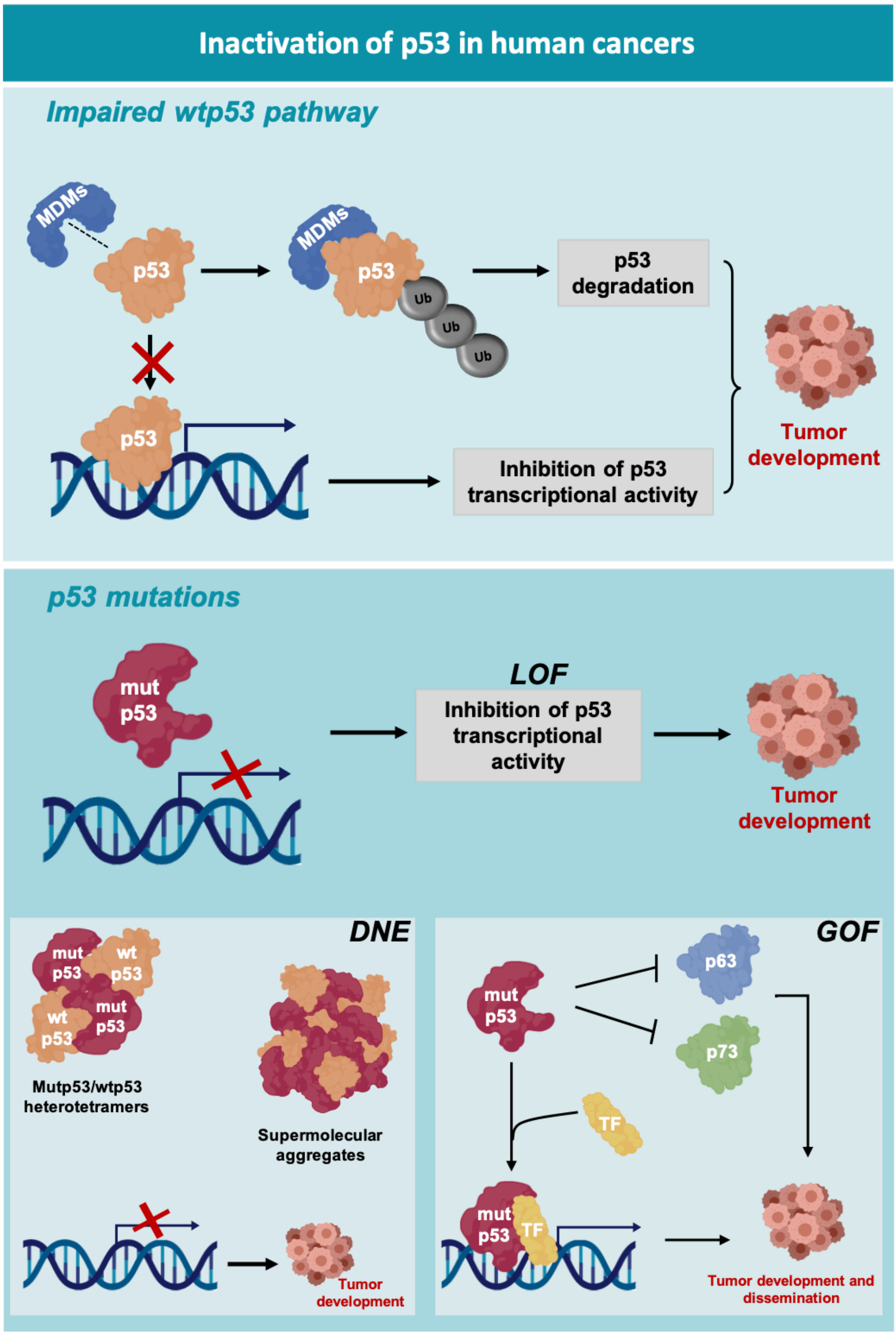
Inactivation of p53 in human cancers
Impaired wtp53 pathway
MDMs
p53
MDMs
p53
Ub
Ub
Ub
p53 degradation
p53
Inhibition of p53 transcriptional activity
Tumor development
p53 mutations
mut p53
LOF
Inhibition of p53 transcriptional activity
Tumor development
DNE
mut p53
wt p53
wt p53
mut p53
Mutp53/wtp53 heterotetramers
Supermolecular aggregates
Tumor development
GOF
mut p53
p63
p73
TF
mut p53
TF
Tumor development and dissemination

Figure 6. Modes of p53 inactivation in human cancers. The upper panel illustrates the impairment of the wtp53 pathway in human cancers due to overexpression of p53 major endogenous negative regulators MDM2 and MDMX (MDMs), leading to the inhibition of p53 transcriptional activity and p53 degradation. The lower panel summarizes the different functional profiles of mutant p53 (mutp53). In general, p53 mutations lead to loss of DNA-binding ability and impairment of the p53 response (loss of function, LOF). Dominant negative effect (DNE) of mutp53 over wtp53 occurs through the formation of heterotetramers and supramolecular aggregates with wtp53. Mutp53 also acquires new oncogenic activities, called gain-of-function (GOF), mainly through inhibition of p63 and p73 tumor suppressor proteins, and recruitment of additional transcription factors (TF), with upregulation of tumor development- and dissemination-promoting genes.

1.3.1. Impaired wtp53 pathway

The perturbation of the intricated p53-MDMs network has pronounced implications for tumorigenesis. In fact, a significant percentage of human tumors exhibit an inactivated wtp53, due to enhanced activity of its major endogenous negative regulators MDM2 and MDMX [167-169] (Figure 6). The increased activity of these two proteins can occur through different oncogenic mechanisms, namely: amplification of *MDM2* and *MDMX* genes, enhanced transcription or translation, altered PTM patterns, overexpression of their positive regulators (*e.g.* Twist, WIP1, Akt), or loss of their negative regulators (*e.g.* p14ARF, ATM, CHK2) [170, 171]. Furthermore, a single-nucleotide polymorphism at position 309 (SNP309) in *MDM2* promoter generates a binding-site for the SP1 transcription factor, increasing MDM2 expression and impairing p53 function [172]. Overexpression of MDM2 is frequently found in osteosarcoma, glioblastoma and prostate cancers [173], while MDMX overexpression is more common in melanoma, retinoblastoma, neuroblastoma, hepatocellular carcinoma and breast cancers [174-176]. MDM2/X overexpression appears in the majority of hematological malignancies and in pediatric tumors, such as sarcomas, gliomas and leukemias, as the main cause of p53 impairment [177].

Oncogenic viruses have developed strategies to inactivate p53 in both infected and transformed cells. Particularly, the E6 oncoprotein produced by Human Papilloma viruses (HPV) is responsible for cervical carcinomas and an increasing number of head-and-neck cancers. It was shown to form a ternary complex with the cellular E3 ubiquitin ligase E6AP and p53, leading to ubiquitin-mediated degradation of p53 [178].

1.3.2. *TP53* mutations

The sequencing of human cancer genomes unveiled a myriad of genomic and chromosomal aberrations, settling that *TP53* mutations are the most frequent genetic alterations [179]. The frequency of p53 mutations fluctuates among different cancer types, with colorectal (43,28%), head and neck (42,51%), esophagus (41,21%), female genital organs (38,64%), lung (37,23%), pancreas (34,67%), and skin (34,63%) cancers exhibiting the highest prevalence [180]. Germline *TP53* mutations have been also identified in approximately 70% of families displaying a rare, but extremely penetrant cancer syndrome known as Li-Fraumeni syndrome (LFS) [181]. This autosomal dominant disorder predisposes individuals to a broad range of childhood- and adult-onset cancers, including premenopausal breast cancer, bone and soft tissue sarcomas, leukemia, adrenocortical carcinomas, and brain tumors [181]. The distribution of germline *TP53* mutations is similar to those documented for sporadic tumors, although the order of frequency differs between the two groups [181].

TP53 mutations can occur throughout all its domains, although mutations occurring in the intrinsically disordered regions of p53 are relatively rare [50]. TAD mutants are described of having selective transactivation activity, being unable to induce the expression of genes involved in cell cycle arrest, such as *CDKN1A*, but without compromising apoptotic cell death. OD mutants have impaired tetramerization, with partial or complete loss of p53 transactivation potential [182]. Mutations in the OD have a low frequency among somatic mutations, but the germline mutant p53 (mutp53) R337H is responsible for an exceptionally high incidence of LFS in Southern Brazil. The study of tumor patterns in R337H carriers unveiled all the common features of conventional DBD mutations in LFS, predisposing carriers to several types of cancer. Comparing to classic LFS, it was observed some onset age differences and a higher risk for other types of cancers, namely colorectal, thyroid, and childhood adrenocortical [183]. The vast majority of cancer-associated *TP53* mutations occur in the p53 DBD (~95%), being mainly missense (~80%), and resulting in protein structure destabilization, abrogation of the DNA-binding ability, and impairment of the p53 response [184, 185]. Six amino acid residues are substantially more frequently mutated in human cancers and are referred as “hotspots” codons (R175, G245, R248, R249, R273, and R282) [184]. p53 mutations can be classified as either “contact” (*e.g.* R248W, R273C, R273H, and R280K), removing essential DNA interaction sites without significant structural alterations, or “structural” (*e.g.* R175H, Y220C, G245D, G245S, R249S, and R282W), leading to p53 DBD conformational distortions that reduce its kinetic and thermodynamic stability [184, 186].

Typically, first stage human tumors are commonly heterozygotes, expressing both wt- and mutp53, as *TP53* mutations occur only in a single allele [179]. Nevertheless, although wtp53 is retained, mutp53 may exert a dominant negative effect (DNE) over wtp53 [182] (Figure 6). The mechanisms by which DNE can occur include either the formation of mut/wtp53 heterotetramers or the incorporation of wtp53 into mutp53 supramolecular aggregates, both rendering transcriptionally inactive p53 [184] (Figure 6). The DNE was shown to be dependent on different factors, namely the mut:wt ratio (generally 3:1) within the heterotetramers, the mutp53 conformation, and the DNA-binding affinity of the mutp53 subunits within the heterotetramers [187]. As such, DNE might be critical in determining the therapeutic outcome with DNA-damaging agents, as mutp53-expressing tumors exhibit a selective advantage under conditions that stimulate a p53-dependent cell death. Thus, therapeutic strategies capable of reducing mutp53 levels will increase the therapeutic response [182].

During tumor progression, cancer cells frequently lose the second wt allele, mostly by deletion (loss of heterozygosity, LOH). The complete loss of wtp53 provides cancer cells, only expressing mutp53, a selective advantage [185]. Observations that relate *TP53* mutations and LOH to poor therapeutic response and worse outcomes indicated a different cancer scenario from loss of function (LOF) [184]. Furthermore, recent data have shown that p53 LOH is a requisite for mutp53 stabilization and the execution of additional oncogenic functions [188]. Indeed, there are clear evidences that mutp53 proteins can exert additional oncogenic activities (called gain-of-function, GOF), shown to promote tumor development and dissemination [182] (Figure 6).

The first evidences of mutp53 GOF arose from the observation that mutp53 expressed in p53-null cells led to increased cellular growth, also enhancing tumorigenic potential when injected in nude mice [189]. Furthermore, it has been described that knock-in mice expressing mutp53 R248Q, R273H, or R175H exhibited accelerated tumor growth, being the developed tumors more aggressive and invasive than those observed for *TP53*$^{-/-}$ and *TP53*$^{+/+}$ mice, although the similar spectrum of developed tumors [190-192]. These results are consistent with clinical data, which showed that patients with mutp53-expressing tumors have a higher incidence of metastatic disease and poorer overall survival, with the development of chemoresistance [193]. However, some mutp53, namely G245S and R249S, did not exhibit GOF properties, indicating that these activities are not transversal to all mutp53 [192, 194]. It should also be noted that the data obtained so far indicate that the conformational state does not determine mutp53 GOF, as both contact (*e.g.* R248Q) and structural (*e.g.* R175H) mutants present GOF activity *in vivo* [192, 195].

GOF activities exhibited by mutp53 are extensive and include the promotion of tumor cell proliferation, survival, stemness, genomic instability, migration and invasion, angiogenesis, inflammation, and enhancement of chemoresistance [196] (Figure 7). These outcomes induce cancer cells to become addicted to the presence of mutp53, a phenomenon called “oncogene addiction” [182, 184, 197]. The underlying mechanisms by which mutp53 exerts its GOF activities have been extensively investigated in the last years, and have disclosed several aberrant interactions particularly with transcription factors and co-factors, with the reprograming of tumor cell behavior to adopt a more aggressive phenotype [197] (Figures 6 and 7). In fact, although the DNA-binding ability of mutp53 is lost or largely inhibited, mutp53 can recruit different transcriptional factors (*e.g.* NF-kB, NF-Y, ETS2, E2F1, VDR, SP1, SREBP, ID4, and STAT2), coordinating the expression of target genes involved in tumor cell proliferation, invasion and metastasis [196, 198-201] (Figure 7). Moreover, mutp53 has been shown to potentiate oncogenic cellular changes by interacting with the chromatin remodeling complex SWI/SNF, leading to alterations in the cellular transcriptional profiles [202] (Figure 7). Remarkably, mutp53 block ATM-dependent activation of the DNA damage response by disrupting the MRE-RAD50-NSB complex, rendering cells dependent on the activity of the enzyme poly(ADP ribose) polymerase 1 (PARP1) [203]. Interestingly, mutp53 potentiates the PARP1 activity, assuring tumor cell survival in the presence of high levels of DNA damage [203] (Figure 7).

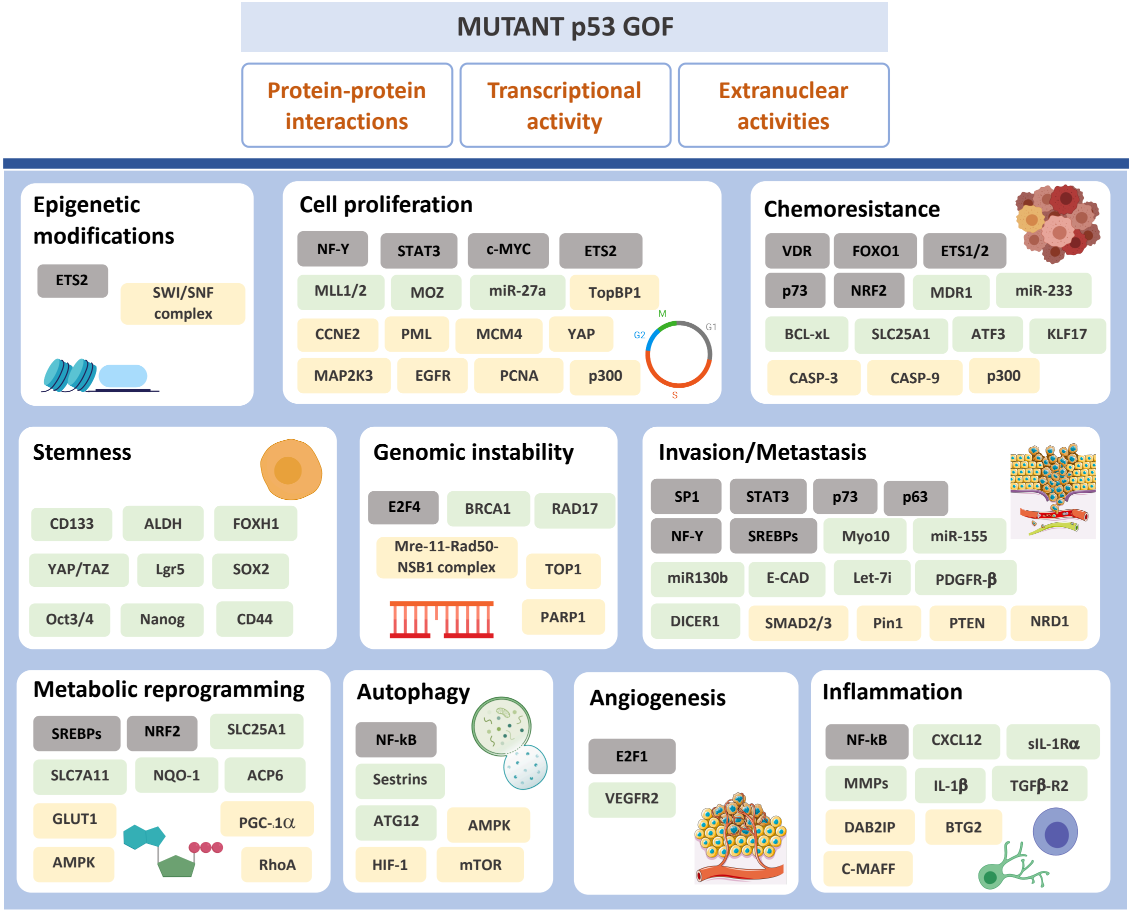
MUTANT p53 GOF
Protein-protein interactions
Transcriptional activity
Extranuclear activities
Epigenetic modifications
ETS2
SWI/SNF complex
Cell proliferation
NF-Y
STAT3
c-MYC
ETS2
MLL1/2
MOZ
miR-27a
TopBP1
CCNE2
PML
MCM4
YAP
MAP2K3
EGFR
PCNA
p300
M
G1
G2
S
Chemoresistance
VDR
FOXO1
ETS1/2
p73
NRF2
MDR1
miR-233
BCL-xL
SLC25A1
ATF3
KLF17
CASP-3
CASP-9
p300
Stemness
CD133
ALDH
FOXH1
YAP/TAZ
Lgr5
SOX2
Oct3/4
Nanog
CD44
Genomic instability
E2F4
BRCA1
RAD17
Mre-11-Rad50-NSB1 complex
TOP1
PARP1
Invasion/Metastasis
SP1
STAT3
p73
p63
NF-Y
SREBPs
Myo10
miR-155
miR130b
E-CAD
Let-7i
PDGFR-β
DICER1
SMAD2/3
Pin1
PTEN
NRD1
Metabolic reprogramming
SREBPs
NRF2
SLC25A1
SLC7A11
NQO-1
ACP6
GLUT1
PGC-1α
AMPK
RhoA
Autophagy
NF-kB
Sestrins
ATG12
AMPK
HIF-1
mTOR
Angiogenesis
E2F1
VEGFR2
Inflammation
NF-kB
CXCL12
sIL-1Rα
MMPs
IL-1β
TGFβ-R2
DAB2IP
BTG2
C-MAFF

Figure 7. Mutp53 GOF activities impact multiple hallmarks of cancer cell biology, affecting the chromatin structure, transcriptional regulation, and microRNA biogenesis, shaping the proteome, and rewiring tumor cell metabolic pathways. It also encompasses cytoplasmic functions and cell-extrinsic effects, namely affecting tumor microenvironment and the inflammatory response. Essentially, oncogenic functions of mutp53 proteins driving tumor development and dissemination rely on the direct interaction with transcription factors (grey boxes) or co-factors, and other protein effectors (yellow boxes), altering their activity, or through transcriptional modulation of target genes (green boxes). ACP6, Acid Phosphatase 6; ALDH, Aldehyde dehydrogenase; AMPK, AMP-activated protein kinase; ATF3, Activating transcription factor 3; ATG12, Autophagy Related 12; BTG2, BTG Anti-Proliferation Factor 2; CASP-3, Caspase-3; CASP-9, Caspase-9; CXCL12, C-X-C motif chemokine 12; E-CAD, E-cadherin; DAB2IP, DAB2 interacting. protein; FOXH1, Forkhead Box protein H1; FOXO1, Forkhead box protein O1; GLUT1, Glucose transporter 1; HIF-1, hypoxia-inducible factor-1; KLF17, Krueppel-like factor 17; MDR1, multidrug resistance protein 1; MMPs, Metalloproteinases; mTOR, Mammalian target of rapamycin; NF-kB, Nuclear factor kappa B; NF-Y, Nuclear transcription factor Y; NQO-A, NAD(P)H quinone dehydrogenase 1; NRF2, Nuclear factor erythroid 2-related factor 2; PARP1, Poly(ADP ribose) polymerase 1; PGC-1α, Peroxisome proliferator-activated receptor gamma coactivator 1-alpha; RhoA, Ras homolog family member A; SOX2, SRY-Box Transcription Factor 2; SREBPs, Sterol regulatory element-binding proteins; STAT,

Signal transducer and activator of transcription; TAZ, Tafazzin; TOP1, DNA topoisomerase 1; TGFβ-R12, Transforming growth factor, beta receptor II; TopBP1, DNA Topoisomerase II Binding Protein 1; VDR, Vitamin D Receptor; VEGFR2, Vascular endothelial growth factor receptor 2; YAP, yes-associated protein. Data retrieved and adapted from [166, 179, 184, 204].

Furthermore, mutp53 was shown to hetero-oligomerize with other members of the p53 tumor suppressors family, p63 and p73, inhibiting their transcriptional activities, or stimulating the transcription of non-canonical oncogenes, to promote oncogenesis [184, 205-207]. In fact, the inhibitory effect of mutp53 over p63 has been mostly associated with an enhanced invasive and metastatic behavior of tumor cells, via regulation of Sharp1, Cyclin G2, and miR-155 [197, 208]. On the other hand, besides the stimulation of the expression of ABCB1, an ATP-binding cassette (ABC) transporter, mediating the efflux of drugs from cancer cells [184], the chemoresistance commonly observed in mutp53-expressing tumors has been also partly attributed to its inhibitory interaction with p73 [197] (Figure 7).

Recently, mutp53s were also implicated in the rewiring of cancer cell metabolism, in order to meet the biosynthetic demands for tumor growth and progression, as a novel GOF [209]. Conversely to wtp53, mutp53 stimulates the Warburg effect, via the RhoA–ROCK–GLUT1 cascade, and the lipid synthesis [209]. Particularly, in a context of breast cancer, mutp53 was shown to interact with the sterol regulatory element-binding proteins (SREBPs), main regulators of fatty-acid and cholesterol biosynthesis, with induction of the mevalonate pathway [210]. Moreover, alterations of cancer cell metabolism by mutp53 also encompasses the direct inhibition of AMP-activated protein kinase (AMPK), a major sensor of cellular energy metabolism and a master regulator of metabolic homeostasis [211]. Cytoplasmatic mutp53 was shown to suppress autophagy [212] and apoptosis, through interference with the ability of pro-caspase-3 to become proteolytically activated by caspase-9 [213], thereby supporting tumor cell survival.

Mutp53 proteins are recurrently expressed at higher levels in human cancers than wtp53 in normal cells, suggesting that mutp53 are quite stable and often accumulate in tumor cells. In fact, the stabilization and accumulation of mutp53 in cancer cells is a prerequisite for its GOF phenotypes. Early assumptions considered that mutations in p53 lead to the abrogation of the auto-regulatory feedback loop between p53 and MDM2, once mutp53 fails to transactivate *MDM2* [184]. Later, this concept was challenged by different *in vitro* and *in vivo* evidences showing that mutp53 levels can be regulated by MDM2 in normal tissues, but not in tumor tissues [190, 191, 195, 214]. This suggested that additional events occurring during tumorigenesis are important for mutp53 stability and accumulation.

The overexpression of different MDM2 short isoforms was frequently found in human tumors, being correlated with poorer prognosis [215, 216]. These MDM2 isoforms differ from MDM2 full-length by lacking critical function domains important for p53 regulation. In fact, MDM2 isoforms lack the nuclear localization signal domain, mainly localizing in the cytoplasm, and cannot bind p53, due to lack of a p53-binding domain. They are also incapable of p53 degradation [215, 217]. Studies using MDM2 isoform B, the most frequently expressed MDM2 isoform in human cancers, unveiled that this protein can sequester MDM2 full length in the cytoplasm, limiting the interaction of MDM2 full length with mutp53 in the nucleus [218]. Hence, the inhibition of MDM2-mediated mutp53 degradation promotes mutp53 accumulation and the subsequent execution of its GOF [218].

The heat shock proteins (HSPs) machinery is highly active in tumor cells, being involved in the stabilization of oncoproteins, including mutp53 [219]. Different studies have shown that, at elevated levels, HSP70 and/or HSP90 bind and stabilize mutp53, by trapping it and MDM2 (or other E3 ubiquitin ligases) in complexes such as the carboxy terminus of HSP70-interacting protein (CHIP), preventing the ubiquitination and degradation of mutp53 [220]. Moreover, HSPs were shown to stabilize mutp53 polypeptides in a folding intermediate state prone to form pseudo-aggregates, described to localize mainly in the cytoplasm and perinuclear region, rather in the nucleus as functional wtp53. Also, these intermediate mutp53 protein forms were described to sequester other functional proteins or transcription factors, namely wtp53, p63 and p73, effectively suppressing the antitumor response [219].

Bcl-2 associated athanogene (BAG) proteins function as adapters or co-chaperones and were found overexpressed in many types of human cancers. BAGs interact with different proteins, participating in diverse cellular processes, including cell division, cell death, and differentiation [221, 222]. Particularly, BAG2 and BAG5 were shown to interact with mutp53, inhibiting its degradation and promoting its stabilization and accumulation in tumors [223, 224].

1.4. Anticancer therapeutic approaches targeting p53

As already mentioned, once p53 negatively controls virtually all cancer hallmarks, its inactivation is a required factor for tumor development and progression. In addition, the high frequency of impaired p53 in human cancers underlines that its targeting constitutes an appealing anticancer therapeutic strategy. Since its discovery that p53 has been a challenging target for drug discovery, being frequently assumed as “undruggable”. In fact, wtp53 and most of mutp53 (except for Y220C) lack binding pockets or allosteric sites, other than the DNA-binding groove itself, hindering rational drug design [171]. Importantly, over 2,000 mutp53 forms can be found in human tumors, with differences in their structure, stability, and biological functions, being virtually impossible to target all of them with a single drug [50, 225]. Nonetheless, *in vitro* and *in vivo* evidences have proved that restoration of p53 activity elicits impressive tumor regression and cell death, with minimal toxic effects in normal tissues [170, 226-228].

Distinct therapeutic approaches reconstituting p53 pathway are currently available. Mutp53-expressing tumors benefit from therapeutic strategies focusing on reactivation of wt-like activity to mutp53, elimination of mutp53, and/or circumvention of its GOF. Conversely, in wtp53-expressing tumors, therapeutic approaches have mainly focused on inhibition of the p53 interaction with its negative regulators [229]. Different approaches involving gene therapy and vaccination were also developed. Adenovirus-based gene therapy (Gendicine), which involves the introduction of a functional copy of p53 into tumors, was approved by China Food and Drug administration in 2003, and it is still currently used in China. Gendicine has been successfully used to treat several cancer types, and its combination with chemotherapy and radiotherapy has demonstrated improved survival rates compared to single standard therapies [230]. p53 has been considered a promising target antigen, which led to the development of DNA-based and dendritic cell-delivered p53 vaccines, eliciting specific anti-p53 immune responses without toxicity [231-234]. Particularly, phase II clinical trials testing the effects of immunotherapy on small cell lung cancer, using the dendritic cell-based p53 vaccine (INGN-225) in combination with Nivolumab and Ipilimumab, are currently underway (NCT03406715).

In the last years, several drug discovery strategies have been combined in an attempt to identify effective p53-activating agents, including p53 dynamic structure studies, virtual screening and rational drug design, and protein- and cell-based drug screening approaches [225]. In particular, engineered yeast-based models have proven to be a valuable cell system to study human cancer-related proteins such as p53. In fact, relevant insights about the pharmacology of p53 family proteins have been disclosed by our research group, using “humanized” yeasts heterologously expressing these proteins and their modulators MDM2 and MDMX [235-238] (Figure 8). Most importantly, with this yeast approach, new small molecule activators of p53 have been successfully identified, including SLMP53-1 [239] and SLMP53-2 [240] as reactivators of mutp53 R280K and Y220C, respectively, DIMP53-1 as dual inhibitor of p53-MDM2/MDMX interactions [241], and LEM2 as a dual inhibitor of p73-mutp53 and p73-MDM2 interactions [242].

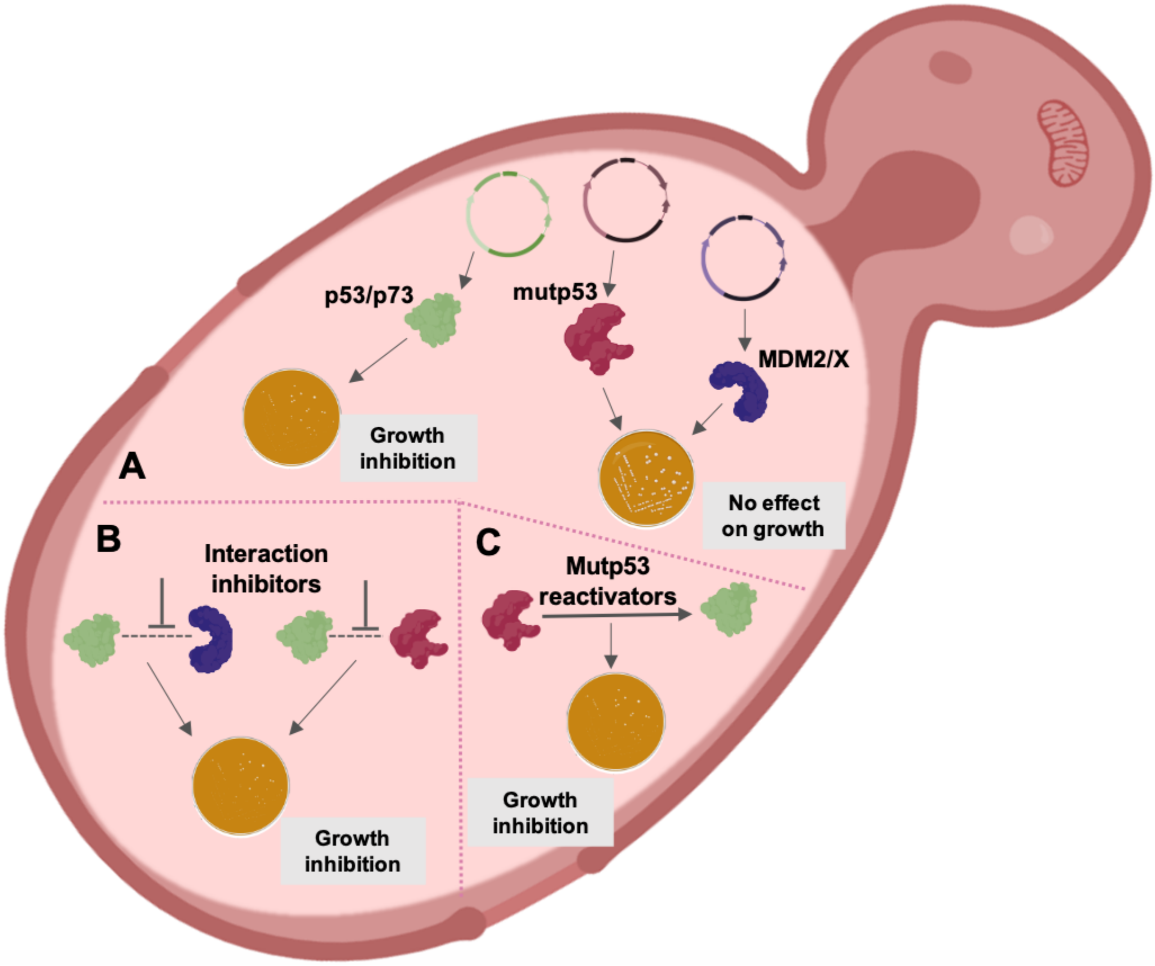
p53/p73
mutp53
MDM2/X
Growth inhibition
No effect on growth
A
B
Interaction inhibitors
Growth inhibition
C
Mutp53 reactivators
Growth inhibition

Figure 8. Yeast-based assay for the screening of p53-targeting agents. (A) The heterologous expression of human p53 or p73 induces *Saccharomyces cerevisiae* growth inhibition, while the expression of human mutp53, MDM2 or MDMX have no effect on yeast growth. The yeast cell growth is evaluated by counting the number of colony-forming units [235, 236, 238]. **(B)** Yeast cells co-expressing p53/p73 and MDM2/MDMX have a normal growth, and small molecule inhibitors of p53-MDMs (*e.g.* DIMP53-1), p73-MDMs or p73-mutp53 (*e.g.* LEM2) interactions reestablish the p53/p73-dependent growth inhibition [241, 242]. **(C)** Small molecule reactivators of mutp53 (*e.g.* SLMP53-1 and SLMP53-2) reestablish the p53-dependent growth inhibition [239, 240].

1.4.1. Targeting wtp53-expressing tumors

The inhibition of p53-MDM2/MDMX interactions is a key therapeutic strategy to stabilize p53 levels, especially in tumors overexpressing MDM2 or MDMX. Different small molecules, peptides and aptamer-based approaches targeting MDM2 or/and MDMX or their upstream regulators, or p53 itself have been reported [243].

In particular, the inhibitory activity of MDM2 over p53 can be targeted directly either by blocking the ubiquitin ligase activity of MDM2 and/or by inhibiting the p53-MDM2 interaction [229, 243]. Some compounds were already identified as inhibitors of MDM2-

mediated p53 degradation. Particularly, the MDM2 ligase inhibitor 98 (HLI98) class of compounds, sempervirine and MEL23/MEL24, were shown to inhibit the E3-ligase activity of MDM2, leading to p53 stabilization and p53-mediated tumor cell death [170, 171]. Different small molecules have been developed to target the p53-MDM2 interaction by mimicking the structure of the three key amino acid residues (*Phe19*, *Trp23*, *Leu26*) of p53 TAD that bind to the MDM2 hydrophobic cleft [171, 229]. In fact, the co-crystallization of p53 and MDM2 led to the identification of the first MDM2 antagonist small molecules with *in vivo* activity, the nutlins (cis-imidazoline compounds) [244]. Nutlin-3a was shown to bind to MDM2, leading to p53 stabilization and activation, promoting the expression of p53 targets, such as p21 and PUMA, and inducing cell cycle arrest and apoptosis [244]. Later, the nutlin analogues RG7112 [245, 246] and RG7388 [247] were developed. Due to superior affinity and potency *in vitro* and *in vivo*, as well as improved bioavailability and toxicity profiles, these nutlin analogues have entered clinical trials. Particularly, RG7388 entered phase III clinical trials for relapsed or refractory acute myeloid leukemia in combination with cytarabine (DNA synthesis inhibitor). Other small molecules targeting MDM2, which block the p53-binding site of MDM2, include benzodiazepinediones [248], piperidinones [249] and spiro-oxindoles (or MIS compounds) [250]. Some “stapled” p53-based peptides have been also described to bind to the p53-binding hydrophobic pocket on MDM2, preventing the p53-MDM2 interaction, namely SAH-p53-8, and sMTide analogues [171]. Importantly, the safety and efficacy of some inhibitors of the p53-MDM2 interaction have been tested in clinical trials, namely of SAR405838, AMG232, RO6839921, MK-8242, DS3032b, HDM201, and CGM097 [171, 251, 252].

Small molecule inhibitors of MDM2 can also bind MDMX, however differences between the p53-binding pockets of the two proteins decrease the affinity of these compounds to MDMX. As such, given the limited efficacy of the p53-MDM2 interaction inhibitors in tumors overexpressing MDMX [67], the development of specific MDMX inhibitors and/or dual MDM2/MDMX inhibitors became imperative. The first small molecule inhibitor of MDMX identified was SJ-172550, which forms covalent adducts with MDMX, preventing p53 binding and inducing apoptosis in retinoblastoma cells expressing high levels of MDMX. Interestingly, SJ-172550 showed additive effects in combination with nutlin-3a [253]. Moreover, the compounds XI-011 and XI-006 act in a different manner by blocking MDMX transcription [254]. Although the dual targeting of MDM2/MDMX is thought to be required for a full p53 reactivation, few dual inhibitors have been reported. The small molecule RO-5963 was shown to block homo- and heterodimerization of both MDM2 and MDMX, triggering a p53 tumor suppressive response [255]. The small molecule reactivation of p53 and induction of tumor cells apoptosis (RITA) showed efficient induction of apoptosis by inhibiting both MDMX and MDM2 *in vitro* and *in vivo* [256-258]. However, the precise mechanism of RITA remains to be elucidated because, besides eliciting a p53-dependent growth suppression, other p53-independent effects have been described [171, 259]. The stapled peptide ALRN-6924 was also described to disrupt the p53 interaction with both MDM2 and MDMX, recently entering phase I/II clinical trials [171].

Some challenges and limitations are frequently associated with the pharmacological reactivation of wtp53. Firstly, the harmful effects and clinical implications of MDM2/MDMX inhibition in normal cells should be taken at high consideration, as these proteins exhibit crucial p53-independent cellular functions other than p53 regulation [171]. Also, the existence of a subset of tumors with a wtp53 inactivated by other means than the p53-MDM2/MDMX pathway must also be considered [260]. Therefore, reliable biomarkers should be identified for improved patient stratification and, consequently, wtp53 restoration strategies. Lastly, the treatment with MDM2 inhibitors promotes a strong selection pressure for p53 inactivation so that cancer cells can resist to the effects of therapy [171]. In fact, the occurrence of p53 DBD mutations upon prolonged treatment of cancer cells with nutlin-3a was noticed [261]. Even during phase I clinical trial testing MI-773 in liposarcoma patients, an increase of *TP53* mutations over time was registered and it was associated with the resistance to this MDM2 inhibitor [262].

1.4.2. Targeting mutp53-expressing tumors

Different approaches of mutp53 targeting have been explored, with several molecules demonstrating great potential (Table 1). One feasible strategy is related to the use of compounds that reactivate wt-like transcriptional function to mutp53, by binding to p53 DBD and restoring DNA contacts or stabilizing the wt conformation. In fact, despite conserving essential DNA-binding residues, structural mutp53 are kinetically and thermodynamically destabilized, in a temperature-dependent (*e.g.*, β-sandwich mutations) or -independent (*e.g.*, zinc region mutations) manner. As such, small molecule stabilizers, acting as molecular chaperones, should restore the correct folded p53 conformation [50]. Conversely, given the lack of surface crevices to be docked by small molecules, the reactivation of contact mutp53 constitutes a higher challenge. Nevertheless, the introduction of functional groups that can compensate for the missing DNA contacts has been advocated [50]. Other approaches targeting mutp53 include the abrogation of its GOF or DNE activities, by effective depletion of mutp53, inhibition of mutp53 aggregation, and targeting of mutp53 downstream pathways, disrupting protein-protein interactions [225, 263].

Table 1. Mutp53-targeting agents. Compounds are organized according to their mechanism of mutp53 targeting.

Molecule	Mechanism of mutp53 targeting	Targeted mutp53	Structure	Ref
Restoration of wt-like function to mutp53				
Covalent binding to mutp53				
CP-31398 Styrylquinazoline	Michael acceptor; probable Michael addition involving cysteine-targeting by thiol-binding	V173A S241F R249S R273H	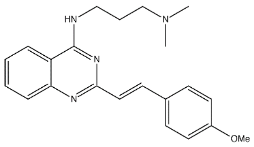	[264, 265]
STIMA-1 Styrylquinazoline derivative	Michael acceptor; probable Michael addition involving cysteine-targeting by thiol-binding	R175H R273H	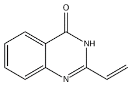	[266]
MIRA-1 Maleimide analogue	Michael acceptor; probable Michael addition involving cysteine-targeting by thiol-binding	R273H R175H P176Y/R248W R248Q R248W R282W R273H/P309S R280K	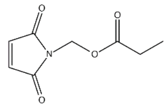	[267]
PRIMA-1 **PRIMA-1^{MET} (APR-246)** Quinuclidinones	Metabolized to methylene quinuclidinone Michael addition involving cysteine-targeting by thiol-binding	R175H R273H R248Q D259Y/K286E K286E S241F R273C P223L/V274F	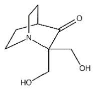 PRIMA-1 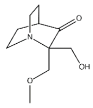 PRIMA-1^{MET}	[268-276]
PK11007 Sulfonylpyrimidine	Alkylation of the thiol groups through nucleophilic aromatic substitution	Y220C V143A R273H/P309S	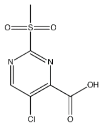	[277]
HO-3867 Diarylidenyl piperidone curcumin analogue	Michael addition involving cysteine-targeting by thiol-binding	R273H R175H R248Q R248W L194F M237K G245S H193R R196* Y205F S241F C277F K132Q R249S R280K E285K R156P C238Y R158H/N239D Y163H M246I G245V P223L P153A/S241F	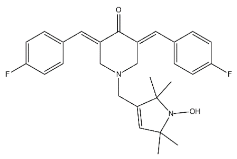	[278]

		P223L/V274F		
KSS-9 Piperlongumine derivative	Michael acceptor; probable Michael addition involving cysteine-targeting by thiol-binding	R175H	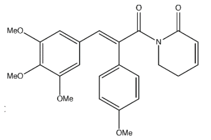	[279]

Non-covalent binding to mutp53

PhiKan083 Carbazole	Binding to the mutp53 Y220C-induced surface cleft	Y220C	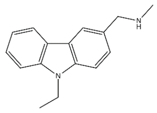	[280]
PK7088 Pyrazole	Binding to the mutp53 Y220C-induced surface cleft	Y220C	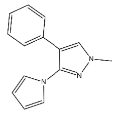	[281]
PK5196 Halogen-phenol derivative	Binding to the mutp53 Y220C-induced surface cleft	Y220C	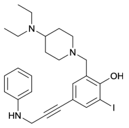	[282]
SCH529074 Piperazinylquinazoline	Binding to mutp53 nearby DNA binding surface	R249S R273H R175H R248W S241F	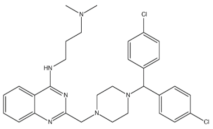	[283]
MB725 **MB710** Aminobenzothiazoles derivatives	Binding to the mutp53 Y220C-induced surface cleft	Y220C	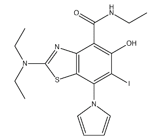 MB725 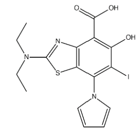 MB710	[284]
Stictic acid	Binding to a transiently open pocket between loop L1 and sheet S3 of the p53 DBD	R175H G245S	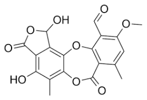	[285]
CDB3 Peptide	Binding to wt/mutp53 nearby DNA binding surface (R249S and R273H) or unknown local (G245S and R175H)	R249S G245S R175H I195T R273H	Sequence: REDEDEIEW	[286-288]
pCAPs Peptides	Binding to unknown local of mutp53	R175H A135V S241F R249S R280K		[289]

Zinc ion chelators

ZMC1 (NSC319726) Thiosemicarbazone	Zinc chelation	R175H C176F C238S C242S C242F	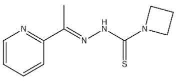	[290, 291]

		G245S		
COTI-2 Thiosemicarbazone	Zinc chelation	R175H	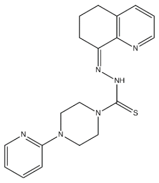	[292, 293]
Chaperone-mediated effect				
Chetomin Epidithiodioxopiperazine	Binding to HSP40	R175H	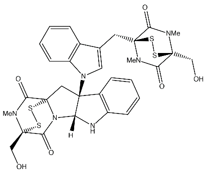	[294]
SLMP53-2 Tryptophanol-derived oxazoloisoindolinone	Enhancement of the interaction between mutp53 Y220C and HSP70	Y220C	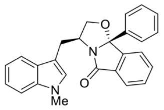	[240]
Unknown mechanism				
Ellipticine Alkaloid2	*ND*	R175H R248W R249S R273H D281G L194F S241F H233L R273C	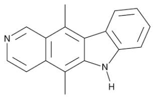	[295]
P53R3 Piperazinylquinazoline	*ND*	R175H R273H M237I R248W	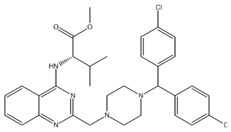	[296]
PEITC Phenethyl isothiocyanate	*ND*	R175H	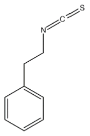	[297]
WR-1065 Aminothiol	*ND*	V272M	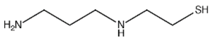	[298]
Inducers of mutp53 degradation				
17-AAG **17-DMAG** Demethoxygeldanamycin derivatives	Inhibition of HSP90, with the increase of MDM2 and CHIP function	R273H R273H/P309S R280K L194F	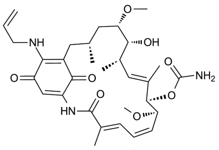 17-AAG	[220]

			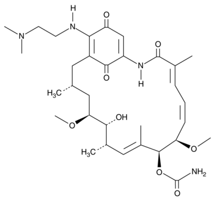 17-DMAG	
SAHA Suberoylanilide hydroxamic acid	Inhibition of HDAC6/8 (HSP90 machinery), leading to the release of mutp53 and its MDM2- and CHIP-mediated degradation Suppression of the association between HDAC8 and YY1 transcriptional factor, with decreased mutp53 expression	R280K L194F P223L/V274F R249S R273H R273H/P309S	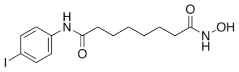	[299, 300]
Sodium butyrate	Inhibition of HDAC8 (HSP90 machinery) Suppression of the association between HDAC8 and YY1 transcriptional factor, with decreased mutp53 expression	R249S R280K	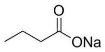	[300]
Geldanamycin Benzoquinone ansanamycin	Inhibition of HSP90 with increase of MDM2 and CHIP function	R175H L194F R248Q R273H R280K R175H	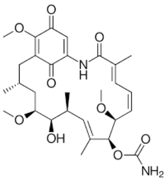	[301, 302]
Ganetespib Phenylindolyl triazolone	Inhibition of HSP90 with mutp53 degradation	R248Q C124R P223L/V274F L194F S241F R273H C275F	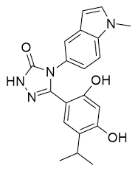	[303]
Gambogic Acid Xanthone	Disruption of the HSP90-mutp53 interaction, with mutp53 CHIP-mediated degradation	R175H G266E R273H R280K	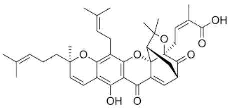	[304]
NSC59984 Methylpiperazinyl nitrofuranyl propenone	Degradation of mutp53 through MDM2-mediated ubiquitination	R273H/P309F S241F R175H/L	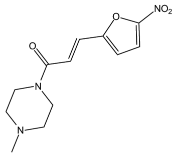	[305] 247
Arsenic compounds	Nuclear export of mutp53 and promotion of its proteasome-mediated degradation	R175H R273h H179Y/R282W R248W R273H/P309	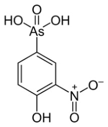	[306]
YK-3-237 Boronic acid chalcone	Deacetylation of mtp53 through SIRT1 activation, with a reduction of mutp53 levels	R249S V157F R273H M237I R280K	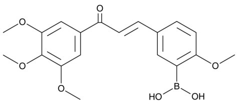	[307]
Spautin-1 Fluorobenzylquinazolin amine	Inhibition of deubiquitinating enzymes, with mutp53 lysosome-mediated degradation	R248Q/L/W S241F R158InF R280K	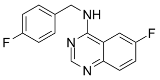	[308]

		G266E R282W P151H R175H/C/D P98S R273H/L G245C L194F A161T S227R/K E258K		
Disulfiram Bis-diethylthiocarbamoyl disulfide	Thiol-conjugation with mutp53 proteasome-mediated degradation	R273H	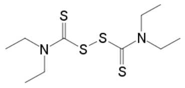	[309]
Disruptors of protein-protein interactions				
RETRA Thiazolthiophenyl ethanone	Disruption of mutp53-p73 interaction	R273H	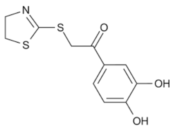	[310]
Prodigiosin Pyrrolyl pyrromethane	Disruption of mutp53-p73 interaction	R273H/P309S S241F R273H R248Q	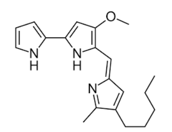	[311]
LEM2 Xanthone	Disruption of mutp53-p73 and MDM2-p73 interactions	R273H	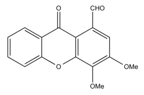	[242]
ATRA Retinoic acid; tretinoin	Inhibition and degradation of Pin1, with disruption of mutp53-Pin1 interaction	R273H R280K	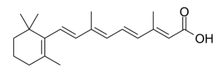	[312]
Statins	Inhibition of the mevalonate pathway, with CHIP-mediated mutp53 degradation	R175H R156P V157F Y220C R248W	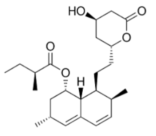	[313]
Reacp53 Peptide	Binding to mutp53 aggregation prone region (S9)	R175H R248Q	Sequence: RRRRRRRRRLTRITLE	[314]

ND – Not determined.

1.4.2.1. Restoration of wt-like function to mutp53

Covalent binding to mutp53

Some of the identified mutp53 reactivators were shown to covalently modify the cysteines residues within mutp53 DBD, stabilizing its conformation and, consequently, rescuing wt-like transcriptional activity. These molecules act as soft eletrophiles or Michael acceptors, reacting with nucleophiles of the cellular environment, namely protein thiol groups and cysteines. Particularly, p53 DBD exhibits ten cysteines, three of which (*C124*, *C182* and *C277*) have been implicated in mutp53 refolding [315].

CP-31398 was the first small molecule reported to reactivate mutp53 [264]. Its derivative STIMA-1 [266], MIRA-1 and analogues [267], and KSS-9 [279] were shown to stabilize and reactivate wt-like transcriptional activity to mutp53. Since they all exhibit reactive carbon-carbon double bonds, being potential Michael acceptors, their mechanism of mutp53 reactivation is thought to involve cysteine-targeting by thiol-binding [225, 263] (Table 1). Nevertheless, these compounds were shown to exert additional p53-independent antitumor activity [279, 315, 316].

PRIMA-1 was identified through a cell-based screening of a library of 2,000 low-molecular-mass compounds. It promotes the refolding of mutp53, inducing the expression of p53 targets such p21, BAX, and PUMA in tumor cells [268]. Its derivative, PRIMA-1^{MET} (or APR-246) was later found to be more effective due to its higher lipophilicity and cell permeability. It is currently in phase Ib/II clinical trials [269, 317]. These compounds are pro-drugs, being converted intracellularly into the active Michael acceptor methylene quinuclidinone (MQ), which covalently binds to cysteines of mutp53 R175H and R273H, particularly to *C124* residue [271]. Some authors have also unveiled that the thermal stabilization of wtp53, mutp53 R175H and R273H by MQ occur through its binding to *C277* residue, while the reactivation of mutp53 R175H occurs by MQ binding to both *C124* and *C277* residues [276] (Table 1). Interestingly, residue *C277* directly interacts with DNA, being in close proximity to residue R273. As such, the *C277* adduct formed may establish additional contacts with DNA to compensate for the R273H mutation [318]. Nevertheless, some redox-related effects underlying the antitumor properties of MQ have also been described, namely the inhibition of thioredoxin reductase 1 (TRXR1) [319] and depletion of glutathione [320].

The 2-sulfonylpeyrimide, PK11000, was found to stabilize the DBD of both wt- and mutp53 proteins by covalent cysteine modification, alkylating *C182* and *C277* residues, without compromising DNA-binding affinity. PK11000 and its derivative PK11007 showed to promote the highest thermal stabilization of mutp53 Y220C, while PK11007 exhibited higher cytotoxicity against mutp53 Y220C- and V143A-expressing tumor cells (Table 1), with upregulation of the p53 targets p21, MDM2, and PUMA. Like MQ, also PK11007 presented redox-related effects, namely glutathione depletion via thiol-binding with increase of ROS levels [277].

The curcumin analog HO-3867 was recently identified as mutp53 reactivator by cysteine-thiol-binding ability to *C182* and *C277* residues in mutp53 Y220C. The compound restored folded wt-like conformation and the transcriptional activity to mutp53, with *in vitro* and *in vivo* antitumor activity [278] (Table 1).

Non-covalent binding to mutp53

The disclosure of mutp53 Y220C crystal structure revealed a druggable crevice on the DNA-binding surface, appealing for rational drug design [186, 280]. *In silico*- and NMR-based screening identified different compounds as potential binders of the Y220C cleft, namely carbazole derivative PhiKan083 (PK083) [280], the pyrazole PK7088 [281], and aminobenzothiazole derivatives MB710 and MB725 [284] (Table 1). Both PK083 and PK7088 were shown to thermodynamically stabilize mutp53 Y220C. Consistently with a mutp53 reactivation, PK7088 also induced growth inhibition and apoptosis in tumor cells harboring mutp53 Y220C, through restoration of wt-like p53 conformation, with upregulation of the p53 targets p21 and NOXA and relocation of BAX to the mitochondria [281]. In the same way, MB710 and MB725 were shown to bind tightly to the mutp53 Y220C pocket, stabilizing mutp53 and leading to its wt-like reactivation. Particularly, MB725 induced growth inhibition in several cancer cell lines carrying mutp53 Y220C [284].

CDB3 is a peptide derived from the p53-binding protein 53BP2, a co-factor that enhances p53-mediated transactivation. It was shown that CDB3 interact and partially overlap the edge of mutp53 DNA-binding site, restoring the wt-like conformation and DNA-binding *in vitro* to hotspot mutp53 G245S, R249S, and I195T [286] (Table 1). Similarly, the small molecule SCH529074 was shown to non-covalently bind to mutp53 R273H and R249S DBD (Table 1), in a similar manner to peptide CDB3, restoring p53 tumor suppressor activity. Interestingly, it was also shown that this compound prevents p53 ubiquitination by MDM2, leading to its stabilization [283]. Both CDB3 and SCH529074 induced the transcription of wtp53 target genes in cancer cells expressing different mutp53 forms. Moreover, SCH529074 exhibited *in vivo* antitumor activity.

Lead p53 conformation activating peptides (pCAPs), sharing sequence similarity with known p53-binding partners, were shown to bind and rescue wt-like conformation to structural mutp53 R175H and R249S (Table 1), with restoration of their DNA-binding ability. Furthermore, these lead peptides elicited potent tumor regression in mouse xenograft models [289].

A virtual screening led to the identification of stictic acid as a potential mutp53 reactivator by binding with high affinity to a transiently open pocket in mutp53 DBD. As such, the compound induced *in vitro* thermal stabilization of mutp53 R175H and G245S (Table 1), and effectively induced the expression of p21 and PUMA in cancer cells carrying mutp53 R175H [285].

Zinc ion chelators

Zinc ion is fundamentally required for wtp53 structure stabilization, and specific mutp53 (*e.g.* R175H) structures fail to coordinate zinc [321]. Moreover, the concentration of zinc affects the conformation and aggregation of p53. As such, *in vitro* and *in vivo* zinc supplementation was shown to increase the wt-like tumor suppressive activity of mutp53 R175H and R273H by restoring their active conformations [322, 323]. The addition of zinc also prevented the DNE of mutp53 over wtp53, by promoting the clearance of misfolded mutp53 through autophagy [324].

The small molecule thiosemicarbazone ZMC1 (NSC319726) is a zinc chelator that enables the transport of the ion across cell membranes (ionophore activity) (Table 1). It was able to restore the wt function to mutp53 R175H, buffering optimal intracellular zinc concentration for refolding mutant DBD. ZMC1 efficiently inhibited the growth of mutp53 R175H-expressing human tumor xenografts in mice [290]. Later studies showed that ZMC1 also restored the wt function to other mutp53 with impaired zinc binding, such as C242S, C242F, and C176F [291].

COTI-2 was first described as mutp53 reactivator with effective antitumor activity in several human tumor cells and in mouse xenograft models [292]. It was shown that COTI-2 also inhibited the PI3K/AKT/mTOR pathway, suggesting other mechanisms underlying its antitumor activity. Nevertheless, likewise ZMC1, COTI-2 has also a thiosemicarbazone structure and it is likely that this small molecule functions as a mutp53 reactivator by zinc chelation [292] (Table 1). COTI-2 is now being tested in a phase I clinical trials in gynecological and head and neck cancers [315].

Chaperone-mediated effect

The natural compound chetomin (CTM) was first identified in a p53 reporter screening assay as a reactivator of mutp53 R175H (Table 1). CTM was described to inhibit the growth of mutp53 R175H-expressing tumor cells *in vitro* and *in vivo*, with upregulation of the expression levels of the p53 targets MDM2, p21, and PUMA. The evidences showed that CTM binds to the HSP40, enhancing its interaction with mutp53 R175H, with refolding and reactivation of wt-like transcriptional activity to mutp53 [294]. In fact, HSP40 is a p53 chaperone, assisting in protein active conformation and stability for DNA binding [219].

Recently, the tryptophanol-derived oxazoloisoindolinone SLMP53-2 was identified as a new reactivator of mutp53. SLMP53-2 promoted the interaction of HSP70 with mutp53, restoring its wt-like conformation and transcriptional activity (Table 1). The small molecule elicited cell cycle arrest, apoptosis, and endoplasmic reticulum stress in mutp53-expressing hepatocellular carcinoma cells. Most importantly, SLMP53-2 exhibited potent *in vivo* antitumor activity against human hepatocellular carcinoma xenografts, with no apparent undesirable toxicity [240].

1.4.2.2. Depletion of mutp53

The rationale of this mutp53-targeting strategy includes the selective degradation of mutp53, expressed at high levels in human cancers and exhibiting oncogenic DNE or GOF properties. In fact, several evidences have suggested that various tumor cells became addicted to mutp53 and its GOF activities. Also, the knockdown of mutp53 in tumor cells was shown to significantly reduce tumor growth and metastasis. As such, drugs that efficiently eliminate mutp53 might be useful to improve therapeutic responses and the survival of cancer patients [222]. One potential therapeutic approach is to target cellular proteins responsible for mutp53 stabilization, namely HSP90. In fact, the inhibition of HSP90 by 17-AAG, geldanamycin, or ganetespib showed to destabilize mutp53, with inhibition of its transcriptional GOF, by inducing MDM2 or CHIP-mediated mutp53 degradation [303] (Table 1). A similar approach includes histone deacetylase (HDAC, inducers of HSP90) inhibitors such as SAHA and sodium butyrate, which were described to promote mutp53 elimination [299, 300] (Table 1).

1.4.2.3. Disruption of protein-protein interactions

As discussed above, among the different mutp53 GOF activities, mutp53 is able to bind and thereby inhibit the tumor suppressor activity of p73 and p63. Thus, the disruption of mutp53-p63/p73 complexes constitutes an appealing therapeutic alternative to reestablish the p63/p73-mediated antitumor responses [252]. The small molecule RETRA was identified in a p53 reporter assay, leading to a significant increase in expression levels of both p73 and different p53 target genes in mutp53-expressing tumor cells, an effect that was reverted by inhibition of p73 by RNAi. In fact, it abrogated mutp53-p73 complexes, with restoration of p73 transcriptional activity and tumor suppression, *in vitro* and *in vivo* [310] (Table 1). Also, the natural compound prodigiosin showed to restore the p53 signaling pathway in tumor cells carrying mutp53, by inducing the expression of p73 and abrogating mutp53-p73 complexes [311] (Table 1). Very recently, the xanthone derivative LEM2 was shown to inhibit the mutp53-p73 interaction, eliciting p73 transcriptional activity, cell cycle arrest, and apoptosis in p53-null and mutp53-expressing tumor cells (Table 1). Moreover, the pronounced antitumor activity against patient-derived neuroblastoma cells displayed by LEM2 was consistent with an activation of the p73 pathway [242].

The disruption of the mutp53 interaction with other transcription factors or co-factors, involved in the transcription of key players of oncogenic pathways, has been constituted an attractive therapeutic approach. The prolyl isomerase Pin1, frequently overexpressed in human cancers, supports the inhibition of p63 by mutp53 and also stimulates the induction of the oncogenic mutp53 transcriptional program [325]. As such, Pin1 inhibitors such as All-trans Retinoic Acid (ATRA) and KPT-6566 prevent mutp53 oncogenic activation in tumor cells, decreasing viability of mutp53-expressing cancer cell lines [203] (Table 1).

The transcription factor SREBP activates the expression of numerous oncogenic enzymes involved in the mevalonate pathway (*e.g*. Ras, Rho, YAP/TAZ), which potentiate cancer aggressiveness. On the other hand, the mevalonate pathway contributes to mutp53 stabilization, whilst mutp53 was shown to bind to and activate SREBP, thus upregulating mevalonate pathway-associated oncogenic proteins. As such, a positive-feedback loop between mutp53 and the mevalonate pathway is generated, and the inhibition of the mevalonate pathway by statins induces degradation of misfolded mutp53 and ultimately leads to reduced malignant properties of human cancer cells [326] (Table 1).

1.4.2.4**. Inhibitors of mutp53 aggregation**

Recent findings showed that mutp53 can form amyloid aggregates *in vitro* and *in vivo*, which play a crucial role in cancer development. p53 aggregation greatly contributes to the malignant properties of cancer cells, as it leads to the loss of p53 functionality, and the co-aggregation of mutp53 with other p53 family members, resulting in DNE of mutp53 [327]. Thus, the development of new drugs that can inhibit mutp53 aggregation will open new directions in cancer therapy. Mutp53 unfolded forms frequently expose specific self-adhesive amino acid segments (residues 252-258) in the p53 DBD, highly prone to aggregation, resulting in a favorable process of protein aggregation [328]. Based on this, the cell penetrating peptide Reacp53 was rationally designed to dock this region, preventing the amyloid-like aggregation of mutp53, converting aggregated mutp53 to a soluble wt-like p53 folded conformation, and triggering cell cycle arrest and cell death (Table 1). Reacp53 also exhibited activity in ovarian cancer organoids and inhibited intraperitoneal growth of mutp53-carrying ovarian cancer cells in mice [314].

1.5. Targeting p53 in cancer chemoprevention

Despite considerable advances in cancer treatment, the anticancer therapies currently available are of limited therapeutic efficacy and commonly associated with physical, emotional and social suffering to the patients. This strongly indicates that more attention should be devoted to prevention as an effective strategy to avoid the damaging impact of the disease. The premise that most cancers are preceded by a long latent period of premalignant lesions, which suppression would stop the carcinogenic process, has framed the concept of cancer prevention. The chemoprevention has therefore arisen to inhibit, delay or reverse the onset of cancer by using natural or synthetic agents [329]. In a clinical setting, the chemopreventive strategy can be classified as primary, secondary and tertiary. The first class encompasses the concept of chemoprevention for the general population and for people with increased susceptibility to develop cancer. The second class aims the prevention of premalignant lesions, avoiding the progression to more advanced stages. The third class is based on the prevention of disease recurrence or development of a second primary tumor in patients already subjected to therapy [330]. At the molecular level, the concept of cancer chemoprevention falls on the capacity of a certain drug to disrupt, or even to delay, pathways of the carcinogenic events without significant toxicity, given the expected long-term consumption regimens [331]. Since perturbations of p53 pathway can be observed across all stages of the neoplastic transformation, p53 represents a valuable molecular risk signature in cancer prevention. The assessment of *TP53* status may enhance the overall opportunity of risk reduction by identifying patients with premalignant conditions. Additionally, it may act as predictive marker for therapeutic response in cancer patients.

The concept of cancer prevention is particularly valuable in a context of mutp53-related LFS. In fact, since LFS carriers have a high probability of developing multiple tumors over their lifetime, risk management strategies to decrease cancer incidence and mortality mostly fall into cancer prevention and early detection (surveillance). In general, surveillance is more suitable for solid tumors, since normally the total resection of smaller tumors does not require chemo- or radiation therapy, minimizing for instance the risk of therapy-associated second cancers. The “Toronto protocol” includes a feasible multi-modal screening scheme, in which LFS individuals are closely monitored to improve their survival [332]. The management of cancers with germline *TP53* mutations has been the subject of intense debate and there are still no consensus recommendations. However, there is agreement in reducing the exposure to ionizing radiation and chemotherapy, to decrease the risk of therapy-associated second cancers, and in the type of chemotherapeutic agent chosen, particularly alkylating agents that are commonly associated with increased risk of leukemia or myelodysplasia development [181]. Several dietary compounds that specifically act in early stages of cellular transformation, by targeting p53, have been considered promising chemopreventive candidates for individuals at high-risk of cancer development, namely the phytochemicals curcumin [333-335] and its analogue HO-3867 [278], andrographolide, and D-limonene [336], resveratrol [337-341], epigallocatechin gallate [342-345], apigenin [346, 347], silibinin [348], isothiocyanates [349], and PEITC [297]. Also, a small pilot study found that LFS patients carrying *TP53* mutations typically present increased oxidative phosphorylation and oxygen consumption associated with their higher risk of developing cancer. In a subsequent study, it was uncovered that inhibition of mitochondrial respiration increased cancer-free survival in a mouse model of LFS expressing mutp53 [350]. Based on this, the authors suggested that the disruption of mitochondrial respiration using metformin would be considered for cancer prevention in LFS patients. In fact, metformin inhibits respiratory complex I, with consequent downregulation of OXPHOS and lower ATP production, inciting an energetic stress state, which may be detrimental for cancer proliferation [351]. Consistently, a phase I clinical study was carried out to assess the safety and tolerability of metformin in non-diabetic LFS patients [352]. Collectively, numerous *in vitro* and *in vivo* studies have unveiled several dietary compounds, particularly polyphenols, which seem to be safe and well-tolerated, and effective on attenuating various stages of carcinogenesis. The finding of mutp53 reactivation by these dietary compounds has further reinforced their promising application in cancer prevention, especially in LFS individuals. However, results are frequently controversial and inconsistent since these compounds also present p53-independent cytotoxic effects. More studies are required to further elucidate their mechanism of action, which will be essential for their successful clinical translation as chemopreventive agents.

Additionally, the chemopreventive effect of several synthetic p53-activating agents has also been explored. In particular, the preventive potential of two p53 activators, CP-31398 and PRIMA-1 (described in the previous section), was investigated on 4-(methylnitrosamino)-1-(3-pyridyl)-1-butanone (NNK)-induced lung adenoma and adenocarcinoma formation in mice [353]. The oral intake of CP-31398 or PRIMA-1 by mice significantly suppressed the lung adenocarcinoma formation and delayed the progression of adenoma to adenocarcinoma. Moreover, the immunohistochemical analysis of lung tumors from the exposed mice showed a significant reduction of tumor growth with wtp53 nuclear accumulation and increased p21 and apoptotic-positive cells [353]. The preventive effect of CP-31398 on the incidence of spontaneously occurring epithelial ovarian and oviductal carcinomas of egg-laying hens (with similar clinical and molecular ovarian cancer alterations to humans, including the high frequency of mutp53) was also evaluated [354]. The authors verified a significant reduction in the incidence of localized and metastatic ovarian cancer with moderate- and high-doses of CP-31398, supporting the effectiveness of CP-31398 in ovarian cancer prevention. In another study, it was demonstrated that CP-31398 inhibited UVB-induced skin carcinogenesis in mice through restoration of mutp53 activity [355]. As CP-31398 and PRIMA-1, it would be of great interest to investigate other p53 reactivators with demonstrated *in vitro* and *in vivo* antitumor activity, such as SLMP53-1 [239] and SLMP53-2 [240], as potential chemopreventive agents in cancer-prone LFS individuals.

1.6. Aims

The present doctoral thesis focused on advancing the knowledge related to the biology and pharmacology of the tumor suppressor p53, envisioning new and improved anticancer therapeutic opportunities by targeting p53. Particularly, it was intended to:

i) Further elucidate the molecular mechanism of action of the wt- and mutp53 reactivator SLMP53-1 (**Chapter 2**);

ii) Exploit the ability of SLMP53-1 to induce non-canonical p53 antitumor responses, through modulation of glucose metabolism of cancer cells (**Chapter 3**);

iii) Identify improved p53-activating agents, with potential clinical application as anticancer drug (**Chapter 4**).

To carry out the proposed goals, the thesis encompassed a multidisciplinary research approach, integrating different scientific areas, namely molecular biology, pharmacology, microbiology, oncobiology, biotechnology, and medicinal chemistry.

CHAPTER 2

SLMP53-1 interacts with wild-type and mutant p53 DNA-binding domain and reactivates multiple hotspot mutations

Ana Sara Gomes[#], **Helena Ramos[#]**, et al, 2020. *SLMP53-1 interacts with wild-type and mutant p53 DNA-binding domain*. Biochim Biophys Acta Gen Subj, 1864 (1), 129440. DOI: 10.1016/j.bbagen.2019.129440

[#]Authors equally contributed to this work

2.1. Background

Reactivation of mutp53 through restoration of wt-like function represents one of the most promising therapeutic strategies in cancer treatment [182]. Although several small molecule mutp53 reactivators have been reported to date, only two (PRIMA-1^{MET} and COTI-2) are under clinical trials, and so far, none has reached the clinic [268, 293, 315, 356]. Recently, our group have reported the (*S*)-tryptophanol-derived oxazoloisoindolinone, SLMP53-1, as a new activator of wtp53 with the ability to also reactivate contact mutp53 R280K [239, 357]. SLMP53-1 restored DNA-binding ability, and subsequent transcriptional activity, to mutp53 R280K. Additionally, it displayed *in vitro* and *in vivo* p53-dependent antitumor activity against tumors bearing wtp53 or mutp53 R280K, with no apparent undesirable toxicity [239]. However, there was still a lack of understanding about the molecular mechanism by which SLMP53-1 reactivates mutp53 R280K, as well as its potential to reactivate other mutp53 besides R280K. An additional aspect requiring further elucidation was related to the inactivity of SLMP53-1 (*R*)-enantiomer [239]. In this chapter, these issues were deeply investigated/analyzed.

2.2. Materials and methods

2.2.1. Compounds

The (*S*)-tryptophanol-derived oxazoloisoindolinone SLMP53-1 was synthesized as described [239]. For all experiments, SLMP53-1 was dissolved in dimethyl sulfoxide (DMSO) from Sigma-Aldrich (Sintra, Portugal).

2.2.2. Construction of yeast and mammalian expression vectors

2.2.2.1. Yeast expression vectors

The yeast expression vectors pLLS89 (GAL1–10, *LEU2*) encoding full-length human mutp53 (R175H, G245D, G245S, R248Q, R248W, R273H, R273C or R282W) were constructed through SgraI/StuI (New England Biolabs, Ipswich, Massachusetts, USA) digestion of available pLS76 (*ADH1*, *LEU2*) vectors [358], and subsequent ligation (T4 DNA ligase, New England Biolabs) of the gel purified mutp53 fragment in a SgraI/StuI digested and gel purified pLLS89-based vector (generous gift of Prof. Alberto Inga). The creation of the mutp53 expression vectors was confirmed after XL1-Blue *Echerichia coli* extraction (GenEluteTM Plasmid Miniprep Kit, Sigma-Aldrich, St. Louis, Missouri, USA) by digestion and DNA sequencing (BMR Genomics, Padua, Italy).

2.2.2.2. Mammalian expression vectors

The full-length coding sequence of mutp53 was PCR-amplified from the yeast vector with Vent DNA polymerase (New England Biolabs, Werfen, Porto, Portugal), using the primers pair 5′ GG**G GTA CC**A TGG AGG AGC CGC AGT CAG 3′ and 5′ CCG **CTC GAG** TCA GTC TGA GTC AGG CCC TTC 3′, where the restriction sites for KpnI/XhoI (in bold) were included, respectively. The PCR products and the mammalian expression vector pcDNA3 (Invitrogen, Alfagene, Lisboa, Portugal) were digested with KpnI/XhoI (New England Biolabs, Werfen), purified from agarose gel, and ligated with T4 DNA ligase (Promega, VWR, Carnaxide, Portugal), originating the expression vectors pcDNA3-mutp53. These constructs were propagated in NZY5α *Echerichia coli* cells (NZYTech, Lisboa, Portugal) as described [359]. The sequence of each mutp53 in the constructed vectors was confirmed by sequencing (Eurofins GATC Biotech, Konstanz, Germany) with specific pcDNA3 primers. pcDNA3-mutp53 vectors were extracted using the PureYieldTM Plasmid Miniprep System kit (Promega, VWR).

2.2.3. Modeling

The starting structure for the modeling was the crystal structure of the wtp53 DBD tetramer bound to a DNA target (Protein Data Bank (PDB) code: 2AC0) [55]. Missing hydrogen atoms were added to these structures according to the assigned protonation states. The DNA bound mutp53 R280K was obtained by replacing the guanidine group in residue 280 by the butylammonium side chain of lysine in the wtp53 model, and was subjected to a geometry optimization with the Amber 18 (parm99SB) force field [360].

The ligands (*S*)-tryptophanol-derived oxazoloisoindolinone SLMP53-1 and the corresponding enantiomer (*R*)-tryptophanol-derived oxazoloisoindolinone were geometry optimized in Gaussian09 using B3LYP [361] and a Polarizable Continuum Model (PCM) solvent description [362]. Atomic partial charges were calculated resorting to the Restrained Electrostatic Potential (RESP) method [363] from HF/6- 31G(d) single point energy calculations. The zinc atoms in p53 were described with the semi-bonded model [364, 365].

2.2.3.1. Molecular docking

The ligands SLMP53-1 and respective enantiomer were docked to the wtp53 and mutp53 R280K DBD models. Molecular docking was performed using the AutoDock 4.2 suite of programs with the Lamarckian genetic algorithm (LGA) [366]. A grid box was centered on residue 280 of chain A. A total of 100 LGA runs were carried out for each DNA:protein complex or free protein. The population was 300, the maximum number of generations was 27,000 and the maximum number of energy evaluations was 2,500,000.

2.2.3.2. Molecular dynamics (MD) simulations

MD simulations were performed for the following complexes: DNA:wtp53 with SLMP53-1 and its enantiomer; DNA:mutp53 R280K with SLMP53-1 and its enantiomer. All MD simulations were performed using the Amber 18 molecular dynamics program with the parm99SB [360] and GAFF force fields [367]. The structures were placed within an octahedral box of TIP3P waters [368, 369] and counter ions were added to make the entire system neutral. The systems were subjected to two initial energy minimizations and to 500 ps of equilibration in a NVT ensemble using Langevin dynamics with small restraints on the protein (10 kcal/mol) to heat the system from 0 to 300 K. Production simulations were carried out at 300 K in the NPT ensemble using Langevin dynamics with a collision frequency of 1.0 ps^{-1}. Constant pressure periodic boundary conditions were imposed with an average pressure of 1 atm. Isotropic position scaling was used to maintain pressure with a relaxation time of 2 ps. The time step was set to 2 fs. SHAKE constraints were applied to all bonds involving hydrogen atoms [370, 371]. The particle mesh Ewald (PME) method [372] was used to calculate electrostatic interactions with a cut off distance of 10 Å. Three replicas with different initial velocities were performed for each system. The total combined time of the simulations was 280 ns. The reference structures of the simulations were calculated as described [373].

2.2.4. Yeast assay

Saccharomyces cerevisiae CG379 (Yeast Genetic Stock Center, University of California, Berkeley, CA, USA) was transformed with the pLLS89 expressing human mutp53 (or empty vector as control) obtained in 2.2.2.1., using the LiAc/SS Carrier DNA/PEG method [374]. Yeast cells expressing human wtp53 were obtained in previous work [239]. For expression of human wt or mutp53, cells (routinely grown in minimal selective medium) were incubated in galactose selective medium with all the amino acids required for yeast growth (50 µg/mL) except leucine as described [239], in the presence of 10 µM of SLMP53-1 or 0.1% DMSO, for approximately 42 h (time required by control yeast incubated with DMSO to achieve 0.4 OD_{600}). Yeast growth was analyzed by colony forming unit (CFU) counts as described [239]. Percentage of growth inhibition was calculated considering the wtp53-induced yeast growth inhibition as 100%.

2.2.5. Human tumor cell lines and growth conditions

Colon adenocarcinoma wtp53-expressing HCT116, breast adenocarcinoma MDA-MB-23 and MDA-MB-468, and human non-small cell lung cancer H1299 human cell lines (Annex I, Table S1) were cultured in RPMI-1640 with UltraGlutamine (Lonza, VWR), supplemented with 10% fetal bovine serum (Merck Millipore, VWR), and incubated at 37 °C with 5% CO_2. Cells were routinely tested for mycoplasma infection using the MycoAlert™ PLUS mycoplasma detection kit (Lonza, VWR). Cells were recently characterized and authenticated, by short tandem repeat DNA profiling [375].

2.2.6. Cellular thermal shift assay (CETSA)

To evaluate drug target interactions in cells, the CETSA analysis was performed basically as described [241, 376, 377]. Briefly, HCT116 or MDA-MB-231 cell lysates were incubated with SLMP53-1 or solvent for 1 h at room temperature, and then heated at different temperatures for 3 min, cooled to room temperature for 3 min, and placed on ice. Soluble protein was detected by western blot. At 39 °C (HCT116) or 40 °C (MDA-MB-231), the increase in non-denatured p53 of lysates treated with 1 – 50 μM SLMP53-1 was calculated relative to solvent at 25 °C, set as 1.

2.2.7. Transient transfection assay of mutp53 in human H1299 tumor cells

H1299 cells were transfected at 7.5×10^3 cells/well density in 96-well plates with 75 ng of the pcDNA3-mutp53 (or empty vector) constructed in 2.2.2.2., using ScreenFect®A (Screenfect GmbH, GRiSP, Porto, Portugal) according to the manufacturer's instructions.

2.2.8. Sulforhodamine B (SRB) assay

H1299 transfected cells were seeded in 96-well plates at 7.5×10^3 cells/well density, followed by analysis of SLMP53-1 effect on cell proliferation after 48 h treatment with serial dilutions (3.13 – 50 μM) of compound, as described [237]. The solvent (DMSO; maximum concentration used 0.25%) was included as control. Half maximal inhibitory concentration (IC_{50}) values were determined as described [237].

2.2.9. Western blot analysis

To evaluate the expression levels of human wt and mutp53 in yeast, cells were grown in galactose selective medium for 42 h. To evaluate the expression levels of p53 targets (in MDA-MB-468 cells) and ectopic human mutp53 (in transfected H1299 cells), cells were seeded in 6-well plates at 2.25×10^5 cells/well density for 48 h. Yeast and human tumor cells were lysed and protein fractions were analyzed as described [237]. Briefly, Protein fractions were quantified using the Pierce BCA Protein Assay Kit (Bioportugal, Porto, Portugal). Proteins were run in SDS–PAGE and transferred to a Whatman nitrocellulose membrane from Protan (VWR). After membranes blocking, proteins were probe using specific primary antibodies followed by HRP-conjugated secondary antibodies, all listed in Annex I, Table S2. GAPDH was used as loading control. The signal was detected with the ECL Amersham kit from GE Healthcare (VWR) and the detection was made by

ChemiDoc Imaging Systems (Bio-Rad, Amadora, Portugal). Band intensities were quantified using the Image Lab software v6.0.1 (Bio-Rad). Signal intensity is relative to the respective loading and normalized to control (DMSO) set as 1.

2.2.10. Statistical analysis

Data were statistically analyzed using the GraphPad Prism software v7.0 (San Diego, CA, USA). Differences between means were tested for significance using the Student's *t*-test (**$p < 0.01$; ***$p < .001$).

2.3. Results

2.3.1. SLMP53-1 binds to wt and mutp53 R280K

To uncover the molecular mechanism by which SLMP53-1 reactivates wtp53 and mutp53 R280K, we performed the CETSA analysis. This technique enlightens about the possibility of direct binding of small molecules to macromolecules. Specifically, it gives insights about the ability of small molecules to induce thermal stabilization of cellular proteins as a consequence of intermolecular interactions [378]. As such, using HCT116 and MDA-MB-231 tumor cells expressing wtp53 and mutp53 R280K, respectively, it was evaluated the impact of SLMP53-1 on wt and mutp53 R280K thermal stabilization. For that, the amount of soluble wt and mutp53 R280K was measured upon heating of HCT116 or MDA-MB-231 cell lysates. In fact, whereas unbound (non-stabilized) proteins denature and precipitate after heating, ligand-bound (stabilized) proteins remain in solution [378]. The results showed that 10 μM SLMP53-1 induced a slight mutp53 R280K thermal stabilization at 39 °C and 40 °C (Figure 9A). Consistently, at 40 °C, SLMP53-1 caused concentration-dependent mutp53 R280K thermal stabilization, with a two-fold increase of non-denatured mutp53 R280K thermal stabilization achieved at 50 μM SLMP53-1, when compared to solvent (Figure 9B). In fact, considering the amount of mutp53 R280K obtained with DMSO at 25 °C, a complete protein stabilization was achieved with 50 μM SLMP53-1 at 40 °C. Similarly, in wtp53-expressing tumor cells, SLMP53-1 induced a dose-dependent thermal stabilization at 39 °C (Figure 9C), with a complete stabilization achieved with 10 μM (Figure 9C). These results showed that SLMP53-1 led to wt and mutp53 R280K thermal stabilization, which was indicative of intermolecular interactions between the compound and wt/mutp53.

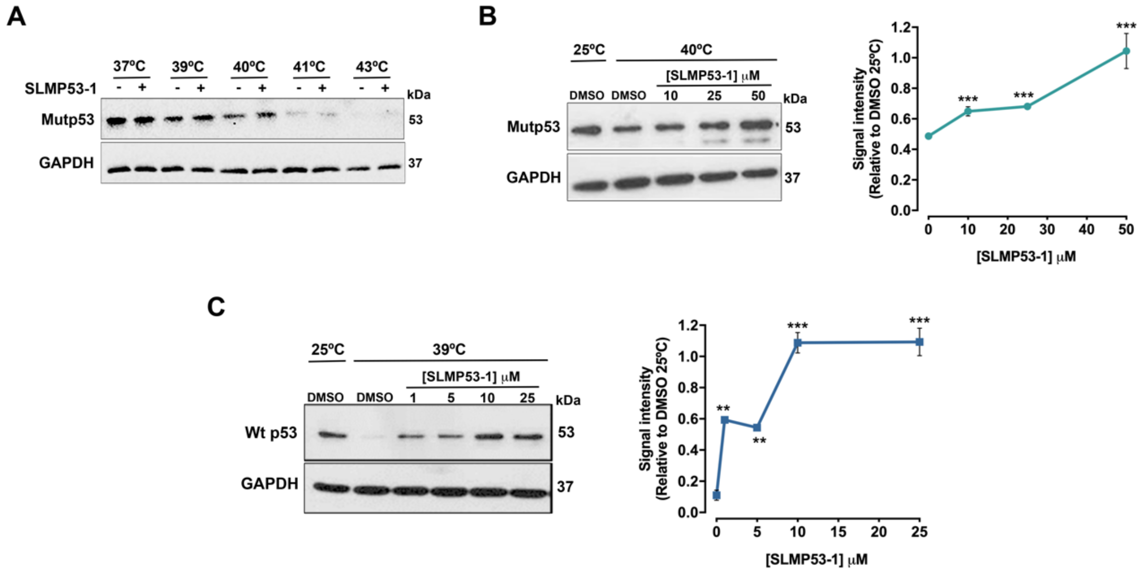

Figure 9. SLMP53-1 thermally stabilizes wt and mutp53 R280K. CETSA experiments were performed in mutp53 R280K-expressing MDA-MB-231 lysates **(A** and **B)** and in wtp53-expressing HCT116 lysates **(C)**. **(A)** Lysate samples treated with DMSO (−) or 10 μM SLMP53-1 (+) were heated at different temperatures; immunoblot represents one of three independent experiments. Lysate samples treated with increasing concentrations of SLMP53-1 were heated at 40 °C **(B)** or 39 °C **(C)**; immunoblot represents one of five independent experiments; plotted data represent the amount of non-denatured mutp53 after heating in SLMP53-1-treated lysates relatively to DMSO at 25 °C (set as 1); data are mean ± SEM of five independent experiments; values significantly different from DMSO at 40 °C: $**p < 0.01$, $***p < 0.001$ (unpaired Student's *t*-test). In (A-C), GAPDH was used as a loading control.

2.3.2. SLMP53-1 potentially binds to a hydrophobic pocket formed at the interface of the p53 homodimer with the DNA minor groove

To predict SLMP53-1 binding in a more biologically relevant context with p53 DNA recognition, the models of wt and mutp53 R280K DBD tetramer in complex with DNA were used. Consistently with previous data [55], the MD simulations showed that, in the wtp53 DBD crystal structure, the R280 establishes two hydrogen bonds with a conserved guanine base at the DNA major groove (Figure 10A). Moreover, as reported [359] in mutp53 R280K, the arginine to lysine substitution abolishes these direct interactions with DNA (Figure 10A), and no substantial differences were found in the structural motifs' conformational rearrangements. Docking and MD simulations of wt and mutp53 R280K DBD with SLMP53-1 showed that the compound binds at the interface of the p53 homodimer with the minor groove of the DNA target half-site (Figure 10B). This pocket is located on the opposite DNA side from residue 280. SLMP53-1 interacted with p53, mainly with a methionine from each monomer (M243A and M243B), through its indole moiety via sulfur-π and methyl-π interactions, being closer to M243A (Figure 10B and C; Annex II, Table S5). Furthermore, these interactions were closer in mutp53 R280K:SLMP53-1 compared to wtp53:SLMP53-1 complex (Annex II, Table S5). The isoindolinone moiety of SLMP53-1 further established stacking interactions with the DNA bases (DA18, DT19, DA6, DT7), and a hydrogen bond (with DG12) through its carbonyl group (Figure 10B and C; Annex II, Table S5). Consequently, the loss of direct contacts between residue 280 and the DNA major groove was partially compensated by the indirect protein-DNA interactions mediated by SLMP53-1 at the DNA minor groove (Figure 10B and C). Although the SLMP53-1 enantiomer could bind to the same pocket in the wtp53 and mutp53 R280K DBD models, its different arrangement prevented the formation of the same interactions established by SLMP53-1 with p53. In fact, due to its spatial orientation, the SLMP53-1 enantiomer interacted mainly with the DNA minor groove in detriment of protein interactions (Figure 10D), justifying its inactivity as a mutp53 reactivator [239].

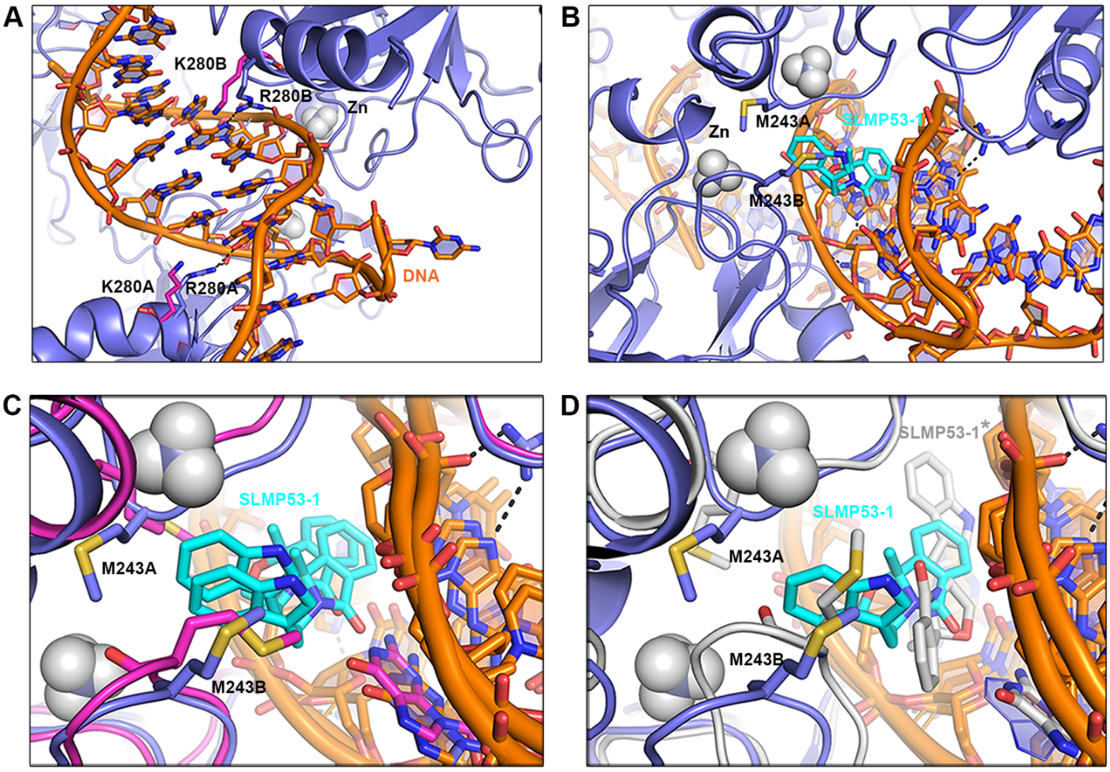

Figure 10. SLMP53-1 potentially binds at the interface of the p53 homodimer with the DNA minor groove. (A-D) MD reference structures. **(A)** Image from the DNA major groove side showing the wtp53:SLMP53-1 complex superposed with mutp53 R280K:SLMP53-1 complex (only residue K280, in pink, is depicted from the mutp53 R280K:SLMP53-1 complex). **(B)** Image from the DNA minor groove side showing the binding of SLMP53-1 to the protein and to the DNA. **(C)** Superposition of wtp53:SLMP53-1 complex (in purple) with mutp53 R280K:SLMP53-1 complex (in pink) showing the similar binding pose for SLMP53-1. **(D)** wtp53:SLMP53-1 complex (in purple) superposed with wtp53:SLMP53-1 enantiomer (*) complex (in gray).

2.3.3. SLMP53-1 reactivates distinct hotspot mutp53

It was previously demonstrated that SLMP53-1 was able to restore wt-like function to contact mutp53 R280K, but not to structural mutp53 Y220C [239]. Based on that, we interrogated whether the activity of SLMP53-1 was restricted to mutp53 R280K, or instead it would be also observed in other mutp53, including structural mutp53. To answer this question, the yeast assay, previously developed to screen reactivators of mutp53 R280K and Y220C [239], was extended to other contact (R248Q, R248W, R273H, R273C) and structural (R175H, G245D, G245S, R282W) mutp53, known for their high prevalence and clinical relevance in human cancers [184, 205, 379]. To this end, the heterologous expression of each human mutp53 was carried out in yeast, and their effect on the growth of transformed yeast was analyzed (Figure 10A and B). By western blot analysis, we confirmed no substantial differences among mutp53 protein expression levels (Figure 11A). Contrary to the growth inhibitory effect induced by wtp53, none of the expressed mutp53 considerably interfered with yeast cell growth (Figure 11B, DMSO; Annex II, Figure S1). Since potential reactivators of mutp53 would restore the wt-like growth inhibitory effect to mutp53 expressed in yeast, as observed for R280K [239], we next evaluated the effect of SLMP53-1, at 10 µM (concentration that caused the maximal effect on mutp53 R280K, reestablishing over 79% of wtp53-induced growth inhibitory effect) [239], on the growth of mutp53-expressing yeast cells. Despite the negligible effect on G245S and R273C, SLMP53-1 was able to restore more than 50% of the wtp53-induced growth inhibition to the remaining tested mutp53 (Figure 11B).

To validate the results obtained in yeast, the effect of SLMP53-1 was evaluated on the same set of hotspot mutp53 ectopically expressed in p53-null H1299 tumor cells, through analysis of cell proliferation by SRB assay, after 48 h treatment (Figure 11C and D). No considerable differences among mutp53 protein expression levels were detected by western blot analysis in mutp53-transfected H1299 cells (Figure 11C). Notably, like in yeast, SLMP53-1 caused a significant reduction of the IC_{50} values in H1299 cells expressing R175H, G245D, R248Q, R248W, R273H, and R282W, when compared to empty vector (Figure 11D). These results further supported the ability of SLMP53-1 to reactivate distinct contact and structural hotspot mutp53. Moreover, they reinforced the mutp53-dependent cytotoxic effect of SLMP53-1 evidenced in previous work by knocking down mutp53 R280K by siRNA, in MDA-MB-231 tumor cells [239]. To further confirm the growth inhibition induced by SLMP53-1 in mutp53-transfected tumor cells, this effect was also evaluated in human breast adenocarcinoma MDA-MB-468 cells endogenously expressing one of the most prevalent hotspot mutp53 (R273H). As expected, a significant growth arrest was observed (Figure 11E) with an IC_{50} value of 10.3 ± 2.4 µM (n = 5) determined by SRB assay, after 48 h treatment with SLMP53-1. This was associated with alterations in the protein levels of p53 transcriptional targets. In fact, 10.3 μM SLMP53-1 increased the levels of the cell cycle inhibitor p21 and the pro-apoptotic protein PUMA, while decreasing the anti-apoptotic BCL-2 protein levels (Figure 11F).

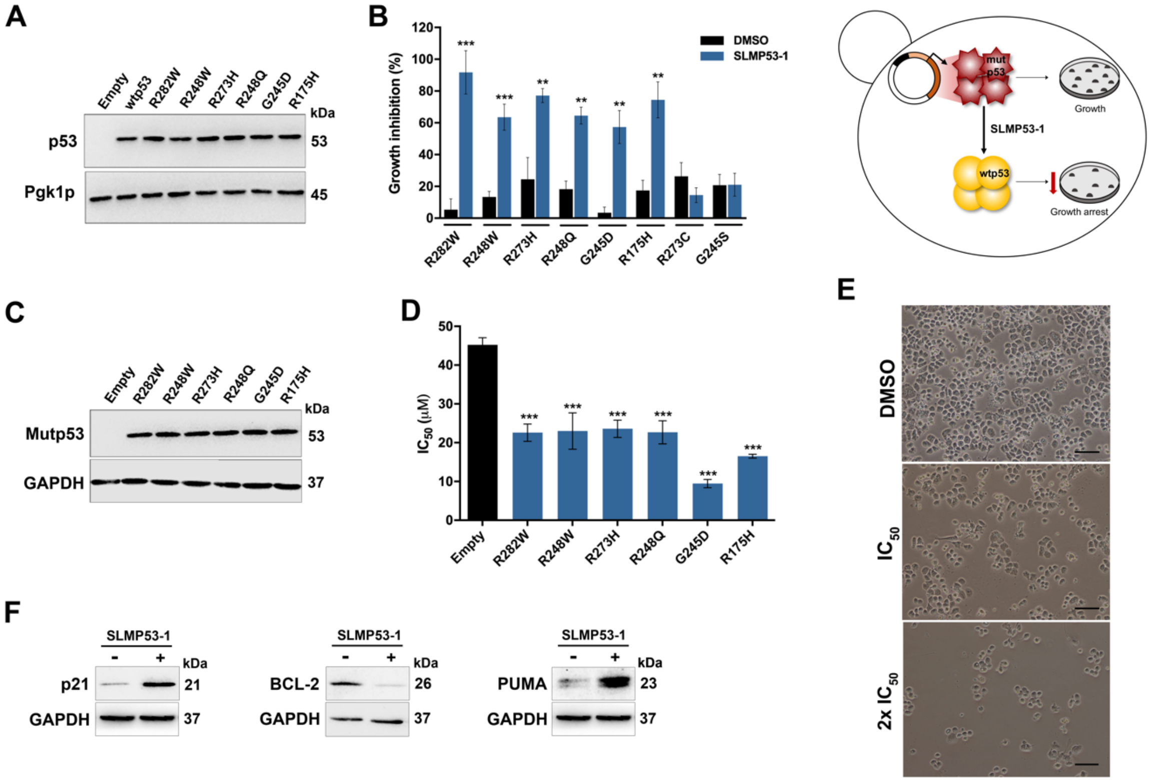

Figure 11. SLMP53-1 reactivates distinct hotspot mutp53. (A) Immunoblot of human wt and mutp53 expressed in yeast, after 42 h incubation of yeast cells treated with solvent; results represent one of three independent experiments; Pgk1p was used as loading control. **(B)** Percentage of wt-like growth inhibition obtained in mutp53-expressing yeast treated with 10 μM SLMP53-1 or DMSO, for 42 h (yeast assay is schematically represented). Plotted data correspond to the percentage of growth inhibition achieved with wtp53-expressing yeast cells treated with DMSO (set as 100%); data are shown as mean ± SEM of 4–8 independent experiments; values significantly different from DMSO: $^{**}p < 0.01$; $^{***}p < 0.001$ (unpaired Student's *t*-test). **(C)** Immunoblot of mutp53 ectopically expressed in p53-null H1299 tumor cells after 72 h incubation; results represent one of three independent experiments; GAPDH was used as loading control. **(D)** Growth inhibitory effect of SLMP53-1 on H1299 tumor cells transfected with pcDNA3 encoding human mutp53 (or empty vector). Plotted data of IC_{50} values were determined by SRB assay after 48 h treatment with SLMP53-1; data are shown as mean ± SEM of 3–8 independent experiments; values significantly different from empty vector: $^{***}p < 0.001$ (unpaired Student's *t*-test). **(E)** Representative microscopy images of MDA-MB-468 cells treated with IC_{50} (10.3 μM) and 2× IC_{50} (20.6 μM) SLMP53-1 or DMSO, for 48 h (Scale bar = 50 μm, magnification = ×200). **(F)** Protein levels of p53 targets p21, PUMA, and BCL-2, after 48 h treatment with 10.3 μM SLMP53-1 (+) or DMSO (−), in MDA-MB-468 cells. Immunoblots are representative of three independent experiments.

2.4. Discussion

The promising pre-clinical results attained with SLMP53-1 in our previous work [239] led us to further delve into the molecular mechanism of action of this potential anticancer drug candidate. The results obtained in this work support a direct interaction of SLMP53-1 to wt and mutp53 with subsequent enhancement of their thermal stability. It is worth noting that despite this thermal stability, additional results unveiled that SLMP53-1 did not interfere with wt/mutp53 half-life (Annex II, Figure S2), supporting that its activity is not related to an inhibition of p53 degradation pathways. Most importantly, in a complementary work to that carried out in this thesis, the direct interaction of SLMP53-1 to mutp53 was confirmed by microscale thermophoresis (MST) analysis, using recombinant human mutp53 R280K DBD (Kd of 10.7 μM, Annex II, Figure S3).

To better understand the binding mode of SLMP53-1 to wt and mutp53 R280K, *in silico* docking studies were performed using structural models of wtp53 tetramer in complex with DNA, and the equivalent model with R280K mutagenesis. With this strategy, we intended to simulate a more biologically relevant context, in which the p53 transcriptional activity depends on its DNA-binding ability. In fact, it was previously demonstrated that SLMP53-1 enhanced wtp53 and mutp53 R280K DNA-binding ability, at the promoter regions of target genes, and subsequent transcriptional activity [239]. In the presence of DNA, the p53 protein organizes as a dimer of dimers (homotetramer) [380]. The results showed that SLMP53-1 binds to a hydrophobic pocket of the p53 homodimer, establishing an interface with the DNA minor groove, and compensating for the loss of direct contacts between the K280 residue and the DNA. Interestingly, the superposition of wt and mutp53 R280K models showed that SLMP53-1 has a similar binding pattern to the wtp53 model, which is consistent with the reported activation of wtp53 by SLMP53-1 [239]. The *in silico* studies also revealed that SLMP53-1 enantiomer presented different binding pattern to p53, therefore justifying the described inability of the SLMP53-1 enantiomer to activate both wt and mutp53 R280K [239]. In fact, whereas SLMP53-1 interacts with the protein via sulfur-π and sulfur-hydrogen bonds and with DNA via stacking interactions and a hydrogen bond, its enantiomer interacts mainly with the DNA minor groove. As such, SLMP53-1 seems to bridge an extra interaction between the protein and DNA, on the opposite site to the mutation, rescuing the DNA binding and subsequent transcription activity to mutp53.

This work also showed that, besides wt and mutp53 R280K [239], SLMP53-1 also has the ability to reactivate other hotspot p53 mutations with high clinical relevance. The ability of SLMP53-1 to activate wtp53, as well as contact and structural mutp53, supports that its molecular mechanism of action is irrespective of the formation of pockets derived from specific mutation sites. In fact, *in silico* models of wtp53, contact mutp53 R280K, and structural mutp53 R282W (Annex II, Figure S4) indicate that the region of L3 (involved in the homodimer interface) is also conserved in this particular structural mutp53.

Altogether, the results herein obtained denote a distinct molecular mechanism of mutp53 reactivation by SLMP53-1, non-dependent on covalent bonds or mutation-created hydrophobic pockets as described for other mutp53 reactivators. In fact, PRIMA-1^{MET} is transformed into a metabolite that is a Michael acceptor, which binds covalently to p53 free cysteines (C124 and C277), with adducts formation, inducing protein stabilization in both contact and structural mutp53 [270, 276]. On the other hand, the carbazole PK08325 and the pyrazole derivative PK708826 bind to a hydrophobic pocket in the cleft induced by the Y220C amino acid substitution in mutp53 structure [280, 281]. Since wt and many mutp53 do not have well-defined pockets to accommodate ligands (particularly contact mutants, such as R280K), our work highlights alternatives to the design and development of new mutp53 reactivators. Consistently, it was previously suggested that an interesting strategy to reactivate mutp53 would rely on bridging the interaction between the protein and DNA through a small molecule [381]. Furthermore, an *in silico* study of mutp53 R273H with curcumin, alpinetin and flavokawain has hypothesized that these small molecules might also rescue mutp53:DNA contact by binding between the protein and DNA next to the mutation site [382].

It is worth noting that this work also validates the yeast model as a reliable cell system for the high-throughput screening of mutp53 reactivators. This simplified and highly effective yeast-based assay may streamline the identification of improved mutp53 reactivators with therapeutic application in cancer treatment.

Interestingly, all mutp53 tested appear to have a similar functional activity in yeast. Nevertheless, this homogeneity contrasts with the heterogeneous ability of SLMP53-1 to reactivate mutp53 occurring at the same codon but with different amino acid substitutions. Thus, it would be worth doing further studies to better understand the inability of SLMP53-1 to reactivate mutp53 Y220C, R273C, and G245S. By addressing this issue, deeper insights on mutp53 pharmacology will be achieved, paving new ways in anticancer drug discovery by targeting mutp53.

CHAPTER 3

SLMP53-1 inhibits tumor cell growth through regulation of glucose metabolism and angiogenesis in a p53-dependent manner

Helena Ramos, et al, 2020. *SLMP53-1 inhibits tumor cell growth through regulation of glucose metabolism and angiogenesis in a p53-dependent manner*. Int J Mol Sci, 21 (2). DOI: 10.3390/ijms21020596

3.1. Background

As mentioned in the Literature Overview (item 1.2.2.2.), a common property of cancer cells is an altered glucose metabolism compared to normal cells [7]. Even in the presence of sufficient oxygen, most cancer cells increase glucose consumption and convert it to lactate, instead of relying on mitochondrial OXPHOS [7, 383]. In fact, the Warburg effect confers several advantages to cancer cells, favoring its unrestrained proliferation and dissemination [142].

Numerous studies have shown that p53 intervenes at many steps in the glucose metabolism by slowing down glycolysis and promoting OXPHOS [161]. Herein, we carried out an in-depth analysis of the molecular events underlying the antitumor activity of the (*S*)-tryptophanol-derived oxazoloisoindolinone (SLMP53-1) [239], by studying its effect on glucose metabolism and angiogenesis.

3.2. Materials and Methods

3.2.1. Compounds and reagents

The (*S*)-tryptophanol-derived oxazoloisoindolinone (SLMP53-1) was synthesized by using the protocol previously described in [239]. For all experiments, SLMP53-1 was dissolved in DMSO from Sigma-Aldrich (Sintra, Portugal). Dichloroacetic acid (DCA) from Sigma-Aldrich was dissolved in water.

3.2.2. Human cell lines and growth conditions

Human colon adenocarcinoma HCT116 cells (Annex I, Table S1) were routinely cultured as described in Chapter 2 (section 2.2.5.). Dermal microvascular endothelial HMVEC-D cells (Lonza, VWR, Carnaxide, Portugal) were cultured in endothelial cell growth basal medium supplemented with SingleQuots™ Kit (Lonza, VWR). Both cells were maintained at 37 °C in a humidified atmosphere of 5% CO_2, and routinely tested for mycoplasma, as described in Chapter 2 (section 2.2.5.). Cells were recently characterized and authenticated using short tandem repeat DNA profiling.

3.2.3. Immunohistochemistry (IHC)

Tumor tissues from $p53^{+/+}$ and $p53^{-/-}$ colon HCT116 cancer xenografts treated with 50 mg/kg SLMP53-1 or vehicle by intraperitoneal injection twice a week, for a total of five administrations, were obtained in a previous study [239]. Tissues were fixed in 10% formalin, embedded in paraffin, sectioned at 4 μm, and stained with hematoxylin and eosin

(H&E) or antibodies, as described in [239]. Briefly, antigen retrieval was performed by boiling the sections for 20 min in citrate (pH 6.0) or EDTA (pH 8.0) buffer. Antibodies used are listed in Annex I, Table S2. Immunostaining was performed by using the UltraVision Quanto Detection System HRP DAB Kit, from Lab Vision Thermo Scientific (Grupo Taper SA, Sintra, Portugal), according to the manufacturer's instructions. Evaluation of DAB (3,3′-diaminobenzidine) intensity and quantification of marked cells were performed by using Image J software (Laboratory for optical and computational instrumentation, University of Wisconsin-Madison, USA). Images were obtained by using an Eclipse E400 fluorescence microscope (Nikon) with ×200 magnification, with a Digital Sight camera system (Nikon DS-5Mc) and software Nikon ACT-2U, from Izasa Scientific (Carnaxide, Portugal).

3.2.4. Western Blot

To evaluate the expression levels of HK2, GLUT1, PFKFB3, SCO2, cytochrome *c* oxidase subunit 4 (COX4), E-CAD, N-cadherin (N-CAD), and VEGF1, HCT116 cells were seeded in 6-well plates at 1.5×10^5 cells/well density for 24 h. Cancer cells were lysed and protein fractions were analyzed as described in Chapter 2 (section 2.2.9.); GAPDH or α-Tubulin were used as loading controls. Antibodies used are described in Annex I, Table S2.

3.2.5. Measurement of extracellular lactate

The levels of lactate exported by HCT116 were determined using the Lactate-Glo^{TM} assay kit (Promega, J5021, VWR), according to the manufacturer's instructions. Briefly, 5.0×10^3 HCT116 cells/well were seeded in 96-well plates, followed by treatment with SLMP53-1 or solvent for 24 h. The culture medium was then collected and diluted in phosphate saline buffer. After that, 50 µL was transferred to a 96-well assay plate, and 50 µL of Lactate Detection Reagent was added. After 60 min at room temperature, luminescence was read by using the BioTek Synergy HT plate reader (Izasa Scientific).

3.2.6. Angiogenesis assay

Endothelial tube formation was evaluated by using the *in vitro* Angiogenesis Assay Kit (Millipore, VWR) according to the manufacturer's instructions. Briefly, 3×10^4 HMVEC-D cells/well were seeded in 24-well plates coated with ECMatrix, treated with SLMP53-1 or solvent for 12 h. Cells were photographed by using the inverted Nikon TE 2000-U microscope at ×100 magnification, with a DXM1200F digital camera and NIS-Elements microscope imaging software (VWR).

3.2.7. Generation of colon cancer spheroids

HCT116 cells were resuspended in serum-free stem cell culture media consisting of DMEM/F12 supplemented with 10 ng/mL of bFGF, 20 ng/mL of EGF from Biotechne (Citomed Lda, Lisboa, Portugal), 1 × B27 from Life Technologies (Porto, Portugal), and 5 µg/mL of insulin (Sigma-Aldrich). HCT116 cells were plated in 24-well ultra-low attachment plates (one spheroid per well; Corning Inc., Sigma-Aldrich), at a density of 1×10^3 cells/well [384]. To assess the synergistic effect of SLMP53-1 with DCA in spheroids development, colonospheres were allowed to form for 3 days, followed by treatment with 20 µM SLMP53-1 and/or 12 mM DCA, for an additional 9 days. During this period of time, new medium with the drugs (or DMSO only) was added to the wells each three days. Spheroids were photographed by using an inverted Nikon TE 2000-U microscope at ×100 magnification, with a DXM1200F digital camera and NIS-Elements microscope imaging software (VWR). Determination of spheroids diameter was performed by using Image J software.

3.2.8. Combination therapy assays

To assess the synergistic effect of SLMP53-1 with DCA, HCT116 cells were treated with 9 µM SLMP53-1 and/or increasing concentrations of DCA (5.93 – 20 mM) for 48 h. The effect of combined treatments on cell proliferation was analyzed by SRB assay. For each combination, the combination index (CI) values were calculated by using the CompuSyn software v1.0 (ComboSyn, Inc., Paramus, NJ, USA), according to the following equation: $CI = (D)_1/(Dx)_1 + (D)_2/(Dx)_2$, where the numerators $(D)_1$ and $(D)_2$ are the concentrations of each drug in the combination $(D)_1 + (D)_2$ that inhibit x %, and the denominators $(Dx)_1$ and $(Dx)_2$ are the concentrations of drug one and two alone that inhibit x %; dose reduction index (DRI) measures how much the dose of a drug may be reduced in synergistic combination compared to the dose of each drug alone; CI values < 1, $1 < CI < 1.1$, and > 1.1 indicate synergistic, additive and antagonistic effects, respectively [385].

3.2.9. Cell cycle analysis

The analyses were performed basically as described in [239]. Briefly, HCT116 cells were seeded in 6-well plates at a density of 1.5×10^5 cells/well for 24 h, followed by treatment with SLMP53-1, DCA, or both, for an additional 48 h. Cells were then stained with propidium iodide (PI; Sigma-Aldrich) and analyzed by flow cytometry; cell cycle phases were identified and quantified by using the FlowJo software v10.0.7 (Treestar, Ashland, OR, USA). The AccuriTM C6 flow cytometer and the BD Accuri C6 software (BD Biosciences, Enzifarma, Porto, Portugal) were used.

3.2.10. Statistics

Data were statistically analyzed by using GraphPad Prism software v7.0 (San Diego, CA, USA). Different statistical tests were used, accordingly, to the dataset; *p* values < 0.05 were considered statistically significant.

3.3. Results

3.3.1. SLMP53-1 regulates the Warburg effect and angiogenesis in cancer cells, with interference in ECM remodeling and EMT events

To investigate whether SLMP53-1 could interfere with the Warburg effect, the expression levels of major proteins involved in glycolysis and OXPHOS were investigated in HCT116 cancer cells. When compared to solvent, SLMP53-1 downregulated the protein levels of GLUT1, HK2, and PFKFB3, while it upregulated the mitochondrial markers SCO2 and COX4, particularly for 32 µM (Figure 12A). Moreover, 16 µM SLMP53-1 upregulated the levels of OXPHOS mitochondrial complexes, with a more pronounced effect on complexes III and V (Figure 12B). These results indicated the modulation of the Warburg effect by SLMP53-1, with glycolysis inhibition and OXPHOS stimulation, in HCT116 cells. The anti-glycolytic activity of SLMP53-1 was further sustained by the reduction of extracellular lactate levels in SLMP53-1-treated HCT116 cells, when compared to solvent (Figure 12C).

In HCT116 cells, it was also observed that SLMP53-1, particularly at 32 µM, increased the protein levels of E-CAD, while decreasing the levels of N-CAD and MMP-9 (Figure 12D). These data were consistent with an inhibition of ECM remodeling and EMT processes.

We next checked the anti-angiogenic potential of SLMP53-1. To this end, we started by assessing the effect of SLMP53-1 on VEGF1 expression levels, in HCT116 cells. The results showed that 16 and 32 µM SLMP53-1 visibly decreased the VEGF1 protein levels (Figure 12E). In addition, we tested the effect of SLMP53-1 on endothelial cell tube formation. For that, the anti-proliferative effect of SLMP53-1 on HMVEC-D endothelial cells was previously determined. An IC_{50} value of 74 ± 10.2 µM (three independent experiments; 48 h treatment) indicated low toxicity of SLMP53-1 toward endothelial cells. Thereafter, using the endothelial cell tube formation assay, a pronounced anti-angiogenic effect of SLMP53-1 could be observed. In fact, 36 and 42 µM of SLMP53-1 led to a significant decrease in HMVEC-D tube formation, upon 12 h treatment (Figure 12F). Notably, for these concentrations and treatment time, SLMP53-1 had no significant cytotoxic effect on

HMVEC-D cells. Consistently, 42 µM SLMP53-1 also decreased the VEGF1 protein levels in HMVEC-D cells (Figure 12G).

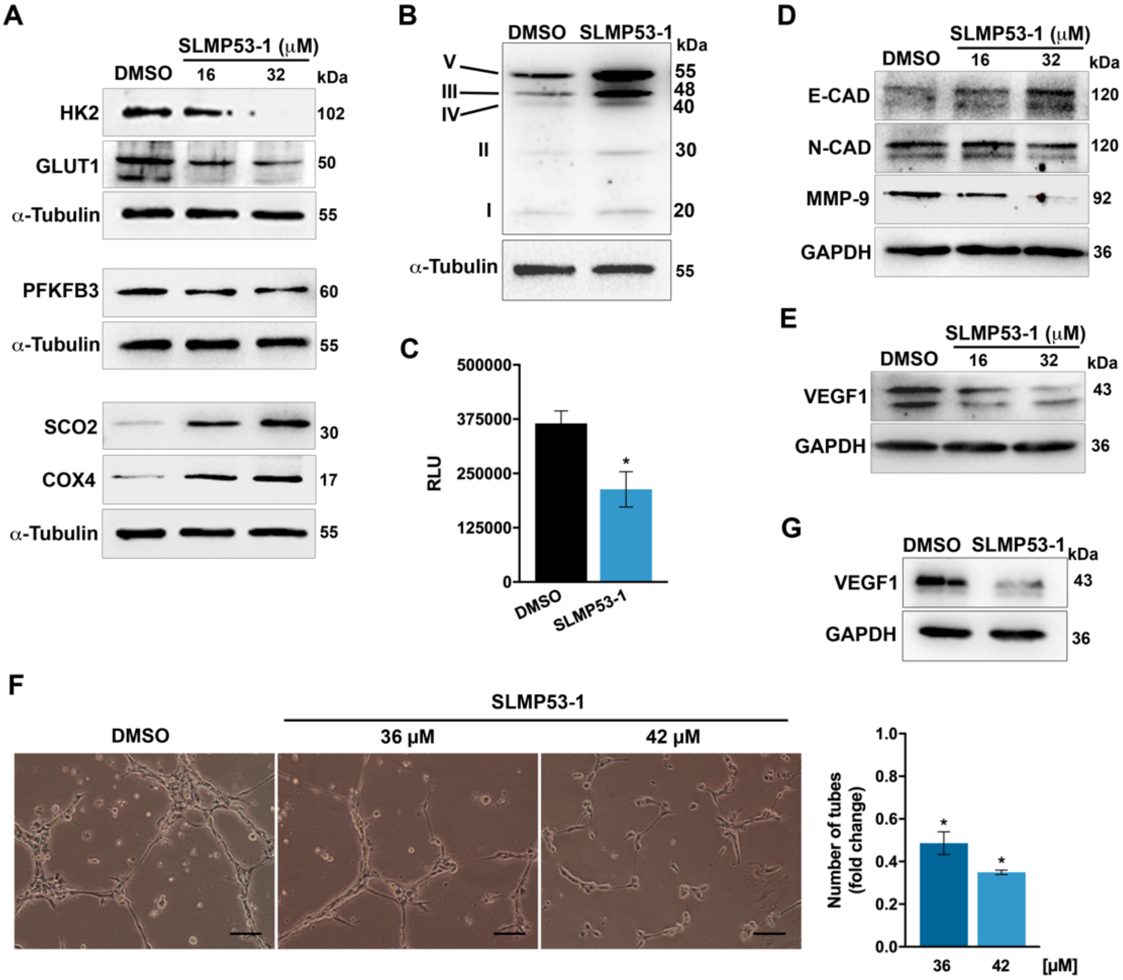
A
SLMP53-1 (µM)
DMSO
16
32
kDa
HK2
102
GLUT1
50
α-Tubulin
55
PFKFB3
60
α-Tubulin
55
SCO2
30
COX4
17
α-Tubulin
55
B
DMSO
SLMP53-1
kDa
V
III
IV
II
I
55
48
40
30
20
α-Tubulin
55
C
500000
375000
250000
125000
0
RLU
*
DMSO
SLMP53-1
D
SLMP53-1 (µM)
DMSO
16
32
kDa
E-CAD
120
N-CAD
120
MMP-9
92
GAPDH
36
E
SLMP53-1 (µM)
DMSO
16
32
kDa
VEGF1
43
GAPDH
36
G
DMSO
SLMP53-1
kDa
VEGF1
43
GAPDH
36
F
SLMP53-1
DMSO
36 µM
42 µM
1.0
0.8
0.6
0.4
0.2
0.0
Number of tubes (fold change)
*
*
36
42
[µM]

Figure 12. SLMP53-1 modulates the Warburg effect and angiogenesis in cancer cells, with impact on endothelial cell tube formation, ECM remodeling and EMT events *in vitro*. (A) Expression levels of proteins involved in glycolysis and OXPHOS after 24 h treatment with SLMP53-1, in HCT116 cancer cells. **(B)** Expression levels of OXPHOS mitochondrial complexes I–V, after 24 h treatment with 16 µM SLMP53-1, in HCT116 cells. **(C)** Effect of 16 µM SLMP53-1 on lactate secretion by HCT116 cells, after 24 h treatment. Relative luminescence units (RLU) signal was normalized to the respective cell number and corresponds to mean ± SEM of three independent experiments. Values significantly different from DMSO (*$p < 0.05$; unpaired Student's *t*-test). **(D, E)** Expression levels of proteins involved in migration (D) and angiogenesis (E) after 24 h treatment with SLMP53-1, in HCT116 cells. **(F)** Anti-angiogenic effect of SLMP53-1, in HMVEC-D cells, after 12 h treatment, using the endothelial cell tube formation assay. Representative images are shown (scale bar = 50 µm and magnification = ×100; zoomed-out pictures are shown in Annex III, Figure S5A). Quantification of tube-like structures in five randomly selected microscopic fields; fold changes are relative to solvent (DMSO) and correspond to mean ± SEM of three independent experiments. Values significantly different from DMSO (*$p < 0.05$; one-way ANOVA with Dunnett's multiple comparison test); quantification of total tube length, using Image J software, is shown in Annex III, Figure S5B. **(G)** Expression levels of VEGF1, after 48 h treatment with 42 µM SLMP53-1, in HMVEC-D cells. In A, B, D, E, and G, immunoblots are representative of three independent experiments; α-tubulin or GAPDH were used as a loading control.

3.3.2. SLMP53-1 regulates the Warburg effect and angiogenesis, interfering with ECM remodeling and EMT events in a p53-dependent manner, in tumor tissues of xenograft mouse models

To assess the *in vivo* effect of SLMP53-1 on glucose metabolism, the expression levels of glycolytic and OXPHOS molecular markers were evaluated by IHC staining in tumor tissues of xenograft mouse models carrying $p53^{+/+}$ and $p53^{-/-}$ HCT116 cells obtained in previous work [239] (Figure 13A, B). The results showed that SLMP53-1 treatment (50 mg/kg, twice a week during two weeks) modulated the protein levels of typical glycolytic and OXPHOS markers in p53-expressing, but not in p53-null, tumor tissues. In fact, when compared to vehicle, SLMP53-1 treatment decreased the expression levels of GLUT1, HK2, monocarboxylate transporter 4 (MCT4), and PFKFB3 in $p53^{+/+}$, but not in $p53^{-/-}$, HCT116 tumors (Figure 13A, B). Conversely, SLMP53-1 promoted OXPHOS by enhancing the expression of SCO2 and COX4, only in p53-expressing HCT116 tumors.

In the same tumor tissue, the expression levels of markers associated with angiogenesis (VEGF1) and migration (MMP-9 and E-CAD) were also evaluated. When compared to vehicle, SLMP53-1 treatment decreased the expression levels of MMP-9 and VEGF1, while increasing the levels of E-CAD in $p53^{+/+}$, but not in $p53^{-/-}$, HCT116 tumors (Figure 13A, B).

Collectively, likewise *in vitro*, SLMP53-1 displayed the *in vivo* potential to antagonize the Warburg effect, also inhibiting angiogenesis and modulating key signatures of ECM remodeling and EMT processes, in a p53-dependent manner.

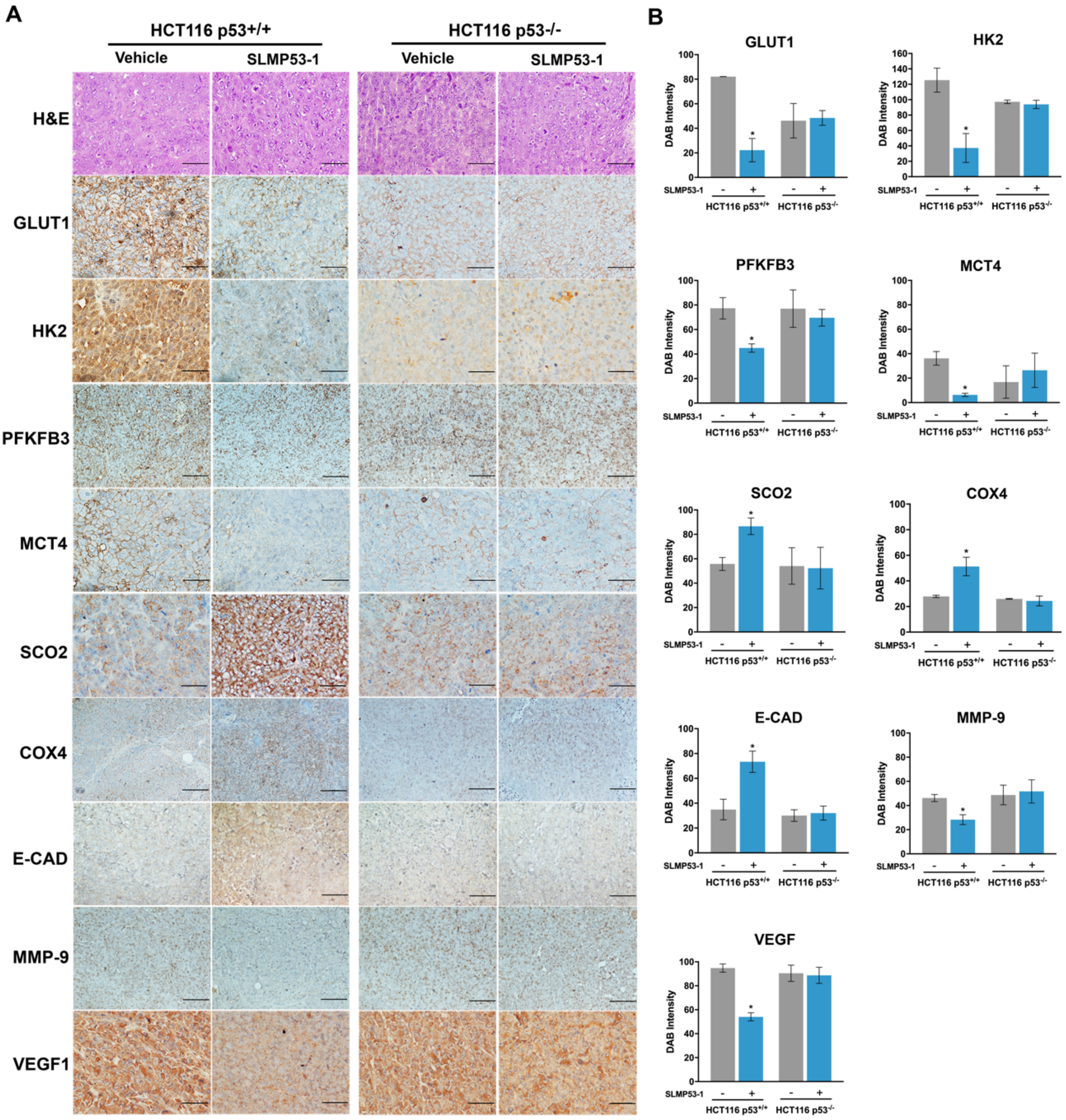
A
HCT116 p53+/+
HCT116 p53-/-
Vehicle
SLMP53-1
Vehicle
SLMP53-1
H&E
GLUT1
HK2
PFKFB3
MCT4
SCO2
COX4
E-CAD
MMP-9
VEGF1
B
GLUT1
HK2
PFKFB3
MCT4
SCO2
COX4
E-CAD
MMP-9
VEGF
DAB Intensity
0
20
40
60
80
100
120
140
160
*
SLMP53-1
-
+
-
+
HCT116 p53+/+
HCT116 p53-/-

Figure 13. SLMP53-1 modulates the Warburg effect and angiogenesis, interfering with ECM remodeling and EMT events, through a p53-dependent manner, in tumor tissues of xenograft mouse models. (A, B) Detection of molecular markers involved in glycolysis, OXPHOS, angiogenesis, and migration, in tumor tissues of p53$^{+/+}$ and p53$^{-/-}$ HCT116 xenografts treated with 50 mg/kg SLMP53-1 or vehicle (intraperitoneal injection twice a week, for a total of five administration [239]); in **(A)** representative images of IHC are shown; scale bar =20 μm; magnification = ×200; hematoxylin and eosin (H&E); in **(B)** quantification of IHC staining in tumor tissues of p53$^{+/+}$ and p53$^{-/-}$ HCT116 xenografts treated with SLMP53-1 (+) or vehicle (−). Staining quantification was assessed by evaluation of DAB (3,3′-diaminobenzidine) intensity. Data are mean ± SEM, values significantly different from vehicle (*p < 0.05, unpaired Student's *t*-test).

3.3.3. SLMP53-1 synergizes with dichloroacetic acid (DCA), enhancing its antitumor efficacy in cancer cells

We also assessed the ability of SLMP53-1 to enhance the antitumor activity of the well-established metabolic regulator DCA, in HCT116 cells. For that, cancer cells were treated with SLMP53-1 at 9 μM (concentration with no significant anti-proliferative effect on HCT116 cells [239]) and/or with 5.93–20 mM of DCA. The results showed a significant enhancement of the growth inhibitory effect of DCA by SLMP53-1 (Figure 14A). A multiple-drug-effect analysis was performed with the calculation of the combination index (CI) for each combination. As depicted in Figure 14B, synergistic effects between SLMP53-1 and DCA could be observed for the four concentrations tested (CI < 1). Moreover, for the combination of 13.3 mM DCA with 9 μM SLMP53-1, the synergic effect was associated with an increase of G0/G1-phase cell cycle arrest, when compared to DCA only-treated cells (Figure 14C). Accordingly, in a 3D HCT116 spheroid model, we could corroborate that the growth inhibitory activity of DCA was visibly potentiated by SLMP53-1 at 20 μM (concentration with no significant effect on HCT116 colonosphere growth), after nine days treatment (Figure 14D, E).

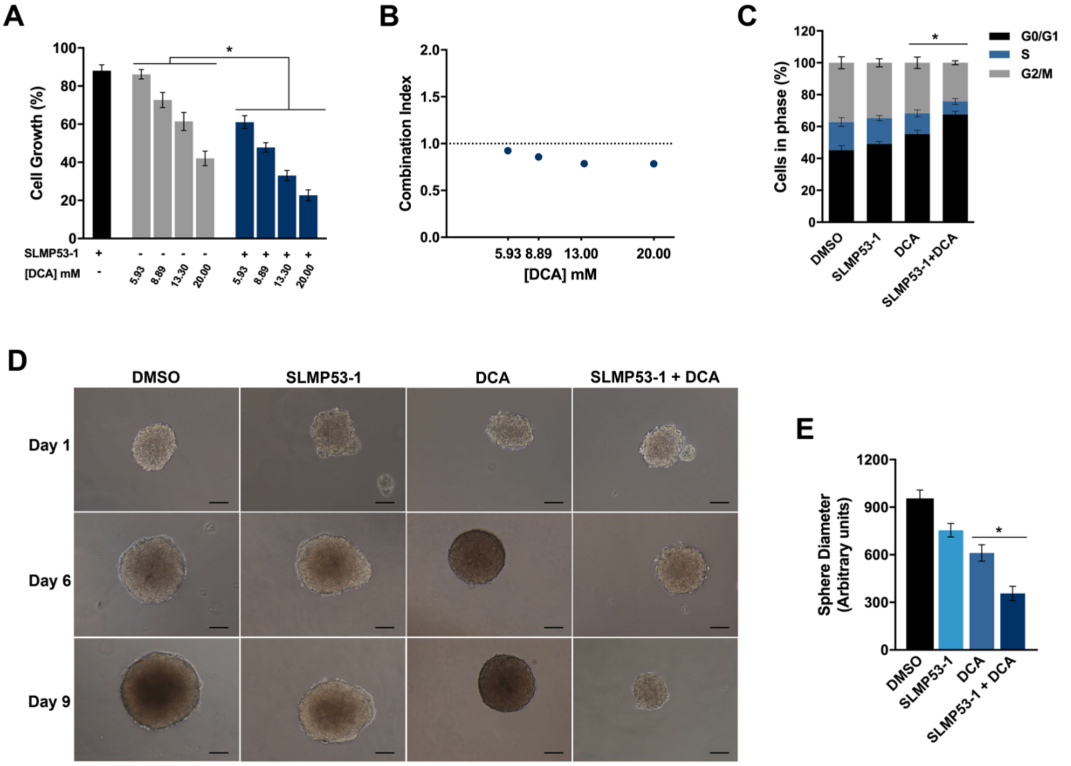

Figure 14. SLMP53-1 sensitizes cancer cells to DCA. (A) HCT116 cells were treated with 5.93 – 20 mM DCA alone and in combination with 9 μM SLMP53-1; cell proliferation was determined after 48 h treatment; growth obtained with solvent (DMSO) was set as 100%. Data are mean ± SEM of six independent experiments. Values significantly different from DCA alone (*$p < 0.05$, two-way

ANOVA followed by Sidak's test). **(B)** Combination index (CI) values calculated by using the CompuSyn software for each combined treatment. CI < 1, synergy; 1 < CI < 1.1, additive effect; CI > 1.1, antagonism. CI values were calculated by using a mean value effect of six independent experiments. **(C)** Effect of 13.3 mM DCA alone and in combination with 9 μM SLMP53-1 in cell cycle of HCT116 cells, after 48 h treatment. Data are mean ± SEM of three independent experiments. Values significantly different from DCA alone (**p* < 0.05, two-way ANOVA followed by Dunnett's test). **(D, E)** Effect of 20 μM SLMP53-1 alone and in combination with 12 mM DCA on three-day-old HCT116 colonosphere, for up to nine days of treatment. **(D)** Images are representative of three independent experiments (scale bar = 50 μm; magnification = ×100). **(E)** Determination of spheroid diameter at the end of treatment; data represent mean ± SEM of three independent experiments. Values significantly different from DCA alone (**p* < 0.05, one-way ANOVA followed by Dunnett's test).

3.4. Discussion

The high sensitivity of cancer cells to the counteraction of Warburg effect has been considered a valuable target in anticancer therapy. In particular, activation of p53, a major regulator of glucose metabolism, can conduct to a robust inhibition of energy production in cancer cells and subsequently to their efficient elimination. In fact, among the wide set of genes regulated by p53, important regulators of glucose metabolism are included, which have central roles in maintaining mitochondrial health, increasing mitochondrial respiration, and lowering glycolysis [386]. In earlier studies, SLMP53-1 was identified as a new activator of wt- and mutp53, with encouraging *in vitro* and *in vivo* p53-dependent antitumor activity [239]. Data from SwissADME analysis [387] also showed that SLMP53-1 followed criteria for drug-likeness, gastrointestinal adsorption, lipophilicity, and solubility (Annex III, Tables S6-S12). This evidence led us to further investigate the potential of SLMP53-1 as an anticancer drug candidate, particularly through an in-depth analysis of its impact on OXPHOS and glycolysis. In fact, it was shown that SLMP53-1 triggered a p53-dependent mitochondrial apoptotic cell death in cancer cells, involving upregulation of BAX and PUMA expression levels (considered a consequence of the stimulation of both pro-oxidant and mitochondrial p53 functions [388]) mitochondrial membrane potential dissipation, p53 and BAX mitochondrial translocation, cyt *c* release, and p53-dependent ROS generation [239]. ROS are a toxic by-product of OXPHOS, playing a major role in the progressive accumulation of damages in cancer cells and in their efficient elimination through apoptosis [389].

In this work, the results in cancer cells and xenograft human tumor tissues unveiled that SLMP53-1 potentially stimulated OXPHOS through upregulation of SCO2, which in turn is involved in ROS accumulation and apoptotic cell death. In fact, some authors have reported that SCO2 upregulation provides an alternative pathway of p53-dependent apoptosis [390]. SLMP53-1 also caused *in vitro* and *in vivo* upregulation of COX4, a nuclear-encoded subunit of mitochondrial complex IV, and increased the levels of OXPHOS mitochondrial complexes in cancer cells, which further reinforced the stimulation of OXPHOS by the compound. Additionally, SLMP53-1 inhibited glycolysis, with downregulation of several glycolytic intervenient, including glucose transporters (GLUT1) and enzymes (HK2 and PFKFB3), which are direct p53 targets, in cancer cells and xenograft tumor tissue. Thus, p53 activation by SLMP53-1 ablates the first step of glycolysis, namely glucose uptake, primary phosphorylation of glucose molecules, and the rate-limiting step of glycolysis, the conversion of fructose-6-phosphate to fructose-1,6-biphosphate. Notably, these effects of SLMP53-1 on OXPHOS and glycolysis were shown to be dependent on p53 in xenograft tumor tissues. Moreover, consistently with *in vivo* data, it was further confirmed *in vitro* that SLMP53-1 did not interfere with the expression levels of glycolytic markers such as HK2 and GLUT1, in HCT116 $p53^{-/-}$ cells (Annex III, Figure S6).

As previously mentioned, elevated lactate levels are correlated with poor prognosis and decreased overall survival in cancer patients [391]. In fact, high lactate production promotes the metastatic disease, which largely remains the main cause of cancer-associated morbidity and mortality [392]. Herein, it is shown that SLMP53-1 also significantly reduced the extracellular lactate levels in cancer cells. Accordingly, a significant downregulation of MCT4 expression levels, a plasma membrane lactate transporter, was observed in SLMP53-1-treated tumor tissues. The MCT4 expression is not directly regulated by p53. Instead, its expression is induced via HIF-1 [393]. Indeed, in response to the hypoxic conditions in tumors, activated HIF-1 upregulates transporters and enzymes of the glycolysis pathway, while reducing mitochondrial respiration [394]. However, p53 makes part of a triad with c-Myc and HIF-1, which is responsible for the transcription of multiple genes that tightly regulate cell metabolism through feedback mechanisms [394]. Activation of p53 keeps the levels of HIF-1 low, with downregulation of transporters regulated by HIF-1, including MCT4 [394]. Interestingly, MCT4 is overexpressed in several cancers, which is correlated with cancer progression, infiltration, and angiogenesis [395]. MCT4 is therefore recognized as a marker of poor prognosis [396]. As such, several inhibitors of MCTs, including MCT4, have been evaluated as promising anticancer therapeutic options. For example, the MCT1/4 inhibitor syrosingopine [397] and the MCT1 inhibitor AZD3965 [398] have shown promising preclinical anticancer activity. In fact, AZD3965 is currently under phase I trial for refractory and advanced solid tumors and lymphoma (NCT07197595).

Herein, we also showed that SLMP53-1 modulated *in vitro* and *in vivo* key signatures of ECM remodeling and EMT processes, increasing E-CAD, while decreasing MMP-9. Importantly, this effect showed to be dependent on p53 in xenograft tumor tissues. In fact, this is in accordance with our previous work, in which low doses of SLMP53-1 significantly inhibited the migration of colon cancer cells (wound healing assay) [399].

In this work, the anti-angiogenic activity of SLMP53-1 was further confirmed. In fact, a pronounced reduction of VEGF production by SLMP53-1 was observed in p53-expressing cancer cells. Indeed, it was reported that p53 indirectly suppresses VEGF expression by repressing transcription factors like SP1 [400] and E2F [401, 402]. Interestingly, SLMP53-1 also inhibited the VEGF expression levels in endothelial cells, an effect associated with reduction in cell tube formation. Furthermore, although this negative effect of SLMP53-1 on VEGF production could be also observed in p53-expressing tumor tissue, it was depleted in p53-null tumor tissue. These results evidenced that the anti-angiogenic activity of SLMP53-1 was highly dependent on tumor environment, particularly on its p53 status. In fact, the high VEGF expression levels by p53-null cancer cells seem to counteract the inhibitory effect of SLMP53-1 on VEGF production by endothelial cells. Given the fact that angiogenesis is an essential event in tumor dissemination and metastases formation [403], these results reinforced the p53-dependent anti-metastatic activity of SLMP53-1.

Our data further corroborated the combination of drugs targeting glucose metabolism with p53-activating agents as an efficient therapeutic approach to counteract resistances and undesirable toxicity commonly observed in cancer therapy. Indeed, SLMP53-1 was shown to synergize with DCA both in 2D and 3D cancer cell models. DCA is a well-established inhibitor of the mitochondrial pyruvate dehydrogenase kinase (PDK) [404, 405] that was shown to reverse the Warburg effect [406]. DCA binds to PDK and attenuates the inhibition of pyruvate dehydrogenase (PDH) activity, which shifts metabolism from glycolysis to OXPHOS, with subsequent increase of ROS production, decrease of mitochondrial membrane potential, efflux of pro-apoptotic mediators from the mitochondria, and induction of mitochondria-dependent apoptosis [406]. Interestingly, some authors have recently shown that DCA restored colorectal cancer chemosensitivity through the p53/miR-149-3p/PDK2-mediated glucose metabolic pathway [407]. Accordingly, it was also reported that the antitumor activity of DCA was dependent on a functional p53 status, exhibiting synergistic growth inhibitory effects in combination with the p53 activator Nutlin-3 [408].

As a whole, this work further reinforces the great potential of SLMP53-1, as single or combined anticancer drug, by targeting major hallmarks of cancer growth and dissemination.

CHAPTER 4

MANIO: MECHANISM OF WILD-TYPE AND MUTANT P53 ACTIVATION AND THERAPEUTIC POTENTIAL IN COLORECTAL CANCER

Helena Ramos, et al, 2020. *MANIO: mechanism of wild-type and mutant p53 activation and therapeutic potential in colorectal* cancer. Manuscript in preparation*.*

Lucília Saraiva; Teresa Melo; **Helena Ramos**; Joana Soares; Maria Isabel Soares. (3*S*)- and (3*R*)-6,7-Bis(hydroxymethyl)-1H,3H-Pyrrolo [1,2-c]thiazoles as p53 activators. International Patent Application nº PCT/IB2019/053603, Publication Number WO 2019/243906 A1.

4.1. Background

As previously mentioned in the Literature Overview, the disruption of the p53 pathway, either by p53 mutation or inhibition by negative regulators, is a major pathological event in local and advanced CRC [409]. Notably, around 80% of metastatic and advanced CRC present *TP53* mutations, greatly contributing to the aggressiveness and invasiveness of these cancers [410]. It is well-accepted that restoration of p53 function is an encouraging strategy for CRC therapy. Among the compounds targeting p53 under clinical trials [252], the Nutlins family of p53 activators [411] does not target mutp53-expressing cancers, and the mutp53 reactivator PRIMA-1^{MET} (APR-246) has a p53-independent inhibitory activity in CRC [412]. Also, the precise antitumor mechanism of action of the mutp53 reactivator COTI-2 remains not comprehensively understood in many cancers, including CRC [292]. Therefore, additional research has been required in order to find novel p53-targeting agents that would be used as effective anticancer therapeutic options in CRC patients, including those with advanced and metastatic disease.

In this work, the (3*S*)-6,7-bis(hydroxymethyl)-5-methyl-3-phenyl-1*H*,3*H*-pyrrolo[1,2-c]thiazole (MANIO) was identified as a new wt- and mutp53-activating agent, with promising therapeutic application in cancer therapy, particularly of CRC.

4.2. Materials and Methods

4.2.1. Compounds and reagents

MANIO was synthesized as previously described [413]. Doxorubicin (DOXO) and etoposide (ETOP) were from Calbiochem (VWR, Carnaxide, Portugal); cisplatin and 5-fluorouracil (5-FU) were from Enzo Life Science (Palex Medical, Algés, Portugal). All tested compounds were dissolved in DMSO (Sigma-Aldrich, Sintra, Portugal), except cisplatin that was dissolved in saline. In all experiments, the solvent (0.1–0.25% DMSO) was included as control.

4.2.2. Human cell lines and culture conditions

HCT116 $p53^{+/+}$, HCT116 $p53^{-/-}$, MCF-7, MDA-MB-468, H460, H1299, HCC1937, HT-29, SW837, LS-1034, A431, IGROV-1 and SK-OV-3 human cell lines were routinely cultured as described in 2.2.5. Cells were also routinely tested for mycoplasma infection as described in Chapter 2 (section 2.2.5.). Cells were recently characterized and authenticated using short tandem repeat DNA profiling.

4.2.3. Patient-derived CRC cells

Patient-derived CRC cell lines (CCA2, CCA8, CCZ1, CCZ2, CCZ3, CCZ4, CCZ5, CCZ6, CCZ7, CRCJS1) were established from tumor tissue samples with written informed consent approved by Ethics Committee of Faculty Hospital St. Ann's Brno (reference number 74V/2018). Tumors were histologically characterized according to WHO classification. The specimens were briefly washed in 70% ethanol, followed by two washes in phosphate buffered saline (PBS); the specimens were then mechanically disintegrated into pieces about ⌀2 mm. Tissue pieces were washed three times in PBS, and seeded into 25 cm^2 cell culture flasks containing 1 ml of DMEM complete medium (Biosera, Nuaille, France), supplemented with 10% fetal calf serum (Biosera), 2 mM glutamine and antibiotics: 100 IU/mL of penicillin, 100 µg/mL of streptomycin (Biosera), 10 µg/mL Ciprofloxacine, 400 µg/mL Piperacilin plus Tazobactam and 1.25 µg/mL Amphotericin B (Merck, Darmstadt, Germany). The cells were cultivated under standard conditions at 37 °C and in an atmosphere of 5% CO_2. Once the specimen pieces had attached, the volume of the medium was gradually increased to 5 mL over the next 48 h. As soon as the outgrowing cells covered about 60% of the surface, they were detached, diluted and transferred into a new flask with fresh medium, this time with penicillin and streptomycin only.

4.2.4. Cell viability and proliferation assays

For SRB assays, cells were seeded in 96-well plates at a density of 4.0×10^3 (H460), 5.0×10^3 (HCT116, MCF-7, MDA-MB-468, LS-1034, HT-29, IGROV-1, H1299, A431, and SK-OV-3), 7.5×10^3 (SW837) and $1.0\text{x}10^4$ (HCC1937) cells/well, for 24 h. Cells were treated with serial dilutions of MANIO, for additional 48 h, and IC_{50} values were determined for each cell line using the GraphPad Prism software v7.0 (San Diego, CA, USA), as described in [242].

For MTT assays, patient-derived CRC cells were seeded in 96-well plates at a density of 3×10^3 cells/well. Cells were treated with serial dilutions of MANIO, for additional 48 h, and IC_{50} values were determined for each cell line using the GraphPad Prism software v7.0 as described [242].

For colony formation assays, HCT116 (p53$^{+/+}$ and p53$^{-/-}$) and SW837 cells were seeded in 6-well plates at a density of 1.0×10^3 and 2.5×10^3 cells/well, respectively, followed by incubation with MANIO for 11-14 days. Formed colonies were fixed with a solution of 10% methanol and 10% acetic acid for 10 min, and then stained with 0.5% crystal violet (Sigma-Aldrich) in 1:1 methanol/H2O for 15 min. Colonies having more than 20 cells were counted.

4.2.5. Transient transfection assay of mutp53 in human H1299 tumor cells

For ectopic expression of mutp53, p53-null H1299 cells were transfected with 75 ng of pcDNA3 mammalian expression vectors, encoding full-length human mutp53 (R175H, G245D, G245S, R248Q, R248W, R273H, R273C, Y220C or R282W), or empty pcDNA3, constructed as described in Chapter 2 (section 2.2.2.2.). Briefly, cells in suspension were transfected using the ScreenFect®A reagent from Screenfect GmbH (GRiSP, Porto, Portugal), according to the manufacturer's instructions, and then seeded at 7.5×10^3 cells/well density in 96-well plates. After 24 h incubation, transfected cells were treated with serial dilutions of MANIO, for additional 48 h, and IC_{50} values were determined by the SRB assay, as described in section 4.2.4.

4.2.6. Cell cycle and apoptosis analysis

Cell cycle and apoptosis were analyzed as described in [242]. Briefly, HCT116 (p53$^{+/+}$ and p53$^{-/-}$) cell lines were seeded in 6-well plates at a density of 1.5×10^5 cells/well, followed by treatment with MANIO or solvent. For cell cycle analysis, cells were stained with PI (Sigma-Aldrich); cell cycle scattering was analyzed by flow cytometry and cell cycle phases were quantified using FlowJo software v10.0.7 (Treestar, Ashland, OR, USA).

For apoptosis analysis, cells were stained using the Annexin V-FITC Apoptosis Detection Kit I (BD Biosciences, Enzifarma, Porto, Portugal), according to the manufacturer's instructions. For both, the Accuri™ C6 flow cytometer and the BD Accuri C6 software (BD Biosciences, Enzifarma) were used.

Patient-derived CRC cells were seeded in ⌀100 mm petri dishes at a density of 3×10^5 cells/dish, followed by treatment with MANIO or solvent. Cell cycle was analyzed using the BD FACSVerse™ flow cytometer with BD FACSuite software (Beckton Dickinson, NJ, USA). Cell cycle phases were quantified using Flowing software v2.5.1 (Cell Imaging Core, Turku Centre for Biotechnology, Turku, Finland).

4.2.7. Western blot analysis

HCT116 (p53$^{+/+}$ and p53$^{-/-}$) and SW837 cells were seeded in 6-well plates at a density of 1.5×10^5 and 2.25×10^5 cells/well respectively, and patient-derived CRC cells in ⌀100 mm petri dishes at 3×10^5 cells/dish, for 24 h, followed by treatment with MANIO or solvent. Protein fractions were analyzed as described in Chapter 2 (section 2.2.9.); GAPDH was used as loading control. Antibodies are listed in Annex I, Table S2.

4.2.8. Cycloheximide (CHX) assay

HCT116 p53$^{+/+}$ cells were seeded in 6-well plates at a density of 1.5×10^5/well for 24 h, followed by treatment with MANIO or solvent for additional 48 h. After that, cells were treated with 150 µg/mL CHX (Sigma-Aldrich) for 0, 1, 2, 3 and 4 h. p53 protein expression was detected by western blot, as described in Chapter 2 (section 2.2.9.); GAPDH was used as loading control.

4.2.9. RNA extraction and RT-qPCR

HCT116 ($p53^{+/+}$ and $p53^{-/-}$) and SW837 cells were seeded in 6-well plates at a density of 1.5×10^5 and 2.25×10^5 cells/well respectively, and patient-derived CRC cells in ⌀100 mm petri dishes at 3×10^5 cells/dish, for 24 h, followed by treatment with MANIO or solvent.

For HCT116 and SW837 cells, total RNA was extracted using the IllustraTM RNAspin Mini RNA Isolation Kit (GE Healthcare, Milan, Italy). After that, 1 µg of RNA was reverse transcribed into cDNA using the RevertAid cDNA Synthesis kit (Thermo Fisher, Monza and Brianza, Italy) according to the manufacturer’s instructions. The amplification process, using 25 ng of cDNA, was performed in a 384-well plate on a Real-Time PCR Detection System v3.1. (Bio-Rad, Milan, Italy). The 2X KAPA SYBR® FAST qPCR Kit (Kapa Biosystems, Rome, Italy) and specific primers (Eurofins, MWG, Milan, Italy) listed in Annex I, Table S3 were used; *GAPDH* and *B2M* were used as reference genes.

For patient-derived CRC cells, total RNA was extracted using GenElute™ Mammalian Total RNA Miniprep Kit (Sigma-Aldrich, Steinheim, Germany), and RNA concentration and purity were determined spectrophotometrically. 50 $ng\cdot\mu L^{-1}$ of RNA were reverse transcribed into cDNA using M-MLV reverse transcriptase (Top-Bio, Prague, Czech Republic). qPCR was carried out in 10 µL reaction volumes using the KAPA SYBR® FAST qPCR Kit (Kapa Biosystems, Wilmington, MA, USA) and analyzed using the 7500 Fast Real-Time PCR System and 7500 software v2.0.6 (both Life Technologies, Carlsbad, CA, USA). The sequences of primers used are listed in Annex I, Table S3; *HSP90AB1* was used as reference gene.

4.2.10. Chromatin immunoprecipitation (ChIP) assay

HCT116 $p53^{+/+}$ and SW837 cells were seeded in 75 cm^2 flasks at a density of 1.5×10^6 and 2.25×10^6 cells/well respectively, for 24 h, and treated with MANIO or solvent for additional 24 h. ChIP experiments were carried out as previously described [414]. Mouse monoclonal anti-p53 antibody (Annex I, Table S2) was used for immunoprecipitation, and normal mouse IgG immunoglobulin (sc-2025; Santa Cruz Biotechnology) was used as negative control. DNA was recovered and purified using the QIAquick PCR purification kit (Qiagen, Milan, Italy). Purified immunoprecipitated DNA (2 µL) was then used for qPCR analysis and calculation was performed using the ΔCt method in respect to nonimmunoprecipitated DNA (% of input) as previously described [415]. Primers used are listed in Annex I, Table S4.

4.2.11. RNA sequencing (RNA-seq)

Cells were seeded in 75 cm^2 flasks at a density of 1.5×10^6 cells/well, treated with MANIO or solvent in quadruplicate for 24 h. Cells were then collected, and total RNA was extracted using the IllustraTM RNAspin Mini RNA Isolation Kit (GE Healthcare, Milan, Italy). RNA integrity was checked by the Agilent 2100 Bioanalyzer (Agilent Technologies, Milan, Italy), discarding preparations with RIN (RNA integrity number) values ≤ 8. Sequencing libraries were produced following the TruSeq RNA Library kit v2 protocol (Illumina, Thermo Fisher) and using 1 µg of RNA as input. A total of eight samples, four treatment and four controls, were sequenced using HiSeq 2500, obtaining ≈25M raw reads per sample. Raw sequence files were subjected to quality control analysis using FastQC v1.3 (http://www.bioinformatics.babraham.ac.uk/projects/fastqc/). Transcript quantification was conducted with STAR v2.5.3a [416] (assigned to a gene using the GENCODE annotation v27, using the STAR function “quantMode GeneCounts”) mapped to the human genome version GRCh38 and with reference annotation. Read counts generated by STAR were analyzed by using DESeq2 package [417] for detecting genes that were differentially expressed. An adjusted *p*-value cut off of 0.05 was decided as threshold for detection of differentially expressed genes (DEGs). Starting from the expression matrix, genes that were considered as differentially regulated, were analyzed using hierarchical clustering method (cluster function, stats package). Visualization of the clustering and heatmap of log2-normalized counts (TMM method) were obtained using gplots package. To explore the high-dimensional property of the data, the PCA (Principal Component Analysis), as dimensionality reduction algorithm implemented in stats package, was used. For the Functional Annotation analyses, Enricher web tools were used. The enriched annotation table results, obtained in the web site, were then downloaded to be processed in R/bioconductor and visualized using ggplot2 package. The combined score is a combination of the logarithm of the *p*-value computed using the Fisher's exact test and the rank score computed using a modification to Fisher's exact test, in which it was computed a z-score for deviation from an expected rank.

4.2.12. p53 small interfering RNA (siRNA)

SW837 cells were transfected with 100 nM of siRNA against p53 (SMARTpool p53) and negative nonspecific siRNA (Non-targeting Pool), both from Thermo Scientific (Bioportugal, Porto, Portugal), using Lipofectamine 2000 (Invitrogen, Alfagene, Lisboa Portugal), following the manufacturer's instructions. After 72 h transfection, cells were seeded in 6-well plates at a density of 2.25×10^5 cells/well, followed by MANIO or solvent treatment. The expression of the different proteins analyzed was detected by western blot, as described in Chapter 2 (section 2.2.9.); GAPDH was used as loading control.

4.2.13. CETSA

CETSA experiments were performed as described in Chapter 2 (section 2.2.6.). Briefly, HCT116 $p53^{+/+}$ and SW837 cell lysates were incubated with MANIO or solvent for 1 h at room temperature and then heated at different temperatures for 3 min, cooled to room temperature for 3 min, and placed on ice. Soluble protein was detected by western blot as described in Chapter 2 (section 2.2.9.). The increase in non-denatured p53 of lysates treated with MANIO was calculated relative to solvent at 25 ºC, set as 1.

4.2.14. Comet assay

HCT116 $p53^{+/+}$ cells were seeded in 6-well plates at a density of 1.5×10^5 cells/well for 24 h, followed by treatment with 50 µM ETOP (positive control) or 1 and 2.5 µM MANIO, for additional 48 h. To evaluate DNA damage, an alkaline comet assay was performed using the OxiSelect Comet Assay kit (Cell Biolabs, MEDITECNO, Carcavelos, Portugal), according to the manufacturer's instructions, as described [242]. Tail DNA quantification considered the percentage of cells with more than 5% of DNA in the tail (comet-positive cells). Cells were photographed using a Nikon DS-5Mc camera and a Nikon Eclipse E400 fluorescence microscope, and images processed using a Nikon ACT-2U software (all Izasa Scientific, Carnaxide, Portugal). Images were quantified using Fiji Software (Open Comet/ImageJ, Laboratory for optical and computational instrumentation, University of Wisconsin-Madison, USA). For each condition, five independent experiments were performed, and in each sample 100 cells were quantified.

4.2.15. Micronucleus test

The cytokinesis block micronucleus assay in human lymphocytes was performed as described [242]. Briefly, fresh peripheral blood samples were collected from healthy volunteers into heparinized vacutainers. Blood samples were suspended in RPMI-1640 medium supplemented with 10% FBS and treated with 1 and 2.5 µM MANIO, 1 µg/mL cyclophosphamide (CP, positive control; Sigma-Aldrich), or solvent for 44 h. Cells were thereafter treated with 3 µg/mL cytochalasin B (cytokinesis preventive; Sigma-Aldrich) for 28 h. Lymphocytes were isolated by density gradient separation (Histopaque-1077 and -1119; Sigma-Aldrich), fixed in 3:1 methanol/glacial acetic acid, and stained with Wright stain. For each sample, 1000 binucleated lymphocytes were blindly scored using a Leica light optical microscope (Leica Microsystems, Wetzlar, Germany); the number of micronuclei per 1000 binucleated lymphocytes was recorded.

4.2.16. Recombinant human wt- and mutp53 R248W protein DBD production

Human wt- and mutp53 R248W protein DBD were subcloned into the vector pETM-20 as described [359] with some modifications. Briefly, proteins were expressed in *Echerichia coli* strain BL21(DE3), which were grown at 37 ºC in Luria-Bertani broth medium, supplemented with 100 μg/mL ampicillin, to an OD_{600} of 1.2. Bacterial cultures were supplemented with 10 μM $Zn(CH_3CO_2)_2$ before overnight induction at 25 ºC with 1 mM isopropyl β-D-thiogalactoside. Cells were harvested by centrifugation and chemically lysed in NZY Bacterial Cell Lysis Buffer (Nzytech, Lisboa, Portugal), 5mM dithiothreitol (DTT), and 10 μM $Zn(CH_3CO_2)_2$ following manufacturer's instructions. Samples were filtrated (0.2 μm), loaded onto a HiTrap™ Heparin HP column (GE Healthcare, VWR), and proteins eluted with a NaCl step gradient (0 - 0.3 M) at 1.5 mL/min. Further purification was achieved by gel filtration chromatography using a HiPrep 16/60 Sephacryl S-100 High-Resolution column (GE Healthcare, VWR) in a Fast Protein Liquid Chromatography (FPLC) system (Pharmacia Biotechnology, GE Healthcare, VWR). Running buffer contained 50 mM HEPES pH 7.5, 5 mM DTT, 10 μM $Zn(CH_3CO_2)_2$, and 150 mM NaCl. Pure protein fractions were analyzed using SDS-polyacrylamide gel electrophoresis, while protein concentration was measured spectrophotometrically.

4.2.17. Protein-ligand interaction by fluorescence quenching

Evaluation of the binding of MANIO to recombinant human wtp53 and mutp53 R248W DBD was based on the quenching of the proteins intrinsic fluorescence. Phosphate buffer consisting of 50 mM HEPES, 5 mM DTT, 10 μM $Zn(CH_3CO_2)_2$, and 150 mM NaCl (pH 7.5) was used in the preparation of all solutions. Briefly, 5 μM of each protein, increasing concentrations of drug solution (0 – 75 μM) and phosphate buffer solution (pH 7.5) were mixed to a final volume of 280 μL. Fluorescence emission spectra were recorded at room temperature (23 ± 1°C) in a microplate reader (Synergy™ HT Multi-Detection Microplate Reader, BioTek®, Izasa Scientific) in the range of 300 – 350 nm upon excitation at 260 nm.

Proteins-MANIO binding parameters were calculated using the Origin 8.5.1 software v8.5.1 (OriginLab Corporation, Northampton, MA, USA). The fitting of the experimental values was made according to the Langmuir binding equation. The protein binding parameters of the interaction monitored by fluorescence were calculated through the fitting of the experimental points to the following equation (adapted from [418]):

$$[protein - MANIO] = \frac{I_0}{I} - 1 = \frac{y_{max}^{n}}{1 + \frac{K_d}{[MANIO]}}$$

where I_0 and I are the fluorescence intensities in the absence and presence of MANIO, respectively, y_{max} corresponds to the highest quenching induced by MANIO, *n* accounts for the number of binding sites, and K_d corresponds to the dissociation constant of protein-MANIO complexes.

4.2.18. *In vivo* antitumor and toxicity assays

Animal experiments were conducted according to the EU Directive 2010/63/EU and to the National Authorities. The study was approved by the local Animal Welfare Body (Ref. ORBEA-5-2016). Female Swiss nude mice (Charles-River Laboratories, Barcelona, Spain) were housed under pathogen-free conditions in ventilated cages. Xenograft tumor assays were performed with HCT116 p53$^{+/+}$, HCT116 p53$^{-/-}$ and SW837 tumor cells. Briefly, 1×10^6 (HCT116 cells) or 5×10^6 (SW837 cells) (in PBS) were inoculated subcutaneously in mice dorsal flank. Tumor dimensions were assessed by caliper measurement, and their volumes were calculated using the equation *tumor volume = (*L × W^2*)/2*, where *L* and *W* represent the longest and shortest axis of the tumor, respectively. Treatment started when tumors reached approximately 100 mm^3 volume (14 or 8 days after the HCT116 and SW837 grafts, respectively). Mice were thereafter treated twice a week with MANIO or vehicle by intraperitoneal injection for two weeks. Tumor volumes, body weights or any signs of morbidity were regularly monitored until the end of the treatment. Animals were sacrificed by cervical dislocation at the end of the study. At the time of sacrifice, blood samples and organs (kidneys, spleen, heart, and liver) were collected for toxicological analysis. Each experimental group included six animals.

4.2.19. IHC

Tissues of HCT116 (p53$^{+/+}$ and p53$^{-/-}$) and SW837 tumors were prepared and stained with H&E or antibodies, as described in Chapter 3 (section 3.2.3.). Antibodies used are listed in Annex I, Table S2. TUNEL assay was performed using the *In situ Cell Death Detection Kit Fluorescein* (Roche, Ingrenor, Porto, Portugal), according to the manufacturer's instructions. Tissues were counterstained with DAPI (0.1 µg/mL).

4.2.20. Combination therapy assays

To assess the synergistic effect of MANIO with conventional chemotherapeutic drugs, SW837 and patient-derived primary CRC cells (CCZ3) were treated with 0.9 µM or 2 µM MANIO, respectively, and increasing concentrations of DOXO (0.313 – 1.330 µM), cisplatin (1.25 – 20 µM), or 5-FU (2.5 – 20 µM) for 24 h (SW837 cells) or 48 h (patient-derived CRC cells). The effect of combined treatments on cell proliferation was analyzed by SRB (for SW837 cells) or MTT (for patient-derived CRC cells) assays as described in 4.2.4. For each combination, CI and DRI values were calculated as described in 3.2.8.

4.2.21. Statistical analysis

Data were statistically analyzed using GraphPad Prism software v7.0. Different statistical tests were used accordingly to the dataset; *p* values < 0.05, < 0.01 and < 0.001 were considered statistically significant.

4.3. Results

4.3.1. MANIO displays p53-dependent growth inhibitory effect in human cancer cells, inducing cell cycle arrest and apoptosis, but not genotoxicity

In an attempt to identify new effective p53-activating agents with antitumor activity, the anti-proliferative activity of a small chemical library of 6,7-bis(hydroxymethyl)-1*H*,3*H*-pyrrolo[1,2-c]thiazoles was investigated in a panel of human cancer cells with different p53 status, by the SRB assay. Based on the IC_{50} values obtained for the tested compounds, the (3*S*)-6,7-bis(hydroxymethyl)-5-methyl-3-phenyl-1*H*,3*H*-pyrrolo[1,2-c]thiazole (MANIO; Figure 15A) was selected due to its noticeable selectivity to cancer cells expressing p53 (Figure 15B). Actually, the IC_{50} values of MANIO ranged from 0.20 – 0.97 µM (in wtp53-expressing cells) and 0.088 – 6.27 µM (in mutp53-expressing cells) to 26.20 – 48.25 µM in p53-null cells (Figure 15B). These results clearly demonstrated that MANIO had a p53-dependent anti-proliferative activity, with much lower IC_{50} values in cancer cells expressing p53, when compared to p53-null cells (Figure 15C). In fact, the IC_{50} value of MANIO in colon adenocarcinoma HCT116 cells expressing wtp53 (HCT116 $p53^{+/+}$; 0.97 µM) was approximately 50-fold lower to that obtained in its p53-null isogenic derivative (HCT116 $p53^{-/-}$; 48.25 µM) (Figure 15B). Accordingly, MANIO did not significantly affect colony formation in HCT116 $p53^{-/-}$ cells, while a pronounced growth inhibitory effect was observed in HCT116 $p53^{+/+}$ cells (Figure 15D; Annex IV, Figure S7). Consistently, 1 and 2.5 µM MANIO induced G2/M-phase cell cycle arrest (Figure 15E) and increased the percentage of Annexin V-positive cells (Figure 15F), in $p53^{+/+}$, but not in $p53^{-/-}$, HCT116 cells. The stimulation of a p53-dependent apoptotic cell death by MANIO was further evidenced by the induction of PARP cleavage, at 1 µM, in $p53^{+/+}$, but not in $p53^{-/-}$, HCT116 cells (Figure 15G).

We also checked whether the anti-proliferative effect of MANIO was associated with the induction of DNA damage. The potential genotoxicity of MANIO was therefore evaluated in tumor and normal cells, by comet assay and micronucleus test, respectively. Contrary to the positive controls, 1 and 2.5 μM MANIO did not increase the percentage of comet-positive HCT116 p53$^{+/+}$ cells (Figure 15H; Annex IV, Figure S8), and the number of formed micronuclei in peripheral lymphocytes of normal individuals (Figure 15I).

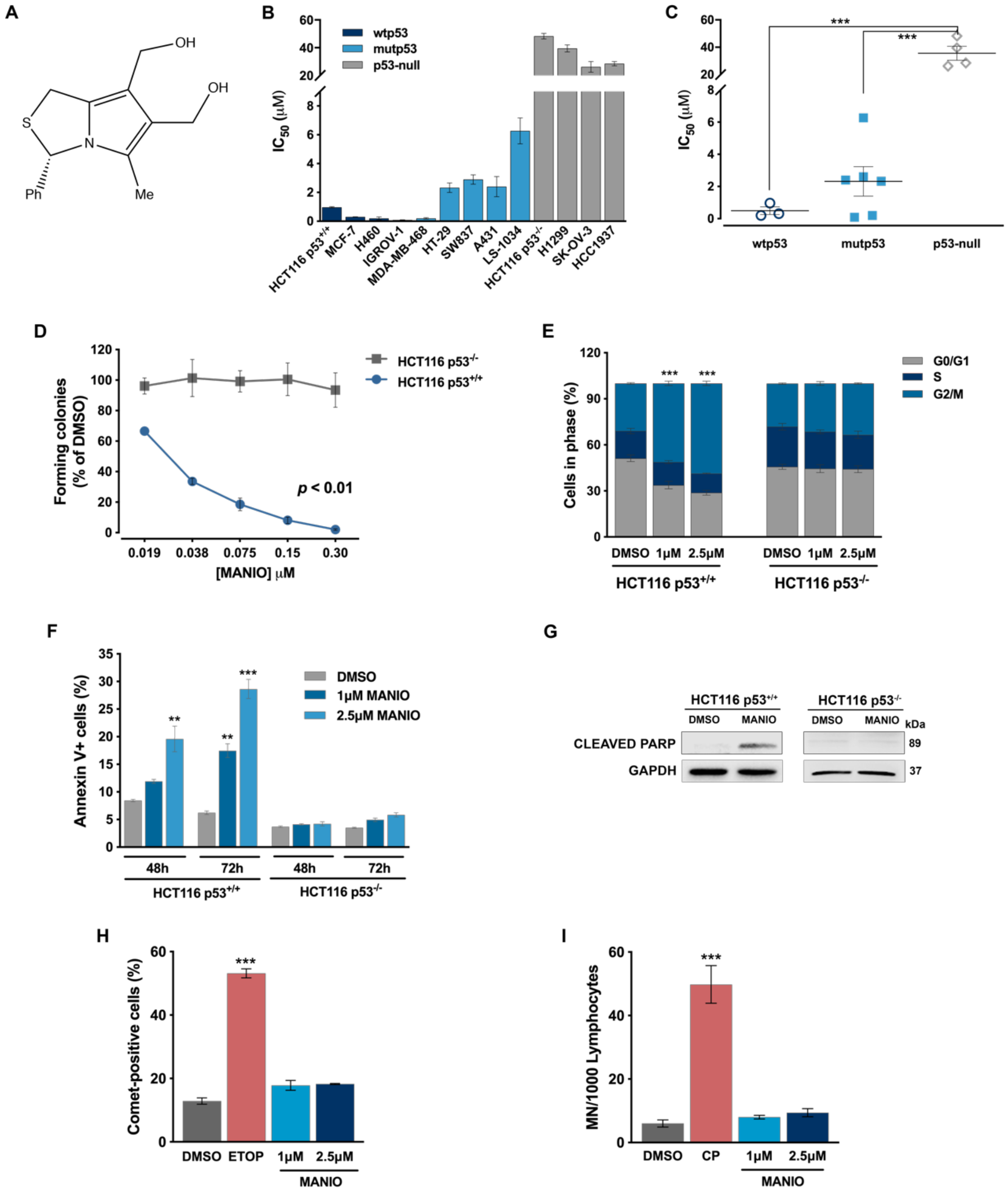

Figure 15. Growth inhibitory effect of MANIO in human cancer cells is dependent on p53 and is associated with induction of cell cycle arrest and apoptosis, but not genotoxicity. (A) Chemical structure of MANIO. **(B)** IC_{50} values of MANIO in a panel of human cancer cell lines with

distinct p53 status. Growth inhibitory effect of MANIO was determined by the SRB assay, after 48 h treatment. Growth obtained with control (DMSO) was set as 100%. Data are mean ± SEM of 4-5 independent experiments. **(C)** Scatter-plot representation of the relationship between MANIO IC_{50} values and p53 status in cancer cells. Data are mean ± SEM of 4-5 independent experiments; values significantly different: ****p* < 0.001; two-way ANOVA with Dunnett's multiple comparisons test. **(D)** Effect of MANIO on colony formation of $p53^{+/+}$ and $p53^{-/-}$ HCT116 cells, after 14 days of treatment. Data are mean ± SEM of 4 independent experiments; *p* < 0.01; two-way ANOVA with Sidak's multiple comparisons test. **(E)** Effect of MANIO on cell cycle progression of $p53^{+/+}$ and $p53^{-/-}$ HCT116 cells, after 48 h treatment. Cell cycle phases were analyzed by flow cytometry using PI, and quantified using the FlowJo software. Data are mean ± SEM of 3 independent experiments; values significantly different from DMSO: ****p* < 0.001; two-way ANOVA with Dunnett's multiple comparisons test. **(F)** Effect of MANIO on apoptosis of $p53^{+/+}$ and $p53^{-/-}$ HCT116 cells, after 48 and 72 h treatment. Apoptosis was analyzed by flow cytometry using FITC-Annexin V and PI. Data are mean ± SEM of 3 independent experiments; values significantly different from DMSO: ****p* < 0.001; two-way ANOVA with Dunnett's multiple comparisons test. **(G)** Effect of 1 µM MANIO on PARP cleavage, after 72 h treatment, in $p53^{+/+}$ and $p53^{-/-}$ HCT116 cells. Immunoblots represent one of three independent experiments. GAPDH was used as a loading control. **(H)** Measurement of DNA damage in HCT116 $p53^{+/+}$ cells with 1 and 2.5 µM MANIO and 25 µM etoposide (ETOP; positive control), after 48 h treatment, using the alkaline comet assay. Quantification of comet-positive cells (containing more than 5% of DNA in the tail; assessed by OPEN COMET/IMAGEJ); 100 cells were analyzed in each group (representative images are shown in Annex III, Figure S8); 3 independent experiments; values significantly different from DMSO: ****p* < 0.001; one-way ANOVA with Dunnett's multiple comparisons test. **(I)** Cytokinesis-block micronucleus (MN) assay after 72 h treatment, in human lymphocyte cells; 5 µg/mL cyclophosphamide (CP): positive control; the number of MN per 1000 binucleated lymphocytes was recorded (3 independent experiments); values significantly different from DMSO: ****p* < 0.001; one-way ANOVA with Dunnett's multiple comparisons test.

4.3.2. Activation of the p53 response pathway by MANIO in HCT116 cells is associated with p53 stabilization, and enhancement of p53 DNA-binding and transcriptional activity

To gain more evidence of the potential to engage the p53 response pathway, HCT116 $p53^{+/+}$ cells were treated with 1 µM MANIO for 24 h followed by RNA-seq. Results indicated that MANIO treatment led to broad changes in gene expression with nearly 900 upregulated and 500 downregulated differentially expressed genes (DEGs) (four replicates for each treatment and DMSO control, log fold change < -1 or > 1, multiple tests correction, adjusted *p* value < 0.05; data is deposited in GEO - accession GSE145482) (Figure 16A, B). Gene ontology, pathway, and upstream regulator enrichment analysis using the EnrichR webtool [419] showed strong evidence for the activation of the p53-response pathway (Figure 16C, upper panel). Instead, the list of genes repressed by MANIO diverged from a canonical p53-dependent signature, as it was not enriched for cell proliferation, DNA repair, DNA replication, or cell division (Figure 16C, lower panel). Similar results were obtained using GSEA or Metascape (Annex IV, Figure S9A, S9B and data not shown). Indeed, about 65 established p53 target genes were upregulated by MANIO in the RNA-seq data (Figure

16D). Hence, the upregulated gene signature of MANIO-treated HCT116 p53$^{+/+}$ cells is indisputably p53-related. The p53-dependent gene repression is thought to be mostly indirect and largely dependent on the modulation of the DREAM complex via p21 [420], which is induced by MANIO. Based on this, we compared MANIO downregulated DEGs with an extended list of DREAM complex targets, and found a very small overlap (Annex III, Figure S9C). However, we observed a trend for down-modulation by MANIO of several DREAM targets (Annex IV, Figure S9D). We then explored if the lack of a canonical p53-dependent gene repression signature could be dependent on the timepoint of our RNA-seq analysis by following four targets expression of MANIO-treated cells for 16, 24, and 48 h (Annex IV, Figure S9E). Results confirmed the RNA-seq data and showed the same trend also for the earlier time point, while the 48 h treatment showed a trend for downregulation, paralleled by higher induction of p21. As such, it appears that MANIO engages the p53-dependent response, with its effects persisting and increasing over at least a 48 h time window.

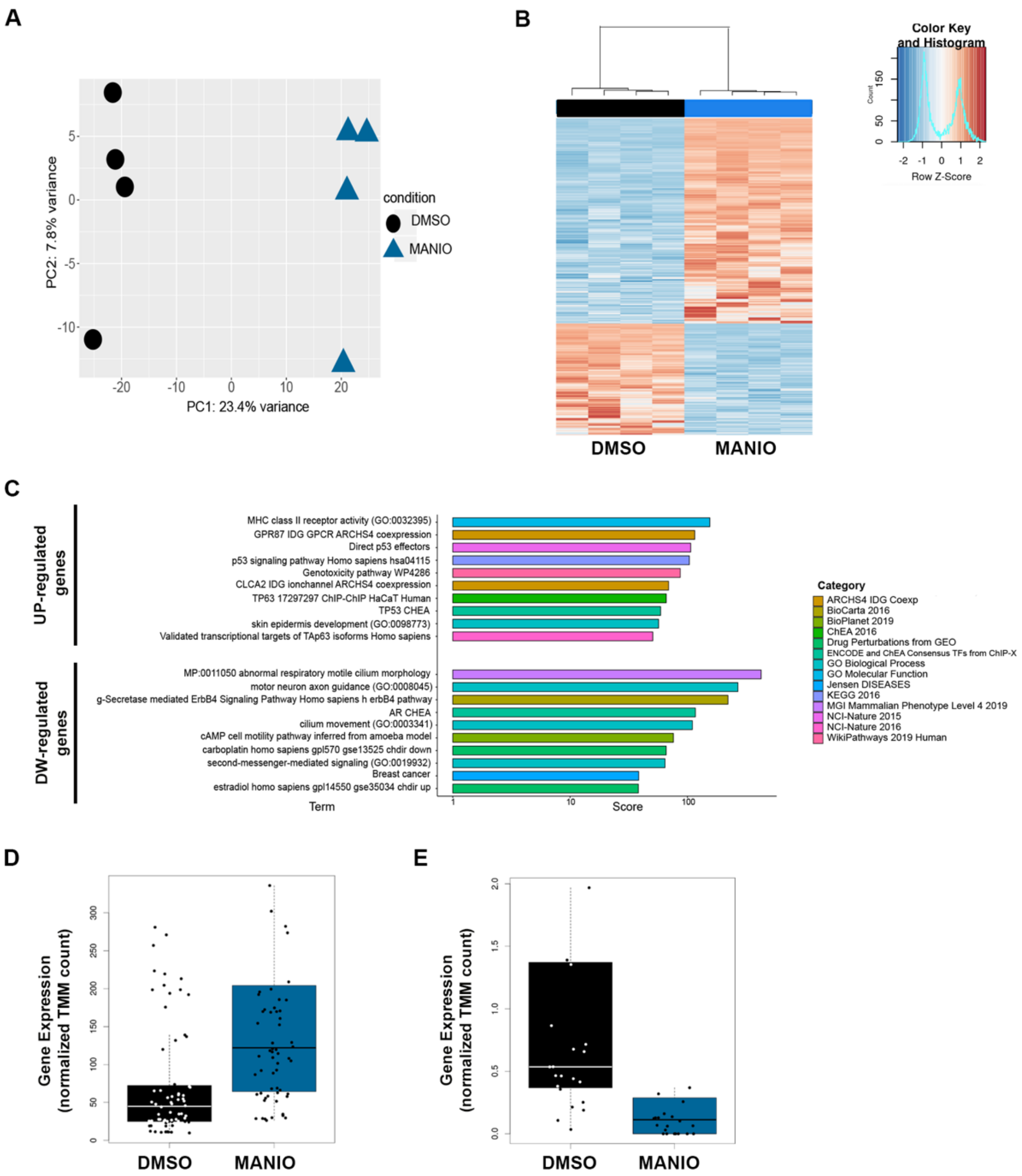

Figure 16. Gene expression profile changes in human cancer cells by MANIO reveal a p53-activating signature. (A) Principal component analysis (PCA) of the gene expression counts (log2 normalized Trimmed Mean of M-values (TMM) method counts) showing the first versus the second principal component (PC). In the axes, the percentage of the explained variance by the component is reported. Samples in the two conditions (DMSO, 1 µM MANIO) are highlighted in different colors and different shapes. **(B)** Heatmap showing the differentially expressed genes (log2 Fold change < -1 or > 1, multiple tests correction adjusted *p* value < 0.05) in the comparison MANIO vs DMSO. Gene expression counts were normalized by the TMM method, hierarchically clustered with average linkage and uncentered correlation metric was applied. Two main clusters of genes were obtained: the first one is composed by the genes upregulated through the samples cluster and a second one composed by the genes downregulated. **(C)** Barplot graphs represent the enrichment of the biological terms based on the Combined score (x-axis), as calculated by the EnrichR web tool; upper panel: upregulated (UP) gene cluster, bottom panel: downregulated (DW) gene cluster. Since this tool provides a large collection of gene set databases, a few key elements were selected for each. For the full results please see Annex IV (Figure S9). All terms have multiple tests correction adjusted *p* value < 0.05. **(D, E)** Boxplot representations of the RNA-seq based gene expression for one element from the upregulated gene cluster (p53 signaling pathway, **D**) and one element from the downregulated gene cluster (cAMP-mediated cell motility pathway genes, **E**).

Consistently, in HCT116 p53$^{+/+}$ cells, MANIO treatment increased p53 protein levels in a dose- and time-dependent manner (Figure 17A), which was related to p53 stabilization. In fact, an enhancement of p53 half-life by 1 µM MANIO was observed upon inhibition of protein synthesis with 150 µg/mL cycloheximide (Figure 17B).

Moreover, 1 µM MANIO regulated the protein levels of major p53 transcriptional targets, increasing MDM2, p21, GADD45, PUMA, and Killer/DR5, while decreasing the anti-apoptotic BCL-2, in p53$^{+/+}$, but not in p53$^{-/-}$, HCT116 cells (Figure 17C). Accordingly, 1 and 2.5 µM MANIO increased the mRNA levels of the p53 transcriptional targets *MDM2*, *CDKN1A/p21*, *GADD45A*, *BAX*, *TNFRSF10B/DR5*, *PUMA*, and *NOXA* in HCT116 p53$^{+/+}$ cells, without affecting their expression in p53-null HCT116 cells (Figure 17D). By ChIP assay, we further verified that the increase of p53 transcriptional activity by MANIO resulted from an enhancement of p53 DNA-binding ability in HCT116 p53$^{+/+}$ cells. In fact, treatment with 1 and 2.5 µM MANIO increased p53 occupancy at *MDM2* and *CDKN1A* promoters (Figure 17E).

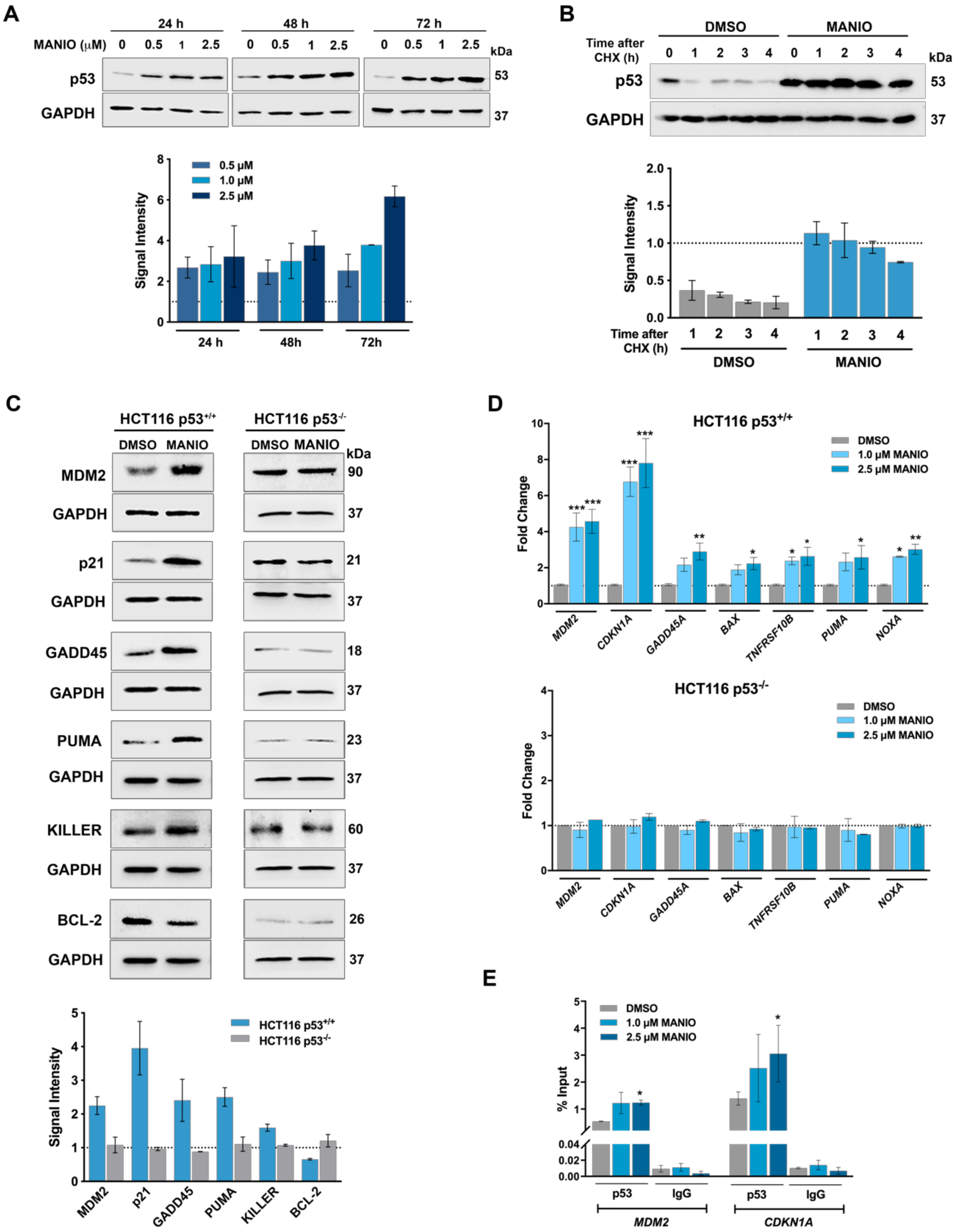

Figure 17. MANIO enhances p53 stabilization and transcriptional activity, regulating the expression of several p53 target genes by increasing its DNA-binding ability, in HCT116 p53$^{+/+}$ cells. (A) Effect of 0.5, 1.0, and 2.5 μM MANIO on the protein expression levels of p53, after 24, 48, and 72 h treatment, in HCT116 p53$^{+/+}$ cells. Quantification of p53 protein levels relative to DMSO (set as 1); data are mean ± SEM of 3 independent experiments. **(B)** p53 protein levels in HCT116 p53$^{+/+}$ cells treated with 1 μM MANIO or solvent for 48 h followed with 150 μg/mL cycloheximide (CHX). Quantification of p53 protein levels relative to 0 h (no CHX treatment) was set as 1; data are mean ± SEM of 3 independent experiments. **(C)** Effect of 1 μM MANIO on the protein expression levels of p53 target genes, after 48 h (MDM2, p21, and GADD45) and 72 h (BCL-2, KILLER, and PUMA) treatment, in p53$^{+/+}$ and p53$^{-/-}$ HCT116 cells. Quantification of protein expression levels in

$p53^{+/+}$ and $p53^{-/-}$ HCT116 cells, relative to DMSO (set as 1); data are mean ± SEM of 3 independent experiments. In A-C, immunoblots represent 1 of 3 independent experiments; GAPDH was used as loading control. **(D)** Effect of 1 and 2.5 μM MANIO in mRNA levels of p53 target genes in $p53^{+/+}$ and $p53^{-/-}$ HCT116 cells, after 48 h treatment, determined by RT-qPCR. Fold of induction is relative to DMSO. Data are mean ± SEM of 3 independent experiments; values significantly different from DMSO: *$p < 0.05$; **$p < 0.01$; ***$p < 0.001$; two-way ANOVA with Dunnett's multiple comparison test. **(E)** Analysis of p53 occupancy at *MDM2* and *CDKN1A* promoters, in HCT116 $p53^{+/+}$ cells, determined by ChIP, after 48 h treatment with 1 and 2.5 µM MANIO. Immunoprecipitation was performed using the anti-p53 antibody (DO-1) or an anti-mouse IgG as a negative control (IgG). The enrichment of DNA fragments was analyzed by qPCR, using site-specific primers. Data are mean ± SEM of 3 independent experiments; values significantly different from DMSO: *$p < 0.05$; two-way ANOVA with Dunnett's multiple comparison test.

4.3.3. MANIO reactivates distinct contact and structural mutp53, restoring wt-like properties to mutp53 R248W in CRC cells

Given the prominent anti-proliferative activity of MANIO in mutp53-expressing cancer cells (Figure 15B, C), we analyzed its capacity to reactivate distinct structural and contact mutp53, with high prevalence and clinical relevance in human cancers [198]. With this aim, these mutp53s were ectopically expressed in p53-null H1299 tumor cells, and the anti-proliferative effect of MANIO was evaluated by SRB assay (Figure 18A). Importantly, no significant differences were detected between the protein expression levels of the different mutp53 (Figure 18A, lower panel). When compared to cells transfected with the empty vector, MANIO showed a significant reduction of its IC_{50} values in H1299 cells expressing mutp53 R282W, R248W, R280K, R273H, R273C, G245D, R175H, R248Q or G245S (Figure 18A). Interestingly, MANIO presented its highest inhibitory effect on cells expressing mutp53 R248W and R248Q, while no reduction in IC_{50} was observed for mutp53 Y220C, suggesting some level of specificity (Figure 18A). The high IC_{50} values of MANIO in both parental (39.50 ± 2.50 µM, Figure 15B) and empty vector-transfected (41.25 ± 1.61 µM, Figure 18A) H1299 cells further reinforced its mutp53-dependent anti-proliferative activity.

To further support the ability of MANIO to reactivate mutp53, we focused on mutp53 R248W. As expected, a prominent growth inhibition was induced by MANIO treatment in SW837 CRC cells, which endogenously express mutp53 R248W, as demonstrated by SRB (IC_{50} of 2.9 ± 0.32 µM; Figure 15B) and colony formation (Figure 18B; Annex IV, Figure S7) assays. Consistently with a reactivation of mutp53 R248W, 3 μM MANIO increased the protein levels of p53 transcriptional targets, including MDM2 and PUMA, an effect abolished by p53 siRNA silenced SW837 cells (Figure 18C; Annex IV, Figure S10). Moreover, the mRNA levels of *MDM2*, *CDKN1A/p21*, and *NOXA,* were upregulated in a dose-dependent manner (Figure 18D). Additionally, 6 μM MANIO enhanced mutp53 R248W occupancy at

MDM2 and *CDKN1A* promoters, evidencing the restoration of mutp53 DNA-binding ability (Figure 18E).

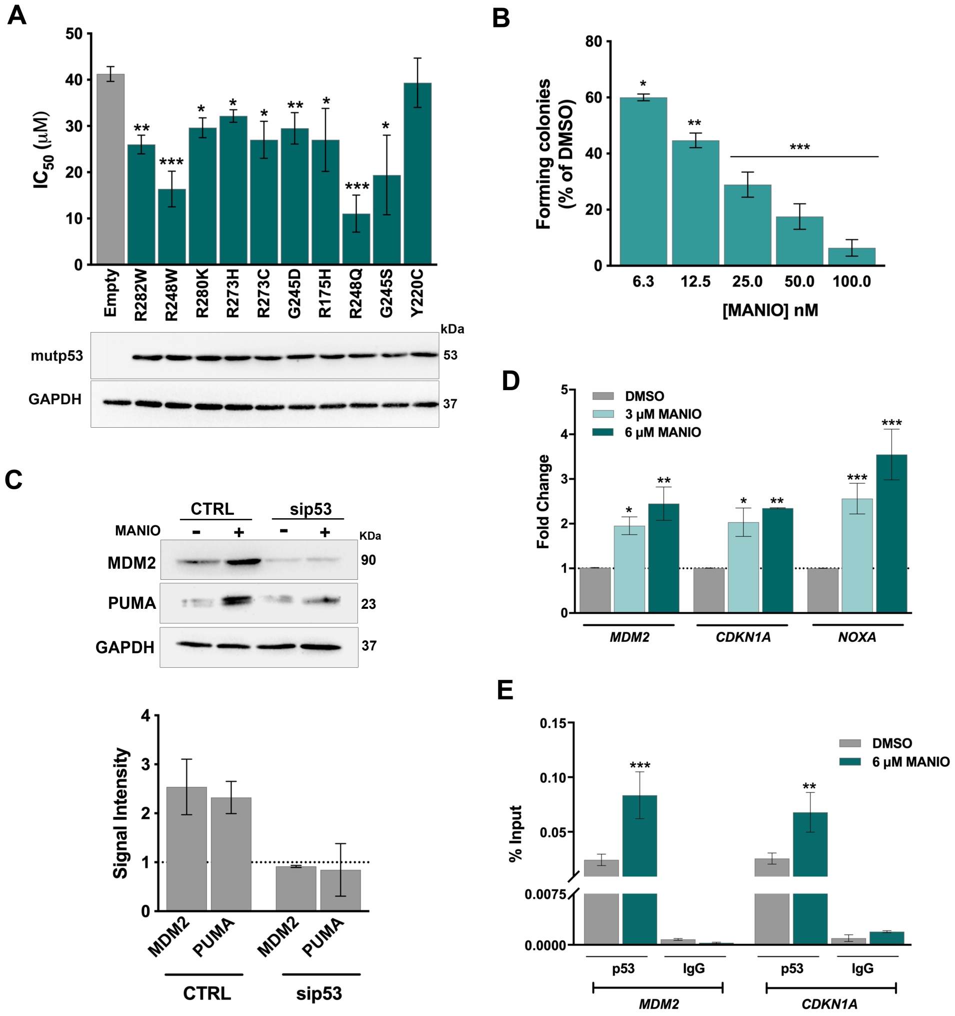

Figure 18. MANIO reactivates distinct contact and structural mutp53, inhibiting the growth of mutp53 R248W-expressing SW837 cells through restoration of wt-like p53 transcriptional activity and DNA-binding ability. (A) p53-null H1299 cells were transfected with pcDNA3 plasmid expressing mutp53, or with the empty pcDNA3 plasmid, using ScreenFect®A. Growth inhibitory effect of 3.125 – 50 µM MANIO, in H1299 cells, was determined by SRB assay, after 48 h treatment. Data are mean ± SEM of 4-8 independent experiments; values significantly different from empty vector: $^{*}p < 0.05$; $^{**}p < 0.01$; $^{***}p < 0.001$, unpaired Student's *t*-test. Immunoblot represent the protein expression levels of mutp53 in untreated H1299-transfected cells, after 72 h incubation. **(B)** Effect of MANIO on SW837 cell colony formation, after 11 days of treatment. Data are mean ± SEM of 4 independent experiments; values significantly different from empty vector: $^{*}p < 0.05$ $^{**}p < 0.01$; $^{***}p < 0.001$, one-way ANOVA with Dunnett's multiple comparisons test. **(C)** Protein levels of MDM2 and PUMA, after 24 h treatment with 3 µM MANIO, in mutp53 R248W-silenced (sip53) and control (CTRL) SW837 cells. Quantification of protein expression levels is relative to DMSO (set as 1). **(D)** Effect of 3 and 6 µM MANIO on the mRNA expression levels of p53 target genes in SW837 cells, after 24 h treatment, determined by RT-qPCR. Fold of induction is relative to DMSO. Data are mean ± SEM of 3 independent experiments; values significantly different from DMSO: $^{*}p < 0.05$; $^{**}p < 0.01$; $^{***}p < 0.001$; two-way ANOVA with Dunnett's multiple comparisons test. **(E)** Analysis of

the p53 occupancy at *MDM2* and *CDKN1A* promoters in SW837 cells, after 24 h treatment with 6 μM MANIO, determined by ChIP. Immunoprecipitation was performed with the anti-p53 antibody (DO-1) or an anti-mouse IgG as a negative control (IgG). The enrichment of DNA fragments was analyzed by qPCR, using site-specific primers. Data are mean ± SEM of 3 independent experiments; values significantly different from DMSO: $^{**}p < 0.01$; $^{***}p < 0.001$; two-way ANOVA with Dunnett's multiple comparisons test. In A and C, immunoblots are representative of 3 independent experiments; GAPDH was used as a loading control.

4.3.4. MANIO leads to wt and mutp53 R248W thermal stabilization through direct binding to protein DBD

To ascertain the mechanism by which MANIO would affect wt and mutp53 function leading to a pronounced p53-dependent antitumoral activity, we investigated whether it could directly bind to these proteins. With such purpose, we started performing the CETSA analysis, checking the impact of MANIO on the thermal stabilization of wt and mutp53 R248W, as a consequence of potential interactions with these proteins. In fact, in CETSA, analysis, upon gradual heating, unbound proteins denature and precipitate, while a small molecule ligand can counteract this effect by providing thermodynamic stability to a target protein and subsequently increasing its fraction in solution [421]. Based on this premise, the amount of soluble wt and mutp53 R248W was measured after heating of HCT116 and SW837 cell lysates, respectively. In HCT116 cells, 30 μM MANIO induced wtp53 thermal stabilization at 38 °C and 39 °C (Figure 19A), causing a concentration-dependent wtp53 thermal stabilization at 39 °C, when compared to solvent (Figure 19B). Also, in SW837 cells, 0.75 μM MANIO induced mutp53 R248W thermal stabilization between 39 °C and 41 °C (Figure 19C). Moreover, at 40 °C, MANIO caused a concentration-dependent mutp53 R248W thermal stabilization, when compared to solvent (Figure 19D). In fact, 0.75 μM MANIO promoted a complete protein stabilization, with reestablishment of the non-denatured mutp53 protein levels observed with solvent at 25 °C (Figure 19D).

To confirm the potential interaction between MANIO and p53 evidenced by CETSA, the human wt and mutp53 R248W DBD were produced in *Echerichia coli* cells and purified for a binding fluorescence quenching assay. The binding assay corroborated the direct interaction of MANIO with the DBD of wtp53 (Kd of 590 ± 90 μM) and mutp53 R248W (Kd of 320 ± 90 μM) (Figure 19E).

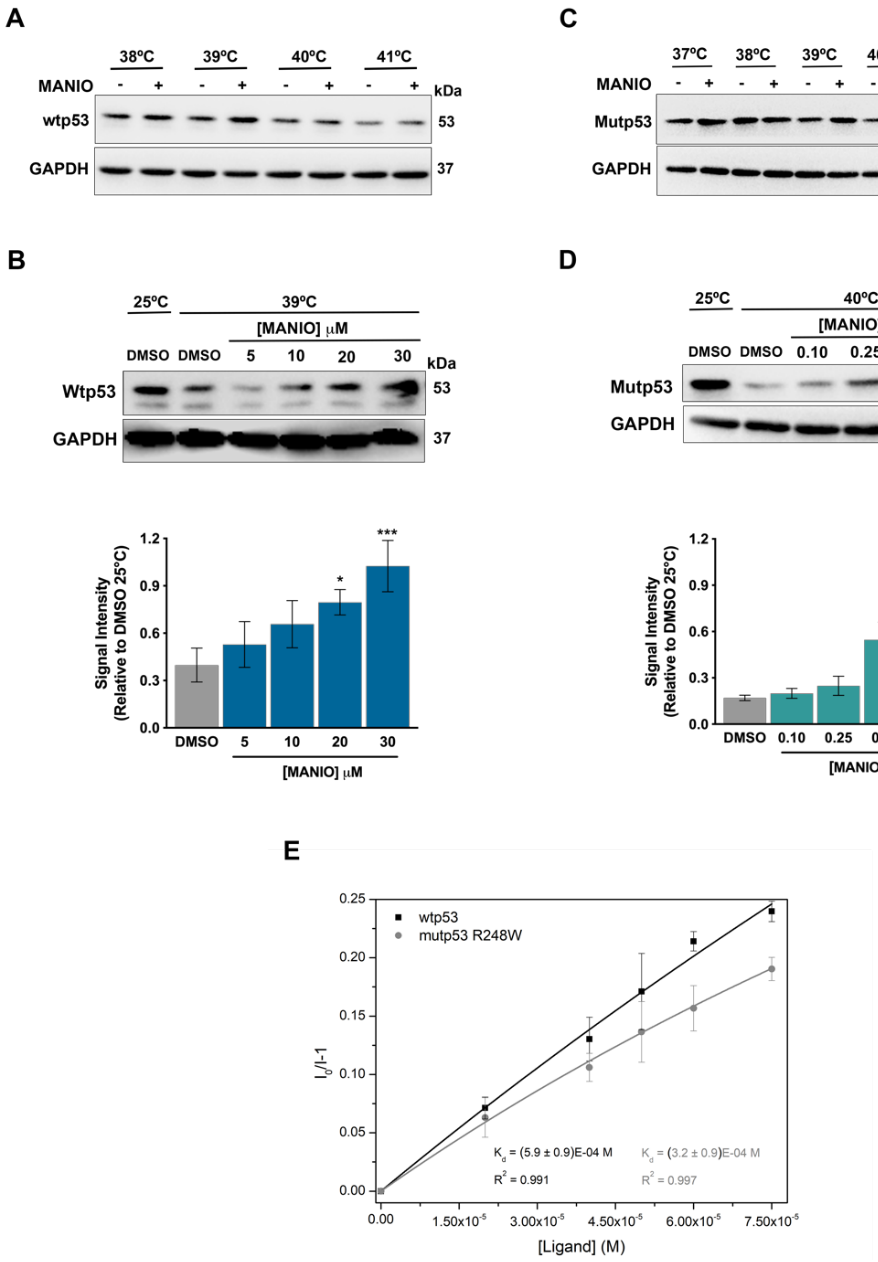

Figure 19. MANIO binds directly to the DBD of wt and mutp53 R248W, leading to their thermal stabilization. (A-D) CETSA experiments were performed in HCT116 **(A, B)** and SW837 **(C, D)** lysates. In **A** and **C**, lysate samples, treated with DMSO (-) or MANIO (+; 30 µM in HCT116 cells; 0.75 µM in SW837 cells), were heated at different temperatures. In **B** and **D**, lysate samples were treated with increasing concentrations of MANIO and heated at 39 °C **(B)** or 40 °C **(D)**; plotted data represent the amount of non-denatured p53 after heating, in MANIO-treated lysates relatively to DMSO (3 independent experiments); fold increase was calculated setting the amount of non-denatured mutp53 obtained with DMSO at 25 °C as 1. Data are mean ± SEM (3 independent experiments); values significantly different from DMSO: $^{**}p < 0.01$; $^{***}p < 0.001$; two-way ANOVA with Dunnett's multiple comparisons test. **(E)** p53-MANIO binding interactions measured by fluorescence quenching of *5* µM *wt*p53 (black squares) and mutp53 R248W (gray circles) proteins upon MANIO titration. The Kd for the interactions were determined via nonlinear regression using equation described in 4.2.17.

4.3.5. MANIO has *in vivo* p53-dependent antitumor activity in CRC xenograft mouse models, with no apparent toxic side effects

The *in vivo* antitumor activity of MANIO was assessed using human tumor xenograft mouse models of HCT116 p53$^{+/+}$, HCT116 p53$^{-/-}$ and SW837 CRC cells. Four intraperitoneal administrations of 100 mg/kg MANIO inhibited the growth of wtp53-expressing HCT116 and mutp53-expressing SW837 tumors, when compared to vehicle (Figure 20A, B, D, E). Conversely, for the same conditions, MANIO did not interfere with the growth of p53-null HCT116 tumors (Figure 20G, H), supporting its *in vivo* p53-dependent antitumor activity. Of notice that a pronounced antitumor activity was also achieved with 50 mg/kg MANIO in xenograft mouse models of SW837 cells (Figure 20D, E).

During the experimental time, no significant loss of body weight or morbidity signs were observed in mice treated with MANIO (Figure 20C, F, I). We also examined potential primary toxicity signs in mice induced by MANIO treatments. For that, at the time of sacrifice, organs relative weight, and biochemical and hematological blood parameters were determined (Table 2). No significant differences concerning the weight of heart, spleen, liver, or kidneys, as well as hematological and biochemical parameters were observed between MANIO and vehicle groups.

Tumor sections were subsequently analyzed by immunohistochemistry staining (Figure 20J-N). In both HCT116 p53$^{+/+}$ and SW837 tumors, MANIO treatment decreased Ki-67-positive staining (indicative of a lower proliferative status; Figure 20J, K), increased Bax expression (indicative of an apoptotic cell death; Figure 20J, L), and DNA fragmentation demonstrated by TUNEL-positive staining (Figure 20J, M), when compared to vehicle. Conversely, no significant differences were observed between the Ki-67, Bax and TUNEL staining of MANIO- and vehicle-treated HCT116 p53$^{-/-}$ tumors (Figure 20J-M). The alteration in p53 expression levels was also evaluated in the different experimental groups. Noteworthy, the expression of p53 was higher in mutp53-expressing SW837 tumors than in wtp53-expressing HCT116 tumors (vehicle-treated tumors; Figure 20J, N). On the other hand, it was observed an increase of wtp53 expression levels in MANIO-treated HCT116 p53$^{+/+}$ tumors, compared to the vehicle (Figure 20J, N). Conversely, in SW837 tumors, MANIO significantly decreased the mutp53 expression levels (Figure 20J, N). As expected, no p53 expression was detected in MANIO- and vehicle-treated HCT116 p53$^{-/-}$ tumors (Figure 20J).

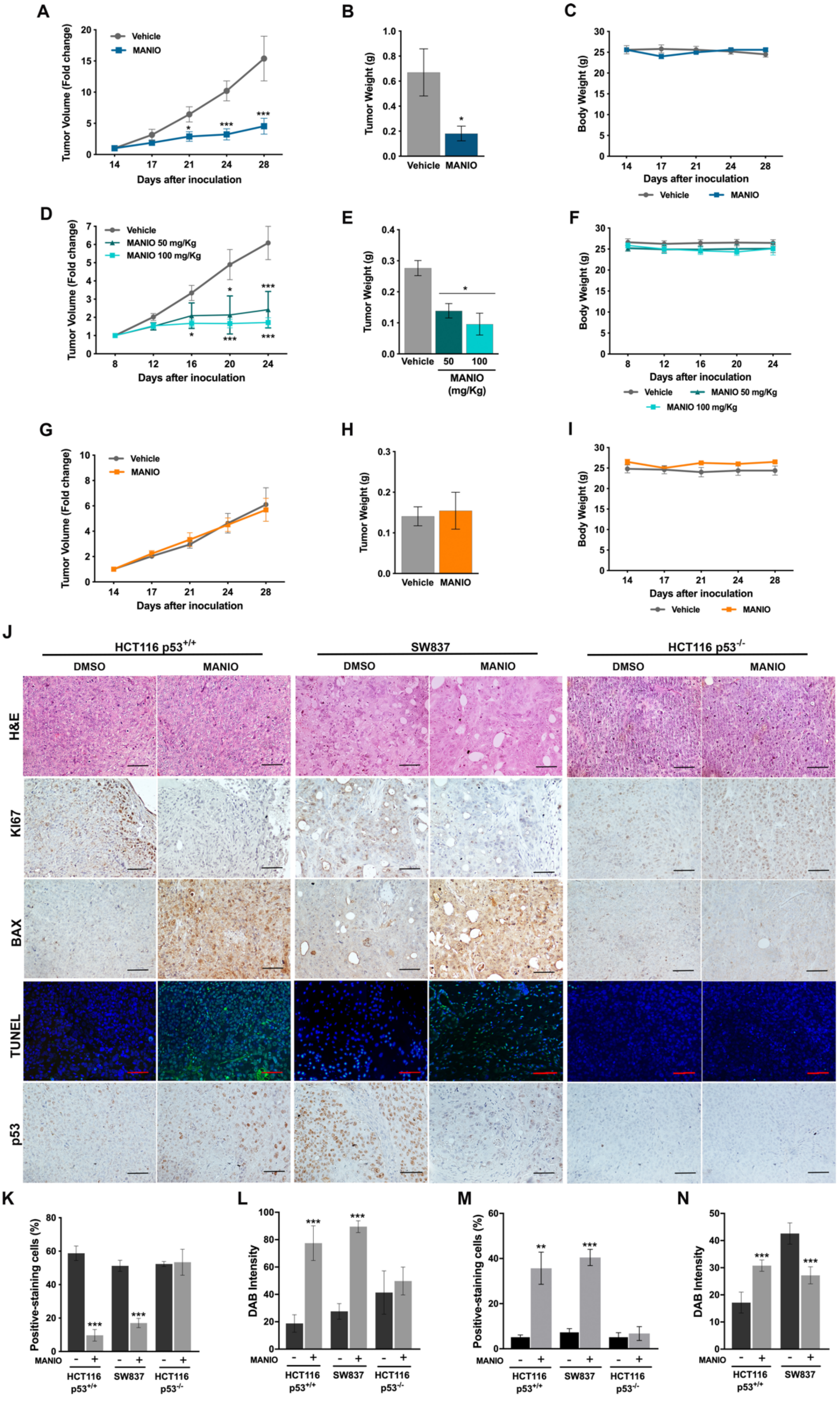
A
Tumor Volume (Fold change)
Vehicle
MANIO
Days after inoculation
14
17
21
24
28
*
***
***
B
Tumor Weight (g)
Vehicle
MANIO
*
C
Body Weight (g)
Days after inoculation
Vehicle
MANIO
D
Tumor Volume (Fold change)
Vehicle
MANIO 50 mg/Kg
MANIO 100 mg/Kg
Days after inoculation
8
12
16
20
24
E
Tumor Weight (g)
Vehicle
50
100
MANIO (mg/Kg)
F
Body Weight (g)
Days after inoculation
Vehicle
MANIO 50 mg/Kg
MANIO 100 mg/Kg
G
Tumor Volume (Fold change)
Vehicle
MANIO
Days after inoculation
H
Tumor Weight (g)
Vehicle
MANIO
I
Body Weight (g)
Days after inoculation
Vehicle
MANIO
J
HCT116 p53+/+
SW837
HCT116 p53-/-
DMSO
MANIO
DMSO
MANIO
DMSO
MANIO
H&E
KI67
BAX
TUNEL
p53
K
Positive-staining cells (%)
MANIO
HCT116 p53+/+
SW837
HCT116 p53-/-
L
DAB Intensity
MANIO
HCT116 p53+/+
SW837
HCT116 p53-/-
M
Positive-staining cells (%)
MANIO
HCT116 p53+/+
SW837
HCT116 p53-/-
N
DAB Intensity
MANIO
HCT116 p53+/+
SW837

Figure 20. MANIO has *in vivo* p53-dependent antitumor activity by inhibiting proliferation and enhancing apoptotic cell death. Swiss nude mice carrying HCT116 p53$^{+/+}$ **(A-C)**, SW837 **(D-F)**, and HCT116 p53$^{-/-}$ **(G-I)** xenografts were treated intraperitoneally with 50 or 100 mg/kg MANIO or vehicle (control), twice a week during two weeks (5 animals/group); values significantly different from vehicle: **p* < 0.05, ****p* < 0.001; two-way ANOVA with Dunnett's multiple comparisons test. Tumor weight of mice carrying HCT116 p53$^{+/+}$ **(B)**, SW837 **(E)**, and HCT116 p53$^{-/-}$ **(H)** xenografts, at the end of the treatment with MANIO or vehicle; data are mean ± SEM; values significantly different from vehicle: **p* < 0.05; unpaired Student's *t*-test. Body weight of mice carrying HCT116 p53$^{+/+}$ **(C)**, SW837 **(F)**, and HCT116 p53$^{-/-}$ **(I)** xenografts, during MANIO or vehicle treatment; no significant differences between vehicle and MANIO-treated mice: *p* > 0.05; two-way ANOVA with Dunnett's multiple comparisons test. **(J)** Representative images of Ki-67, BAX, DNA fragmentation (TUNEL) and p53 detection in tumor tissues of HCT116 p53$^{+/+}$, SW837 and HCT116 p53$^{-/-}$ xenografts treated with MANIO or vehicle, collected at the end of the treatment (scale bar = 10 µm; magnification = ×200). **(K)** Percentage of positive-staining Ki-67 cells. **(L)** Quantification of BAX staining evaluated by 3,3′-diaminobenzidine (DAB) intensity. **(M)** Percentage of positive-staining TUNEL cells. **(N)** Quantification of p53 staining evaluated by DAB intensity. In **(K-N)**, data are mean ± SEM of 3 independent experiments; values significantly different from vehicle: ***p* < 0.01, ****p* < 0.001, unpaired Student's *t*-test.

Table 2. Toxicological studies of MANIO in Swiss nude mice.

	Vehicle	**Treated**
Relative tissue weight (trophism)		
Spleen/BW (g/kg)	5.97 ± 0.50	7.08 ± 0.79
Heart/BW (g/kg)	6.23 ± 0.46	5.84 ± 0.68
Liver/BW (g/kg)	54.03 ± 2.65	64.05 ± 3.76
Kidney/BW (g/kg)	8.39 ± 0.60	9.51 ± 0.84
Hematological data		
WBC count (×10^3/µL)	1.68 ± 0.03	1.40 ± 0.10
RBC count (×10^6/µL)	9.03 ± 0.33	8.41 ± 0.42
HGB (g/dL)	13.58 ± 0.54	12.88 ± 0.43
HCT (%)	43.10 ± 1.74	41.60 ± 1.60
PLT counts (×10^3/µL)	953.0 ± 275.43	1195.67 ± 172.42
Biochemical data		
Blood glucose (mg/dL)	201.89 ± 9.61	185.57 ± 9.25
Urea (mg/dL)	24.80 ± 1.19	22.41 ± 1.93
Creatinine (mg/dL)	0.32 ± 0.06	0.28 ± 0.04
Total Protein (g/dL)	5.03 ± 0.12	4.47 ± 0.13
Albumin (g/dL)	2.88 ± 0.14	2.47 ± 0.08
ALT (U/L)	20.71 ± 3.62	20.50 ± 13.30
AST (U/L)	79.67 ± 10.17	69.25 ± 11.95
Total Cholesterol (mg/dL)	87.89 ± 5.08	80.67 ± 4.96
Triglycerides (mg/dL)	99.11 ± 4.92	111.00 ± 9.01

Data were analyzed for vehicle and 100 mg/kg MANIO (treated) mice groups, after four intraperitoneal administrations (twice a week). Results are mean ± SEM (6 independent experiments). ALT, alanine aminotransferase; AST, aspartate aminotransferase; BW, body weight; HCT, hematocrit; HGB, hemoglobin concentration; PLT, platelet; RBC, red blood cell count; RET, reticulocytes; WBC, white blood cells.

4.3.6. MANIO inhibits the growth of patient-derived CRC cells through regulation of p53 transcriptional targets

In order to assess the effectiveness of MANIO in a more disease-relevant model system, closer to the heterogeneity and intrinsic drug sensitivity of the original tumors [422], the growth inhibitory effect of MANIO was determined in a panel of patient-derived primary CRC cells. All CRC cells expressed wtp53, excepting CCA8 that harbored the mutp53 P151S (Table 3). By the MTT assay, it was observed that MANIO inhibited the growth of all patient-derived CRC cells with IC_{50} values ranging from 0.09 to 15.43 μM (Figure 21A; Table 3). MANIO displayed the highest growth inhibitory effect on CCZ2 cells, which has high clinical relevance. CCZ2 cells were from a patient diagnosed with liver metastatic adenocarcinoma that was first subjected to conventional chemotherapy, namely 5FU and oxaliplatin plus anti-angiogenic agent bevacizumab (Table 3), following by surgical removal of the remaining liver metastasis. In CCZ1, CCZ2, CCZ3, and CCZ5 cells, it was verified that MANIO interfered with the mRNA expression levels of several p53 transcriptional targets, increasing *BAX*, *CDKN1A/p21*, and *MDM2*, while decreasing the levels of the angiogenic factor *VEGF* in CCZ1, CCZ3, and CCZ5 (Figure 21B). Importantly, in CCZ1, CCZ2, and CCZ3 cells, MANIO also decreased the mRNA expression levels of the pro-survival *BIRC5* (Figure 21B), which is a critical gene in cancer cell growth and chemoresistance.

Table 3. Characterization of patient-derived CRC cells and growth inhibitory effect of MANIO.

PATIENT	SEX	Diagnosis	p53 status*	Prior Therapy	IC_{50} (μM)
CCA2	F	Adenocarcinoma	wt	---	15.43 ± 0.46
CCA8	M	Adenocarcinoma	c.451C>T p.Pro151Ser	---	14.50 ± 1.76
CCZ1	F	Adenocarcinoma	wt	---	14.00 ± 0.81
CCZ2	F	Metastatic adenocarcinoma	wt	5-FU + oxaliplatin + bevacizumab	0.09 ± 0.01
CCZ3	F	Adenocarcinoma	wt	---	11.46 ± 1.34
CCZ4	F	Adenocarcinoma	wt	---	13.33 ± 0.49
CCZ5	M	Adenocarcinoma	wt	---	9.46 ± 0.83
CCZ6	M	Mucinous Adenocarcinoma	wt	---	9.51 ± 1.51
CCZ7	F	Adenocarcinoma	wt	---	12.22 ± 1.51
CRCJS1	F	*ND*	wt	---	13.64 ± 1.49

*Obtained by sequencing. F, Feminine; M, Masculine; *ND*, not defined.

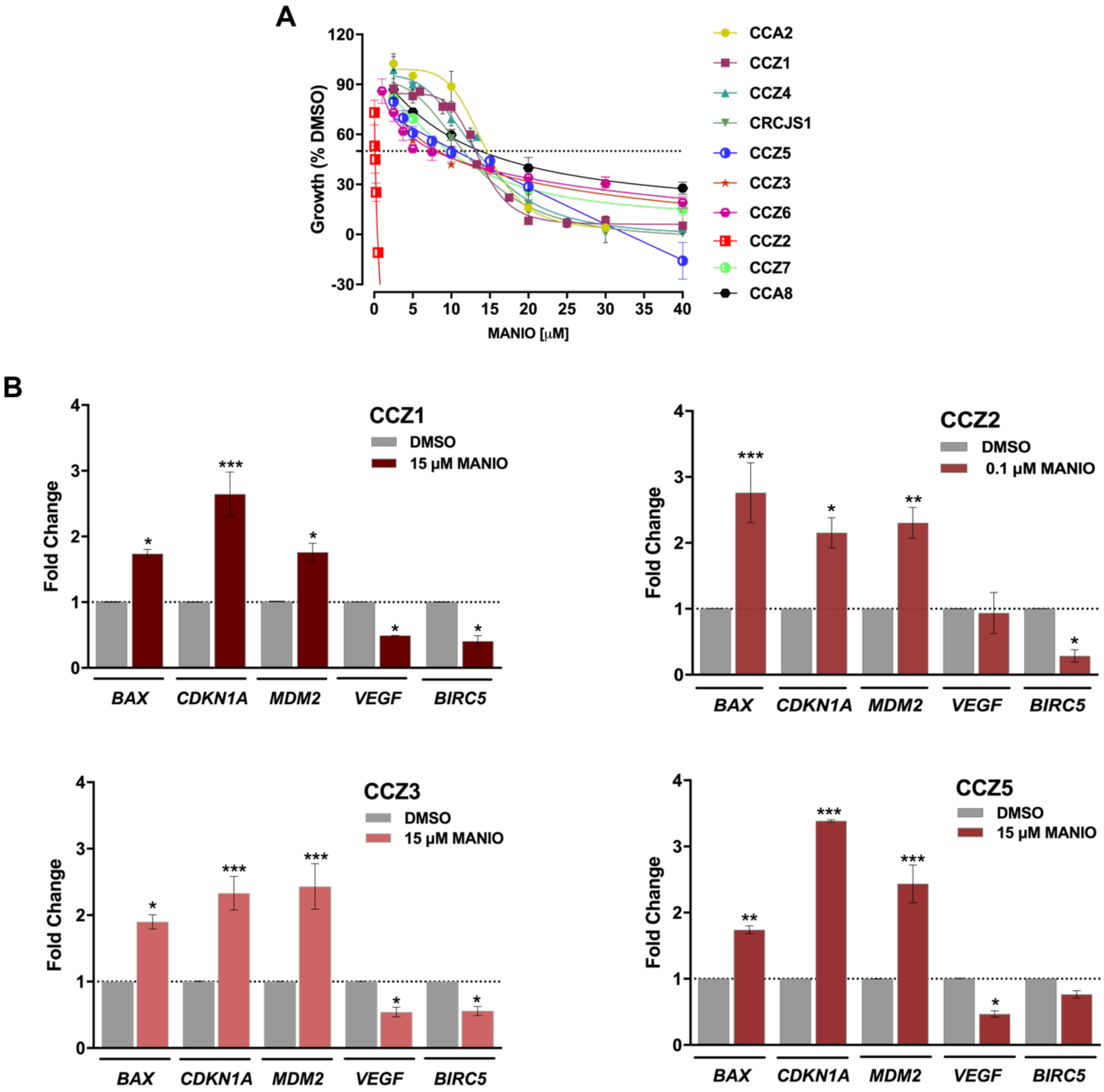

Figure 21. MANIO inhibits the growth of patient-derived CRC cells through regulation of p53 transcriptional targets. (A) Concentration-response curves of the growth inhibitory effect of MANIO in patient-derived CRC cells was determined by MTT assay, after 48 h treatment. Data are mean ± SEM (5-8 independent experiments). **(B)** Effect of MANIO on the mRNA expression levels of p53 target genes in CCZ1, CCZ2, CCZ3, and CCZ5 cells, after 48 h treatment, determined by RT-qPCR. Fold of induction is relative to DMSO. Data are mean ± SEM of 3 independent experiments; values significantly different from DMSO: *$p < 0.05$; **$p < 0.01$; ***$p < 0.001$; unpaired Student's *t*-test.

4.3.7. MANIO has synergistic effects with conventional chemotherapeutics, in immortalized and patient-derived CRC cells

The ability of MANIO to enhance the anticancer activity of conventional chemotherapeutics typically used in CRC treatment was investigated in SW837 cells. For that, cells were treated with MANIO at 0.9 μM (concentration without significant effect on cancer cell growth) and a range of concentrations of DOXO, cisplatin or 5-FU. The results showed that MANIO enhanced the growth inhibitory effect of the three chemotherapeutic drugs (Annex IV, Figure S11). In fact, the CI values determined for each combination revealed that MANIO had synergistic effects with DOXO, cisplatin and 5-FU, at all the concentrations tested (Table 4).

The effect of MANIO on the sensitization of patient-derived CRC cells to DOXO was also evaluated. For that, CCZ3 cells were treated with increasing concentrations of DOXO, alone and in combination with MANIO at 2 μM (concentration without significant effect on cell growth). When compared to DOXO alone, the combination with MANIO sensitized CCZ3 cells to the cytotoxicity of DOXO (Annex IV, Figure S11). In fact, the CI values for each combination tested showed that MANIO had synergistic effects with all concentrations tested of DOXO (Table 4). The synergistic effects obtained with MANIO would allow a significant reduction of the effective dose of chemotherapeutic drug (translated by DRI values; Table 4), and therefore of the undesirable toxicity and chemoresistance commonly observed with these drugs [423].

Table 4. Effect of MANIO in combination with conventional chemotherapeutic agents, in SW837 and patient-derived CCZ3 cells.

	Mutually nonexclusive CI		**Dose reduction index (DRI)**
Drug combination with MANIO	**CI**	**Profile**	**Conventional Drug**
SW837 cells			
DOXO (nM)			
31.25	0.378	Synergy	8.194
62.5	0.342	Synergy	6.353
125	0.393	Synergy	4.142
250	0.512	Synergy	2.604
500	0.324	Synergy	3.580
5-FU (μM)			
1.25	0.314	Synergy	36.524
2.5	0.257	Synergy	33.966
5	0.249	Synergy	22.510
10	0.250	Synergy	15.154
20	0.246	Synergy	11.309
Cisplatin (μM)			
2.5	0.630	Synergy	9.312
5	0.684	Synergy	5.359
10	0.698	Synergy	3.850
20	0.369	Synergy	8.839

Patient-derived CRC CCZ3 cells			
DOXO (μM)			
0.39	0.522	Synergy	2.628
0.59	0.535	Synergy	2.701
0.89	0.588	Synergy	2.869
1.33	0.614	Synergy	1.629

The synergistic effect of 0.9 μM (SW837 cells) or 2 μM (CCZ3 cells) MANIO in combination with DOXO, 5-FU or cisplatin was evaluated using CompuSyn software to calculate combination index (CI) and conventional chemotherapeutic dose reduction index (DRI) values. CI<1, synergy; 1 < CI < 1.1, additive effect; CI > 1.1, antagonism. Data were calculated using a mean value effect (6 independent experiments).

4.4. Discussion

In the era of precision medicine, an in-depth knowledge on CRC molecular pathogenesis and the improved patient stratification based on molecular subtypes of CRC has greatly advanced the therapy of this type of cancer. In particular, the inactivation of the p53 pathway is an indisputable event in the pathogenesis of CRC, which has made its functional restoration an appealing strategy in anticancer targeted therapy. In fact, mutations in *TP53* are frequently found in CRC, having a profound clinical impact based on the activation of additional oncogenic pathways that contribute to the invasiveness and aggressiveness of this type of cancer. Since no p53-based therapy has been successfully translated into clinical CRC treatment, new effective p53-activating agents are still needed as potential therapeutic alternatives.

Herein, we report the identification of the new p53-activating agent MANIO, with the ability not only to activate the wtp53, but also of restoring wt-like function to mutp53. In fact, MANIO displayed an evident p53-dependent antitumor activity, with much higher growth inhibitory effect on wt/mutp53-expressing cancer cells than on p53-null cells. Particularly, in wtp53-expressing CRC cells, MANIO induced cell cycle arrest and apoptosis. Consistently, it interfered with the protein and mRNA expression levels of major p53 transcriptional targets, increasing the cell cycle regulators p21 and GADD45 and the pro-apoptotic PUMA and KILLER/DR5, while decreasing the anti-apoptotic regulator BCL-2. These effects were shown to be associated with an induction of wtp53 stabilization by MANIO. Although the major mechanism of p53 stabilization and activation has relied on the inhibition of the p53 interaction with MDM2 [424], we were unable to detect this inhibitory effect by MANIO (Annex IV, Figure S12). However, we uncovered that MANIO directly bound to the p53 DBD, leading to its cellular thermal stabilization.

A pronounced growth inhibitory effect of MANIO was also unveiled in cancer cells expressing distinct contact and structural mutp53 forms with high clinical prevalence. This indicated that its binding mode might be irrespective of the formation of particular pockets derived from specific mutation sites, as observed with the binding of Phikan083 to mutp53 Y220C [280]. Interestingly, MANIO was highly effective against mutations with particular interest in a CRC context, particularly at residue R248 [425]. Both mutations R248Q and R248W have similar frequencies and may exert oncogenic GOF activities in CRC [425]. In fact, cancer patients carrying mutp53 R248Q/W have been associated with lower survival rates than those with other mutp53 forms [425]. Particularly, mutp53 R248Q GOF accelerated tumor onset [192], and knockin mice exhibited a broader tumor spectrum, shorter overall survival and metastasis development [425]. Mutp53 R248W was also shown to interact with the nuclease Mre11, suppressing the binding of the Mre11–Rad50–NBS1 (MRN) complex to DNA double-stranded breaks, and subsequently inhibiting ATM-dependent repair [426]. Compelling evidences are herein provided demonstrating the restoration of the wt-like DNA-binding ability and transactivation function to mutp53 R248W by MANIO, with subsequent upregulation of p53 transcriptional targets involved in cell cycle arrest (p21) and apoptosis (BAX and PUMA). As with wtp53, the direct interaction of MANIO with mutp53 R248W, leading to its thermal stabilization, was also demonstrated.

The p53-dependent antitumor activity of MANIO was further confirmed in CRC xenograft mouse models. In fact, in tumors expressing wt or mutp53, MANIO inhibited tumor cell proliferation and induced apoptosis, while it did not significantly interfere with the growth of p53 knockout tumors. Interestingly, in accordance with the wtp53 stabilization observed in CRC cells, a marked increase in the p53 levels was also observed in wtp53-expressing tumor tissues treated with MANIO. However, in mutp53-expressing tumor tissues, MANIO significantly reduced the levels of mutp53. It is also worth noting that much higher levels of p53 could be observed in control tumors expressing mutp53 compared to those expressing wtp53. Although the mechanism of mutp53 accumulation in tumors remains not well-understood, the disruption of the p53-MDM2 loop can constitute a potential explanation. Actually, the inability of mutp53 to transcriptionally induce MDM2 and of MDM2 to interact and degrade mutp53 greatly reduce the overall mutp53 degradation by ubiquitination [222]. In fact, mutp53 accumulation in tumors has been considered critical for the occurrence of mutp53 GOF, contributing to the development of more advanced tumors. As such, low mutp53 levels have been correlated with increased survival rates [427], strongly supporting the depletion of mutp53 as a positive marker of cancer therapeutic response [222]. The restoration of the wt-like function to mutp53 by MANIO, with reestablishment of the p53-MDM2 feedback loop, may therefore explain the reduction in mutp53 expression to similar levels to wtp53-expressing tumors tissues.

Notably, no signs of toxicity or morbidity were noticed in MANIO-treated mice. In fact, in case of wtp53 activators, it would be expected that these agents might also activate p53 in normal cells, exhibiting undesirable toxic side effects. Accordingly, some authors have shown that normal tissues were not significantly affected by genetic re-establishment of p53 [226]. In particular, it was demonstrated that p53-activating signals triggered by acute radiation injury in normal radiosensitive tissues rapidly attenuated, as the damage was promptly resolved. Conversely, tumor cells have irreparable DNA lesions and p53-activating signals (*e.g.* oncogene activation) are persistent features of established tumors. As such, the combination of p53-activating sustained endogenous signals with exogenous stimuli for p53 restoration in tumor cells will lead to a robust p53-mediated tumor growth suppression [226, 428].

The antitumor potential of MANIO through activation of a p53 pathway was also validated in patient-derived CRC cells. In fact, in these cells, MANIO also upregulated the mRNA levels of several p53 transcriptional targets involved in cell cycle arrest and apoptosis, while downregulating genes involved in angiogenesis (*VEGF*) and cancer development and chemoresistance (*BIRC5*/Survivin). In fact, several evidences have demonstrated that survivin has a crucial role in the pathogenesis of CRC [429], being its upregulation strongly associated with poor prognosis [430], and resistance of tumor cells to both radiotherapy and chemotherapy [431]. As such, this downregulation of survivin expression levels by MANIO will greatly improve CRC therapeutic response.

Notably, MANIO displayed its highest antiproliferative effect on patient-derived CCZ2 cells, which is of high clinical relevance, as CCZ2 cells derived from a metastatic CRC patient, previously subjected to standard therapeutic regimens (5-FU, Oxaliplatin) combined with the anti-angiogenic agent bevacizumab. MANIO also showed marked antitumor activity against CCA8 patient-derived cells, which expressed the missense p53 DBD mutation P151S. Although not being a “hotspot” *TP53* mutation, its clinical relevance should not be disregarded, since these mutations within the exon 5 of *TP53* are associated with worse outcomes in proximal colon cancers [432].

CRC treatments have embraced the use of conventional chemotherapeutic drugs, including 5-FU, platinum-based agents, and topoisomerases inhibitors [29]. Although the approved chemotherapy had a positive impact on CRC therapy, their combination with targeted therapy has greatly improved the median overall survival of CRC patients, minimizing toxicity and counteracting frequent drug resistance [24]. Herein, we showed that low doses of MANIO had synergistic effects with chemotherapeutic agents used in CRC therapy, both in immortalized and patient-derived CRC cells. Indeed, DNA-damaging drugs, like DOXO, 5-FU or cisplatin, are highly dependent on functional p53 to trigger cell death, therefore benefiting CRC patients harboring wt but not mutp53 [433]. As such, the occurrence of promising synergistic combinations between the studied chemotherapeutics and MANIO was predictable in mutp53-expressing SW837 cells. Despite this, an evident potentiation of DOXO cytotoxic effect could also be obtained with MANIO in wtp53-expressing patient-derived CCZ3 cells.

Altogether, compelling pre-clinical evidences are herein provided supporting the therapeutic potential of MANIO in the personalized treatment of cancer, particularly of CRC, either as single agent or in combination with conventional chemotherapeutics.

CHAPTER 5

GENERAL DISCUSSION

In the last years, it has become clear that different patients with the same type of cancer can manifest variable responses to conventional cancer treatments, namely chemotherapy and radiation. In fact, these generic cancer treatments rely on “one-size-fits-all” approach, being overly unspecific, frequently ineffective, and causing patients’ suffering from severe side effects. In an attempt to maximize the antitumor therapeutic response and minimize the toxicity, precision medicine has emerged as a more efficient treatment approach, focused on specific subtypes of cancer [28]. Particularly, it relies on tumors heterogeneity and on the effort of classifying and subclassifying cancers based on histological, biological, genetic, and molecular characteristics. The identification of proteins and/or pathways that are specifically altered in human cancers made it possible to treat subtypes of tumors with drugs, which have been tailored to those specific molecular targets. In fact, targeted therapies currently constitute the foundation of the personalized therapy [28].

In this context, the tumor suppressor protein p53 has arisen as an extremely attractive target in cancer therapeutics, as an impairment of its function or pathway represents the most common alterations in human cancers. Actually, p53-targeting agents, able to activate p53 tumor suppressive function or pathway, have shown great promising as potential anticancer drug candidates, currently being tested in several clinical trials. Nevertheless, no p53-based therapy has yet been successfully translated to the clinic. Hence, new and improved options are still highly needed.

For several years, our group has been focused on the discovery of new anticancer drug candidates by targeting p53. Particularly, the enantiopure tryptophanol-derived oxazoloisoindolinone SLMP53-1 was first identified as a wt- and mutp53 R280K (re)activator, with considerable p53-dependent anti-proliferative activity in wt- and mutp53 R280K-expressing tumor cells [239]. That work also demonstrated that SLMP53-1 was able to restore wt-like activity to mutp53 R280K by reestablishing its transcriptional activity. Importantly, SLMP53-1 showed promising *in vivo* p53-dependent antitumor activity, without apparent toxicity [239]. These promising pre-clinical results encouraged an in-depth elucidation of the molecular mechanism of mutp53 reactivation by SLMP53-1, which was the basis of Chapter 2 of this doctoral thesis. Thermal stability assays have suggested the direct interaction of SLMP53-1 to wt- and mutp53. In fact, in a complementary work to this thesis, the direct interaction of SLMP53-1 to mutp53 R280K DBD was confirmed [434]. As such, it became imperative to identify the type of interactions involved in the SLMP53-1 interaction with mutp53, restoring its wt-like DNA-binding ability and transcriptional activity. This assumed particular relevance in the case of contact mutp53 R280K, in which the replacement of the lost protein-DNA contact points by exogenous molecules has proved to be very defiant [186]. Still, p53 reputation of being undruggable has been continuously confronted by different studies reporting new molecules with potential to reactivate mutp53. Some of the first molecules reported to activate p53 are Michael acceptors that form adducts by covalently binding to p53 cysteines, causing its stabilization and reactivation [270, 276-278]. On the other hand, the hydrophobic crevice suitable for binding exhibited by mutp53 Y220C prompted the design of several molecules able to reactivate its wt-like function [280, 281, 284]. Notably, the affinity of Y220C-cavity binders has progressively improved since PhiKan083, and further optimizations may be predicted. Furthermore, *in silico* studies have identified new druggable p53 regions, namely two transiently open putative binding pockets in the p53 DBD, in its folded conformation, suitable to accommodate small molecules, thermodynamically stabilizing p53 in its native conformation and reactivating its transcriptional function [285]. The targeted therapy using zinc metallochaperones is unique, without a direct protein-ligand interaction but increasing the intracellular levels of zinc that are appropriate for remetallating and refolding of conformational mutp53 DBD [291]. A different approach targeting the DNA-binding surface mutp53 DBD with peptides or small molecules supports a chaperone mechanism for rescuing an unfolded mutp53, shifting the equilibrium to the native state and being displaced in the presence of DNA [286, 287, 289]. Herein, *in silico* results denoted a distinct molecular mechanism of mutp53 reactivation by SLMP53-1, non-dependent on covalent bonds or mutation-created hydrophobic pockets as described above for other mutp53 reactivators. SLMP53-1 reactivates mutp53 R280K through binding to a hydrophobic pocket of the protein homodimer, establishing an interface with the DNA minor groove, and compensating for the loss of direct contacts between the K280 residue and the DNA. Interestingly, the superposition of wt- and mutp53 R280K models showed that SLMP53-1 has a similar binding pattern to wtp53, which is consistent with the reported activation of wtp53 by SLMP53-1 [239]. Besides, this study also unveiled that SLMP53-1 is able to reactivate other mutp53, both contact and structural, with high clinical relevance, which supports a molecular mechanism unrelated to the formation of pockets derived from specific mutation sites. Importantly, these conclusions resulted from the extension of the yeast assay, previously established for mutp53 R280K and Y220C [239], to other mutp53, namely the hotspot R175H, G245S/D, R248Q/W, and R273C/H. These data obtained in yeast were corroborated in cancer cells ectopically expressing the same mutp53 form, which further validates the yeast model as a reliable and efficient cell system to search for new mutp53 reactivators. As a whole, in Chapter 2, a novel mechanism of mutp53 reactivation involving a p53-DNA bridging molecule was revealed (Figure 22), which may be a valuable contribution to the design of new p53-activating agents.

Great progresses have been made in clarifying the non-canonical p53 functions [59, 126]. Particularly, the antitumor activity due to the restoration of p53 function has been frequently related to the reprogramming of tumor glucose metabolism. Depending on the stimuli inflicted in tumor cells, the p53 response will influence the balance between glycolysis and OXPHOS [161]. Notably, different studies have demonstrated that the status and the activity of p53 in tumor cells are determinant for the success of metabolic therapy [435-437]. In that context, the modulation of glucose metabolism by p53-activating agents, for a tumor-selective elimination, has been explored. In 2011, Zawacka-Pankau *et al* showed *in vitro* and *in vivo* that the reinstatement of p53 function by the small molecule p53-activator RITA inhibited aerobic glycolysis in cancer cells, which contributed to the robust induction of apoptosis by p53 in cancer cells [438]. The authors also found that the depletion of HK2 by siRNA or inhibition by 2-deoxyglucose potentiated the induction of apoptosis, suggesting that the simultaneous inhibition of the glycolytic intervenient contributed to the robust apoptosis triggered by RITA [438].

According to former studies, SLMP53-1 suppresses tumorigenesis primarily by inducing a p53 canonical response, mainly involving cell cycle arrest and apoptosis [239]. In Chapter 3, we unveiled that SLMP53-1 also stimulates non-canonical functions of p53, directly impacting the glucose metabolism of colon adenocarcinoma cells, which contributes to the efficient inhibition of tumor growth and dissemination. In fact, *in vitro* and *in vivo* evidences are herein provided showing the ability of SLMP53-1 to counteract the Warburg effect, with inhibition of migration and angiogenesis of tumor cells (Figure 22).

Combination therapy has been denoted as the cornerstone of cancer therapy, with the main purpose of reducing drug resistance, while improving tumor suppressor activity [439]. Drug combinations comprising DNA-damaging agents have been explored and were found to synergistically combine with p53 activators [171]. In our previous study, SLMP53-1 has already demonstrated combinatorial therapeutic potential, showing evident synergistic effects with doxorubicin and etoposide, in wt/mut p53-expressing tumor cells [239]. Herein, synergism effects between SLMP53-1 and DCA metabolic modulator were also observed, further reinforcing that p53-activating agents may greatly contribute to a more efficient and safe anticancer therapy by decreasing the doses of metabolic therapies and by redirecting the treatment to cancer cells with compromised p53 [161].

All data collected in this thesis regarding SLMP53-1 activity indisputably corroborate the promising clinical potential of this p53-activating agent, as single or combined anticancer drug, by targeting major hallmarks of cancer growth and dissemination. Notably, the encouraging application of SLMP53-1 in personalized cancer therapy is strengthened by its capacity to reach a broader panel of patients harboring both wtp53 and distinct structural or contact mutp53 forms.

In Chapter 4, a new p53-activating agent from a different chemical family, the (3*S*)-6,7-bis(hydroxymethyl)-5-methyl-3-phenyl-1*H*,3*H*-pyrrolo[1,2-c]thiazole (MANIO) is reported. MANIO exhibited a remarkable p53-dependent antitumor activity, particularly when compared to that observed with the well-established p53 reactivator under clinical trials PRIMA-1^{MET} (APR-246; Annex IV, Table S13). The tumor growth inhibitory effect triggered by MANIO, associated with cell cycle arrest and apoptosis, resulted from an enhancement of p53 DNA-binding and transcriptional activity. MANIO was also able to reactivate distinct contact and structural hotspot mutp53. In particular, several evidences are provided showing the restoration of wt-like tumor suppressive activities to contact mutp53 R248W. Importantly, MANIO is able to bind directly to wt- and mutp53 R248W DBD, although the characterization of the type of interactions established with the target protein is still missing. To accomplish this issue, future biophysical studies, including X-ray crystallography and NMR, should be performed. These studies would also provide the first crystal structure of mutp53 R248W, which would be of crucial relevance for the design of optimized reactivators. However, even though without these data, we can anticipate a type of interaction similar to that observed with SLMP53-1, transversal to several mutp53 and, therefore independent of mutation-created hydrophobic pockets. Despite this, the absence of activity in mutp53 Y220C suggests some level of selectivity of MANIO towards mutp53, which should deserve further investigation.

This work also highlights the encouraging clinical application of MANIO as anticancer drug candidate in CRC therapy. This fact assumes particular relevance considering that despite the frequent impairment of the p53 signaling in CRC, effective p53-targeted agents against this type of cancer are still missing. In fact, MANIO displayed potent p53-dependent antiproliferative activity both in human immortalized cells and in xenograft mouse models of human wt/mutp53-expressing CRC. Most importantly, MANIO also showed potent antiproliferative activity against patient-derived CRC primary cells, through engagement of the p53 pathway. Regarding chemoresistance, which has been recognized as one of the key causes for chemotherapeutic failure and CRC relapse [440], MANIO revealed promising synergistic effects in combination with chemotherapeutics generally used in CRC therapy, namely 5-FU and cisplatin, both in immortalized and patient-derived CRC cells. Therefore, MANIO reveals great potential to minimize the toxicity and the frequent drug resistance observed in the current therapeutic regimens of CRC [24].

Mutations in *TP53* gene occur in approximately 40%-50% of sporadic CRC, and mutp53 GOF activities are closely associated to the more aggressive CRC phenotypes and poor outcomes [441]. *In vivo* evidences of inhibition of mutp53 stabilization and accumulation in mutp53-expressing tumor tissues treated with MANIO are provided, which constitutes a positive prognostic marker in CRC [222]. Despite this, as future perspectives, it would be interesting to further investigate the MANIO ability of inhibiting mutp53 GOF in CRC.

The characterization of the pharmacokinetic (PK) profile of MANIO study shows to be critical for its potential clinical translation. Based on this, different absorption, distribution, metabolism, and elimination (ADME) parameters of MANIO were assessed both *in vitro* and *in vivo* (Annex V). Most anticancer agents are administered intravenously (IV) or orally. Regarding the bioavailability of oral drugs, it has to be considered that they are subjected to absorption barriers and the hepatic first-pass effect. The compound solubility is particularly important in determining the rate and extent of its absorption because it will be transported within different environments before crossing the biological membranes. Although MANIO was soluble in aqueous solvents of neutral and basic pH, it presented poor solubility in low pH aqueous solvents (Annex V, Table S16), which indicated its pH-dependent solubility. To overcome this limitation, the use of pharmaceutically acceptable counter ions can provide favorable pH conditions upon dissolution in water. This may render the pH of resulting solution closer to maximum pH of the compound, translating into better absorption rates [442]. In fact, many approved orally administered anticancer drugs exhibit this pH-dependent solubility, and the oral bioavailability of these agents was significantly influenced when co-administered with acid-reducing agents (*e.g.* proton pump inhibitors, H2-receptor antagonists, and antacids) [443]. On the other hand, salt forms of the compounds may occasionally avoid pH adjustments necessary for their solubilization, as salt formation has been reported to improve crystallinity, stability and pharmaceutical processing of drugs [442]. For instance, the anticancer drug imatinib is marketed as a salt form, the imatinib mesylate, which exhibits increased solubility and stability [444].

We also observed that MANIO coefficient partition (LogD) was 1.09, indicating an adequate lipophilicity of MANIO and, consequently, its suitability to easily cross cellular membranes. In fact, in an attempt to evaluate the properties of thousands of drugs, some authors identified structural parameters related with solubility and permeability used as an initial assessment of a compound oral absorption potential [445]. This was termed the “rule of 5”, stating that good oral absorption is more likely when there are less than 5 hydrogen bond donors (expressed as the sum of OHs and NHs), the molecular weight (MW) is inferior to 500, the calculated logP is < 5, and there are less than 10 hydrogen bond acceptors (expressed as the sum of Ns and Os) [445]. MANIO complied with all of these parameters.

The study of the transport of MANIO across a Caco-2 cell monolayer to predict human intestinal permeability revealed that, despite the good permeability, with high percentage of MANIO recovery, some level of MANIO efflux was occurring (Annex V, Table S17), which can limit the drug absorption in the intestine. In fact, P-glycoprotein (P-gp), a drug efflux pump, recurrently confers a multi-drug resistance phenotype to cancer cells. In addition, it is frequently overexpressed in the intestinal epithelium, where it can limit the oral bioavailability of anticancer drugs. Different P-gp inhibitors, such as tariquidar, elacridar, zosuquidar, laniquidar, and ONT093, have advanced to clinical development as a combination anticancer therapy in an effort to increase oral bioavailability of anticancer drugs [446].

Regarding MANIO susceptibility to undergo hepatic first-pass metabolism, *in vitro* models of hepatic clearance using human liver microsomes showed that MANIO exhibited relatively low intrinsic clearance (CL_{int} < 115.5 µg/min/pmol, Annex V, Table S18), which increases the prospect of MANIO being more slowly cleared *in vivo*, having therefore a longer duration. Also, contrary to most drugs that bind in a large proportion to plasma proteins, such as albumin, α1-acid glycoprotein, globulins, and lipoproteins [447], a negligible fraction of MANIO bound to plasmatic albumin was detected (Annex V, Table S19), which means that a great percentage of MANIO is pharmacological active and free to distribute.

The *in vivo* kinetics was analyzed in mice treated with MANIO via IV bolus injection, which constitutes the most direct route of administration, resulting in rapid and complete compound bioavailability. Given the evidences of protein-bound MANIO fraction being very low (Annex V, Table S19), with free compound around 99.6%, mice plasma levels determinations were expected to represent almost all MANIO free-fraction available at a given moment. The obtained results (Annex V: curve of total plasm concentration of MANIO versus time, in Figure S13; summarized MANIO PK parameters, Table S20) indicated an apparent volume of distribution at steady state (Vss) of 4 L/kg, which can be interpreted as the rapid distribution of MANIO within the body. In fact, drugs that slightly bind to plasma proteins or with good lipophilicity, like MANIO, present relatively high Vss [448]. The PK of MANIO was also characterized by a relatively high clearance (CL = 26 mL/min/kg, Annex V, Table S20), and MANIO concentrations declined in plasma with an elimination half-life ($t_{1/2}$) of about 6.83 h (Annex V, Table S20). Collectively, these results may predict adequate PK properties for MANIO.

As a whole, MANIO is a new p53-activating agent, exhibiting potent *in vitro* and *in vivo* antitumor activity against CRC, without apparent toxicity, and suitable drug-likeness (Figure 22). This lead compound represents therefore a promising anticancer therapeutic candidate, both as a single drug or in combination, particularly for CRC therapy. Alternatively, it may be the basis for new derivatives with improved efficacy on other cancer types.

In conclusion, significant contributions to p53 pharmacology and precision cancer therapy arise from the findings disclosed in the present doctoral thesis, with the identification of promising clinical candidates that may integrate the panel of p53-targeted anticancer therapeutic options. Particularly, MANIO is currently the base of an international patent request for technology protection and is attracting the interest of several pharmaceutical companies.

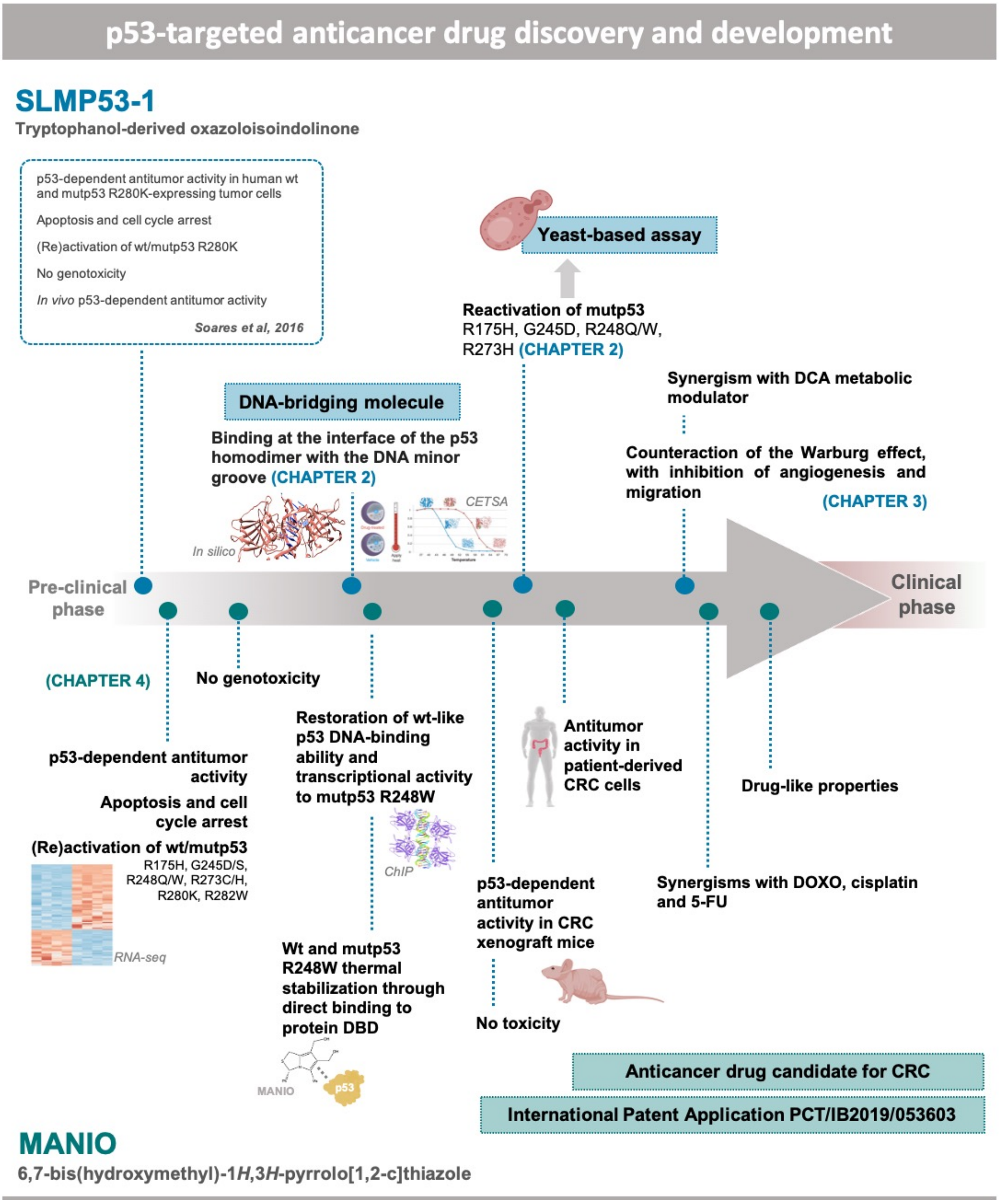
p53-targeted anticancer drug discovery and development
SLMP53-1
Tryptophanol-derived oxazoloisoindolinone
p53-dependent antitumor activity in human wt and mutp53 R280K-expressing tumor cells
Apoptosis and cell cycle arrest
(Re)activation of wt/mutp53 R280K
No genotoxicity
In vivo p53-dependent antitumor activity
Soares et al, 2016
Yeast-based assay
Reactivation of mutp53 R175H, G245D, R248Q/W, R273H (CHAPTER 2)
DNA-bridging molecule
Binding at the interface of the p53 homodimer with the DNA minor groove (CHAPTER 2)
In silico
CETSA
Synergism with DCA metabolic modulator
Counteraction of the Warburg effect, with inhibition of angiogenesis and migration
(CHAPTER 3)
Pre-clinical phase
Clinical phase
(CHAPTER 4)
No genotoxicity
p53-dependent antitumor activity
Apoptosis and cell cycle arrest
(Re)activation of wt/mutp53
R175H, G245D/S, R248Q/W, R273C/H, R280K, R282W
RNA-seq
Restoration of wt-like p53 DNA-binding ability and transcriptional activity to mutp53 R248W
ChIP
Wt and mutp53 R248W thermal stabilization through direct binding to protein DBD
MANIO
p53
Antitumor activity in patient-derived CRC cells
p53-dependent antitumor activity in CRC xenograft mice
No toxicity
Drug-like properties
Synergisms with DOXO, cisplatin and 5-FU
Anticancer drug candidate for CRC
International Patent Application PCT/IB2019/053603
MANIO
6,7-bis(hydroxymethyl)-1H,3H-pyrrolo[1,2-c]thiazole

Figure 22. Schematic representation of the major outcomes achieved in this doctoral thesis. Chapter 2 comprised the elucidation of the molecular mechanism underlying wt/mutp53 R280K (re)activation by SLMP53-1, and the disclosure of SLMP53-1 capability to reactivate several mutp53 forms. **Chapter 3** covered the activation of non-canonical tumor suppressor functions of p53 by SLMP53-1, with inhibition of the glucose metabolism in CRC cells. **Chapter 4** reported the discovery of the lead compound MANIO as a new p53-activating agent, exhibiting effective *in vitro* and *in vivo* antitumor activity against CRC, either as single drug or in combination, without apparent toxic side

effects, and suitable drug-like properties. Major outcomes are highlighted in blue (SLMP53-1) or green (MANIO) boxes.

CHAPTER 6

REFERENCES

1. Bray, F., et al., 2018, *Global cancer statistics 2018: GLOBOCAN estimates of incidence and mortality worldwide for 36 cancers in 185 countries.* CA Cancer J Clin, **68**(6): p. 394-424.
2. Ferlay, J., et al., 2018, *Global Cancer Observatory: Cancer Today. Lyon, France: International Agency for Research on Cancer*. [cited 2019 December]; Available from: http://gco.iarc.fr/today/home.
3. Siegel, R.L., K.D. Miller, and A. Jemal, 2019, *Cancer statistics, 2019.* CA Cancer J Clin, **69**(1): p. 7-34.
4. Lopes, J.M., et al., 2017, *The cost of cancer treatment in Portugal.* Ecancermedicalscience, **11**: p. 765.
5. Fouad, Y.A. and C. Aanei, 2017, *Revisiting the hallmarks of cancer.* Am J Cancer Res, **7**(5): p. 1016-1036.
6. Hanahan, D. and R.A. Weinberg, 2000, *The hallmarks of cancer.* Cell, **100**(1): p. 57-70.
7. Hanahan, D. and R.A. Weinberg, 2011, *Hallmarks of cancer: the next generation.* Cell, **144**(5): p. 646-74.
8. Wang, L.H., et al., 2018, *Loss of Tumor Suppressor Gene Function in Human Cancer: An Overview.* Cell Physiol Biochem, **51**(6): p. 2647-2693.
9. Arnold, M., et al., 2017, *Global patterns and trends in colorectal cancer incidence and mortality.* Gut, **66**(4): p. 683-691.
10. Dekker, E., et al., 2019, *Colorectal cancer.* Lancet, **394**(10207): p. 1467-1480.
11. Amaro, A., S. Chiara, and U. Pfeffer, 2016, *Molecular evolution of colorectal cancer: from multistep carcinogenesis to the big bang.* Cancer Metastasis Rev, **35**(1): p. 63-74.
12. Welch, H.G. and D.J. Robertson, 2016, *Colorectal Cancer on the Decline--Why Screening Can't Explain It All.* N Engl J Med, **374**(17): p. 1605-7.
13. Fearon, E.R. and B. Vogelstein, 1990, *A genetic model for colorectal tumorigenesis.* Cell, **61**(5): p. 759-67.
14. Fearon, E.R., 2011, *Molecular genetics of colorectal cancer.* Annu Rev Pathol, **6**: p. 479-507.
15. Vogelstein, B., et al., 2013, *Cancer genome landscapes.* Science, **339**(6127): p. 1546-58.
16. Matano, M., et al., 2015, *Modeling colorectal cancer using CRISPR-Cas9-mediated engineering of human intestinal organoids.* Nature medicine, **21**(3): p. 256-262.
17. Drost, J., et al., 2015, *Sequential cancer mutations in cultured human intestinal stem cells.* Nature, **521**(7550): p. 43-7.
18. Grady, W.M. and J.M. Carethers, 2008, *Genomic and epigenetic instability in colorectal cancer pathogenesis.* Gastroenterology, **135**(4): p. 1079-99.
19. Ionov, Y., et al., 1993, *Ubiquitous somatic mutations in simple repeated sequences reveal a new mechanism for colonic carcinogenesis.* Nature, **363**(6429): p. 558-61.
20. Pino, M.S. and D.C. Chung, 2010, *The chromosomal instability pathway in colon cancer.* Gastroenterology, **138**(6): p. 2059-72.
21. Dienstmann, R., et al., 2017, *Consensus molecular subtypes and the evolution of precision medicine in colorectal cancer.* Nature reviews. Cancer, **17**(2): p. 79-92.
22. Nakayama, M. and M. Oshima, 2019, *Mutant p53 in colon cancer.* J Mol Cell Biol, **11**(4): p. 267-276.
23. Guinney, J., et al., 2015, *The consensus molecular subtypes of colorectal cancer.* Nature medicine, **21**(11): p. 1350-1356.
24. Yau, T.O., 2019, *Precision treatment in colorectal cancer: Now and the future.* JGH Open, **3**(5): p. 361-369.
25. Burness, C.B. and S.T. Duggan, 2016, *Trifluridine/Tipiracil: A Review in Metastatic Colorectal Cancer.* Drugs, **76**(14): p. 1393-402.
26. Mayer, R.J., et al., 2015, *Randomized trial of TAS-102 for refractory metastatic colorectal cancer.* N Engl J Med, **372**(20): p. 1909-19.
27. O'Neil, B.H., et al., 2017, *Safety and antitumor activity of the anti-PD-1 antibody pembrolizumab in patients with advanced colorectal carcinoma.* PLoS One, **12**(12): p. e0189848.
28. Verma, M., 2012, *Personalized medicine and cancer.* J Pers Med, **2**(1): p. 1-14.
29. Cremolini, C., et al., 2015, *First-line chemotherapy for mCRC-a review and evidence-based algorithm.* Nat Rev Clin Oncol, **12**(10): p. 607-19.
30. Oda, K., et al., 2005, *A comprehensive pathway map of epidermal growth factor receptor signaling.* Mol Syst Biol, **1**: p. 2005 0010.
31. Shitara, K., et al., 2010, *Cetuximab plus FOLFOX for Patients with Metastatic Colorectal Cancer with Poor Performance Status and/or Severe Tumor-Related Complications.* Case Rep Oncol, **3**(2): p. 282-6.

32. Peeters, M., et al., 2014, *Final results from a randomized phase 3 study of FOLFIRI {+/-} panitumumab for second-line treatment of metastatic colorectal cancer.* Ann Oncol, **25**(1): p. 107-16.
33. Hashim, A.F., et al., 2010, *Vascular endothelial growth factor (VEGF) receptor expression correlates with histologic grade and stage of colorectal cancer.* Libyan J Med, **5**.
34. Martins, S.F., et al., 2013, *Clinicopathological correlation and prognostic significance of VEGF-A, VEGF-C, VEGFR-2 and VEGFR-3 expression in colorectal cancer.* Cancer Genomics Proteomics, **10**(2): p. 55-67.
35. Ferrara, N. and A.P. Adamis, 2016, *Ten years of anti-vascular endothelial growth factor therapy.* Nat Rev Drug Discov, **15**(6): p. 385-403.
36. Van Cutsem, E., et al., 2012, *Addition of aflibercept to fluorouracil, leucovorin, and irinotecan improves survival in a phase III randomized trial in patients with metastatic colorectal cancer previously treated with an oxaliplatin-based regimen.* J Clin Oncol, **30**(28): p. 3499-506.
37. Bennouna, J., et al., 2013, *Continuation of bevacizumab after first progression in metastatic colorectal cancer (ML18147): a randomised phase 3 trial.* Lancet Oncol, **14**(1): p. 29-37.
38. Tabernero, J., et al., 2015, *Ramucirumab versus placebo in combination with second-line FOLFIRI in patients with metastatic colorectal carcinoma that progressed during or after first-line therapy with bevacizumab, oxaliplatin, and a fluoropyrimidine (RAISE): a randomised, double-blind, multicentre, phase 3 study.* Lancet Oncol, **16**(5): p. 499-508.
39. Lane, D.P. and L.V. Crawford, 1979, *T antigen is bound to a host protein in SV40-transformed cells.* Nature, **278**(5701): p. 261-3.
40. Linzer, D.I. and A.J. Levine, 1979, *Characterization of a 54K dalton cellular SV40 tumor antigen present in SV40-transformed cells and uninfected embryonal carcinoma cells.* Cell, **17**(1): p. 43-52.
41. Menendez, D., A. Inga, and M.A. Resnick, 2009, *The expanding universe of p53 targets.* Nat Rev Cancer, **9**(10): p. 724-37.
42. Binayke, A., et al., 2019, *Awakening the "guardian of genome": reactivation of mutant p53.* Cancer Chemother Pharmacol, **83**(1): p. 1-15.
43. Wei, C.L., et al., 2006, *A global map of p53 transcription-factor binding sites in the human genome.* Cell, **124**(1): p. 207-19.
44. Joerger, A.C. and A.R. Fersht, 2008, *Structural biology of the tumor suppressor p53.* Annu Rev Biochem, **77**: p. 557-82.
45. Li, M., et al., 2012, *Distinct regulatory mechanisms and functions for p53-activated and p53-repressed DNA damage response genes in embryonic stem cells.* Mol Cell, **46**(1): p. 30-42.
46. Fischer, M., 2017, *Census and evaluation of p53 target genes.* Oncogene, **36**(28): p. 3943-3956.
47. Chen, Y., et al., 2013, *Structure of p53 binding to the BAX response element reveals DNA unwinding and compression to accommodate base-pair insertion.* Nucleic Acids Research, **41**(17): p. 8368-8376.
48. Natan, E., et al., 2011, *Interaction of the p53 DNA-binding domain with its n-terminal extension modulates the stability of the p53 tetramer.* J Mol Biol, **409**(3): p. 358-68.
49. Joerger, A.C. and A.R. Fersht, 2010, *The tumor suppressor p53: from structures to drug discovery.* Cold Spring Harb Perspect Biol, **2**(6): p. a000919.
50. Joerger, A.C. and A.R. Fersht, 2016, *The p53 Pathway: Origins, Inactivation in Cancer, and Emerging Therapeutic Approaches.* Annu Rev Biochem, **85**: p. 375-404.
51. Chillemi, G., et al., 2017, *Structural Evolution and Dynamics of the p53 Proteins.* Cold Spring Harb Perspect Med, **7**(4).
52. Venot, C., et al., 1999, *Definition of a p53 transactivation function-deficient mutant and characterization of two independent p53 transactivation subdomains.* Oncogene, **18**(14): p. 2405-10.
53. Jeffrey, P.D., S. Gorina, and N.P. Pavletich, 1995, *Crystal structure of the tetramerization domain of the p53 tumor suppressor at 1.7 angstroms.* Science, **267**(5203): p. 1498-502.
54. Chen, Y., R. Dey, and L. Chen, 2010, *Crystal structure of the p53 core domain bound to a full consensus site as a self-assembled tetramer.* Structure, **18**(2): p. 246-56.
55. Kitayner, M., et al., 2006, *Structural basis of DNA recognition by p53 tetramers.* Mol Cell, **22**(6): p. 741-53.
56. Kenzelmann Broz, D. and L.D. Attardi, 2010, *In vivo analysis of p53 tumor suppressor function using genetically engineered mouse models.* Carcinogenesis, **31**(8): p. 1311-8.
57. Riley, T., et al., 2008, *Transcriptional control of human p53-regulated genes.* Nat Rev Mol Cell Biol, **9**(5): p. 402-12.
58. Brady, C.A. and L.D. Attardi, 2010, *p53 at a glance.* J Cell Sci, **123**(Pt 15): p. 2527-32.

59. Vousden, K.H. and C. Prives, 2009, *Blinded by the Light: The Growing Complexity of p53.* Cell, **137**(3): p. 413-31.
60. Brooks, C.L. and W. Gu, 2006, *p53 ubiquitination: Mdm2 and beyond.* Mol Cell, **21**(3): p. 307-15.
61. Linares, L.K., et al., 2003, *HdmX stimulates Hdm2-mediated ubiquitination and degradation of p53.* Proc Natl Acad Sci U S A, **100**(21): p. 12009-14.
62. Kussie, P.H., et al., 1996, *Structure of the MDM2 oncoprotein bound to the p53 tumor suppressor transactivation domain.* Science, **274**(5289): p. 948-53.
63. Sabbatini, P. and F. McCormick, 2002, *MDMX inhibits the p300/CBP-mediated acetylation of p53.* DNA Cell Biol, **21**(7): p. 519-25.
64. Cross, B., et al., 2011, *Inhibition of p53 DNA binding function by the MDM2 protein acidic domain.* J Biol Chem, **286**(18): p. 16018-29.
65. Clegg, H.V., K. Itahana, and Y. Zhang, 2008, *Unlocking the Mdm2-p53 loop: ubiquitin is the key.* Cell Cycle, **7**(3): p. 287-92.
66. Li, M., et al., 2003, *Mono- versus polyubiquitination: differential control of p53 fate by Mdm2.* Science, **302**(5652): p. 1972-5.
67. Wade, M., Y.C. Li, and G.M. Wahl, 2013, *MDM2, MDMX and p53 in oncogenesis and cancer therapy.* Nat Rev Cancer, **13**(2): p. 83-96.
68. Parant, J., et al., 2001, *Rescue of embryonic lethality in Mdm4-null mice by loss of Trp53 suggests a nonoverlapping pathway with MDM2 to regulate p53.* Nat Genet, **29**(1): p. 92-5.
69. Pei, D., Y. Zhang, and J. Zheng, 2012, *Regulation of p53: a collaboration between Mdm2 and Mdmx.* Oncotarget, **3**(3): p. 228-35.
70. Fan, Q.D., G. Wu, and Z.R. Liu, 2014, *Dynamics of posttranslational modifications of p53.* Comput Math Methods Med, **2014**: p. 245610.
71. Bode, A.M. and Z. Dong, 2004, *Post-translational modification of p53 in tumorigenesis.* Nat Rev Cancer, **4**(10): p. 793-805.
72. Dai, C. and W. Gu, 2010, *p53 post-translational modification: deregulated in tumorigenesis.* Trends Mol Med, **16**(11): p. 528-36.
73. Kumari, R., S. Kohli, and S. Das, 2014, *p53 regulation upon genotoxic stress: intricacies and complexities.* Mol Cell Oncol, **1**(3): p. e969653.
74. Hupp, T.R. and D.P. Lane, 1994, *Allosteric activation of latent p53 tetramers.* Curr Biol, **4**(10): p. 865-75.
75. Craig, A.L., et al., 1999, *Novel phosphorylation sites of human tumour suppressor protein p53 at Ser20 and Thr18 that disrupt the binding of mdm2 (mouse double minute 2) protein are modified in human cancers.* Biochem J, **342 (Pt 1)**: p. 133-41.
76. Toledo, F. and G.M. Wahl, 2006, *Regulating the p53 pathway: in vitro hypotheses, in vivo veritas.* Nat Rev Cancer, **6**(12): p. 909-23.
77. Oda, K., et al., 2000, *p53AIP1, a potential mediator of p53-dependent apoptosis, and its regulation by Ser-46-phosphorylated p53.* Cell, **102**(6): p. 849-62.
78. Ichwan, S.J., et al., 2006, *Defect in serine 46 phosphorylation of p53 contributes to acquisition of p53 resistance in oral squamous cell carcinoma cells.* Oncogene, **25**(8): p. 1216-24.
79. Li, X., et al., 2005, *The codon 47 polymorphism in p53 is functionally significant.* J Biol Chem, **280**(25): p. 24245-51.
80. Reed, S.M. and D.E. Quelle, 2014, *p53 Acetylation: Regulation and Consequences.* Cancers (Basel), **7**(1): p. 30-69.
81. Chen, J., 2016, *The Cell-Cycle Arrest and Apoptotic Functions of p53 in Tumor Initiation and Progression.* Cold Spring Harb Perspect Med, **6**(3): p. a026104.
82. Kastan, M.B., et al., 1991, *Participation of p53 protein in the cellular response to DNA damage.* Cancer Res, **51**(23 Pt 1): p. 6304-11.
83. el-Deiry, W.S., et al., 1993, *WAF1, a potential mediator of p53 tumor suppression.* Cell, **75**(4): p. 817-25.
84. Harper, J.W., et al., 1993, *The p21 Cdk-interacting protein Cip1 is a potent inhibitor of G1 cyclin-dependent kinases.* Cell, **75**(4): p. 805-16.
85. Deng, C., et al., 1995, *Mice lacking p21CIP1/WAF1 undergo normal development, but are defective in G1 checkpoint control.* Cell, **82**(4): p. 675-84.
86. Brugarolas, J., et al., 1995, *Radiation-induced cell cycle arrest compromised by p21 deficiency.* Nature, **377**(6549): p. 552-7.
87. Kastan, M.B., et al., 1992, *A mammalian cell cycle checkpoint pathway utilizing p53 and GADD45 is defective in ataxia-telangiectasia.* Cell, **71**(4): p. 587-97.

88. Hollander, M.C., et al., 1999, *Genomic instability in Gadd45a-deficient mice.* Nat Genet, **23**(2): p. 176-84.
89. Hollander, M.C., et al., 1993, *Analysis of the mammalian gadd45 gene and its response to DNA damage.* J Biol Chem, **268**(32): p. 24385-93.
90. Zhan, Q., et al., 1999, *Association with Cdc2 and inhibition of Cdc2/Cyclin B1 kinase activity by the p53-regulated protein Gadd45.* Oncogene, **18**(18): p. 2892-900.
91. Hermeking, H., et al., 1997, *14-3-3sigma is a p53-regulated inhibitor of G2/M progression.* Mol Cell, **1**(1): p. 3-11.
92. St Clair, S., et al., 2004, *DNA damage-induced downregulation of Cdc25C is mediated by p53 via two independent mechanisms: one involves direct binding to the cdc25C promoter.* Mol Cell, **16**(5): p. 725-36.
93. Yun, J., et al., 1999, *p53 negatively regulates cdc2 transcription via the CCAAT-binding NF-Y transcription factor.* J Biol Chem, **274**(42): p. 29677-82.
94. Krause, K., et al., 2000, *The tumour suppressor protein p53 can repress transcription of cyclin B.* Nucleic Acids Res, **28**(22): p. 4410-8.
95. Adimoolam, S. and J.M. Ford, 2002, *p53 and DNA damage-inducible expression of the xeroderma pigmentosum group C gene.* Proc Natl Acad Sci U S A, **99**(20): p. 12985-90.
96. Chatterjee, A., et al., 2006, *The effect of p53-RNAi and p53 knockout on human 8-oxoguanine DNA glycosylase (hOgg1) activity.* FASEB J, **20**(1): p. 112-4.
97. Oka, S., et al., 2014, *MUTYH, an adenine DNA glycosylase, mediates p53 tumor suppression via PARP-dependent cell death.* Oncogenesis, **3**: p. e121.
98. Scherer, S.J., et al., 2000, *p53 and c-Jun functionally synergize in the regulation of the DNA repair gene hMSH2 in response to UV.* J Biol Chem, **275**(48): p. 37469-73.
99. Gatz, S.A. and L. Wiesmuller, 2006, *p53 in recombination and repair.* Cell Death Differ, **13**(6): p. 1003-16.
100. Tonnessen-Murray, C.A., G. Lozano, and J.G. Jackson, 2017, *The Regulation of Cellular Functions by the p53 Protein: Cellular Senescence.* Cold Spring Harb Perspect Med, **7**(2).
101. Cosme-Blanco, W., et al., 2007, *Telomere dysfunction suppresses spontaneous tumorigenesis in vivo by initiating p53-dependent cellular senescence.* EMBO Rep, **8**(5): p. 497-503.
102. Collado, M., et al., 2005, *Tumour biology: senescence in premalignant tumours.* Nature, **436**(7051): p. 642.
103. Chen, Z., et al., 2005, *Crucial role of p53-dependent cellular senescence in suppression of Pten-deficient tumorigenesis.* Nature, **436**(7051): p. 725-30.
104. Kaiser, A.M. and L.D. Attardi, 2018, *Deconstructing networks of p53-mediated tumor suppression in vivo.* Cell Death Differ, **25**(1): p. 93-103.
105. Attardi, L.D., et al., 1996, *Transcriptional activation by p53, but not induction of the p21 gene, is essential for oncogene-mediated apoptosis.* EMBO J, **15**(14): p. 3693-701.
106. Chen, X., et al., 1996, *p53 levels, functional domains, and DNA damage determine the extent of the apoptotic response of tumor cells.* Genes Dev, **10**(19): p. 2438-51.
107. el-Deiry, W.S., 1998, *Regulation of p53 downstream genes.* Semin Cancer Biol, **8**(5): p. 345-57.
108. Sax, J.K. and W.S. El-Deiry, 2003, *p53 downstream targets and chemosensitivity.* Cell Death Differ, **10**(4): p. 413-7.
109. Jimenez, G.S., et al., 2000, *A transactivation-deficient mouse model provides insights into Trp53 regulation and function.* Nat Genet, **26**(1): p. 37-43.
110. Wu, G.S., et al., 1997, *KILLER/DR5 is a DNA damage-inducible p53-regulated death receptor gene.* Nat Genet, **17**(2): p. 141-3.
111. Owen-Schaub, L.B., et al., 1995, *Wild-type human p53 and a temperature-sensitive mutant induce Fas/APO-1 expression.* Mol Cell Biol, **15**(6): p. 3032-40.
112. Maecker, H.L., C. Koumenis, and A.J. Giaccia, 2000, *p53 promotes selection for Fas-mediated apoptotic resistance.* Cancer Res, **60**(16): p. 4638-44.
113. Sax, J.K., et al., 2002, *BID regulation by p53 contributes to chemosensitivity.* Nat Cell Biol, **4**(11): p. 842-9.
114. Luo, X., et al., 1998, *Bid, a Bcl2 interacting protein, mediates cytochrome c release from mitochondria in response to activation of cell surface death receptors.* Cell, **94**(4): p. 481-90.
115. Liedtke, C., et al., 2003, *The human caspase-8 promoter sustains basal activity through SP1 and ETS-like transcription factors and can be up-regulated by a p53-dependent mechanism.* J Biol Chem, **278**(30): p. 27593-604.
116. Vaseva, A.V. and U.M. Moll, 2009, *The mitochondrial p53 pathway.* Biochim Biophys Acta, **1787**(5): p. 414-20.

117. Miyashita, T., et al., 1994, *Tumor suppressor p53 is a regulator of bcl-2 and bax gene expression in vitro and in vivo.* Oncogene, **9**(6): p. 1799-805.

118. Nakano, K. and K.H. Vousden, 2001, *PUMA, a novel proapoptotic gene, is induced by p53.* Mol Cell, **7**(3): p. 683-94.

119. Kannan, K., et al., 2001, *DNA microarray analysis of genes involved in p53 mediated apoptosis: activation of Apaf-1.* Oncogene, **20**(26): p. 3449-55.

120. MacLachlan, T.K. and W.S. El-Deiry, 2002, *Apoptotic threshold is lowered by p53 transactivation of caspase-6.* Proc Natl Acad Sci U S A, **99**(14): p. 9492-7.

121. Rikhof, B., P.G. Corn, and W.S. El-Deiry, 2003, *Caspase 10 levels are increased following DNA damage in a p53-dependent manner.* Cancer Biol Ther, **2**(6): p. 707-12.

122. Hoffman, W.H., et al., 2002, *Transcriptional repression of the anti-apoptotic survivin gene by wild type p53.* J Biol Chem, **277**(5): p. 3247-57.

123. Mihara, M., et al., 2003, *p53 has a direct apoptogenic role at the mitochondria.* Mol Cell, **11**(3): p. 577-90.

124. Leu, J.I., et al., 2004, *Mitochondrial p53 activates Bak and causes disruption of a Bak-Mcl1 complex.* Nat Cell Biol, **6**(5): p. 443-50.

125. Luo, Q., et al., 2017, *Dynamics of p53: A Master Decider of Cell Fate.* Genes (Basel), **8**(2).

126. Ranjan, A. and T. Iwakuma, 2018, *Emerging Non-Canonical Functions and Regulation of p53.* Int J Mol Sci, **19**(4).

127. Powell, E., D. Piwnica-Worms, and H. Piwnica-Worms, 2014, *Contribution of p53 to metastasis.* Cancer Discov, **4**(4): p. 405-14.

128. Hong, H., et al., 2009, *Suppression of induced pluripotent stem cell generation by the p53-p21 pathway.* Nature, **460**(7259): p. 1132-5.

129. Marion, R.M., et al., 2009, *A p53-mediated DNA damage response limits reprogramming to ensure iPS cell genomic integrity.* Nature, **460**(7259): p. 1149-53.

130. Lin, T., et al., 2005, *p53 induces differentiation of mouse embryonic stem cells by suppressing Nanog expression.* Nat Cell Biol, **7**(2): p. 165-71.

131. Zhao, Z., et al., 2010, *p53 loss promotes acute myeloid leukemia by enabling aberrant self-renewal.* Genes Dev, **24**(13): p. 1389-402.

132. Godar, S., et al., 2008, *Growth-inhibitory and tumor- suppressive functions of p53 depend on its repression of CD44 expression.* Cell, **134**(1): p. 62-73.

133. Choi, Y.J., et al., 2011, *miR-34 miRNAs provide a barrier for somatic cell reprogramming.* Nat Cell Biol, **13**(11): p. 1353-60.

134. Siemens, H., et al., 2011, *miR-34 and SNAIL form a double-negative feedback loop to regulate epithelial-mesenchymal transitions.* Cell Cycle, **10**(24): p. 4256-71.

135. Wang, S.P., et al., 2009, *p53 controls cancer cell invasion by inducing the MDM2-mediated degradation of Slug.* Nat Cell Biol, **11**(6): p. 694-704.

136. Liu, J., et al., 2006, *Wild-type p53 inhibits nuclear factor-kappaB-induced matrix metalloproteinase-9 promoter activation: implications for soft tissue sarcoma growth and metastasis.* Mol Cancer Res, **4**(11): p. 803-10.

137. Iotsova, V. and D. Stehelin, 1996, *Down-regulation of fibronectin gene expression by the p53 tumor suppressor protein.* Cell Growth Differ, **7**(5): p. 629-34.

138. Teodoro, J.G., S.K. Evans, and M.R. Green, 2007, *Inhibition of tumor angiogenesis by p53: a new role for the guardian of the genome.* J Mol Med (Berl), **85**(11): p. 1175-86.

139. Racker, E., 1972, *Bioenergetics and the problem of tumor growth.* Am Sci, **60**(1): p. 56-63.

140. Otto, A.M., 2016, *Warburg effect(s)-a biographical sketch of Otto Warburg and his impacts on tumor metabolism.* Cancer Metab, **4**: p. 5.

141. Jones, R.G. and C.B. Thompson, 2009, *Tumor suppressors and cell metabolism: a recipe for cancer growth.* Genes Dev, **23**(5): p. 537-48.

142. Liberti, M.V. and J.W. Locasale, 2016, *The Warburg Effect: How Does it Benefit Cancer Cells?* Trends Biochem Sci, **41**(3): p. 211-218.

143. Smallbone, K., et al., 2007, *Metabolic changes during carcinogenesis: potential impact on invasiveness.* J Theor Biol, **244**(4): p. 703-13.

144. Canel, M., et al., 2013, *E-cadherin-integrin crosstalk in cancer invasion and metastasis.* J Cell Sci, **126**(Pt 2): p. 393-401.

145. Peppicelli, S., F. Bianchini, and L. Calorini, 2014, *Extracellular acidity, a "reappreciated" trait of tumor environment driving malignancy: perspectives in diagnosis and therapy.* Cancer Metastasis Rev, **33**(2-3): p. 823-32.

146. Suzuki, A., et al., 2014, *Acidic extracellular pH promotes epithelial mesenchymal transition in Lewis lung carcinoma model.* Cancer Cell Int, **14**(1): p. 129.

147. Shi, Q., et al., 2001, *Regulation of vascular endothelial growth factor expression by acidosis in human cancer cells.* Oncogene, **20**(28): p. 3751-6.
148. Beckert, S., et al., 2006, *Lactate stimulates endothelial cell migration.* Wound Repair Regen, **14**(3): p. 321-4.
149. Sonveaux, P., et al., 2012, *Targeting the lactate transporter MCT1 in endothelial cells inhibits lactate-induced HIF-1 activation and tumor angiogenesis.* PLoS One, **7**(3): p. e33418.
150. Liu, Z.J., G.L. Semenza, and H.F. Zhang, 2015, *Hypoxia-inducible factor 1 and breast cancer metastasis.* J Zhejiang Univ Sci B, **16**(1): p. 32-43.
151. Ruckenstuhl, C., et al., 2009, *The Warburg effect suppresses oxidative stress induced apoptosis in a yeast model for cancer.* PLoS One, **4**(2): p. e4592.
152. Cairns, R.A., I.S. Harris, and T.W. Mak, 2011, *Regulation of cancer cell metabolism.* Nat Rev Cancer, **11**(2): p. 85-95.
153. Pavlova, N.N. and C.B. Thompson, 2016, *The Emerging Hallmarks of Cancer Metabolism.* Cell Metab, **23**(1): p. 27-47.
154. Andersen, J.L. and S. Kornbluth, 2013, *The tangled circuitry of metabolism and apoptosis.* Mol Cell, **49**(3): p. 399-410.
155. Kitamura, N., et al., 2011, *Mieap, a p53-inducible protein, controls mitochondrial quality by repairing or eliminating unhealthy mitochondria.* PLoS One, **6**(1): p. e16060.
156. Lebedeva, M.A., J.S. Eaton, and G.S. Shadel, 2009, *Loss of p53 causes mitochondrial DNA depletion and altered mitochondrial reactive oxygen species homeostasis.* Biochim Biophys Acta, **1787**(5): p. 328-34.
157. Schwartzenberg-Bar-Yoseph, F., M. Armoni, and E. Karnieli, 2004, *The tumor suppressor p53 down-regulates glucose transporters GLUT1 and GLUT4 gene expression.* Cancer Res, **64**(7): p. 2627-33.
158. Kawauchi, K., et al., 2008, *p53 regulates glucose metabolism through an IKK-NF-kappaB pathway and inhibits cell transformation.* Nat Cell Biol, **10**(5): p. 611-8.
159. Wang, L., et al., 2014, *Hexokinase 2-mediated Warburg effect is required for PTEN- and p53-deficiency-driven prostate cancer growth.* Cell Rep, **8**(5): p. 1461-74.
160. Franklin, D.A., et al., 2016, *p53 coordinates DNA repair with nucleotide synthesis by suppressing PFKFB3 expression and promoting the pentose phosphate pathway.* Scientific Reports, **6**: p. 38067.
161. Gomes, A.S., et al., 2018, *p53 and glucose metabolism: an orchestra to be directed in cancer therapy.* Pharmacol Res, **131**: p. 75-86.
162. Bensaad, K., et al., 2006, *TIGAR, a p53-inducible regulator of glycolysis and apoptosis.* Cell, **126**(1): p. 107-20.
163. Boidot, R., et al., 2012, *Regulation of monocarboxylate transporter MCT1 expression by p53 mediates inward and outward lactate fluxes in tumors.* Cancer Res, **72**(4): p. 939-48.
164. Matoba, S., et al., 2006, *p53 regulates mitochondrial respiration.* Science, **312**(5780): p. 1650-3.
165. Stambolsky, P., et al., 2006, *Regulation of AIF expression by p53.* Cell Death Differ, **13**(12): p. 2140-9.
166. Stein, Y., V. Rotter, and R. Aloni-Grinstein, 2019, *Gain-of-Function Mutant p53: All the Roads Lead to Tumorigenesis.* Int J Mol Sci, **20**(24).
167. Mandinova, A. and S.W. Lee, 2011, *The p53 pathway as a target in cancer therapeutics: obstacles and promise.* Sci Transl Med, **3**(64): p. 64rv1.
168. Shibagaki, I., et al., 1995, *p53 mutation, murine double minute 2 amplification, and human papillomavirus infection are frequently involved but not associated with each other in esophageal squamous cell carcinoma.* Clin Cancer Res, **1**(7): p. 769-73.
169. Gembarska, A., et al., 2012, *MDM4 is a key therapeutic target in cutaneous melanoma.* Nat Med, **18**(8): p. 1239-47.
170. Selivanova, G., 2014, *Wild type p53 reactivation: from lab bench to clinic.* FEBS Lett, **588**(16): p. 2628-38.
171. Sanz, G., et al., 2019, *Inhibition of p53 inhibitors: progress, challenges and perspectives.* J Mol Cell Biol, **11**(7): p. 586-599.
172. Bond, G.L., et al., 2004, *A single nucleotide polymorphism in the MDM2 promoter attenuates the p53 tumor suppressor pathway and accelerates tumor formation in humans.* Cell, **119**(5): p. 591-602.
173. Rayburn, E., et al., 2005, *MDM2 and human malignancies: expression, clinical pathology, prognostic markers, and implications for chemotherapy.* Curr Cancer Drug Targets, **5**(1): p. 27-41.

174. Riemenschneider, M.J., et al., 1999, *Amplification and overexpression of the MDM4 (MDMX) gene from 1q32 in a subset of malignant gliomas without TP53 mutation or MDM2 amplification.* Cancer Res, **59**(24): p. 6091-6.

175. Danovi, D., et al., 2004, *Amplification of Mdmx (or Mdm4) directly contributes to tumor formation by inhibiting p53 tumor suppressor activity.* Mol Cell Biol, **24**(13): p. 5835-43.

176. Laurie, N.A., et al., 2006, *Inactivation of the p53 pathway in retinoblastoma.* Nature, **444**(7115): p. 61-6.

177. Tisato, V., et al., 2017, *MDM2/X inhibitors under clinical evaluation: perspectives for the management of hematological malignancies and pediatric cancer.* J Hematol Oncol, **10**(1): p. 133.

178. Trave, G. and K. Zanier, 2016, *HPV-mediated inactivation of tumor suppressor p53.* Cell Cycle, **15**(17): p. 2231-2.

179. Blandino, G. and S. Di Agostino, 2018, *New therapeutic strategies to treat human cancers expressing mutant p53 proteins.* J Exp Clin Cancer Res, **37**(1): p. 30.

180. IARC, 2019, *TP53 Database - TP53 mutation prevalence by tumor site*. [cited 2019 January, 3]; Available from: http://p53.iarc.fr/TP53SomaticMutations.aspx.

181. Kamihara, J., H.Q. Rana, and J.E. Garber, 2014, *Germline TP53 mutations and the changing landscape of Li-Fraumeni syndrome.* Hum Mutat, **35**(6): p. 654-62.

182. Sabapathy, K. and D.P. Lane, 2018, *Therapeutic targeting of p53: all mutants are equal, but some mutants are more equal than others.* Nat Rev Clin Oncol, **15**(1): p. 13-30.

183. Malkin, D., 2011, *Li-fraumeni syndrome.* Genes Cancer, **2**(4): p. 475-84.

184. Freed-Pastor, W.A. and C. Prives, 2012, *Mutant p53: one name, many proteins.* Genes Dev, **26**(12): p. 1268-86.

185. Weisz, L., M. Oren, and V. Rotter, 2007, *Transcription regulation by mutant p53.* Oncogene, **26**(15): p. 2202-11.

186. Joerger, A.C., H.C. Ang, and A.R. Fersht, 2006, *Structural basis for understanding oncogenic p53 mutations and designing rescue drugs.* Proc Natl Acad Sci U S A, **103**(41): p. 15056-61.

187. Chene, P., 1998, *In vitro analysis of the dominant negative effect of p53 mutants.* J Mol Biol, **281**(2): p. 205-9.

188. Alexandrova, E.M., et al., 2017, *p53 loss-of-heterozygosity is a necessary prerequisite for mutant p53 stabilization and gain-of-function in vivo.* Cell Death Dis, **8**(3): p. e2661.

189. Dittmer, D., et al., 1993, *Gain of function mutations in p53.* Nat Genet, **4**(1): p. 42-6.

190. Lang, G.A., et al., 2004, *Gain of function of a p53 hot spot mutation in a mouse model of Li-Fraumeni syndrome.* Cell, **119**(6): p. 861-72.

191. Olive, K.P., et al., 2004, *Mutant p53 gain of function in two mouse models of Li-Fraumeni syndrome.* Cell, **119**(6): p. 847-60.

192. Hanel, W., et al., 2013, *Two hot spot mutant p53 mouse models display differential gain of function in tumorigenesis.* Cell Death Differ, **20**(7): p. 898-909.

193. Soussi, T. and C. Beroud, 2001, *Assessing TP53 status in human tumours to evaluate clinical outcome.* Nat Rev Cancer, **1**(3): p. 233-40.

194. Lee, M.K., et al., 2012, *Cell-type, dose, and mutation-type specificity dictate mutant p53 functions in vivo.* Cancer Cell, **22**(6): p. 751-64.

195. Terzian, T., et al., 2008, *The inherent instability of mutant p53 is alleviated by Mdm2 or p16INK4a loss.* Genes Dev, **22**(10): p. 1337-44.

196. He, C., et al., 2017, *Mutant p53 Gain of Function and Chemoresistance: The Role of Mutant p53 in Response to Clinical Chemotherapy.* Chemotherapy, **62**(1): p. 43-53.

197. Muller, P.A. and K.H. Vousden, 2013, *p53 mutations in cancer.* Nat Cell Biol, **15**(1): p. 2-8.

198. Muller, P.A. and K.H. Vousden, 2014, *Mutant p53 in cancer: new functions and therapeutic opportunities.* Cancer Cell, **25**(3): p. 304-17.

199. Strano, S., et al., 2007, *Mutant p53: an oncogenic transcription factor.* Oncogene, **26**(15): p. 2212-9.

200. Bisio, A., et al., 2014, *TP53 mutants in the tower of babel of cancer progression.* Hum Mutat, **35**(6): p. 689-701.

201. Di Agostino, S., et al., 2006, *Gain of function of mutant p53: the mutant p53/NF-Y protein complex reveals an aberrant transcriptional mechanism of cell cycle regulation.* Cancer Cell, **10**(3): p. 191-202.

202. Pfister, N.T., et al., 2015, *Mutant p53 cooperates with the SWI/SNF chromatin remodeling complex to regulate VEGFR2 in breast cancer cells.* Genes Dev, **29**(12): p. 1298-315.

203. Mantovani, F., L. Collavin, and G. Del Sal, 2019, *Mutant p53 as a guardian of the cancer cell.* Cell Death Differ, **26**(2): p. 199-212.

204. Mantovani, F., D. Walerych, and G.D. Sal, 2017, *Targeting mutant p53 in cancer: a long road to precision therapy.* FEBS J, **284**(6): p. 837-850.

205. Muller, P.A., et al., 2014, *Mutant p53 regulates Dicer through p63-dependent and -independent mechanisms to promote an invasive phenotype.* J Biol Chem, **289**(1): p. 122-32.

206. Gaiddon, C., et al., 2001, *A subset of tumor-derived mutant forms of p53 down-regulate p63 and p73 through a direct interaction with the p53 core domain.* Mol Cell Biol, **21**(5): p. 1874-87.

207. Li, Y. and C. Prives, 2007, *Are interactions with p63 and p73 involved in mutant p53 gain of oncogenic function?* Oncogene, **26**(15): p. 2220-5.

208. Neilsen, P.M., et al., 2011, *Mutant p53 uses p63 as a molecular chaperone to alter gene expression and induce a pro-invasive secretome.* Oncotarget, **2**(12): p. 1203-17.

209. Liu, J., et al., 2019, *Tumor suppressor p53 and metabolism.* J Mol Cell Biol, **11**(4): p. 284-292.

210. Freed-Pastor, W.A., et al., 2012, *Mutant p53 disrupts mammary tissue architecture via the mevalonate pathway.* Cell, **148**(1-2): p. 244-58.

211. Zhou, G., et al., 2014, *Gain-of-function mutant p53 promotes cell growth and cancer cell metabolism via inhibition of AMPK activation.* Mol Cell, **54**(6): p. 960-74.

212. Morselli, E., et al., 2008, *Mutant p53 protein localized in the cytoplasm inhibits autophagy.* Cell Cycle, **7**(19): p. 3056-61.

213. Frank, A.K., et al., 2011, *Wild-type and mutant p53 proteins interact with mitochondrial caspase-3.* Cancer Biol Ther, **11**(8): p. 740-5.

214. Suh, Y.A., et al., 2011, *Multiple stress signals activate mutant p53 in vivo.* Cancer Res, **71**(23): p. 7168-75.

215. Bartel, F., H. Taubert, and L.C. Harris, 2002, *Alternative and aberrant splicing of MDM2 mRNA in human cancer.* Cancer Cell, **2**(1): p. 9-15.

216. Harris, L.C., 2005, *MDM2 splice variants and their therapeutic implications.* Curr Cancer Drug Targets, **5**(1): p. 21-6.

217. Sigalas, I., et al., 1996, *Alternatively spliced mdm2 transcripts with loss of p53 binding domain sequences: transforming ability and frequent detection in human cancer.* Nat Med, **2**(8): p. 912-7.

218. Zheng, T., et al., 2013, *Spliced MDM2 isoforms promote mutant p53 accumulation and gain-of-function in tumorigenesis.* Nat Commun, **4**: p. 2996.

219. Wawrzynow, B., A. Zylicz, and M. Zylicz, 2018, *Chaperoning the guardian of the genome. The two-faced role of molecular chaperones in p53 tumor suppressor action.* Biochim Biophys Acta Rev Cancer, **1869**(2): p. 161-174.

220. Li, D., et al., 2011, *Functional inactivation of endogenous MDM2 and CHIP by HSP90 causes aberrant stabilization of mutant p53 in human cancer cells.* Mol Cancer Res, **9**(5): p. 577-88.

221. Kabbage, M. and M.B. Dickman, 2008, *The BAG proteins: a ubiquitous family of chaperone regulators.* Cell Mol Life Sci, **65**(9): p. 1390-402.

222. Yue, X., et al., 2017, *Mutant p53 in Cancer: Accumulation, Gain-of-Function, and Therapy.* J Mol Biol, **429**(11): p. 1595-1606.

223. Yue, X., et al., 2015, *BAG2 promotes tumorigenesis through enhancing mutant p53 protein levels and function.* Elife, **4**.

224. Yue, X., et al., 2016, *A novel mutant p53 binding partner BAG5 stabilizes mutant p53 and promotes mutant p53 GOFs in tumorigenesis.* Cell Discov, **2**: p. 16039.

225. Li, Y., et al., 2019, *Salvation of the fallen angel: Reactivating mutant p53.* Br J Pharmacol, **176**(7): p. 817-831.

226. Christophorou, M.A., et al., 2005, *Temporal dissection of p53 function in vitro and in vivo.* Nat Genet, **37**(7): p. 718-26.

227. Ventura, A., et al., 2007, *Restoration of p53 function leads to tumour regression in vivo.* Nature, **445**(7128): p. 661-5.

228. Xue, W., et al., 2007, *Senescence and tumour clearance is triggered by p53 restoration in murine liver carcinomas.* Nature, **445**(7128): p. 656-60.

229. Zawacka-Pankau, J. and G. Selivanova, 2015, *Pharmacological reactivation of p53 as a strategy to treat cancer.* J Intern Med, **277**(2): p. 248-259.

230. Zhang, W.W., et al., 2018, *The First Approved Gene Therapy Product for Cancer Ad-p53 (Gendicine): 12 Years in the Clinic.* Hum Gene Ther, **29**(2): p. 160-179.

231. van der Burg, S.H., et al., 2001, *Long lasting p53-specific T cell memory responses in the absence of anti-p53 antibodies in patients with resected primary colorectal cancer.* Eur J Immunol, **31**(1): p. 146-55.

232. van der Burg, S.H., et al., 2003, *Magnitude and polarization of P53-specific T-helper immunity in connection to leukocyte infiltration of colorectal tumors.* Int J Cancer, **107**(3): p. 425-33.
233. Speetjens, F.M., et al., 2009, *Induction of p53-specific immunity by a p53 synthetic long peptide vaccine in patients treated for metastatic colorectal cancer.* Clin Cancer Res, **15**(3): p. 1086-95.
234. Chiappori, A.A., et al., 2010, *INGN-225: a dendritic cell-based p53 vaccine (Ad.p53-DC) in small cell lung cancer: observed association between immune response and enhanced chemotherapy effect.* Expert Opin Biol Ther, **10**(6): p. 983-91.
235. Leao, M., et al., 2013, *Discovery of a new small-molecule inhibitor of p53-MDM2 interaction using a yeast-based approach.* Biochem Pharmacol, **85**(9): p. 1234-45.
236. Leao, M., et al., 2013, *Alpha-mangostin and gambogic acid as potential inhibitors of the p53-MDM2 interaction revealed by a yeast approach.* J Nat Prod, **76**(4): p. 774-8.
237. Soares, J., et al., 2015, *Oxazoloisoindolinones with in vitro antitumor activity selectively activate a p53-pathway through potential inhibition of the p53-MDM2 interaction.* Eur J Pharm Sci, **66**: p. 138-47.
238. Gomes, S., et al., 2016, *p53 family interactions and yeast: together in anticancer therapy.* Drug Discov Today, **21**(4): p. 616-24.
239. Soares, J., et al., 2016, *Reactivation of wild-type and mutant p53 by tryptophanolderived oxazoloisoindolinone SLMP53-1, a novel anticancer small-molecule.* Oncotarget, **7**(4): p. 4326-43.
240. Gomes, S., et al., 2019, *SLMP53-2 Restores Wild-Type-Like Function to Mutant p53 through Hsp70: Promising Activity in Hepatocellular Carcinoma.* Cancers (Basel), **11**(8).
241. Soares, J., et al., 2017, *DIMP53-1: a novel small-molecule dual inhibitor of p53-MDM2/X interactions with multifunctional p53-dependent anticancer properties.* Mol Oncol, **11**(6): p. 612-627.
242. Gomes, S., et al., 2019, *New inhibitor of the TAp73 interaction with MDM2 and mutant p53 with promising antitumor activity against neuroblastoma.* Cancer Lett, **446**: p. 90-102.
243. Brown, C.J., et al., 2011, *Reactivation of p53: from peptides to small molecules.* Trends Pharmacol Sci, **32**(1): p. 53-62.
244. Vassilev, L.T., et al., 2004, *In vivo activation of the p53 pathway by small-molecule antagonists of MDM2.* Science, **303**(5659): p. 844-8.
245. Vu, B., et al., 2013, *Discovery of RG7112: A Small-Molecule MDM2 Inhibitor in Clinical Development.* ACS Med Chem Lett, **4**(5): p. 466-9.
246. Andreeff, M., et al., 2016, *Results of the Phase I Trial of RG7112, a Small-Molecule MDM2 Antagonist in Leukemia.* Clin Cancer Res, **22**(4): p. 868-76.
247. Ding, Q., et al., 2013, *Discovery of RG7388, a potent and selective p53-MDM2 inhibitor in clinical development.* J Med Chem, **56**(14): p. 5979-83.
248. Grasberger, B.L., et al., 2005, *Discovery and cocrystal structure of benzodiazepinedione HDM2 antagonists that activate p53 in cells.* J Med Chem, **48**(4): p. 909-12.
249. Sun, D., et al., 2014, *Discovery of AMG 232, a potent, selective, and orally bioavailable MDM2-p53 inhibitor in clinical development.* J Med Chem, **57**(4): p. 1454-72.
250. Gupta, A.K., et al., 2017, *Spiro-oxindoles as a Promising Class of Small Molecule Inhibitors of p53-MDM2 Interaction Useful in Targeted Cancer Therapy.* Top Curr Chem (Cham), **375**(1): p. 3.
251. Nayak, S.K., et al., 2018, *p53-Mdm2 Interaction Inhibitors as Novel Nongenotoxic Anticancer Agents.* Curr Cancer Drug Targets, **18**(8): p. 749-772.
252. Merkel, O., et al., 2017, *When the guardian sleeps: Reactivation of the p53 pathway in cancer.* Mutat Res, **773**: p. 1-13.
253. Reed, D., et al., 2010, *Identification and characterization of the first small molecule inhibitor of MDMX.* J Biol Chem, **285**(14): p. 10786-96.
254. Wang, H., et al., 2011, *A small-molecule inhibitor of MDMX activates p53 and induces apoptosis.* Mol Cancer Ther, **10**(1): p. 69-79.
255. Graves, B., et al., 2012, *Activation of the p53 pathway by small-molecule-induced MDM2 and MDMX dimerization.* Proc Natl Acad Sci U S A, **109**(29): p. 11788-93.
256. Issaeva, N., et al., 2004, *Small molecule RITA binds to p53, blocks p53-HDM-2 interaction and activates p53 function in tumors.* Nat Med, **10**(12): p. 1321-8.
257. Enge, M., et al., 2009, *MDM2-dependent downregulation of p21 and hnRNP K provides a switch between apoptosis and growth arrest induced by pharmacologically activated p53.* Cancer Cell, **15**(3): p. 171-83.
258. Spinnler, C., et al., 2011, *Abrogation of Wip1 expression by RITA-activated p53 potentiates apoptosis induction via activation of ATM and inhibition of HdmX.* Cell Death Differ, **18**(11): p. 1736-45.

259. Wanzel, M., et al., 2016, *CRISPR-Cas9-based target validation for p53-reactivating model compounds.* Nat Chem Biol, **12**(1): p. 22-8.
260. Allen, M.A., et al., 2014, *Global analysis of p53-regulated transcription identifies its direct targets and unexpected regulatory mechanisms.* Elife, **3**: p. e02200.
261. Aziz, M.H., H. Shen, and C.G. Maki, 2011, *Acquisition of p53 mutations in response to the non-genotoxic p53 activator Nutlin-3.* Oncogene, **30**(46): p. 4678-86.
262. Jung, J., et al., 2016, *TP53 mutations emerge with HDM2 inhibitor SAR405838 treatment in de-differentiated liposarcoma.* Nat Commun, **7**: p. 12609.
263. Parrales, A. and T. Iwakuma, 2015, *Targeting Oncogenic Mutant p53 for Cancer Therapy.* Front Oncol, **5**: p. 288.
264. Foster, B.A., et al., 1999, *Pharmacological rescue of mutant p53 conformation and function.* Science, **286**(5449): p. 2507-10.
265. Rippin, T.M., et al., 2002, *Characterization of the p53-rescue drug CP-31398 in vitro and in living cells.* Oncogene, **21**(14): p. 2119-29.
266. Zache, N., et al., 2008, *Mutant p53 targeting by the low molecular weight compound STIMA-1.* Mol Oncol, **2**(1): p. 70-80.
267. Bykov, V.J., et al., 2005, *Reactivation of mutant p53 and induction of apoptosis in human tumor cells by maleimide analogs.* J Biol Chem, **280**(34): p. 30384-91.
268. Bykov, V.J., et al., 2002, *Restoration of the tumor suppressor function to mutant p53 by a low-molecular-weight compound.* Nat Med, **8**(3): p. 282-8.
269. Bykov, V.J., et al., 2005, *PRIMA-1(MET) synergizes with cisplatin to induce tumor cell apoptosis.* Oncogene, **24**(21): p. 3484-91.
270. Lambert, J.M., et al., 2009, *PRIMA-1 reactivates mutant p53 by covalent binding to the core domain.* Cancer Cell, **15**(5): p. 376-88.
271. Lambert, J.M., et al., 2010, *Mutant p53 reactivation by PRIMA-1MET induces multiple signaling pathways converging on apoptosis.* Oncogene, **29**(9): p. 1329-38.
272. Messina, R.L., et al., 2012, *Reactivation of p53 mutants by prima-1 [corrected] in thyroid cancer cells.* Int J Cancer, **130**(10): p. 2259-70.
273. Aryee, D.N., et al., 2013, *Variability in functional p53 reactivation by PRIMA-1(Met)/APR-246 in Ewing sarcoma.* Br J Cancer, **109**(10): p. 2696-704.
274. Li, X.L., et al., 2015, *PRIMA-1met (APR-246) inhibits growth of colorectal cancer cells with different p53 status through distinct mechanisms.* Oncotarget, **6**(34): p. 36689-99.
275. Zhang, W., et al., 2016, *Silencing of CD24 Enhances the PRIMA-1-Induced Restoration of Mutant p53 in Prostate Cancer Cells.* Clin Cancer Res, **22**(10): p. 2545-54.
276. Zhang, Q., et al., 2018, *APR-246 reactivates mutant p53 by targeting cysteines 124 and 277.* Cell Death Dis, **9**(5): p. 439.
277. Bauer, M.R., A.C. Joerger, and A.R. Fersht, 2016, *2-Sulfonylpyrimidines: Mild alkylating agents with anticancer activity toward p53-compromised cells.* Proc Natl Acad Sci U S A, **113**(36): p. E5271-80.
278. Madan, E., et al., 2018, *The curcumin analog HO-3867 selectively kills cancer cells by converting mutant p53 protein to transcriptionally active wildtype p53.* J Biol Chem, **293**(12): p. 4262-4276.
279. Punganuru, S.R., et al., 2016, *Design and synthesis of a C7-aryl piperlongumine derivative with potent antimicrotubule and mutant p53-reactivating properties.* Eur J Med Chem, **107**: p. 233-44.
280. Boeckler, F.M., et al., 2008, *Targeted rescue of a destabilized mutant of p53 by an in silico screened drug.* Proc Natl Acad Sci U S A, **105**(30): p. 10360-5.
281. Liu, X., et al., 2013, *Small molecule induced reactivation of mutant p53 in cancer cells.* Nucleic Acids Res, **41**(12): p. 6034-44.
282. Wilcken, R., et al., 2012, *Halogen-enriched fragment libraries as leads for drug rescue of mutant p53.* J Am Chem Soc, **134**(15): p. 6810-8.
283. Demma, M., et al., 2010, *SCH529074, a small molecule activator of mutant p53, which binds p53 DNA binding domain (DBD), restores growth-suppressive function to mutant p53 and interrupts HDM2-mediated ubiquitination of wild type p53.* J Biol Chem, **285**(14): p. 10198-212.
284. Baud, M.G.J., et al., 2018, *Aminobenzothiazole derivatives stabilize the thermolabile p53 cancer mutant Y220C and show anticancer activity in p53-Y220C cell lines.* Eur J Med Chem, **152**: p. 101-114.
285. Wassman, C.D., et al., 2013, *Computational identification of a transiently open L1/S3 pocket for reactivation of mutant p53.* Nat Commun, **4**: p. 1407.

286. Friedler, A., et al., 2002, *A peptide that binds and stabilizes p53 core domain: chaperone strategy for rescue of oncogenic mutants.* Proc Natl Acad Sci U S A, **99**(2): p. 937-42.

287. Issaeva, N., et al., 2003, *Rescue of mutants of the tumor suppressor p53 in cancer cells by a designed peptide.* Proc Natl Acad Sci U S A, **100**(23): p. 13303-7.

288. Friedler, A., et al., 2004, *Structural distortion of p53 by the mutation R249S and its rescue by a designed peptide: implications for "mutant conformation".* J Mol Biol, **336**(1): p. 187-96.

289. Tal, P., et al., 2016, *Cancer therapeutic approach based on conformational stabilization of mutant p53 protein by small peptides.* Oncotarget, **7**(11): p. 11817-37.

290. Yu, X., et al., 2012, *Allele-specific p53 mutant reactivation.* Cancer Cell, **21**(5): p. 614-25.

291. Yu, X., et al., 2014, *Small molecule restoration of wildtype structure and function of mutant p53 using a novel zinc-metallochaperone based mechanism.* Oncotarget, **5**(19): p. 8879-92.

292. Salim, K.Y., et al., 2016, *COTI-2, a novel small molecule that is active against multiple human cancer cell lines in vitro and in vivo.* Oncotarget, **7**(27): p. 41363-41379.

293. Salim, K.Y., et al., 2016, *COTI-2, a new anticancer drug currently under clinical investigation, targets mutant p53 and negatively modulates the PI3K/AKT/mTOR pathway.* European Journal of Cancer, **69**: p. S19.

294. Hiraki, M., et al., 2015, *Small-Molecule Reactivation of Mutant p53 to Wild-Type-like p53 through the p53-Hsp40 Regulatory Axis.* Chem Biol, **22**(9): p. 1206-16.

295. Peng, Y., et al., 2003, *Rescue of mutant p53 transcription function by ellipticine.* Oncogene, **22**(29): p. 4478-87.

296. Weinmann, L., et al., 2008, *A novel p53 rescue compound induces p53-dependent growth arrest and sensitises glioma cells to Apo2L/TRAIL-induced apoptosis.* Cell Death Differ, **15**(4): p. 718-29.

297. Aggarwal, M., et al., 2016, *Reactivation of mutant p53 by a dietary-related compound phenethyl isothiocyanate inhibits tumor growth.* Cell Death Differ, **23**(10): p. 1615-27.

298. North, S., et al., 2002, *Restoration of wild-type conformation and activity of a temperature-sensitive mutant of p53 (p53(V272M)) by the cytoprotective aminothiol WR1065 in the esophageal cancer cell line TE-1.* Mol Carcinog, **33**(3): p. 181-8.

299. Li, D., N.D. Marchenko, and U.M. Moll, 2011, *SAHA shows preferential cytotoxicity in mutant p53 cancer cells by destabilizing mutant p53 through inhibition of the HDAC6-Hsp90 chaperone axis.* Cell Death Differ, **18**(12): p. 1904-13.

300. Wang, Z.T., et al., 2016, *Histone deacetylase inhibitors suppress mutant p53 transcription via HDAC8/YY1 signals in triple negative breast cancer cells.* Cell Signal, **28**(5): p. 506-515.

301. Blagosklonny, M.V., J. Toretsky, and L. Neckers, 1995, *Geldanamycin selectively destabilizes and conformationally alters mutated p53.* Oncogene, **11**(5): p. 933-9.

302. Whitesell, L., et al., 1997, *Geldanamycin-stimulated destabilization of mutated p53 is mediated by the proteasome in vivo.* Oncogene, **14**(23): p. 2809-16.

303. Alexandrova, E.M., et al., 2015, *Improving survival by exploiting tumour dependence on stabilized mutant p53 for treatment.* Nature, **523**(7560): p. 352-6.

304. Wang, J., et al., 2011, *Gambogic acid-induced degradation of mutant p53 is mediated by proteasome and related to CHIP.* J Cell Biochem, **112**(2): p. 509-19.

305. Zhang, S., et al., 2015, *Small-Molecule NSC59984 Restores p53 Pathway Signaling and Antitumor Effects against Colorectal Cancer via p73 Activation and Degradation of Mutant p53.* Cancer Res, **75**(18): p. 3842-52.

306. Yan, W., et al., 2011, *Mutant p53 protein is targeted by arsenic for degradation and plays a role in arsenic-mediated growth suppression.* J Biol Chem, **286**(20): p. 17478-86.

307. Yi, Y.W., et al., 2013, *Targeting mutant p53 by a SIRT1 activator YK-3-237 inhibits the proliferation of triple-negative breast cancer cells.* Oncotarget, **4**(7): p. 984-94.

308. Vakifahmetoglu-Norberg, H., et al., 2013, *Chaperone-mediated autophagy degrades mutant p53.* Genes Dev, **27**(15): p. 1718-30.

309. Paranjpe, A. and K.S. Srivenugopal, 2013, *Degradation of NF-kappaB, p53 and other regulatory redox-sensitive proteins by thiol-conjugating and -nitrosylating drugs in human tumor cells.* Carcinogenesis, **34**(5): p. 990-1000.

310. Kravchenko, J.E., et al., 2008, *Small-molecule RETRA suppresses mutant p53-bearing cancer cells through a p73-dependent salvage pathway.* Proc Natl Acad Sci U S A, **105**(17): p. 6302-7.

311. Hong, B., et al., 2014, *Prodigiosin rescues deficient p53 signaling and antitumor effects via upregulating p73 and disrupting its interaction with mutant p53.* Cancer Res, **74**(4): p. 1153-65.

312. Wei, S., et al., 2015, *Active Pin1 is a key target of all-trans retinoic acid in acute promyelocytic leukemia and breast cancer.* Nat Med, **21**(5): p. 457-66.

313. Parrales, A., et al., 2016, *DNAJA1 controls the fate of misfolded mutant p53 through the mevalonate pathway.* Nat Cell Biol, **18**(11): p. 1233-1243.
314. Soragni, A., et al., 2016, *A Designed Inhibitor of p53 Aggregation Rescues p53 Tumor Suppression in Ovarian Carcinomas.* Cancer Cell, **29**(1): p. 90-103.
315. Bykov, V.J.N., et al., 2018, *Targeting mutant p53 for efficient cancer therapy.* Nat Rev Cancer, **18**(2): p. 89-102.
316. Bou-Hanna, C., et al., 2015, *Acute cytotoxicity of MIRA-1/NSC19630, a mutant p53-reactivating small molecule, against human normal and cancer cells via a caspase-9-dependent apoptosis.* Cancer Lett, **359**(2): p. 211-7.
317. Bykov, V.J., et al., 2016, *Targeting of Mutant p53 and the Cellular Redox Balance by APR-246 as a Strategy for Efficient Cancer Therapy.* Front Oncol, **6**: p. 21.
318. Loh, S.N., 2020, *Follow the Mutations: Toward Class-Specific, Small-Molecule Reactivation of p53.* Biomolecules, **10**(2).
319. Peng, X., et al., 2013, *APR-246/PRIMA-1MET inhibits thioredoxin reductase 1 and converts the enzyme to a dedicated NADPH oxidase.* Cell Death Dis, **4**: p. e881.
320. Mohell, N., et al., 2015, *APR-246 overcomes resistance to cisplatin and doxorubicin in ovarian cancer cells.* Cell Death Dis, **6**: p. e1794.
321. Butler, J.S. and S.N. Loh, 2003, *Structure, function, and aggregation of the zinc-free form of the p53 DNA binding domain.* Biochemistry, **42**(8): p. 2396-403.
322. Puca, R., et al., 2011, *Restoring p53 active conformation by zinc increases the response of mutant p53 tumor cells to anticancer drugs.* Cell Cycle, **10**(10): p. 1679-89.
323. Margalit, O., et al., 2012, *Zinc supplementation augments in vivo antitumor effect of chemotherapy by restoring p53 function.* Int J Cancer, **131**(4): p. E562-8.
324. Garufi, A., et al., 2014, *Degradation of mutant p53H175 protein by Zn(II) through autophagy.* Cell Death Dis, **5**: p. e1271.
325. Girardini, J.E., et al., 2011, *A Pin1/mutant p53 axis promotes aggressiveness in breast cancer.* Cancer Cell, **20**(1): p. 79-91.
326. Parrales, A., E. Thoenen, and T. Iwakuma, 2018, *The interplay between mutant p53 and the mevalonate pathway.* Cell Death Differ, **25**(3): p. 460-470.
327. Kanapathipillai, M., 2018, *Treating p53 Mutant Aggregation-Associated Cancer.* Cancers (Basel), **10**(6).
328. Xu, J., et al., 2011, *Gain of function of mutant p53 by coaggregation with multiple tumor suppressors.* Nat Chem Biol, **7**(5): p. 285-95.
329. Wu, X., S. Patterson, and E. Hawk, 2011, *Chemoprevention--history and general principles.* Best Pract Res Clin Gastroenterol, **25**(4-5): p. 445-59.
330. Penny, L.K. and H.M. Wallace, 2015, *The challenges for cancer chemoprevention.* Chem Soc Rev, **44**(24): p. 8836-47.
331. Barcellos-Hoff, M.H., D. Lyden, and T.C. Wang, 2013, *The evolution of the cancer niche during multistage carcinogenesis.* Nat Rev Cancer, **13**(7): p. 511-8.
332. Villani, A., et al., 2016, *Biochemical and imaging surveillance in germline TP53 mutation carriers with Li-Fraumeni syndrome: 11 year follow-up of a prospective observational study.* Lancet Oncol, **17**(9): p. 1295-305.
333. Shehzad, A., et al., 2013, *Curcumin induces apoptosis in human colorectal carcinoma (HCT-15) cells by regulating expression of Prp4 and p53.* Mol Cells, **35**(6): p. 526-32.
334. Das, L. and M. Vinayak, 2015, *Long term effect of curcumin in restoration of tumour suppressor p53 and phase-II antioxidant enzymes via activation of Nrf2 signalling and modulation of inflammation in prevention of cancer.* PLoS One, **10**(4): p. e0124000.
335. Talib, W.H., et al., 2018, *Role of curcumin in regulating p53 in breast cancer: an overview of the mechanism of action.* Breast Cancer (Dove Med Press), **10**: p. 207-217.
336. Vukmirovic, D., et al., 2017, *Cytotoxic Profiling of Plant Secondary Metabolites on P53 Variant Human Colon Carcinoma Cell Lines.* Dose Response, **15**(4): p. 1559325817748121.
337. Jang, M., et al., 1997, *Cancer chemopreventive activity of resveratrol, a natural product derived from grapes.* Science, **275**(5297): p. 218-20.
338. Seeni, A., et al., 2008, *Suppression of prostate cancer growth by resveratrol in the transgenic rat for adenocarcinoma of prostate (TRAP) model.* Asian Pac J Cancer Prev, **9**(1): p. 7-14.
339. Ko, J.H., et al., 2017, *The Role of Resveratrol in Cancer Therapy.* Int J Mol Sci, **18**(12).
340. Zheng, X., et al., 2018, *Preventive Potential of Resveratrol in Carcinogen-Induced Rat Thyroid Tumorigenesis.* Nutrients, **10**(3).
341. Honari, M., et al., 2019, *Resveratrol is a promising agent for colorectal cancer prevention and treatment: focus on molecular mechanisms.* Cancer Cell Int, **19**: p. 180.

342. Hastak, K., et al., 2005, *Ablation of either p21 or Bax prevents p53-dependent apoptosis induced by green tea polyphenol epigallocatechin-3-gallate.* FASEB J, **19**(7): p. 789-91.
343. Jin, L., et al., 2013, *Epigallocatechin gallate promotes p53 accumulation and activity via the inhibition of MDM2-mediated p53 ubiquitination in human lung cancer cells.* Oncol Rep, **29**(5): p. 1983-90.
344. Chikara, S., et al., 2018, *Oxidative stress and dietary phytochemicals: Role in cancer chemoprevention and treatment.* Cancer Lett, **413**: p. 122-134.
345. Liao, S., et al., 2019, *Chemoprevention of elite tea variety CFT-1 rich in EGCG against chemically induced liver cancer in rats.* Food Sci Nutr, **7**(8): p. 2647-2665.
346. Zhong, Y., et al., 2010, *Molecular targets of apigenin in colorectal cancer cells: involvement of p21, NAG-1 and p53.* Eur J Cancer, **46**(18): p. 3365-74.
347. Sung, B., H.Y. Chung, and N.D. Kim, 2016, *Role of Apigenin in Cancer Prevention via the Induction of Apoptosis and Autophagy.* J Cancer Prev, **21**(4): p. 216-226.
348. Rigby, C.M., et al., 2017, *Role of p53 in silibinin-mediated inhibition of ultraviolet B radiation-induced DNA damage, inflammation and skin carcinogenesis.* Carcinogenesis, **38**(1): p. 40-50.
349. Nakamura, Y., 2009, *Chemoprevention by isothiocyanates: molecular basis of apoptosis induction.* Forum Nutr, **61**: p. 170-181.
350. Wang, P.Y., et al., 2017, *Inhibiting mitochondrial respiration prevents cancer in a mouse model of Li-Fraumeni syndrome.* J Clin Invest, **127**(1): p. 132-136.
351. Nayak, A.P., et al., 2018, *Oxidative Phosphorylation: A Target for Novel Therapeutic Strategies Against Ovarian Cancer.* Cancers (Basel), **10**(9).
352. Kasznicki, J., A. Sliwinska, and J. Drzewoski, 2014, *Metformin in cancer prevention and therapy.* Ann Transl Med, **2**(6): p. 57.
353. Rao, C.V., et al., 2013, *Chemopreventive effects of the p53-modulating agents CP-31398 and Prima-1 in tobacco carcinogen-induced lung tumorigenesis in A/J mice.* Neoplasia, **15**(9): p. 1018-27.
354. Mocka, E.H., et al., 2017, *Chemoprevention of spontaneous ovarian cancer in the domestic hen.* Poult Sci, **96**(6): p. 1901-1909.
355. Tang, X., et al., 2007, *CP-31398 restores mutant p53 tumor suppressor function and inhibits UVB-induced skin carcinogenesis in mice.* J Clin Invest, **117**(12): p. 3753-64.
356. Duffy, M.J., N.C. Synnott, and J. Crown, 2017, *Mutant p53 as a target for cancer treatment.* Eur J Cancer, **83**: p. 258-265.
357. Saraiva, L.S., M. M. M.; Pereira, N. A. L.; Pereira, C.; Soares, J.; Gomes, S.; Leão, M.; Monteiro, A., *Tryptophanol-Derived Oxazoloisoindolinones: Small-molecule p53 activators. European patent application nº EP14739561.0 (pending) and US patent nº 20160347765 (granted).* 2016.
358. Monti, P., et al., 2011, *Dominant-negative features of mutant TP53 in germline carriers have limited impact on cancer outcomes.* Mol Cancer Res, **9**(3): p. 271-9.
359. Gomes, A.S., et al., 2018, *The Crystal Structure of the R280K Mutant of Human p53 Explains the Loss of DNA Binding.* Int J Mol Sci, **19**(4).
360. Hornak, V., et al., 2006, *Comparison of multiple Amber force fields and development of improved protein backbone parameters.* Proteins, **65**(3): p. 712-25.
361. Stephens, P.J., et al., 1994, *Ab initio calculation of Vibrational Absorption and Circular Dichroism spectra using Density Functional Force Fields.* The Journal of Physical Chemistry **98**: p. 11623-11627.
362. Tomasi, J., B. Mennucci, and R. Cammi, 2005, *Quantum mechanical continuum solvation models.* Chem Rev, **105**(8): p. 2999-3093.
363. Bayly, C.I., et al., 1993, *A well-behaved electrostatic potential based method using charge restraints for deriving atomic charges: the RESP model.* The Journal of Physical Chemistry **97**: p. 10269-10280.
364. Pang, Y.P., 2001, *Successful molecular dynamics simulation of two zinc complexes bridged by a hydroxide in phosphotriesterase using the cationic dummy atom method.* Proteins, **45**(3): p. 183-9.
365. Pang, Y.P., et al., 2000, *Successful molecular dynamics simulation of the zinc-bound farnesyltransferase using the cationic dummy atom approach.* Protein Sci, **9**(10): p. 1857-65.
366. Morris, G.M., et al., 2009, *AutoDock4 and AutoDockTools4: Automated docking with selective receptor flexibility.* J Comput Chem, **30**(16): p. 2785-91.
367. Wang, J., et al., 2004, *Development and testing of a general amber force field.* J Comput Chem, **25**(9): p. 1157-74.

368. Iglesias-Arteaga, M.A., et al., 2005, *The Baeyer-Villiger reaction of 23-oxosapogenins.* ARKIVOC, **vi**: p. 109–126.

369. Cádenas, R., et al., 2000, *Semiempirical studies on the transition structure of the Baeyer and Villiger rearrangement. The reaction of acetone with alkyl and aryl peracids.* Journal of Molecular Structure: THEOCHEM, **497**: p. 211-225.

370. Ryckaert, J., G. Ciccotti, and H. Berendsen, 1977, *Numerical integration of the cartesian equations of motion of a system with constraints: molecular dynamics of n-alkanes.* Journal of Computational Physics, **23**: p. 327-341.

371. Miyamoto, S. and P.A. Kollman, 1992, *Settle: An analytical version of the SHAKE and RATTLE algorithm for rigid water models.* Journal of Computational Chemistry, **13**(8): p. 952-962.

372. Darden, T., D. York, and L. Pedersen, 1993, *Particle mesh Ewald: An N·log(N) method for Ewald sums in large systems. .* The Journal of Chemical Physics, **98**: p. 10089-10092.

373. Dourado, D., M. Swart, and A.T.P. Carvalho, 2018, *Why the Flavin Adenine Dinucleotide (FAD) Cofactor Needs To Be Covalently Linked to Complex II of the Electron-Transport Chain for the Conversion of FADH2 into FAD.* Chemistry, **24**(20): p. 5246-5252.

374. Gietz, R.D. and R.H. Schiestl, 2007, *Quick and easy yeast transformation using the LiAc/SS carrier DNA/PEG method.* Nat Protoc, **2**(1): p. 35-7.

375. Reid, Y., et al., *Authentication of Human Cell Lines by STR DNA Profiling Analysis*, in *Assay Guidance Manual*, G.S. Sittampalam, et al., Editors. 2004: Bethesda (MD).

376. Tan, B.X., et al., 2015, *Assessing the Efficacy of Mdm2/Mdm4-Inhibiting Stapled Peptides Using Cellular Thermal Shift Assays.* Sci Rep, **5**: p. 12116.

377. Raimundo, L., et al., 2018, *Improving anticancer activity towards colon cancer cells with a new p53-activating agent.* Br J Pharmacol, **175**(20): p. 3947-3962.

378. Jafari, R., et al., 2014, *The cellular thermal shift assay for evaluating drug target interactions in cells.* Nat Protoc, **9**(9): p. 2100-22.

379. Walerych, D., K. Lisek, and G. Del Sal, 2015, *Mutant p53: One, No One, and One Hundred Thousand.* Front Oncol, **5**: p. 289.

380. Weinberg, R.L., D.B. Veprintsev, and A.R. Fersht, 2004, *Cooperative binding of tetrameric p53 to DNA.* J Mol Biol, **341**(5): p. 1145-59.

381. Wright, J.D., S.Y. Noskov, and C. Lim, 2002, *Factors governing loss and rescue of DNA binding upon single and double mutations in the p53 core domain.* Nucleic Acids Res, **30**(7): p. 1563-74.

382. Malami, I., et al., 2017, *An in silico approach in predicting the possible mechanism involving restoration of wild-type p53 functions by small molecular weight compounds in tumor cells expressing R273H mutant p53.* EXCLI J, **16**: p. 1276-1287.

383. Warburg, O., 1956, *On the origin of cancer cells.* Science, **123**(3191): p. 309-14.

384. Bessa, C., et al., 2018, *Discovery of a small-molecule protein kinase Cdelta-selective activator with promising application in colon cancer therapy.* Cell Death Dis, **9**(2): p. 23.

385. Chou, T.C. and P. Talalay, 1984, *Quantitative analysis of dose-effect relationships: the combined effects of multiple drugs or enzyme inhibitors.* Adv Enzyme Regul, **22**: p. 27-55.

386. Lago, C.U., et al., 2011, *p53, aerobic metabolism, and cancer.* Antioxid Redox Signal, **15**(6): p. 1739-48.

387. Daina, A., O. Michielin, and V. Zoete, 2017, *SwissADME: a free web tool to evaluate pharmacokinetics, drug-likeness and medicinal chemistry friendliness of small molecules.* Sci Rep, **7**: p. 42717.

388. Macip, S., et al., 2003, *Influence of induced reactive oxygen species in p53-mediated cell fate decisions.* Mol Cell Biol, **23**(23): p. 8576-85.

389. Liou, G.Y. and P. Storz, 2010, *Reactive oxygen species in cancer.* Free Radic Res, **44**(5): p. 479-96.

390. Madan, E., et al., 2013, *SCO2 induces p53-mediated apoptosis by Thr845 phosphorylation of ASK-1 and dissociation of the ASK-1-Trx complex.* Mol Cell Biol, **33**(7): p. 1285-302.

391. Goodwin, M.L., et al., 2014, *Lactate and cancer: revisiting the warburg effect in an era of lactate shuttling.* Front Nutr, **1**: p. 27.

392. Goubran, H.A., et al., 2014, *Regulation of tumor growth and metastasis: the role of tumor microenvironment.* Cancer Growth Metastasis, **7**: p. 9-18.

393. Ullah, M.S., A.J. Davies, and A.P. Halestrap, 2006, *The plasma membrane lactate transporter MCT4, but not MCT1, is up-regulated by hypoxia through a HIF-1alpha-dependent mechanism.* J Biol Chem, **281**(14): p. 9030-7.

394. Obacz, J., et al., 2013, *Cross-talk between HIF and p53 as mediators of molecular responses to physiological and genotoxic stresses.* Mol Cancer, **12**(1): p. 93.

395. Pinheiro, C., et al., 2012, *Role of monocarboxylate transporters in human cancers: state of the art.* J Bioenerg Biomembr, **44**(1): p. 127-39.
396. Baek, G., et al., 2014, *MCT4 defines a glycolytic subtype of pancreatic cancer with poor prognosis and unique metabolic dependencies.* Cell Rep, **9**(6): p. 2233-49.
397. Benjamin, D., et al., 2018, *Dual Inhibition of the Lactate Transporters MCT1 and MCT4 Is Synthetic Lethal with Metformin due to NAD+ Depletion in Cancer Cells.* Cell Rep, **25**(11): p. 3047-3058 e4.
398. Polanski, R., et al., 2014, *Activity of the monocarboxylate transporter 1 inhibitor AZD3965 in small cell lung cancer.* Clin Cancer Res, **20**(4): p. 926-937.
399. Simabuco, F.M., et al., 2018, *p53 and metabolism: from mechanism to therapeutics.* Oncotarget, **9**(34): p. 23780-23823.
400. Pal, S., K. Datta, and D. Mukhopadhyay, 2001, *Central role of p53 on regulation of vascular permeability factor/vascular endothelial growth factor (VPF/VEGF) expression in mammary carcinoma.* Cancer Res, **61**(18): p. 6952-7.
401. Qin, G., et al., 2006, *Cell cycle regulator E2F1 modulates angiogenesis via p53-dependent transcriptional control of VEGF.* Proc Natl Acad Sci U S A, **103**(29): p. 11015-20.
402. Wu, M., et al., 2014, *E2F1 suppresses cardiac neovascularization by down-regulating VEGF and PlGF expression.* Cardiovasc Res, **104**(3): p. 412-22.
403. Bielenberg, D.R. and B.R. Zetter, 2015, *The Contribution of Angiogenesis to the Process of Metastasis.* Cancer J, **21**(4): p. 267-73.
404. Stacpoole, P.W., 1989, *The pharmacology of dichloroacetate.* Metabolism, **38**(11): p. 1124-44.
405. Knoechel, T.R., et al., 2006, *Regulatory roles of the N-terminal domain based on crystal structures of human pyruvate dehydrogenase kinase 2 containing physiological and synthetic ligands.* Biochemistry, **45**(2): p. 402-15.
406. Bonnet, S., et al., 2007, *A mitochondria-K+ channel axis is suppressed in cancer and its normalization promotes apoptosis and inhibits cancer growth.* Cancer Cell, **11**(1): p. 37-51.
407. Liang, Y., et al., 2019, *Dichloroacetate restores colorectal cancer chemosensitivity through the p53/miR-149-3p/PDK2-mediated glucose metabolic pathway.* Oncogene.
408. Agnoletto, C., et al., 2014, *Sodium dichloroacetate exhibits anti-leukemic activity in B-chronic lymphocytic leukemia (B-CLL) and synergizes with the p53 activator Nutlin-3.* Oncotarget, **5**(12): p. 4347-60.
409. Araghi, M., et al., 2019, *Changes in colorectal cancer incidence in seven high-income countries: a population-based study.* Lancet Gastroenterol Hepatol, **4**(7): p. 511-518.
410. Li, X.L., et al., 2015, *P53 mutations in colorectal cancer - molecular pathogenesis and pharmacological reactivation.* World J Gastroenterol, **21**(1): p. 84-93.
411. Kocik, J., et al., 2019, *Helping the Released Guardian: Drug Combinations for Supporting the Anticancer Activity of HDM2 (MDM2) Antagonists.* Cancers (Basel), **11**(7).
412. Lu, T., et al., 2016, *PRIMA-1Met suppresses colorectal cancer independent of p53 by targeting MEK.* Oncotarget, **7**(50): p. 83017-83030.
413. Soares, M.I., et al., 2013, *Chiral 6,7-bis(hydroxymethyl)-1H,3H-pyrrolo[1,2-c]thiazoles with anti-breast cancer properties.* Eur J Med Chem, **60**: p. 254-62.
414. Alessandrini, F., et al., 2018, *ETV7-Mediated DNAJC15 Repression Leads to Doxorubicin Resistance in Breast Cancer Cells.* Neoplasia, **20**(8): p. 857-870.
415. Ciribilli, Y., et al., 2015, *Decoding c-Myc networks of cell cycle and apoptosis regulated genes in a transgenic mouse model of papillary lung adenocarcinomas.* Oncotarget, **6**(31): p. 31569-92.
416. Dobin, A., et al., 2013, *STAR: ultrafast universal RNA-seq aligner.* Bioinformatics, **29**(1): p. 15-21.
417. Love, M.I., W. Huber, and S. Anders, 2014, *Moderated estimation of fold change and dispersion for RNA-seq data with DESeq2.* Genome Biol, **15**(12): p. 550.
418. Fernandes, C., et al., 2017, *Chiral Derivatives of Xanthones: Investigation of the Effect of Enantioselectivity on Inhibition of Cyclooxygenases (COX-1 and COX-2) and Binding Interaction with Human Serum Albumin.* Pharmaceuticals (Basel), **10**(2).
419. Kuleshov, M.V., et al., 2016, *Enrichr: a comprehensive gene set enrichment analysis web server 2016 update.* Nucleic Acids Res, **44**(W1): p. W90-7.
420. Engeland, K., 2018, *Cell cycle arrest through indirect transcriptional repression by p53: I have a DREAM.* Cell Death Differ, **25**(1): p. 114-132.

421. Martinez Molina, D. and P. Nordlund, 2016, *The Cellular Thermal Shift Assay: A Novel Biophysical Assay for In Situ Drug Target Engagement and Mechanistic Biomarker Studies.* Annu Rev Pharmacol Toxicol, **56**: p. 141-61.
422. Jabs, J., et al., 2017, *Screening drug effects in patient-derived cancer cells links organoid responses to genome alterations.* Mol Syst Biol, **13**(11): p. 955.
423. Li, X., et al., 2017, *Prediction of synergistic anti-cancer drug combinations based on drug target network and drug induced gene expression profiles.* Artif Intell Med, **83**: p. 35-43.
424. Lavin, M.F. and N. Gueven, 2006, *The complexity of p53 stabilization and activation.* Cell Death Differ, **13**(6): p. 941-50.
425. Schulz-Heddergott, R., et al., 2018, *Therapeutic Ablation of Gain-of-Function Mutant p53 in Colorectal Cancer Inhibits Stat3-Mediated Tumor Growth and Invasion.* Cancer Cell, **34**(2): p. 298-314 e7.
426. Song, H., M. Hollstein, and Y. Xu, 2007, *p53 gain-of-function cancer mutants induce genetic instability by inactivating ATM.* Nat Cell Biol, **9**(5): p. 573-80.
427. Huang, K., et al., 2014, *Elevated p53 expression levels correlate with tumor progression and poor prognosis in patients exhibiting esophageal squamous cell carcinoma.* Oncol Lett, **8**(4): p. 1441-1446.
428. Martins, C.P., L. Brown-Swigart, and G.I. Evan, 2006, *Modeling the therapeutic efficacy of p53 restoration in tumors.* Cell, **127**(7): p. 1323-34.
429. Williams, N.S., et al., 2003, *Identification and validation of genes involved in the pathogenesis of colorectal cancer using cDNA microarrays and RNA interference.* Clin Cancer Res, **9**(3): p. 931-46.
430. Huang, Y.J., et al., 2013, *The prognostic value of survivin expression in patients with colorectal carcinoma: a meta-analysis.* Jpn J Clin Oncol, **43**(10): p. 988-95.
431. Waligorska-Stachura, J., et al., 2012, *Survivin--prognostic tumor biomarker in human neoplasms--review.* Ginekol Pol, **83**(7): p. 537-40.
432. Russo, A., et al., 2005, *The TP53 Colorectal Cancer International Collaborative Study on the Prognostic and Predictive Significance of p53 Mutation: Influence of Tumor Site, Type of Mutation, and Adjuvant Treatment.* Journal of Clinical Oncology, **23**(30): p. 7518-7528.
433. Iacopetta, B., 2003, *TP53 mutation in colorectal cancer.* Hum Mutat, **21**(3): p. 271-6.
434. Gomes, A.S., et al., 2020, *SLMP53-1 interacts with wild-type and mutant p53 DNA-binding domain and reactivates multiple hotspot mutations.* Biochim Biophys Acta Gen Subj, **1864**(1): p. 129440.
435. Ahmad, I.M., et al., 2008, *2-Deoxyglucose combined with wild-type p53 overexpression enhances cytotoxicity in human prostate cancer cells via oxidative stress.* Free Radic Biol Med, **44**(5): p. 826-34.
436. Sinthupibulyakit, C., et al., 2009, *p53 is an important factor for the radiosensitization effect of 2-deoxy-D-glucose.* Int J Oncol, **35**(3): p. 609-15.
437. Ben Sahra, I., et al., 2010, *Targeting cancer cell metabolism: the combination of metformin and 2-deoxyglucose induces p53-dependent apoptosis in prostate cancer cells.* Cancer Res, **70**(6): p. 2465-75.
438. Zawacka-Pankau, J., et al., 2011, *Inhibition of glycolytic enzymes mediated by pharmacologically activated p53: targeting Warburg effect to fight cancer.* J Biol Chem, **286**(48): p. 41600-15.
439. Bayat Mokhtari, R., et al., 2017, *Combination therapy in combating cancer.* Oncotarget, **8**(23): p. 38022-38043.
440. Li, H., et al., 2019, *Targeting the Oncogenic p53 Mutants in Colorectal Cancer and Other Solid Tumors.* Int J Mol Sci, **20**(23).
441. Takayama, T., et al., 2006, *Colorectal cancer: genetics of development and metastasis.* J Gastroenterol, **41**(3): p. 185-92.
442. Kalepu, S. and V. Nekkanti, 2015, *Insoluble drug delivery strategies: review of recent advances and business prospects.* Acta Pharm Sin B, **5**(5): p. 442-53.
443. Budha, N.R., et al., 2012, *Drug absorption interactions between oral targeted anticancer agents and PPIs: is pH-dependent solubility the Achilles heel of targeted therapy?* Clin Pharmacol Ther, **92**(2): p. 203-13.
444. Beni, S., et al., 2007, *Cyclodextrin/imatinib complexation: binding mode and charge dependent stabilities.* Eur J Pharm Sci, **30**(2): p. 167-74.
445. Lipinski, C.A., et al., 1997, *Experimental and computational approaches to estimate solubility and permeability in drug discovery and development settings.* Advanced Drug Delivery Reviews, **23**(1): p. 3-25.

446. Dash, R.P., R. Jayachandra Babu, and N.R. Srinivas, 2017, *Therapeutic Potential and Utility of Elacridar with Respect to P-glycoprotein Inhibition: An Insight from the Published In Vitro, Preclinical and Clinical Studies.* Eur J Drug Metab Pharmacokinet, **42**(6): p. 915-933.
447. Undevia, S.D., G. Gomez-Abuin, and M.J. Ratain, 2005, *Pharmacokinetic variability of anticancer agents.* Nat Rev Cancer, **5**(6): p. 447-58.
448. Toutain, P.L. and A. Bousquet-Melou, 2004, *Volumes of distribution.* J Vet Pharmacol Ther, **27**(6): p. 441-53.
449. Sangster, J., *Octanol-water partition coefficients : fundamentals and physical chemistry*. 1997, Chichester: John Wiley and Sons.
450. Banker, M.J., T.H. Clark, and J.A. Williams, 2003, *Development and validation of a 96-well equilibrium dialysis apparatus for measuring plasma protein binding.* J Pharm Sci, **92**(5): p. 967-74.
451. Hidalgo, I.J., T.J. Raub, and R.T. Borchardt, 1989, *Characterization of the human colon carcinoma cell line (Caco-2) as a model system for intestinal epithelial permeability.* Gastroenterology, **96**(3): p. 736-49.
452. Obach, R.S., et al., 1997, *The prediction of human pharmacokinetic parameters from preclinical and in vitro metabolism data.* J Pharmacol Exp Ther, **283**(1): p. 46-58.

ANNEX I

Human cell lines, antibodies and primers

Table S1. Human cell lines description.

Cell line	Disease	*TP53* status	Source/Provider
A431	Epidermoid carcinoma	Homozygous Mut R273H	ATCC, Manassas, VA, USA
H1299	Non-small cell lung carcinoma	Homozygous partial deletion No p53 expression	ATCC, Manassas, VA, USA
H460	Large-cell lung carcinoma	wt	ATCC, Manassas, VA, USA
HCC1937	Breast ductal carcinoma	Truncating mutation c.916C>T with wt allele loss No p53 expression	ATCC, Manassas, VA, USA
HCT116 p53$^{+/+}$	Colon adenocarcinoma	wt	B. Vogelstein, The Johns Hopkins Kimmel Cancer Center, Baltimore, MD, USA
HCT116 p53$^{-/-}$		Exon 3 deletion No p53 expression	
HT-29	Colon adenocarcinoma	Homozygous Mut R273H	ATCC, Manassas, VA, USA
IGROV-1	Ovarian adenocarcinoma	Heterozygous Mut Y126C	Leonor David, Instituto de Investigação e Inovação em Saúde, Porto, Portugal
LS-1034	Colon adenocarcinoma	Homozygous Mut G245S	ATCC, Manassas, VA, USA
MCF-7	Breast adenocarcinoma	wt	ATCC, Manassas, VA, USA
MDA-MB-231	Breast adenocarcinoma	Homozygous Mut R280K	ATCC, Manassas, VA, USA
MDA-MB-468	Breast adenocarcinoma	Homozygous Mut R273H	ATCC, Manassas, VA, USA
SK-OV-3	Ovarian adenocarcinoma	Mutation c.267delC No p53 expression	Leonor David, Instituto de Investigação e Inovação em Saúde, Porto, Portugal
SW837	Rectum adenocarcinoma	Hemizygous Mut R248W	ATCC, Manassas, VA, USA

Table S2. List of antibodies used in immunohistochemistry (IHC) or western blot (WB) experiments.

	Final Dilution IHC	Final Dilution WB	Supplier
Primary antibodies			
α-Tubulin Mouse Monoclonal	------	1:5000	Sigma-Aldrich **Cat# T9026**
BAX (6A7) Mouse monoclonal	1:50	------	Thermo Scientific **Cat# MA5-14003**
BCL-2 (C-2) Mouse monoclonal	------	1:200	Santa Cruz Biotechnology **Cat#sc-7382**
CLEAVED PARP (C2-10) Mouse monoclonal	------	1:2000	Santa Cruz Biotechnology **Cat# sc-53643**

COX4 (F-8) Mouse Monoclonal	1:100	1:100	Santa Cruz Biotechnology **Cat#sc-376731**
E-CAD (G-10) Mouse monoclonal	1:50	1:50	Santa Cruz Biotechnology **Cat#sc-8426**
GADD45 alpha Rabbit polyclonal	------	1:200	Merck Millipore **Cat# ABE2696**
GAPDH (6C5) Mouse monoclonal	------	1:10000	Santa Cruz Biotechnology **Cat#sc-32233**
GLUT1 Rabbit polyclonal	1:250	1:500	Abcam **Cat#ab652**
HK2 (3D3) Mouse monoclonal	1:100	1:500	Merck Millipore **Cat#MABN702**
KI67 (SP6) Rabbit monoclonal	1:200	------	Thermo Scientific **Cat# MA5-14520**
KILLER/DR5 (D-6) Mouse monoclonal	------	1:200	Santa Cruz Biotechnology **Cat# sc-166624**
MCT4 (H-90) Rabbit polyclonal	1:200	------	Santa Cruz Biotechnology **Cat#sc-50329**
MDM2 (SMP14) Mouse monoclonal	------	1:100	Santa Cruz Biotechnology **Cat# sc-965**
MMP9 (2C3) Mouse monoclonal	1:100	1:50	Santa Cruz Biotechnology **Cat#sc-21733**
N-CAD (13A9) Mouse monoclonal	1:100	1:100	Santa Cruz Biotechnology **Cat#sc-59987**
p21 (C-19) Rabbit polyclonal	------	1:100	Santa Cruz Biotechnology **Cat#sc-397**
p53 (DO-1) Mouse monoclonal	1:50 – 1:100	1:5000	Santa Cruz Biotechnology **Cat #sc-126**
PFKFB3 Rabbit Polyclonal	1:100	1:1000	ThermoScientific **Cat#PA5-21931**
Pgk1p (22C5D8) Mouse monoclonal	------	1:10000	Invitrogen **Cat#459250**
PUMA (H-136) Mouse monoclonal	------	1:50	Santa Cruz Biotechnology **Cat#sc-28226**
SCO2 Rabbit Polyclonal	1:100	1:500	ProteinTech **Cat#21223-1-AP**
Total OXPHOS cocktail Mouse monoclonal	------	1:1000	Abcam **Cat#ab110413**
VEGF Mouse monoclonal	1:100	1:100	ThermoScientific **Cat#MA1-16629**
Secondary antibodies			
Anti-mouse HRP-conjugated	------	1:5000	Santa Cruz Biotechnology **Cat #sc-2005**
Anti-rabbit HRP-conjugated	------	1:5000	Santa Cruz Biotechnology **Cat#sc-2004**

Table S3. List of primers used in RT-qPCR experiments.

Primer	Sequence
HCT116 and SW837 cells	
B2M FW	AGGCTATCCAGCGTACTCCA
B2M RV	ATGGATGAAACCCAGACACA
BAX FW	GCTGTTGGGCTGGATCCAAG
BAX RV	TCAGCCCATCTTCTTCCAGA
BRCA1 FW	CACTCAGCAGAGGGATACCA
BRCA1 RV	GAGTTGTTCCTTTGGCCATGT
E2F1 FW	CTACGTGACGTGTCAGGACC
E2F1 RV	CTGAAAGTTCTCCGAAGAGTCCA
EXO1 FW	GCCTGGCCCAGAAGAAACTT
EXO1 RV	CTGGGATTCACTAGTTCTCTCAGAT
FANCA FW	TGGAGCTCAAGGGTCAGGG
FANCA RV	CCAGCAGCTCTGCCACG
CDKN1A FW	CTGGAGACTCTCAGGGTCGAAA
CDKN1A RV	GATTAGGGCTTCCTCTTGGAGAA
GADD45A FW	TCAGCGCACGATCACTGTC
GADD45A RV	CCAGCAGGCACAACACCAC
GAPDH FW	GGCCAAGGTCATCCATGA
GAPDH RV	TCAGTGTAGCCCAGGATG
MDM2 FW	GGCCTGCTTTACATGTGCAA
MDM2 RV	GCACAATCATTTGAATTGGTTGTC
NOXA FW	AGCTGGAAGTCGAGTGTGCT
NOXA RV	TCCTGAGCAGAAGAGTTTGGA
PUMA FW	CCTGGAGGGTCCTGTACAATCT
PUMA RV	GCACCTAATTGGGCTCCATCT
TNFRSF10B FW	TGACTCATCTCAGAAATGTCAATTCTTA
TNFRSF10B RV	GGACACAAGAAGAAAACCTTAATGC
YWHAZ1 FW	CAACACATCCTATCAGACTGGG
YWHAZ1 RV	AATGTATCAAGTTCAGCAATGGC
Patient-derived CRC cells	
BAX FW	CCTGGAGGGTCCTGTACAATCT
BAX RV	GCACCTAATTGGGCTCCATCT
BIRC5 FW	GACGACCCCATAGAGGAACAT
BIRC5 RV	CGCACTTTCTCCGCAGTTTC
CDKN1A FW	TTAGCAGCGGAACAAGGAGT
CDKN1A RV	GCCGAGAGAAAACAGTCCAG
HSP90AB1 FW	CGCATGAAGGAGACACAGAA
HSP90AB1 RV	TCCCATCAAATTCCTTGAGC

MDM2 FW	GGCCTGCTTTACATGTGCAA
MDM2 RV	GCACAATCATTTGAATTGGTTGTC
VEGF FW	GCTCGGTGCTGGAATTTGAT
VEGF RV	TCACTCACTTTGCCCCTGTC

Table S4. List of primers used in ChIP experiments.

Primer	**Sequence**
ACTIN B FW	TCTCCCTCCTCCTCTTCCTCAAT
ACTIN B RV	TCGCGCCGCTGGGTTTTATA
CDKN1A FW	GTGGCTCTGATTGGCTTTCTG
CDKN1A RV	CTCCTACCATCCCCTTCCTC
MDM2 FW	GAGGTCCGGATGATCGCAG
MDM2 RV	GGAAAATGCATGGTTTAAATAGCC
NOXA FW	CCTGTTACTGCCCATACTCTTCA
NOXA RV	GACGTCGTCAGCGGCAG

ANNEX II

Supporting information of Chapter 2

Ana Sara Gomes[#], **Helena Ramos[#]**, et al, 2020. *SLMP53-1 interacts with wild-type and mutant p53 DNA-binding domain*. Biochim Biophys Acta Gen Subj, 1864 (1), 129440. DOI: 10.1016/j.bbagen.2019.129440

[#]Authors equally contributed to this work

Table S5. Distances of SLMP53-1 and its enantiomer to wtp53 and mutp53 R280K with DNA models by MD simulations.

	Distances in Å			
	SLMP53-1		SLMP53-1 enantiomer	
	wtp53	mutp53 R280K	wtp53	mutp53 R280K
M243SDA-indole	**4.99 ± 0.50**	**3.78 ± 0.25**	11.57 ± 2.17	10.79 ± 0.25
M243SDB-indole	6.28 ± 0.89	6.35 ± 0.99	8.44 ± 0.48	10.31 ± 0.13
M243CEA-indole	**4.87 ± 0.53**	**4.07 ± 0.03**	11.55 ± 3.41	10.11 ± 0.68
M243CEB-indole	6.65 ± 0.48	6.78 ± 0.61	7.30 ± 2.58	10.84 ± 0.39
Zn-indole	7.33 ± 0.15	7.17 ± 0.40	13.40 ± 0.57	12.24 ± 0.67
Ligand-O2-NH_2-DNA	**2.93 ± 0.17**	**3.10 ± 0.07**	6.88 ± 0.42	6.93 ± 0.32

Wt and mutp53 R280K in complex with DNA models were analyzed with SLMP53-1. Wt and mutp53 R280K in complex with DNA models were analyzed with the inactive SLMP53-1 enantiomer. M243 – methionine 243; SD – sulphur delta; CE – carbon epsilon; A and B – molecules A and B of wtp53 or mutp53 R280K; Zn – zinc (II); indole – center of mass of the substrate indole heavy atoms of the ligand. Data is shown as mean ± SD (n = 3). Distances highlighted in bold indicate interactions.

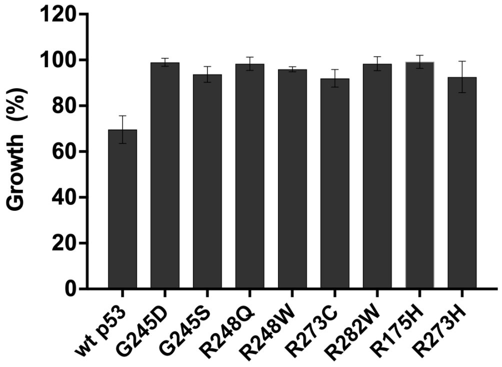

Figure S1. Effect of wtp53 and mutp53 expression on yeast growth. Yeast cells were incubated in induction selective medium for 48 h; the growth of yeast cells expressing wtp53 and mutp53 were analyzed by CFU counts; growth achieved with control yeast (transformed with the empty vector) was set as 100%; data are shown as mean ± SEM of 3-7 independent experiments.

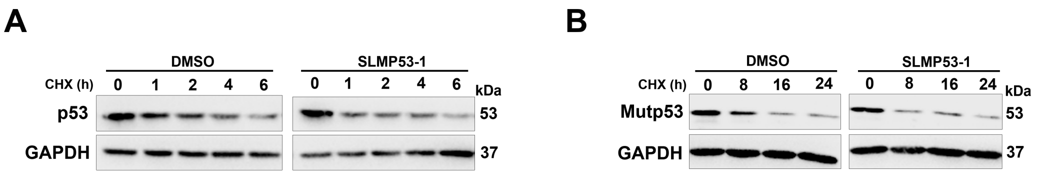

Figure S2. SLMP53-1 does not interfere with wtp53 and mutp53 half-life. (A) Wtp53 protein levels in HCT116 cells treated for 24 h with 15 µM SLMP53-1 or solvent (DMSO), and **(B)** mutp53 protein levels in MDA-MB-468 cells treated for 24 h with 10.3 µM SLMP53-1 or solvent (DMSO)

followed with cycloheximide (CHX; 150 µg/mL; Sigma-Aldrich, Sintra, Portugal) for up to 6 h (A) or 24 h (B).

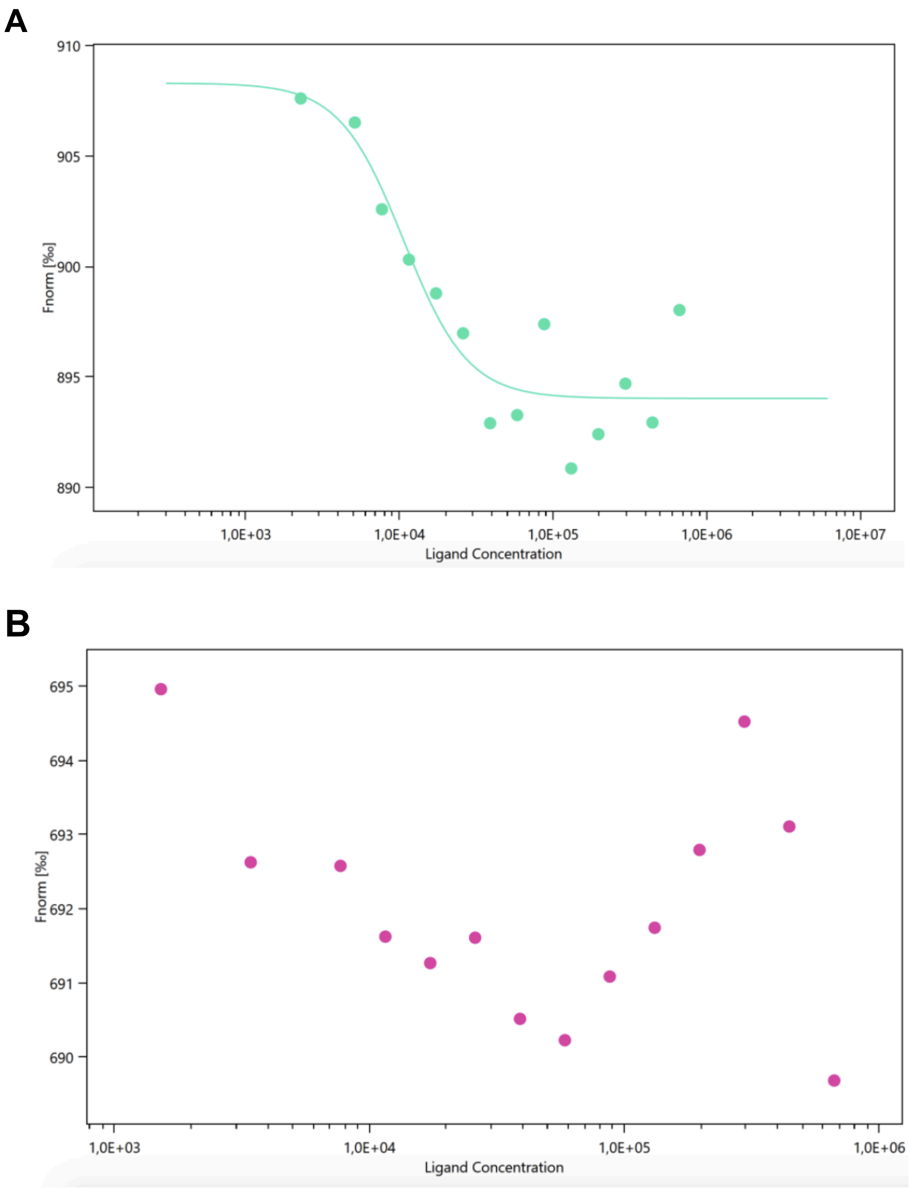

Figure S3. SLMP53-1 binds to human recombinant mutp53 R280K DBD. (A) Fitted dose-response curve of SLMP53-1 indicating interaction with mutp53 R280K, by MST. To accomplish MST analysis, human recombinant mutp53 R280K DBD was produced as described in [359], and fluorescently labelled with NT-647 dye by N-hydroxysuccinimide (NHS) coupling. NT-647-mutp53 R280K at 70 nM was titrated with SLMP53-1 with a concentration range of 1.5 to 666 µM. The assay was performed in Tris.HCl 50 mM pH 7.2, NaCl 300 mM, DTT 1 mM, Tween20 (0.05%) and DMSO (10%). Samples were incubated and loaded into MST NT.115 premium glass capillaries. The MST analysis was performed using the Monolith NT.115, NanoTemper Technologies, (LED: 50%; MST: 80%). Concentrations on the x-axis are plotted in nM. A Kd of 10.7 µM was determined for this interaction. **(B)** Plotted dose-response negative control using the fluorescent dye NT-647 alone in the same buffer, in the absence of the protein, titrated against the same SLMP53-1 concentration range.

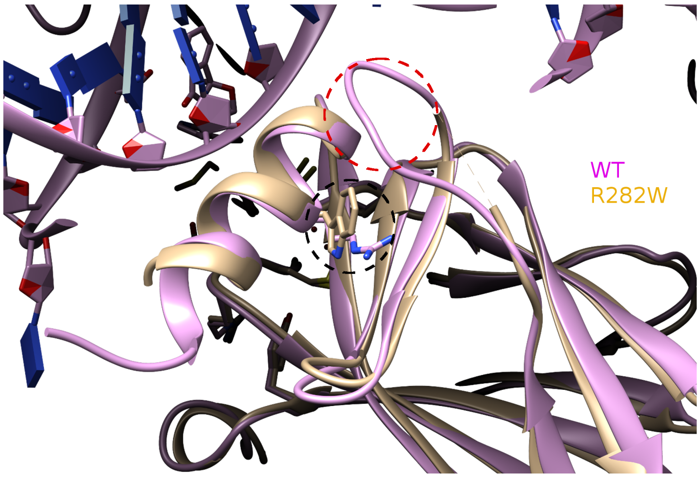

Figure S4. Structural mutp53 R282W DBD exhibits the same conformational structure as wtp53, with exception for L1 region. Image shows the wtp53 DBD:DNA complex superposed with mutp53 R282W DBD (PDB code: 2J21). The black dashed circle indicates the mutation site and the red dashed circle highlights the L1 structural disorganization of mutp53 R282W DBD.

ANNEX III

Supporting information of Chapter 3

Helena Ramos, et al, 2020. *SLMP53-1 inhibits tumor cell growth through regulation of glucose metabolism and angiogenesis in a p53-dependent manner*. Int J Mol Sci, 21 (2). DOI: 10.3390/ijms21020596

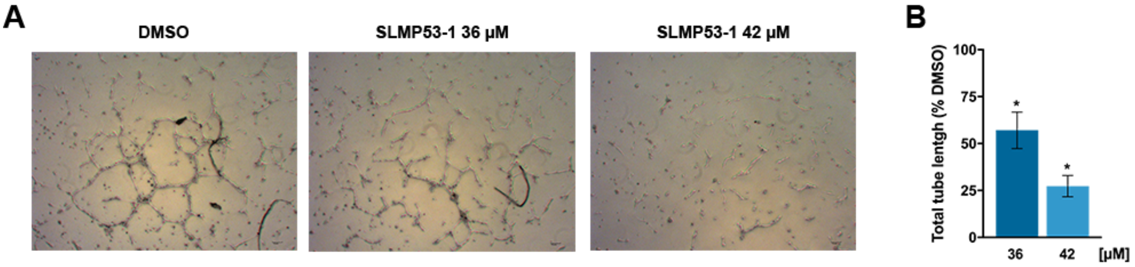

Figure S5. Anti-angiogenic effect of SLMP53-1, in HMVEC-D cells, after 12 h treatment, using the endothelial tube formation assay. (A) Representative images are shown (magnification = ×40). **(B)** Quantification of total endothelial tube length in five randomly selected microscopic fields; percentages are relative to solvent (DMSO) and correspond to mean ± SEM of three independent experiments. Values significantly different from DMSO (*p < 0.05; one-way ANOVA with Dunnett's multiple comparison test).

Physicochemical and pharmacokinetic parameters of SLMP53-1 calculated using SwissADME [387]: The resemblance of the SLMP53-1 compound to other drugs was evaluated with the Ghose, Egan, Veber and Muegee filters. The SLMP53-1 molecule met all the criteria set by those filters. Table S6 provides detailed data regarding the Ghose qualification criteria, which contain physicochemical properties like the molar refractivity (MR; between 40 and 130), molecular weight (MW; between 160 and 480) and number of atoms (20 to 70 atoms). SLMP53-1 also obeyed the Veber model criteria, meaning that it is more likely to have better oral bioavailability (10 or less rotary titers and a polar surface area, PSA, equal to or fewer than 140 Å2 with 12 or fewer hydrogen binding donors and acceptors). Finally, it obeyed the Muegge and Egan filters (Table S7). The Muegge model is an independent database capable of discriminating between drug and chemical substances similar to drugs. The Egan filter is based on the PSA and the AlogP98v, providing a robust prediction of drug absorption. SLMP53-1 was also evaluated against models that exclude molecules that are likely to fail biological assays. The analysis showed no warnings from Pains Alert. In addition, the Brenk selection model and the Leadlikeness criteria also proved to be non-infringing (Table S8). Pharmacokinetic evaluation by SwissADME also estimated that SLMP53-1 has high gastrointestinal absorption, is capable to penetrate the blood brain barrier (BBB), and has an inhibitory function on cytochrome p450 isoenzymes CYP1A2 and CYP2D6 (Table S9). Water solubility was evaluated according to 3 models: the ESOL model, an adapted model from Ali *et* al, and a model developed by SILICOS-IT. The molecule was evaluated as soluble, soluble and moderately soluble respectively. All values given are the decimal logarithm of molar solubility in water (*log S*) (Tables S10 and S11). The lipophilicity of the molecule was further evaluated with

Consensus *Log P*, being in the average value of all *Log P* calculated with various lipophilicity criteria (Table S12).

Table S6. SLMP53-1 physicochemical properties.

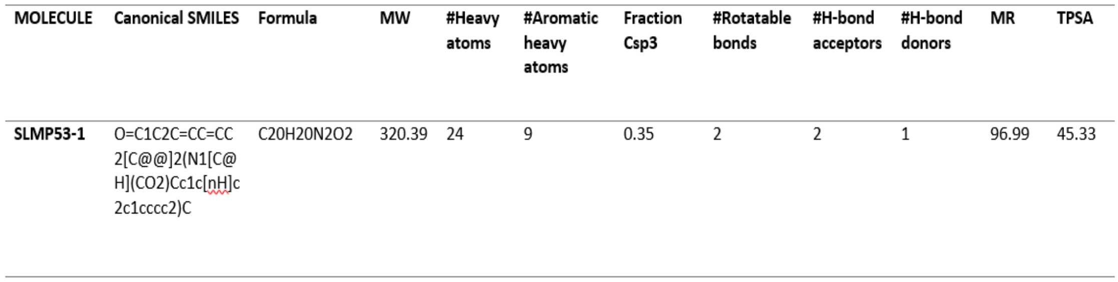

MOLECULE	Canonical SMILES	Formula	MW	#Heavy atoms	#Aromatic heavy atoms	Fraction Csp3	#Rotatable bonds	#H-bond acceptors	#H-bond donors	MR	TPSA
SLMP53-1	O=C1C2C=CC=CC2[C@@]2(N1[C@H](CO2)Cc1c[nH]c2c1cccc2)C	C20H20N2O2	320.39	24	9	0.35	2	2	1	96.99	45.33

(MW; molecular weight, MR; molar refractivity, TPSA; total polar surface area)

Table S7. SwissADME shows that SLMP53-1 do not violate any of the drug-likeness criteria.

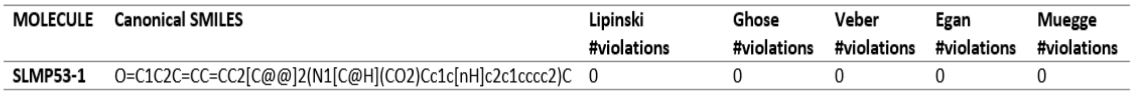

MOLECULE	Canonical SMILES	Lipinski #violations	Ghose #violations	Veber #violations	Egan #violations	Muegge #violations
SLMP53-1	O=C1C2C=CC=CC2[C@@]2(N1[C@H](CO2)Cc1c[nH]c2c1cccc2)C	0	0	0	0	0

Table S8. Medicinal chemistry evaluation of SLMP53-1.

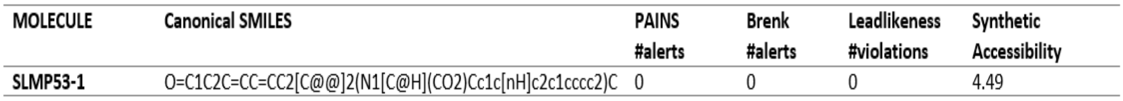

MOLECULE	Canonical SMILES	PAINS #alerts	Brenk #alerts	Leadlikeness #violations	Synthetic Accessibility
SLMP53-1	O=C1C2C=CC=CC2[C@@]2(N1[C@H](CO2)Cc1c[nH]c2c1cccc2)C	0	0	0	4.49

Table S9. Pharmacokinetic evaluation of the SLMP53-1.

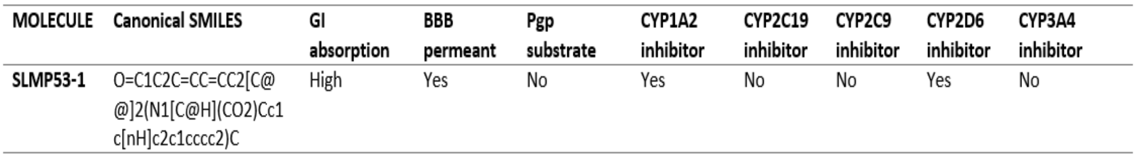

MOLECULE	Canonical SMILES	GI absorption	BBB permeant	Pgp substrate	CYP1A2 inhibitor	CYP2C19 inhibitor	CYP2C9 inhibitor	CYP2D6 inhibitor	CYP3A4 inhibitor
SLMP53-1	O=C1C2C=CC=CC2[C@@]2(N1[C@H](CO2)Cc1c[nH]c2c1cccc2)C	High	Yes	No	Yes	No	No	Yes	No

(GI; gastro-intestinal absorption; BBB, blood brain barrier; nCYP, Cytochromes; P-gp, P-glycoprotein)

Table S10. Water solubility evaluation of SLMP53-1 (ESOL and Ali *et al*. models).

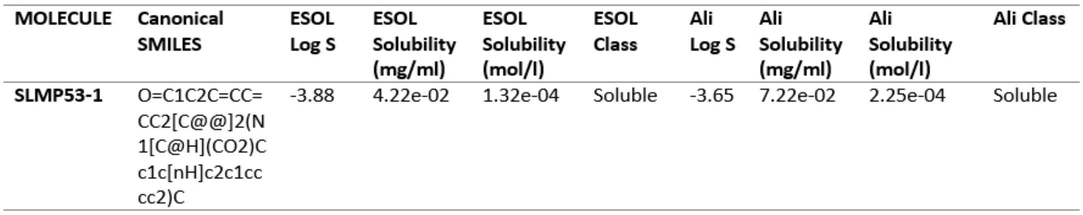

MOLECULE	Canonical SMILES	ESOL Log S	ESOL Solubility (mg/ml)	ESOL Solubility (mol/l)	ESOL Class	Ali Log S	Ali Solubility (mg/ml)	Ali Solubility (mol/l)	Ali Class
SLMP53-1	O=C1C2C=CC=CC2[C@@]2(N1[C@H](CO2)Cc1c[nH]c2c1cccc2)C	-3.88	4.22e-02	1.32e-04	Soluble	-3.65	7.22e-02	2.25e-04	Soluble

Table S11. Water solubility evaluation of SLMP53-1 (SILICOS-IT model).

MOLECULE	Canonical SMILES	Silicos-IT LogSw	Silicos-IT Solubility (mg/ml)	Silicos-IT Solubility (mol/l)	Silicos-IT class
SLMP53-1	O=C1C2C=CC=CC2[C@@]2(N1[C@H](CO2)Cc1c[nH]c2c1cccc2)C	-4.15	2.27e-02	7.08e-05	Moderately soluble

Table S12. Lipophilicity evaluation of SLMP53-1.

MOLECULE	Canonical SMILES	iLOGP	XLOGP3	WLOGP	MLOGP	Silicos-IT Log P	Consensus Log P
SLMP53-1	O=C1C2C=CC=CC2[C@@]2(N1[C@H](CO2)Cc1c[nH]c2c1cccc2)C	2.50	3.03	2.65	2.66	2.74	2.71

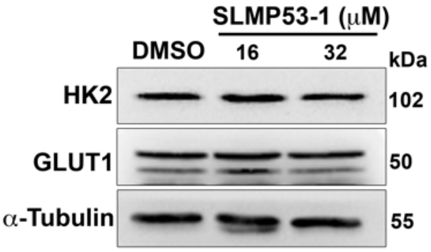

Figure S6. Expression levels of HK2 and GLUT1, after 24 h treatment with SLMP53-1, in HCT116 p53$^{-/-}$ cancer cells. Immunoblots are representative of two independent experiments; α-tubulin was used as a loading control.

ANNEX IV

Supporting information of Chapter 4

Helena Ramos, et al, 2020. *MANIO: mechanism of wild-type and mutant p53 activation and therapeutic potential in colorectal* cancer. Manuscript in preparation.

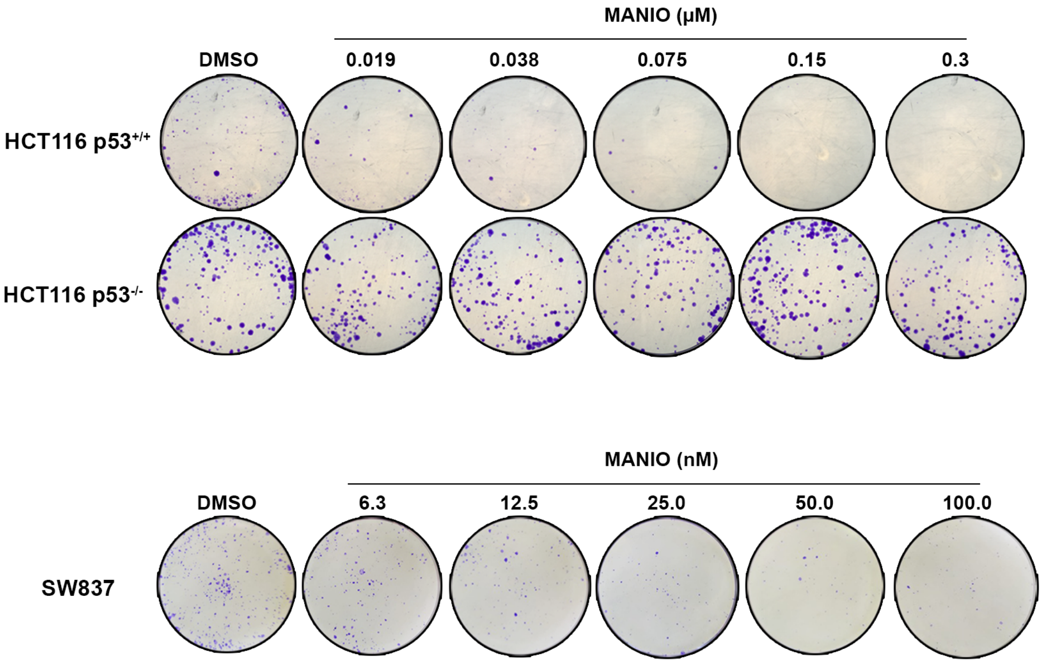
MANIO (µM)
DMSO
0.019
0.038
0.075
0.15
0.3
HCT116 p53+/+
HCT116 p53-/-
MANIO (nM)
DMSO
6.3
12.5
25.0
50.0
100.0
SW837

Figure S7. Representative images of the colony forming assays in HCT116 (p53$^{+/+}$ and p53$^{-/-}$) and SW837, after 14 or 11 days of MANIO treatment, respectively.

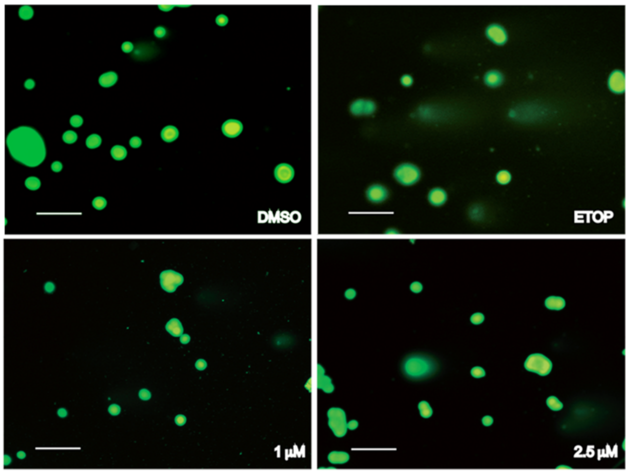
DMSO
ETOP
1 µM
2.5 µM

Figure S8. MANIO is non-genotoxic in tumor cells. Representative images of DNA damage in HCT116 p53$^{+/+}$ cells treated with 1 and 2.5 µM MANIO and 25 µM etoposide (ETOP; positive control), for 48 h, using the alkaline comet assay (scale bar = 50 µm; magnification = ×100).

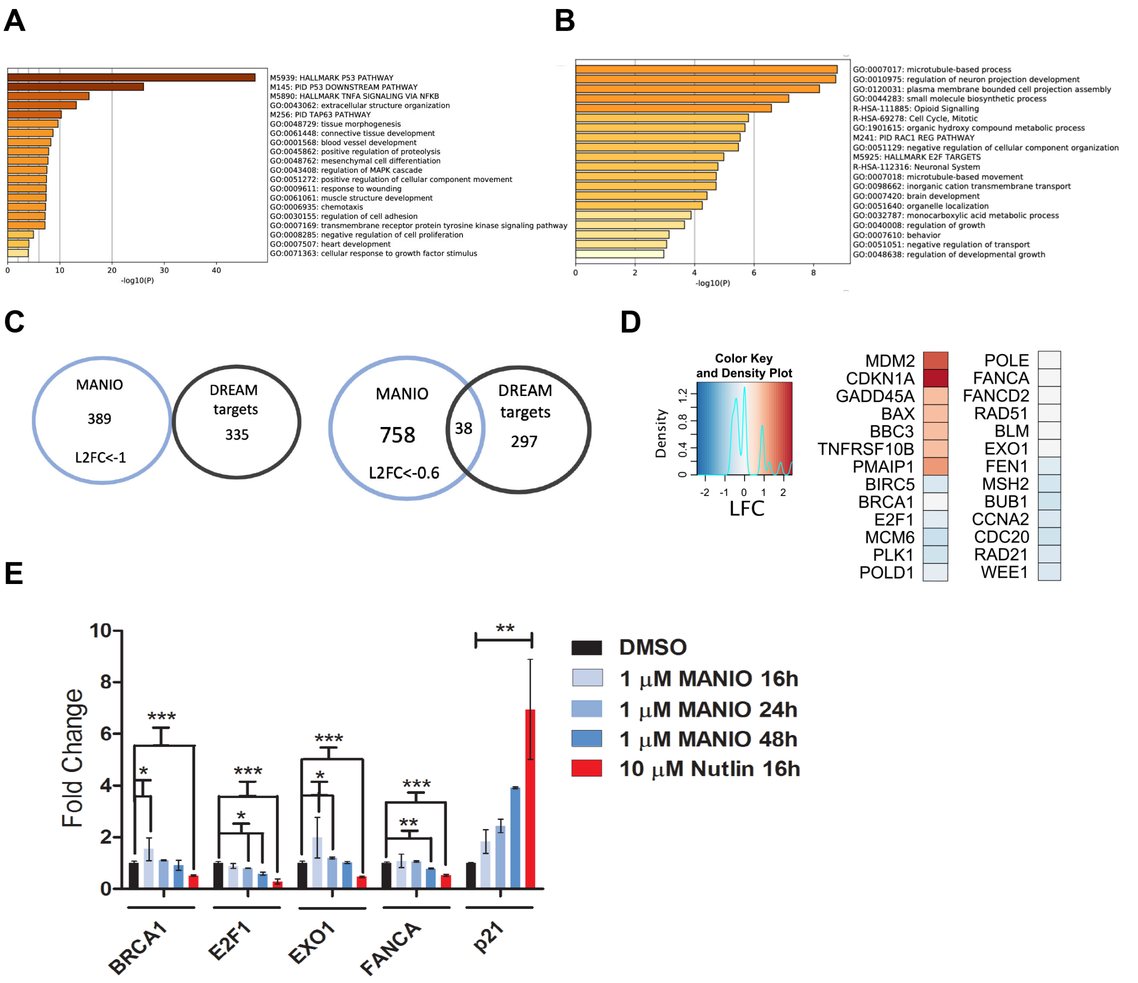

Figure S9. Pathway analysis and features of the repressed gene signature elicited by MANIO treatment in HCT116 cells. **(A)** Metascape results obtained with the differentially Upregulated gene list confirm that the p53 pathway signature as the most enriched semantic terms. See EnrichR data presented in Figure 16. **(B)** Metascape results obtained with the differentially Downregulated gene list confirm the weak enrichment for terms related to cell cycle arrest. See EnrichR data presented in Figure 16. **(C)** Venn Diagram comparing the list of coding genes differentially Downregulated by MANIO treatment and an established list of genes that are modulated by the DREAM complex and can thus be indirectly repressed by p53 via the modulation of p21 (reference). Genes significantly repressed by MANIO selected based on log2 Fold change ≤ -1, or on log2 Fold change ≤ 0.6 were used for the comparison respectively in the upper and lower panels. **(D)** Heatmap-view of the RNA-sequencing results for a selection of DREAM targets. The gene expression change of direct p53 target genes validated in the paper are included as control (gene name italic). While few dream targets are significantly Downregulated by MANIO considering the minimum fold change threshold (Log2 Fold change < -0.6), there is a general trend for repression that is statistically significant for several genes (gene names in bold, adjusted *p* value < 0.05). **(E)** Effect of MANIO treatment at different time points. qPCR data for the indicated DREAM target genes and for p21 (*CDKN1A*) is presented as average fold change and standard deviation of three biological replicates. *B2M* and *YWHAZ* were used as reference genes. Nutlin was used as a control of non-genotoxic p53 activation. Repression of E2F1 and FANCA was apparent after 48 h of MANIO treatment, a time point where the induction of p21 was highest.

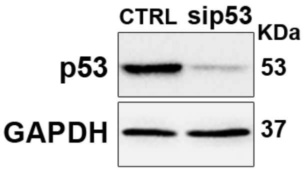

Figure S10. Western blot analysis of mutp53 protein levels in SW837 cells transfected with sip53 or CTRL. Immunoblots represent one of three independent experiments. GAPDH was used as loading control.

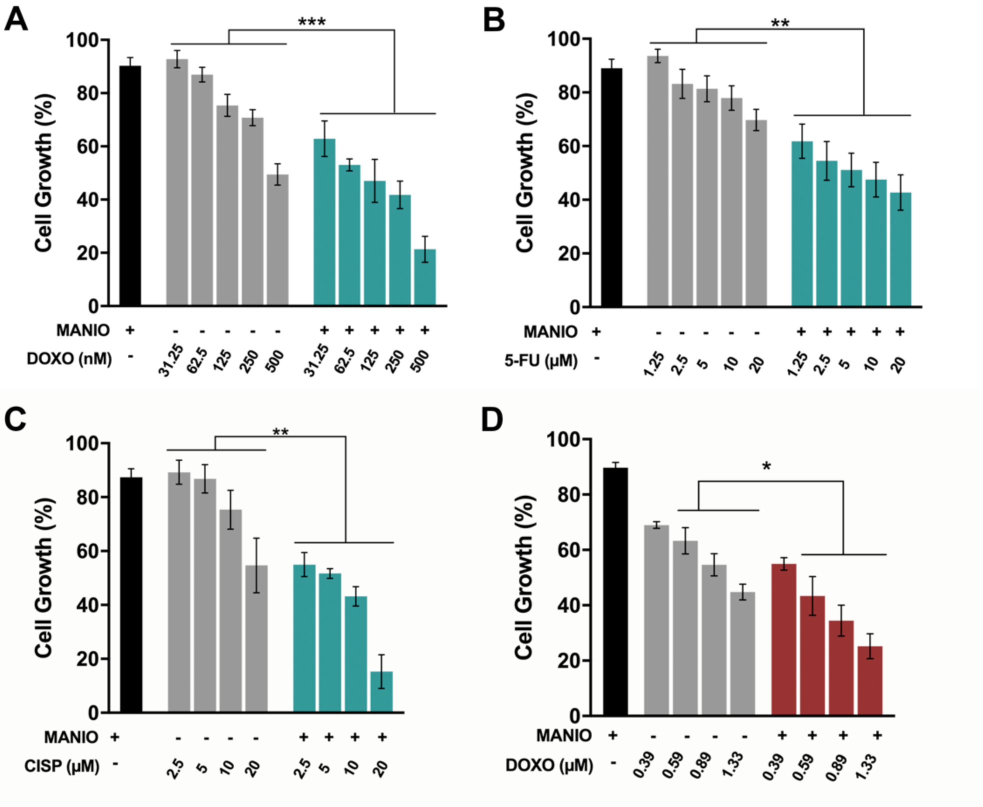

Figure S11. MANIO sensitizes SW837 and patient-derived primary CRC cells to conventional chemotherapeutic agents. (A-C) SW837 cells were treated with a range of concentrations of doxorubicin (DOXO; **A**), 5-fluorouracil (5-FU; **B**) or cisplatin (CISP; **C**) alone and in combination with 0.9 µM MANIO; cell proliferation was measured after 24 h treatment. **(D)** Patient-derived CRC CCZ3 cells were treated with a range of concentrations of DOXO alone and in combination with 2 µM MANIO; cell proliferation was measured after 48 h treatment. In A-D, the growth attained with control (DMSO) was set as 100%. Data shown are mean ± SEM (6 independent experiments); values significantly different from chemotherapeutic drug alone: *$p < 0.05$ **$p < 0.01$, ***$p < 0.001$; two-way ANOVA followed by Sidak's multiple comparison test.

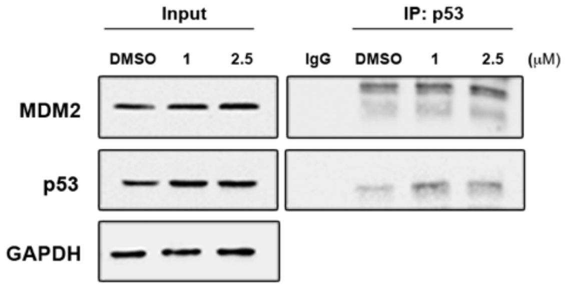

Figure S12. MANIO does not inhibit the p53–MDM2 interaction in HCT116 p53$^{+/+}$ cells. Co-immunoprecipitation was performed with anti-p53 (IP:p53) or anti-immunoglobulin G (IgG) antibodies, followed by immunoblotting with anti-MDM2, and anti-p53 antibodies in cells treated with 1 and 2.5 μm of MANIO or DMSO for 16 h; whole-cell lysate (input). Immunoblots represent one of three independent experiments. GAPDH was used as a loading control.

Table S13. Growth inhibitory effect of MANIO and PRIMA-1^{MET} in human tumor cell lines.

Human tumor cell line	p53 status	PRIMA-1^{MET}	MANIO
HCT116 p53$^{+/+}$	wt	19.50 ± 0.40	0.97 ± 0.04
HCT116 p53$^{-/-}$	null	6.57 ± 0.12	48.25 ± 1.97
SW837	mut	26.50 ± 4.60	2.90 ± 0.317
HT29	mut	39.8 ± 2.0	2.33 ± 0.33
MDA468	mut	13.0 ± 0.0	0.20 ± 0.05
IGROV-1	mut	13.73 ± 3.58	0.09 ± 0.01
SKOV-3	null	> 50	26.20 ± 3.83
OVCAR-3	mut	> 50	11.18 ± 1.69

IC_{50} values were determined by the SRB assay after 48 h treatment with MANIO. Data are mean ± SEM of 4-5 independent experiments.

ANNEX V

Pharmacokinetic studies of MANIO

Data presented in this annex were
provided by Eurofins company

1. Material and methods

1.1 *In vitro* PK assays

Table S14. Description of *in vitro* PK assays.

Assay	Technique	Incubation	Detection method	Reference
Aqueous solubility (simulated gastric fluid)		24 h RT	HPLC-UV/VIS	[445]
Aqueous solubility (simulated intestinal fluid)		24 h RT	HPLC-UV/VIS	[445]
Aqueous solubility (PBS, pH 7.4)		24 h RT	HPLC-UV/VIS	[445]
Partition coefficient (LogD, n-octanol/PBS, pH 7.4)	Shake-flask	60 min RT	HPLC-MS/MS	[449]
Protein binding (plasma, human)	Equilibrium dialysis	4 h 37 °C	HPLC-MS/MS	[450]
A-B permeability (Caco-2, pH 6.5/7.4)		0 and 60 min RT	HPLC-MS/MS	[451]
B-A permeability (Caco-2, pH 6.5/7.4)		0 and 40 min RT	HPLC-MS/MS	[451]
Intrinsic clearance (human liver microsomes – 0.1 mg/mL)		0, 15, 30, 45, 60min RT	HPLC-MS/MS	[452]

A – Apical; B – Basal; HPLC-UV/VIS – High performance liquid chromatography – UV/Visible detector; HPLC-MS/MS – High Performance Liquid Chromatography Mass Spectrometry; RT – Room Temperature.

Aqueous solubility (µM) was determined by comparing the peak area of the principal peak in a calibration standard (200 µM) containing organic solvent (methanol/water, 60/40, v/v) with the peak area of the corresponding peak in a buffer sample. In addition, chromatographic purity (%) was defined as the peak area of the principal peak relative to the total integrated peak area in the HPLC chromatogram of the calibration standard.

The total amount of compound was determined as the peak area of the principal peak in a calibration standard (100 µM) containing organic solvent (methanol/water, 60/40, v/v). The amount of compound in buffer was determined as the combined, volume-corrected, and weighted areas of the corresponding peaks in the aqueous phases of three organic-aqueous samples of different composition. An automated weighting system was used to ensure the preferred use of raw data from those samples with well quantifiable peak signals. The amount of compound in organic was calculated by subtraction. Subsequently, LogD was calculated as the Log10 of the amount of compound in the organic phase divided by the amount of compound in the aqueous phase.

The peak areas of the test compound in the buffer and test samples were used to calculate percent binding and recovery according to the following formulas:

$$\text{Protein binding (\%)} = \frac{Area_p - Area_b}{Area_p} \times 100$$

$$\text{Recovery (\%)} = \frac{Area_p + Area_b}{Area_c} \times 100$$

where

$Area_p$ = Peak area of analyte in protein matrix

$Area_b$ = Peak area of analyte in buffer

$Area_c$ = Peak area of analyte in control sample

The apparent permeability coefficient (P_{app}) of the test compound was calculated as follows:

$$P_{app}\ \text{(cm/s)} = \frac{V_R \times C_{R,end}}{\Delta t} \times \frac{1}{A \times (C_{D,md} - C_{R,mid})}$$

where V_R is the volume of the receiver chamber. $C_{R,end}$ is the concentration of the test compound in the receiver chamber at the end time point, Δt is the incubation time, and A is the surface area of the cell monolayer. $C_{D,mid}$ is the calculated mid-point concentration of the test compound in the donor side, which is the mean value of the donor concentration at time 0 minute and the donor concentration at the end time point. $C_{R,mid}$ is the mid-point concentration of the test compound in the receiver side, which is one half of the receiver concentration at the end time point. Concentrations of the test compound were expressed as peak areas of the test compound.

The recovery of the test compound was calculated as follows:

$$\text{Recovery (\%)} = \frac{V_D \times C_{D,end} + C_{R,end}}{V_D \times C_{D0}} \times 100$$

where V_D and V_R are the volumes of the donor and receiver chambers, respectively. $C_{D,end}$ is the concentration of the test compound in the donor sample at the end time point. $C_{R,end}$ is the concentration of the test compound in the receiver sample at the end time point. C_{D0} is the concentration of the test compound in the donor sample at time zero. Concentrations of the test compound are expressed as peak areas of the test compound.

For permeability assays, lucifer yellow was used as the cell monolayer integrity marker. Lucifer yellow permeability assessment (in the Apical to Basal (A-B) direction at pH 7.4 on both sides) was performed after the permeability assay for the test compound. The cell monolayer that had a Lucifer yellow permeability of less than 1.5×10^{-6} cm/s for Caco-2 and MDR1-MDCKII cells and 2.5×10^{-6} cm/s for MDCKII cells was considered intact, and the permeability result of the test compound from intact cell monolayer is reported.

For intrinsic clearance determinations, metabolic stability, expressed as percent of the parent compound remaining, was calculated by comparing the peak area of the compound at the time point relative to that at time-0. The half-life ($T_{1/2}$) was estimated from the slope of the initial linear range of the logarithmic curve of compound remaining (%) vs. time, assuming the first-order kinetics. The apparent intrinsic clearance (CL_{int}, in µL/min/pmol, µL/min/mg or µL/min/Mcell) was calculated according to the following formula:

$$CL_{int} = \frac{0.693}{T_{1/2} \times (mg\ protein/\mu L\ or\ million\ cells/\mu L\ or\ pmol\ CYP\ isoyme/\mu L)}.$$

1.2. *In vivo* PK assays

1.2.1. Animals

Male ICR mice weighing 25 ± 5 g were provided by BioLasco Taiwan (under Charles River Laboratories Licensee). Animals were acclimated for 3 days prior to use and were confirmed with good health. All animals were maintained in a hygienic environment with controlled temperature (20 - 24ºC), humidity (30% - 70%) and 12 hours light/dark cycles. Free access to sterilized standard lab diet [MFG (Oriental Yeast Co., Ltd., Japan)] and autoclaved tap water were granted. All aspects of this work, including housing, experimentation, and disposal of animals were performed in general accordance with the Guide for the Care and Use of Laboratory Animals: Eighth Edition (National Academy Press, Washington, D. C., 2011) in our AAALAC-accredited laboratory animal facility. The animal care and use protocol was reviewed and approved by the IACUC at Pharmacology Discovery Services Taiwan, Ltd.

1.2.2. Methods

Table S15. Animal Dosing Design - *In vivo* PK, non-fasted animals.

Vehicle	Dose Schedule	Route	Dose		Mice (Male ICR)
			mL/kg	mg/kg	
DMSO/ Solutol® HS15/ PBS (5/10/85, v/v/v)	Bolus	IV	5	20	$24^a + 3^b$

[a]Plasma with 3 mice per timepoint; [b]Normal (untreated) blank control for drug free plasma.

MANIO formulation

MANIO was dissolved in dimethyl sulfoxide (DMSO)/ Solutol® HS15/ PBS (5/10/85, v/v/v) at 4 mg/mL for IV injection. The dosing volume was 5 mL/kg for IV.

Plasma Sample Collection from Mice

Blood aliquots (300-400 µL) were collected via cardiac puncture in tubes coated with lithium heparin, mixed gently, then kept on ice and centrifuged at 2,500 ×g for 15 minutes at 4 °C, within 1 h of collection. The plasma was then harvested and kept frozen at -70 °C until further processing.

Quantitative Bioanalysis (Plasma)

The plasma samples were processed using acetonitrile (ACN) precipitation and analyzed by LC-MS/MS. A plasma calibration curve was generated. Aliquots of drug-free plasma were spiked with the test substance at the specified concentration levels. The spiked plasma samples were processed together with the unknown plasma samples using the same procedure. The processed plasma samples were stored at -70°C until receiving LC-MS/MS analysis, at which time peak areas were recorded, and the concentrations of the test substance in the unknown plasma samples were determined using the respective calibration curve. The reportable linear range of the assay was determined, along with the lower limit of quantitation (LLOQ).

Pharmacokinetics

Plots of plasma concentration of MANIO versus time were constructed. The fundamental pharmacokinetic parameters of each compound after IV ($t_{1/2}$, C_0, AUClast, AUCInf, AUCExtr, MRT, Vss, and CL) was obtained from the non-compartmental analysis (NCA) of the plasma data using WinNonlin. Plots of plasma concentrations of compounds versus dose were constructed.

2. Results

Table S16. Solubility of MANIO in different aqueous samples.

	Test concentration	Wavelength of detection	Solubility (µM)			Flags
			1st	2nd	Mean	
Aqueous solubility (simulated gastric fluid)	200 µM	205	< 1	< 1	**<1**	BLQ
Aqueous solubility (simulated intestinal fluid)	200 µM	205	451.83	438.78	**200.0**	ADJ
Aqueous solubility (PBS, pH 7.4)	200 µM	205	964.35	958.44	**200.0**	ADJ

BLQ: Below the limit of quantitation. Value was below the limit of quantitation in the aqueous sample.
ADJ: Adjusted. When the observed mean solubility is greater than 200 µM, the mean value was adjusted to the maximum assay concentration, which is 200 µM.

Table S17. Human intestinal permeability of MANIO, evaluated in Caco-2 cell monolayer.

	Test concentration	Permeability (10^{-6} cm/s)			% Recovery		
		1st	2nd	Mean	1st	2nd	Mean
A-B permeability (Caco-2, pH 6.5/7.4)	10 µM	0.97	1.00	**0.99**	83	78	80
B-A permeability (Caco-2, pH 6.5/7.4)	10 µM	534.63	605.01	**569.8**	158	173	166

A – Apical; B – Basal.

Table S18. *In vitro* hepatic metabolism of MANIO.

Test concentration	Incubation time (min)	% Compound remaining (% remaining)			Half-life			CL_{int} µL/min/mg
		1st	2nd	Mean	1st	2nd	Mean	
0.1 µM	0	100.0	100.0	100.0	> 60	> 60	> 60	< 115.5
	15	100.4	98.4	99				
	30	91.1	93.2	92				
	45	88.0	90.4	89				
	60	89.1	75.5	82				

CL_{int} – Internal clearance.

Table S19. Protein binding ability of MANIO.

	Test concentration	% Protein Bound			% Recovery		
		1st	2nd	Mean	1st	2nd	Mean
Protein binding (human plasma albumin)	10 µM	0.5	0.4	**0.45**	104	115	109

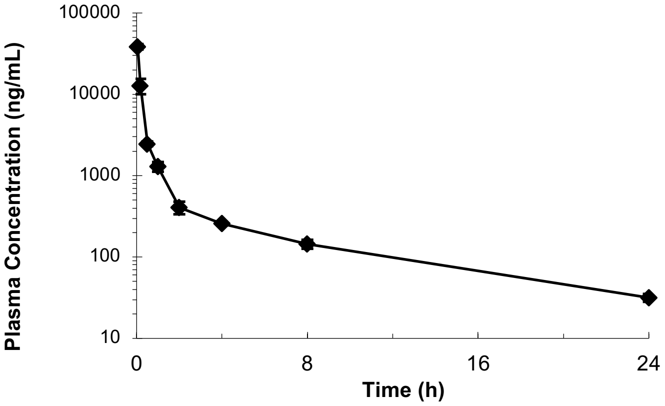

Figure S13. The mean exposure levels of MANIO in plasma samples versus time (semi-log plot). The concentration of MANIO was determined in mice plasma after IV bolus injection of 20 mg/kg MANIO, through LC/MS/MS. Data are mean ± SD (n = 3).

Table S20. The PK parameters of MANIO in mouse plasma samples.

Dose, IV (mg/Kg)	$t_{1/2}$ (h)	C_0 (ng/mL)	AUClast (h*ng/mL)	AUCInf (h*ng/mL)	AUC Extr (%)	MRT (h)	Vss (L/kg)	CL (mL/min/Kg)
20	6.83	61833	12730	13045	2	2.67	4	26

$t_{1/2}$ – Elimination half-life (to be used in one-or noncompartmental model); AUClast – Area under the curve from the time of dosing to the time of the last measurable (positive) concentration (Tlast); AUCInf – AUC from time of dosing extrapolated to infinity; MRT – Mean residence time of drug in the body; CL – Apparent total body clearance of the drug from plasma; Vss – Apparent volume of distribution at steady state; C_0 – Drug concentration at time 0.